NASA Contractor Report 174918

Turbulence Characteristics of Swirling Flowfields

T.W. Jackson and D.G. Lilley
Oklahoma State University
Stillwater, Oklahoma

May 1985

Prepared for
Lewis Research Center
Under Grant NAG 3-74

National Aeronautics and
Space Administration

TABLE OF CONTENTS

NOMENCLATURE

A, B, C	calibration constants
C_μ	k-ε model constant
D	test section diameter
d	inlet nozzle diameter
E	hot-wire voltage
G	pitch factor
K	yaw factor
k	kinetic energy of turbulence
L	contraction nozzle downstream distance
ℓ	turbulence dissipation length scale
P, Q, R	selected hot-wire probe positions
q	local velocity vector
Re	Reynolds number
$\vec{V}$	time-mean vector velocity magnitude
$\underline{v} = (u, v, w)$	time-mean velocity (in x-, r-, θ-directions) in facility coordinates
x, r, θ	axial, radial, and azimuthal cylindrical polar coordinates
x, y, z	Cartesian coordinates
Z	effective cooling velocity acting on a wire
α	side-wall expansion angle
ε	turbulence energy dissipation rate

$\gamma_{Z_i Z_j}$	correlation coefficient (estimated) between cooling velocities of adjacent wire orientations
ϕ	swirl vane angle with respect to facility axis
μ	turbulent viscosity
ρ	time-mean density

Subscripts

1, 2, 3, 4, 5, 6	refer to the six probe measuring positions
P, Q, R	refer to the three selected cooling velocities
i,j	summation indices
o	value at inlet to flowfield
rms	root-mean-squared quantity

Superscripts

$(\bar{})$	time-mean average
$(\,)'$	fluctuating quantity
$(\tilde{})$	relative to probe coordinates

CHAPTER I

INTRODUCTION

1.1 Combustor Design Phenomena

The function of the gas turbine combustion chamber, illustrated in Figure 1, is to heat the air from the compressor up to the design maximum temperature. That is, the temperature that the combustion chamber and turbine will stand without undue creep or distortion for a reasonable period of time. The combustor must also give reasonably uniform velocity and temperature distributions onto the leading edge of the turbine blades. Complete combustion to minimize the formation of carbon particles and pollutants and ignition reliability at high altitudes are both very important criteria for the efficient performance of a gas turbine combustor.

To improve flame stabilization and promote mixing between the incoming fuel and the hot products of combustion, swirl is often imparted to the incoming combustion air prior to entry into the primary zone. The purpose of swirl is to assist in the creation of a toroidal flow reversal to obtain high rates of mixing. This type of recirculation provides better mixing than might be obtained by other means, such as bluff bodies [1].

In design situations, the engineer has to analyze the swirling recirculating turbulent flow within combustors whose complexity is increased manyfold by the processes of combustion and heat transfer. At present

the combustor designer is faced with making only slight modifications to present combustors because of the economic limitations of full-scale testing of combustion chambers. Before a route can be provided which leads to the accomplishments of design objectives more quickly and less expensively than current practice permits greater knowledge is required concerning the flowfields inside gas turbine combustion chambers.

1.2 The Present Research

In gas turbine and ramjet combustion chamber development, designers are aided by both experimental and theoretical studies [2]. Both methods of approach are complementary, theoretical modeling being aided by carefully chosen experiments [3]. A major area of research need, with which the present research work is concerned, is the measurement of time-mean and turbulence properties in nonreacting swirling flow in various combustor geometries, so as to aid in the understanding and development of suitable turbulence models [4].

Some recent researchers [5, 6, 7] have measured the time-mean and turbulence properties of swirling flowfields in the presence of chemical reaction. However, a more fundamental knowledge of the fluctuating velocities and their cross-correlations for a variety of swirl strengths under isothermal conditions is needed before the complex interactions of chemical reaction and turbulent mixing are fully understood. The present research is restricted to isothermal flows.

The specific problem being investigated experimentally is concerned with the steady turbulent flow of air in axisymmetric geometries under low speed conditions. Specifically, flow exits from a round-sectioned contoured nozzle with known velocity and turbulence distributions and

enters a round pipe with an expansion ratio D/d = 2 or ∞, as illustrated in Figure 2. The incoming air may possess a swirl component of velocity via passage through an annular vane swirler with blades at angle ϕ to the undisturbed flow direction. If swirl is present, the resulting flow-field domain may possess a central toroidal recirculation zone (CTRZ). In the sudden expansion case a corner recirculation zone (CRZ) is provoked because of the abrupt change in geometry of the boundary. It is well known that both of these recirculation zones contain large turbulent eddies which promote turbulent mixing. To simulate ramjet combustion chambers, the test section may be equipped with a strong contraction nozzle of area ratio 4.

Of vital concern is the characterization of these turbulent, swirling, confined jet flows in terms of the effects of swirl strength, expansion ratio, and downstream blockage on the time-mean velocities and Reynolds normal and shear stresses. Realization that these flows also play an important role in many other engineering applications has inspired a definite desire for investigation in this area.

1.3 Experimental Investigation

Measurements of the time-mean and turbulence characteristics of confined swirling jet flows are being used to aid in the evolution of turbulence models for these complex flow situations. These measurements are part of a larger ongoing project at Oklahoma State University into the fundamental concepts of swirling flows in combustor geometries.

The present research has included flow visualization techniques using kerosene smoke and neutrally-buoyant helium-filled soap bubbles recorded on still [8] and movie [9] photographs. Time-mean velocities in

swirling and nonswirling confined flowfields have been found by use of a five-hole pitot probe [8, 10]. Turbulence properties using the single hot-wire multi-orientation technique [11] and a crossed hot-wire probe [12] have been measured in nonswirling flowfields. The performance of the annular vane swirler used in this report has also been studied using a five-hole pitot probe [13]. Predictions of the flowfields corresponding to the ones studied have been made using the measured inlet conditions [14, 15, 16]. The predictions are achieved by using the STARPIC computer code which solves the appropriate partial differential equations and simulates turbulence by means of the two-equation k-ε turbulence model [4].

All this previous work has been performed using the low speed wind tunnel, as seen in Figure 3, in the Mechanical Engineering laboratory at Oklahoma State University. The facility consists of an axial-flow fan whose speed can be varied. Numerous fine screens and straws produce flow in the settling chamber of relatively low turbulence intensity. The contoured nozzle leading to the test section has been designed to produce a minimum adverse pressure gradient on the boundary layer and thus avoid any regions of separated flow within the nozzle. The test section consists of either a 15 cm or 30 cm diameter plexiglass tube depending on which expansion ratio is desired. Plexiglass was chosen so as to allow accurate probe positioning and permit flow visualization. The substantial size of the test section provides excellent probe resolution. The swirler, placed upstream of the test section, consists of ten variable angle flat blades with a pitch-to-chord ratio of 0.68. Each individual blade can be set to any desired angle between 0 and 80 degrees. Three swirl flow types are investigated in the present study: nonswirling

flow (ϕ = 0° swirler removed), moderately swirling flow (ϕ = 38 and 45°) and strongly swirling flow (ϕ = 60 and 70°).

1.4 Scope and Objectives

The focus of the present research is the measurement of time-mean and turbulence properties of a confined swirling jet. The measurements provide a data base for the development of turbulence models for these flow situations. Measurements have been made for a full range of swirl strengths and geometric configurations over the entire flowfield of interest. Specifically, these objectives include:

1. Measurements of time-mean velocities and complete Reynolds stress tensor to find the effect of swirl on a suddenly expanding confined jet with an expansion ratio of 2. Swirl vane angles of 0 (swirler removed), 38, 45, 60, and 70 degrees are considered.

2. The effect of a strong contraction nozzle with an area reduction ratio of 4 located at two large chamber diameters downstream of the jet exit is investigated. Time-mean velocities and turbulent stresses are measured for three cases of swirl, ϕ = 0, 45, and 70 degrees.

3. A directional sensitivity analysis is performed on the measuring technique to determine the relative accuracy of the technique to approach time-mean velocity.

4. Measurements of time-mean velocities and Reynolds stress tensor in a nonexpanding confined jet flowfield (D/d = 1) to find the effect of the sudden expansion on three cases of swirl, ϕ = 0, 45, and 70 degrees.

5. Determination of the length scale of energy containing eddies in suddenly expanding and nonexpanding confined jets. The swirl strengths of interest are nonswirling, medium, and strong swirl.

CHAPTER II

REVIEW OF PREVIOUS EXPERIMENTAL STUDIES IN RECIRCULATING FLOWS

Previous experimental work in axisymmetric recirculating flows provide an important background for this investigation. Information regarding nonswirling and swirling turbulent flows have been extensively reviewed. Techniques in the measurement of turbulence are constantly being updated; these require reviewing for their applicability to the present study. Noteworthy results are included in the summary where the emphasis is on nonreacting turbulent swirling flows.

2.1 Confined Nonswirling Flows

One of the first researchers to make a thorough investigation into confined nonswirling jet flow was Chaturvedi [17], who measured the mean velocity and pressure and characteristics of the turbulence in a confined jet with an expansion ratio D/d = 2. The mean velocity and pressure measurements were made by pitot probe and stagnation tube, respectively. Measurements of velocity head were made using a pitot tube of very small diameter with a 15 degree taper machined internally on the leading edge. This was due to regions of high turbulence intensity or where the direction of the velocity vector was unknown. The turbulence characteristics were measured first with a single hot-wire to determine u' and again with cross-wires to determine the radial intensity v'; the measurements

also produced the turbulent shear $\overline{u'v'}$. It was reported that the corner recirculation zone (CRZ) extended to a length of two chamber diameters downstream of the jet exit for the sudden expansion case with high turbulence intensities on the edge of this zone.

Many researchers have studied the recirculation zone behind a pipe step [18-22], in particular, the reattachment length. Krall and Sparrow [18] utilized an orifice in an electrically heated tube to create flow separation with water as the modeling fluid. It was presumed that the peak Nusselt number occurred at the reattachment point which they found existed at 1.25 to 2.50 pipe diameters downstream from the onset of separation. Their results agreed with those of Phaneuf and Netzer [19] in that the reattachment length was unaffected by the Reynolds number in the turbulent range. Also, they found that the peak Nusselt number became spread out into a broad zone for strong separations caused by large step heights. This transition from a point to a broad zone occurred between $h/D = 0.16$ and $h/D = 0.25$, where D is the pipe diameter and h is the step height. It was also found that increasing the step height moved the peak point slightly downstream.

Back and Roshke [20] and Roshke and Back [21] also investigated the reattachment length by visual observation in water flows. The diameter expansion ratio used was 2.6 and a conical contraction section just upstream reduced the boundary layer thickness. Small 0.76 mm diameter holes were located on the larger diameter tube one step height apart. Reattachment locations were determined by slowly metering dye through the holes and observing whether it moved upstream or downstream.

Phaneuf and Netzer [19] measured wall static pressure as well as mean axial velocities behind abrupt steps where the expansion ratios

were 0.303 and 0.195. They found that the reattachment zone spreads out with both increasing Reynolds number (for a given step height) and increasing step height providing the Reynolds number is in the turbulence transition range. It was further concluded that the point of maximum heat transfer does not coincide with the zone of reattachment and furthermore it is dependent upon the inlet mass flux.

Three different step heights of 0.6, 1.6, and 2.0 were studied by Ha Minh and Chassaing [22]. They measured the time-mean axial velocities and the turbulence characteristics of the flow. Agreement between hot-wire and pitot probe measurements were found to exist for the time-mean velocities. The Reynolds stresses were successfully measured using the rotating, inclined, single hot-wire technique, and their results compared well with previous studies [17].

Laser doppler anemometry was used by Moon and Rudinger [23] to study the behavior of recirculating flows. Even though an L.D.A. system was used, only mean axial velocities were measured, particularly those found in regions of recirculation. The L.D.A. system with the aid of a Bragg cell could detect the velocity reversals in the recirculation region.

Johnson and Bennett [24] developed a measuring technique to determine the mean and fluctuating velocity and concentration distributions along with their cross correlations by using a laser doppler velocimeter. This method was developed using coaxial jets in sudden expansions with $D/d = 2.07$. A laser-induced flourescence technique was used to measure the concentration of a flourescent trace material.

Janjua [11] measured the time-mean velocities and complete Reynolds stress tensor for an abrupt and gradual expanding confined jet. The six-orientation single hot-wire technique was employed in a confined jet of

expansion ratio 2. The results obtained using this technique were found to be in good agreement with those found by Chaturvedi [17].

2.2 Free Swirling Jets

Swirl can be imparted upon a flow by many different means. Rose [25] used a very simple method of producing swirl by rotating a pipe at 9500 rpm so as to provide an approximately fully-developed turbulent flow in solid body rotation. By this means it was only possible to obtain a relatively weak degree of swirl. Because of the low swirl number involved, Rose was capable of using a single hot-wire and an X-meter in the flowfield to determine the turbulence intensity components and the direction of the flow velocities, respectively. He found a free swirling jet, in contrast to a nonswirling jet, that the jet spreads at a larger angle, entrains fluid more rapidly, and consequently displays a more rapid reduction of mean velocity and turbulence intensity.

Chigier and Beer [26] generated swirl by introducing varying proportions of air through tangential ports while the remainder of the air was introduced axially. General velocity and static pressure distributions, form and shape of the central toroidal recirculation zone (CTRZ) were obtained for differing degrees of weak swirl and varying discharge nozzle configurations.

Using a three-dimensional probe, Kerr and Fraser [27] found that the jet mass rate, angle of spread, and the reciprocal of the axial velocity all vary linearly with the swirl number. They proposed that the swirl number S be defined as

$$S = \frac{T}{G\ D_e}$$

where T is the nozzle torque, G is the jet thrust, and D_e is the effective nozzle diameter.

Chigier and Chervinsky [28] carried out an experimental investigation on a series of swirling air jets. The swirl generator was composed of axial and tangential air inlets. Measurements of time-mean values of velocity and static pressure were made with a five-hole spherical impact probe. With this instrument they found that there was a progressive decrease in the length of the potential core for an increasing value of degree of swirl. In addition, they noticed that for weak and moderate swirl the velocity profiles are effectively similar from an axial distance of four nozzle diameters downstream of the jet exit. For stronger swirling jets similarity is not achieved until a distance of ten jet diameters has been reached.

Using a rotating pipe similar to Rose [25], Pratte and Keffer [29] measured the time-mean properties, turbulence, and distribution of kinetic energy via means of fine pitot probes and single hot-wire anemometry. Again this was possible because of the weak component of swirl velocity.

The most common and effective method of producing swirling flows is via use of vane swirlers. Mathur and MacCallum [30] conducted an evaluation of swirler efficiency for both annular (with hub) and hubless swirlers. Extensive presentation of velocity profiles and recirculation zone geometry was given as a function of the degree of swirl. They found that for increasing values of swirl a central toroidal recirculation (CTRZ) is formed. This is caused when the adverse pressure gradient along the jet axis cannot be further overcome by the kinetic energy of the fluid flowing in the axial direction. They also concluded that tan ϕ was a good measure of swirl for jets issuing from vane swirlers.

Syred et al. [31] concentrated on turbulence measurements in strongly swirling flows via a single hot-wire six-orientation technique inside the central recirculation zone. Local turbulence intensities were found to be extremely high in and near the CTRZ. Measurements of all six turbulent stress components showed strong variations of absolute kinetic energy levels and strong nonisotropy of the stresses and associated turbulent viscosity.

Claypole and Syred [32] studied the effect of combustion on the CTRZ using a dual beam laser. They found that combustion considerably lowers the level of recirculation even at high levels of swirl. A broader coverage of the measuring techniques and results for free swirling flows can be obtained from Reference [33].

2.3 Confined Swirling Flows

Very little in the open literature has been written concerning turbulence measurements in confined swirling jet flows. The measurements that have been reported have been made with highly expensive nonintrusive instrumentation. However, several researchers have reported on time-mean velocity measurements within confined flows with swirl.

Mathur and MacCallum [34] studied the characteristics of a swirling jet issuing into a model of square cross-section. They used an isothermal air model to obtain time-mean velocity profiles with a five-hole pitot probe and a water model to obtain qualitative data. Mathur and MacCallum found that the initial rates of spread of enclosed jets is more rapid than for free swirling. Also, that the central toroidal recirculation zone is much stronger in enclosed jets than free jets.

Rhode et al. [8] measured the time-mean velocity properties again using a five-hole pitot probe inside a swirling confined jet. By using interchangeable expansion blocks with varying degrees of expansion angle α with increasing swirl strength, they found that the influence of α is negligible for the CRZ. But the effect of the swirl strength was to shorten the length of the CRZ and generate the existence of the CTRZ. The length of the CTRZ was then found to increase for increasing swirl strength. They also noted that on the jet centerline downstream of the CTRZ a precessing vortex core (PVC) existed. This PVC then continued to the exit of the test section. However, this study only included weak and moderate swirl strengths. This work was extended by Yoon and Lilley [10] to include higher swirl strengths and to study the effect of different contraction nozzles placed at various axial locations in the test chamber. They found that a strong contraction nozzle of area ratio 4 greatly affected the size and shape of the CTRZ and PVC.

Beltagui and MacCallum [35] completed a wide range of experiments on annular and hubless swirlers with and without combustion. The expansion ratios they used were D/d = 2.5 and 5.0 with varying degrees of swirl. Mean flow and static pressure measurements were made with a water-cooled five-hole spherical pitot probe. Their investigation concluded that the maximum diameter of the CTRZ is primarily a function of the chamber diameter (approximately 0.65 chamber diameters) and only slightly alters for varying degrees of swirl, by combustion or by D/d ratio. They also noticed that the presence of a central hub in the swirler had little effect on the flow patterns.

Using an expansion ratio of D/d = 2 and a five-hole pitot probe, time-mean velocity measurements were made in a swirling isothermal and

reacting confined jet by Syred and Dahman [36]. They studied the effect of introducing bluff bodies into the jet on the size and shape of the central recirculation zone. Also, they found that by increasing the furnace exit diameter, only a small effect was noticed upon the aerodynamics of the system. They also reported that for furnaces requiring low calorific value gas, only medium swirl produced the desired recirculation zone.

Baker et al. [7] and Hutchinson et al. [6] used laser doppler anemometry to measure the values of mean velocity and turbulence intensity in the recirculation region of a swirling reacting flame. Methane was ignited at the burner and the flow then seeded with TiO_2 particles to enhance the light scattering. As flow reversals are found in swirling flames, a frequency-shifting technique was used to solve the directional ambiguity of the doppler signal. Both groups of researchers found high levels of turbulence near the exit of the jet for even a moderate swirl number.

Laser velocimeter measurements of a confined turbulent diffusion flame burner was made by Owen [5]. Mean and rms turbulent velocity levels were measured for axial and tangential components of the reacting flowfield. He measured four different swirl strengths near the exit of the burner and found there was no significant variation on the time-mean profiles for increasing swirl. He also found that the turbulence is high with significant deviation from isotropy over the initial mixing region of the jet. In this area large scale fluctuations decrease for increase in swirl strength. A bragg cell was used for directional sensitivity of the flow.

Habib and Whitelaw [37] measured the time-mean velocities and directional turbulence intensities in a swirling confined coaxial jet. Two measuring techniques were used to measure the turbulence, hot-wire anemometry, and L.D.A. The two methods were in close agreement even in the corner recirculation zone. These researchers only used low values of swirl strength; therefore, no central recirculation zone was formed.

Using a five-hole pitot probe and a single normal hot-wire, Vu and Gouldin [38] measured the time-mean and turbulent properties of a confined isothermal coaxial jet under co-swirling and counter-swirling conditions. They found that levels of high turbulent fluctuations and large dissipation rates characterize the central flow region for both co- and counter-swirl. They suggested that with chemical reaction the internal structure of the recirculation zone is of much less importance to the combustion process than the turbulent transport properties in the vicinity of the CTRZ and the interjet shear layer. However, they reported that no central recirculation zone was formed for the co-swirling case.

Gouldin et al. [39] continued this work with special emphasis on co-swirling flows with combustion. They found that with the presence of chemical reaction a CTRZ was formed. This seems surprising as mass conservation requires axial flow acceleration with combustion and therefore a favorable pressure gradient must exist over a portion of the test section. Since the formation of the CTRZ requires an adverse pressure gradient on the centerline, one would expect combustion to inhibit recirculation zone formation. However, the researchers showed by application of Bernoulli's equation that the pressure on the centerline increases with combustion.

No PVC was found by Brum and Samuelson [40] in dilute swirl combustors with or without combustion. They suggest that the PVC is an artifact of the modeling process and is not present in full scale combustors as dilution jets are present. The researchers found that if only 70 percent of the inlet air was swirled and the remainder used as dilution air, no PVC existed.

The six-orientation single hot-wire technique was used by Janjua et al. [41] in an isothermal nonswirling and swirling confined jet with an expansion ratio of 2. Measurements in the nonswirling jet compared favorably with those of previous researchers [8, 17]. The swirling jet results presented were quite limited but did show that around regions of recirculation large values of turbulence intensity and shear existed, even for moderate swirl. The researchers also performed an uncertainty analysis on the hot-wire technique. This involved changing certain input parameters to the data reduction and determining the percentage change in output parameters. They found that the most inaccurate output term was $\overline{u'w'}$.

Sommer [42] measured time-mean and fluctuating properties of confined coaxial jets and found that a CTRZ did exist for the co-swirling case. He found that the recirculation zone consisted of a one-celled toroidal vortex characterized by low internal swirl velocity, high turbulence intensity, and large turbulent dissipation rates.

The previous experimental work presented here gives a good indication of the levels of the properties that are quantified in this study. However, before any direct comparison can be made between these reported results and the present measured data, the flows must be similar. This must involve not only geometric similarity but also, and more importantly,

the inlet flow conditions must be dynamically similar. This often involves the use of a similar inlet contoured contraction nozzle and the same number and shape of swirl vane blades.

CHAPTER III

MEASUREMENT TECHNIQUES AND ANALYSIS

Turbulence measurements in a complex flowfield have always been a complicated problem encountered by engineers. In the past turbulence phenomena have been discussed by various authors in detail and various methods of turbulence measurements have been suggested [33, 43, 44]. One of the most widely-used instruments to obtain turbulence quantities is the hot-wire anemometer, the most common of which is the single hot-wire. When used at a single orientation and in a two-dimensional flow with a dominant flow direction, a single hot-wire can measure the streamwise components of the time-mean velocity and the root-mean-square velocity fluctuations at a particular location in the flowfield. A two-wire probe can be used to determine the time-mean velocities, streamwise and cross stream turbulence intensities, and the cross correlation between the two components of the velocity fluctuations [43, 45].

Hot-wire measurements in a complex three-dimensional flowfield are considerably more difficult than in one- or two-dimensional flowfields in which the mean flow is predominantly in one direction. To measure the three velocities and their corresponding fluctuating components in a three-dimensional flowfield such as encountered in combustor simulations, a triple hot-wire technique is typically used.

The three-wire probe technique permits the necessary simultaneous measurements from which three instantaneous velocity components can be

determined. The appropriate signal processing can produce estimates of mean velocity components and the Reynolds stress tensor. However, the three-wire probe technique is very complex, requiring a multi-dimensional probe drive to align the probe in the mean flow direction. Also, sophisticated signal processing electronics is required to handle the three instantaneous hot-wire voltages. Finally, because of the fact that three hot-wires are involved, the dimensions of the instrument tend to be large, causing poor spatial resolution.

In recent years the use of single-wire multiple-orientation techniques is rapidly growing in popularity. This is because of their ability to measure all the time-mean velocities and all the components of normal and shear turbulent stresses in complex flowfields. The method is very cost effective, requiring only standard hot-wire electronics. Assumptions regarding the nature of the turbulence are that it is stationary and that it follows a normal probability distribution. It is for these reasons that makes the six-orientation, single hot-wire technique suitable for swirling confined jet flows.

3.1 Single-Wire Six-Orientation Technique

Multi-orientation of a single hot-wire is a novel way to measure the three components of a velocity vector and their fluctuating components. A method devised by Dvorak and Syred [46] uses a single normal hot-wire oriented at three different positions such that the center one is separated by 45 degrees from the other two. The velocity vector at a location is related to the three orthogonal components using pitch and yaw factors as defined by Jorgensen [47]. The data are obtained in the form of mean and root-mean-square voltages at each orientation. However,

the measurements done with a single wire do not supply all the information needed to obtain the turbulence quantities. Therefore, in addition to a single wire, Dvorak and Syred used a cross-wire probe to obtain the covariances between the voltages obtained at adjacent hot-wire orientations.

King [48] modified the technique developed by Dvorak and Syred. His method calls for a normal hot-wire to be oriented through six different positions, each orientation separated by 30 degrees from the adjacent one. Mean and root-mean-square voltages are measured at each orientation. The data reduction is performed using some assumptions regarding the statistical nature of turbulence, making it possible to solve for the three time-mean velocities, the three normal turbulent stresses, and the three turbulent shear stresses.

The six-orientation, hot-wire technique requires a single, straight, hot-wire to be calibrated for three different flow directions in order to determine the directional sensitivity of such a probe. The three directions and three typical calibration curves are shown in Figures 4 and 5. Each of the calibration curves follows a second order, least square fit of the form:

$$E_i^2 = A_i + B_i \tilde{u}_i^{1/2} + C_i \tilde{u}_i \tag{3.1}$$

which is an extension of the commonly used King's law. In this equation, A_i, B_i, and C_i are calibration constants, and $\tilde{u}_i$ can take on a value of $\tilde{u}$, $\tilde{v}$, and $\tilde{w}$ for the three calibration curves, respectively.

When the wire is placed in a three-dimensional flowfield, the effective cooling velocity experienced by the hot-wire is:

$$Z^2 = \tilde{v}^2 + G^2\tilde{u}^2 + K^2\tilde{w}^2 \tag{3.2}$$

where G and K are the pitch and yaw factors defined by Jorgensen [47] to be:

$$G = \frac{\tilde{v}(\tilde{u} \text{ and } \tilde{w} = 0)}{\tilde{u}(\tilde{v} \text{ and } \tilde{w} = 0)} \tag{3.3a}$$

and

$$K = \frac{\tilde{v}(\tilde{u} \text{ and } \tilde{w} = 0)}{\tilde{w}(\tilde{u} \text{ and } \tilde{v} = 0)} \tag{3.3b}$$

which are evaluated from the three calibration curves (Figure 5) for a constant value of E^2. Equation (3.3) shows that the pitch and yaw factors are calculated with the $\tilde{v}$ component i = 2 in Equation (3.1) of the effective cooling velocity as the reference. Therefore, the calibration constants used in Equation (3.1) are the coefficients in the E versus $\tilde{v}$ calibration of Figure 5, i.e., in a general flowfield:

$$E^2 = A_2 + B_2 Z^{1/2} + C_2 Z$$

with Z as given in Equation (3.2) above.

Figure 6 shows the pitch and yaw factors as a function of hot-wire voltage determined from the calibration curve of Figure 5. Both factors vary with hot-wire voltage, but the yaw factor is far more sensitive. The sensitivity analysis discussed in the next section demonstrates that uncertainties associated with the varying pitch and yaw factors do not seriously affect the accuracy of the estimated flow quantities.

To carry out measurements in the confined jet flowfield, the wire is aligned in the flow in such a way that in the first orientation the wire is normal to the flow in the axial direction and the probe coordinates coincide with the coordinates of the experimental facility. Thus,

the six equations for the instantaneous cooling velocities at the six orientations, as given by King [48], are:

$$Z_1^2 = v^2 + G^2u^2 + K^2w^2 \tag{3.4a}$$

$$Z_2^2 = v^2 + G^2\,(u\cos 30° + w\sin 30°)^2 + K^2\,(w\cos 30° - u\sin 30°)^2 \tag{3.4b}$$

$$Z_3^2 = v^2 + G^2\,(u\cos 60° + w\sin 60°)^2 + K^2\,(w\cos 60° - u\sin 60°)^2 \tag{3.4c}$$

$$Z_4^2 = v^2 + G^2w^2 + K^2u^2 \tag{3.4d}$$

$$Z_5^2 = v^2 + G^2\,(w\sin 120° + u\cos 120°)^2 + K^2\,(u\sin 120° - w\cos 120°)^2 \tag{3.4e}$$

$$Z_6^2 = v^2 + G^2\,(w\sin 150° + u\cos 150°)^2 + K^2\,(u\sin 150° - w\cos 150°)^2 \tag{3.4f}$$

Solving simultaneously any three adjacent equations provide expressions for the instantaneous values of the three velocity components, u, w, and v in terms of the equivalent cooling velocities (Z_1, Z_2, and Z_3, for example, when the first three equations are chosen). It is then possible to obtain the three time-mean velocity components and the three normal turbulent stresses of the Reynolds stress tensor, in a manner described in Reference [41].

To determine the cross-correlations of the turbulent fluctuations, a correlation coefficient has to be assumed. King [48] argued that if two wires are separated by an angle of 30 degrees, the fluctuating signals from the wires at the two locations would be such that their contribution to the cooling of the wire would be related by the cosine of

the angle between the wires. This assumption leads to the following two values of the correlation coefficients:

$$\gamma_{Z_P Z_Q} = \cos 30 = 0.867 \tag{3.5a}$$

$$\gamma_{Z_Q Z_R} = \cos 30 = 0.867 \tag{3.5b}$$

To relate $\gamma_{Z_P Z_Q}$ with $\gamma_{Z_Q Z_R}$ and $\gamma_{Z_P Z_R}$, King [48] introduced the following relationship:

$$\gamma_{Z_P Z_R} = \eta \gamma_{Z_P Z_Q} \cdot \gamma_{Z_Q Z_R} \tag{3.6}$$

where η is given a value of 0.8. A sensitivity analysis presented in Chapter VI demonstrates that there is no significant error magnification in the data reduction due to the correlation terms.

To obtain measurements of the correlation coefficients in a swirling flowfield, a triple hot-wire and a time correlator would have to be used. Dvorak and Syred [46] used a double-wire in a two-dimensional flow and found that the above assumptions are quite good.

3.2 Eddy Dissipation Rate Measurements

Studies of the energy processes in shear flows have all suffered from uncertainty in determining the rate of turbulent dissipation. Hinze [49] shows that this process can be expressed in cartesian coordinates by

$$\varepsilon = \nu \sum_{i,j} \overline{\left(\frac{\partial u_i'}{\partial x_j} + \frac{\partial u_j'}{\partial x_i} \right) \frac{\partial u_i'}{\partial x_j}} \tag{3.7}$$

(where u_i' is the component of the fluctuating velocity in the x_i direction). Assuming incompressible, homogeneous, small scale turbulence, Hinze reduces this equation to the form:

$$\varepsilon = \nu \sum_{i,j} \overline{\left(\frac{\partial u_i'}{\partial x_j}\right)^2} \tag{3.8}$$

Lawn [50] suggests that complete isotropy is not required for Equation (3.8), but the condition that the transfer of energy from one velocity component to another be relatively small suggests that the normal stresses due to these components be approximately equal. This condition is defined as "second class local isotropy" by Bradshaw [43]. The assumption does not neglect the existence of shear, and in fact includes an inherent nonisotropy by giving special emphasis on the mean flow direction. This reasoning states that all the turbulent energy is initially produced in the component of the flow direction and is then distributed among other components. This turbulent energy could be distributed by means of the pressure fluctuations [50].

If Bradshaw's definition applies, and assuming that all the turbulent dissipation occurs in the mean flow direction, then Equation (3.8) reduces to:

$$\varepsilon = 15\, \nu \overline{\left(\frac{\partial q'}{\partial s}\right)^2} \tag{3.9}$$

where s is in the direction of the local time-mean velocity.

Invoking Taylor's hypothesis ($\partial/\partial t = \vec{V}\, \partial/\partial s$), that the fluctuations at any point in the flowfield are caused by the whole turbulent flowfield passing that point with a constant velocity $\vec{V}$, it follows that

$$\varepsilon = 15\, \nu \frac{1}{\vec{V}^2} \overline{\left(\frac{\partial q'}{\partial t}\right)^2} \tag{3.10}$$

Heskestad [51] has suggested that the use of Taylor's hypothesis can possibly overestimate the dissipation rate and therefore introduced a modification to the convective velocity:

$$\frac{1}{\vec{v}^2}\overline{\left(\frac{\partial u'}{\partial t}\right)^2} = \overline{\left(\frac{\partial u'}{\partial x}\right)^2}\left(1 + \frac{\overline{u'^2}}{\vec{v}^2} + 2\,\frac{\overline{v'^2} + \overline{w'^2}}{\vec{v}^2}\right) \qquad (3.11)$$

However, Antonia et al. [52] did not apply this modification to measurements in the fully developed region of axisymmetric free jet at axial locations greater than x/D = 40. They found that there was a linear decrease in dissipation rate for increasing axial location.

Laufer [53] used Equation (3.7) to determine the eddy dissipation rate. He measured five of the nine contributions to the sum and assumed that isotropic relations may be used to derive the remainder. His measurements were performed in a fully-developed turbulent pipe flow, a relatively easy flowfield. However, his results contained several inconsistencies mainly because of the errors incurred while measuring five different derivatives. Lawn [50] also measured the energy dissipation in turbulent pipe flow. He concluded from his own and Laufer's results [53] that Equation (3.8), which assumes complete isotropy, will not be grossly in error if the pipe Reynolds number is greater than 9×10^4. Any slight errors that do exist could be attributed to poor high frequency response of hot-wires and to finite wire length. Isotropy is approached as the Reynolds number increases and is a good approximation at Re = 9×10^4. Lawn [50] used Equation (3.8) with a Reynolds number of 4×10^4 with a single hot-wire and then Equation (3.7) with a double wire; he found that the results did not show a great deal of scatter between the

two methods, indicating that a single hot-wire could be used at the lower Reynolds number.

Habib and Whitelaw [54] measured the dissipation rate in a confined coaxial jet without swirl. They used the isotropic relationship of Equation (3.8) and compared their results with those obtained with the TEACH computer code [55]. The researchers found that the calculated results were a factor of two higher than the measured results. However, the measurements were only of a preliminary nature and the authors concluded that neither the precision nor the detail of the measurements were sufficient for satisfactory appraisal.

In confined coaxial swirling flows, Vu and Gouldin [38] used Equation (3.10) to determine the dissipation rate. From this they were able to calculate the length scale of dissipation from the well-known k-ε relationship. In addition, estimates of the Taylor microscale and the Kolmogorov length scales were obtained using isotropic relationships and the eddy dissipation rates. The fact that Vu and Gouldin [38] have no comparisons to make with their results in swirling recirculating flows attests to the fact that accurate measurements in such a flow are quite difficult.

To avoid errors associated with taking many turbulent derivatives, the isotropic relationship of Equation (3.10) is used in this study to determine the eddy dissipation rate. The high Reynolds numbers employed in this project also gives another point in favor for using the isotropic assumptions.

3.3 Contribution to Turbulence Modeling

The practical need of the turbulence measurements in swirling flows

can be seen from studying the Reynolds equations. In solving the Reynolds equations for time-mean velocities, specification is required of the turbulent stresses, usually via the turbulent viscosity μ_t. While the molecular viscosity is a real property of the fluid, existing whether the fluid is in motion or at rest, the turbulent viscosity requires some flow of fluid to become effective and is thus not a property of the fluid but a parameter of the fluid motion. This parameter describes the behavior of the turbulent stresses in terms of the time-mean velocity gradients, implying the assumption that the turbulence transport is of the gradient type. Although simple models are available for the specification of μ_t, especially in boundary layer flows, for example, they are not useful for recirculating flows.

Increasingly complex flowfields are governed by increasingly complicated equations for the time-mean properties, which contain increasingly more components of the turbulent (Reynolds) stress tensor. For example, the increasing number of components required are:

1. Nonswirling boundary layer flow--rx-component only;

2. Swirling boundary layer flow--rx and rθ components;

3. Nonswirling axisymmetric recirculating flow--rx, xx, rr, and θθ components;

4. Swirling axisymmetric recirculating flow--rx, rθ, xθ, xx, rr, and θθ components;

with more complex flows requiring, again, all six components.

In nonswirling axisymmetric recirculating flow, the turbulent (Reynolds) equations of conservation of axial and radial momentum may be solved (along with the conservation of mass [continuity] equation) so as to obtain time-mean values of p, u, and v (time-mean pressure, axial and

radial velocities) throughout the flowfield. The equations for u and v contain only the following components of the turbulent (Reynolds) stress tensor $\underline{\underline{\tau}}$:

$$\tau_{xx} = -\rho\overline{u'^2} = 2\mu_t \frac{\partial u}{\partial x} - \frac{2}{3}\rho k \tag{3.12a}$$

$$\tau_{rr} = -\rho\overline{v'^2} = 2\mu_t \frac{\partial v}{\partial r} - \frac{2}{3}\rho k \tag{3.12b}$$

$$\tau_{\theta\theta} = -\rho\overline{w'^2} = -2\mu_t \frac{\partial w}{\partial \theta} - \frac{2}{3}\rho k \tag{3.12c}$$

$$\tau_{rx} = -\rho\overline{u'v'} = \mu_t\left(\frac{\partial u}{\partial r} + \frac{\partial v}{\partial x}\right) \tag{3.12d}$$

which are usually related by way of an isotropic turbulent viscosity μ to the appropriate components of strain (velocity gradients) in the form also shown. Incompressibility has also been assumed and the terms containing div $\underline{v}$ have been omitted. Notice that the normal components also contain the term $-\frac{2}{3}\rho k$ (which is often omitted in practice) in order that summation of the normal components and application of the continuity equation are consistent with the definition of $k = (\overline{u'^2} + \overline{v'^2} + \overline{w'^2})/2$.

If swirl is also present, coupled with the above is an equation for conservation of swirl momentum from which the time-mean swirl velocity w may be obtained throughout the flowfield. Additional terms also appear in the other momentum equations. From the turbulence simulation point of view, additional components of the turbulent (Reynolds) stress tensor appear in the swirl equation:

$$\tau_{x\theta} = -\rho\overline{u'w'} = \mu \frac{\partial w}{\partial x} \tag{3.13a}$$

$$\tau_{r\theta} = -\rho\overline{v'w'} = \mu r \frac{\partial}{\partial r}\left(\frac{w}{r}\right) \tag{3.13b}$$

These correlations are usually related by way of an isotropic turbulent viscosity μ to the appropriate components of strain (velocity gradients) in the form shown on the extreme right hand of these equations. Thus all six different components appear in the governing equations. Notice that axisymmetry has reduced the complexity, not only of the governing equations themselves but also of the constitutive relations.

If isotropic turbulent viscosity is not assumed, different values of μ may be appropriate to different components of the turbulent (Reynolds) stress tensor $\underline{\underline{\tau}}$. That is, a double suffix is added so as to indicate the component in question. Then by analogy with Prandtl-Schmidt numbers, viscosity numbers may be defined so as to relate other viscosities to the primary component of turbulent viscosity $\mu = \mu_{rx}$. (This particular one is chosen, since it is the only component which remains in the governing equations of a nonswirling boundary layer flow, on which much previous research has taken place. Swirling boundary layers contain $\mu_{r\theta}$ in addition to μ_{rx} and only one viscosity ratio appears.) Thus one is interested in whether or not the following viscosity numbers are unity (isotropic) or not (nonisotropic):

$$\sigma_{xx} = \mu/\mu_{xx} \tag{3.14a}$$

$$\sigma_{rr} = \mu/\mu_{rr} \tag{3.14b}$$

$$\sigma_{\theta\theta} = \mu/\sigma_{\theta\theta} \tag{3.14c}$$

$$\sigma_{r\theta} = \mu/\mu_{r\theta} \tag{3.14d}$$

$$\sigma_{x\theta} = \mu/\mu_{x\theta} \tag{3.13e}$$

There is some evidence that these values are <u>not</u> unity [31, 55], but general recommendations are not available [56]. The remaining problem is how the main component of turbulent viscosity is to be specified by a

turbulence model. Or, rather, the more complete question of how are all the components of turbulent (Reynolds) stress to be specified, either directly (advanced differential or algebraic stress modeling) or indirectly (via the turbulent viscosity concept).

A turbulence model is a set of differential and/or algebraic equations for things like k, ε, $\overline{u_i' u_j'}$, $\overline{u_i' m_\ell'}$, $\overline{m_\ell'^2}$, etc. which connect statistical properties of turbulence (correlations) with each other and with terms appearing in the time-averaged equations of conservation of mass, momentum, energy, and chemical species. Auxiliary relations are like

$$\overline{u_i' u_j'} = -\text{const}\ k^2 \varepsilon^{-1}\ \partial u_i/\partial x_j \tag{3.15a}$$

$$R_\ell = -\text{const}\ (\overline{m_\ell'^2})^{1/2}\ \rho\varepsilon k^{-1} \tag{3.15b}$$

Models are classified according to the turbulent flux hypothesis (whether or not turbulent exchange coefficients are introduced) and the number of extra differential equations to be solved. If introduced, exchange coefficients have generally been assumed isotropic until recently, even in flows with swirl, but recent experimental, inverse and prediction works have disputed this for swirling flows. Briefly the choice available is:

1. Prandtl mixing length $\mu_{rx} = \rho l^2\ (2\Lambda:\Lambda)^{1/2}$;
2. Energy-length $\mu_{rx} = c_\mu\ k^2 \varepsilon^{-1}$;
3. Differential stress modeling $D\tau_{rx}/Dt = P_{rx} + D_{rx} + R_{rx} + \varepsilon_{rx}$;
4. Algebraic stress modeling $\tau_{rx} = f$ (other τ's, k, ε, Λ).

Here Λ is the time-mean flow rate of strain tensor, k and ε are turbulent kinetic energy and dissipation rate, and P, D, R, and ε stand for production, diffusion, redistribution, and dissipation in the turbulent

stress equation. The first two choices are examples of theories of the exchange coefficient type; the second two are of direct stress specification type.

Currently two-equation energy-length models are to be recommended for application in practical engineering situations; in particular the k-ε model where $\varepsilon = k^{1.5}/\ell$ and ℓ is the macrolength scale of turbulence. Models of this type have been successfully modified and applied to swirling flows, even with nonisotropic assumptions [58, 59]. Recent relevant work is discussed elsewhere [60]. Numerical and analytical inverse solution of the turbulent swirl flow boundary layer equations (which allow turbulence model development directly from time-mean experimental data) have been useful for this purpose. Details of the general turbulence model development in both nonreacting and reacting flows are available via recent conferences [61, 62].

The advantage of a turbulent kinetic energy TKE model over a simple algebraic "local" model is that solution of a PDE for k allows upstream "historical" influence to assert itself on the subsequent flowfield. Application of several such models to flowfields of interest in sudden expansion burners have been reviewed elsewhere [63]. For high speed turbulent reacting flows of specific interest to ramjet dump combustors, two models show significant promise: the Harsha one-equation model [64] and the Rodi two-equation k-ε model [57]. Applications to reacting jet flows shows that both appear to be suitable [65]. More advanced turbulence models, such as those based upon the Reynolds-stress modeling approach, are not yet fully developed to warrant their use in recirculating flowfield problems as encountered in gas-turbine combustors. In

addition, such an approach will appreciably increase the computation effort.

Measurements of the complete Reynolds stress tensor and the time-mean velocity gradients can lead to knowledge of the turbulent eddy viscosities via use of Equations (3.12) and (3.13). Determination of the rate of eddy dissipation in conjunction with the turbulent viscosity can be used to introduce a numerical value to the constant term C_μ in Equation (3.15). Typically, C_μ is given the constant value of 0.09 in swirling flows. However, it has been shown that this value is unrealistic and is more likely to be a function of the velocity gradients [66]. The measured data from this study will be used to obtain a relationship for the values of C_μ [67].

CHAPTER IV

DIRECTIONAL SENSITIVITY ANALYSIS

The analysis is performed at any specific flowfield location by initially placing the probe in a free jet such that the coordinate system of the probe coincides with the coordinate system of the jet, as shown in part (a) of Figure 7. Measurements are then taken by rotating the probe in the manner of the technique just described. To simulate the effect of the flow shifting its dominant flow direction, the probe is rotated by θ degree about its z-axis, as shown in part (b) of the figure. This rotation causes a misalignment between the probe coordinate system and the facility coordinates. This discrepancy can be accounted for by use of the Eulerian matrices described in section 4.1. In this configuration, the measured time-mean values, normal and shear stresses are in a coordinate system oblique to the jet coordinate system. However, they can be transformed back to the facility coordinate system [68]. Notice that the correct directional sense of the rotation must be followed so that standard coordinate transformations may be used on the probe data so as to obtain facility coordinate data. Results shown later in Chapter VI have been obtained in this manner.

To examine the directional sensitivity of the wire further, the probe was subsequently rotated about its new $\hat{x}$-axis, thereby forming a compound angle between probe and the dominant flow velocity, as also shown in Figure 7, part (c). Again, the time-mean velocities and

Reynolds stress tensor can be deduced in terms of the jet coordinate system by the method shown in section 4.1, and the results and their accuracy are also discussed in Chapter VI.

Specifically, the directional sensitivity of the technique is assessed at five flowfield situations for self-consistency using the following five configurations:

Case 1	$\theta = 0°$	$\phi = 0°$
Case 2	$\theta = -45°$	$\phi = 0°$
Case 3	$\theta = -45°$	$\phi = -45°$
Case 4	$\theta = -90°$	$\phi = 0°$
Case 5	$\theta = -90°$	$\phi = -90°$

The above five probe/flow configurations are used at each of five representative situations in a free axisymmetric nonswirling jet at x/d = 0 (laminar in potential core region), 3 and 10 (turbulent in shear layer region) and in a free axisymmetric swirling jet at a location in a region of strong shear just downstream of the exit from a variable-angle vane swirler with swirl vane angles of 45 and 70 degrees, representing moderate and strong swirl cases. In these swirling jet cases, the probe was located just downstream of the swirler exit, outside of any regions of recirculation: this part of the flow was chosen as it is in an area of rapid acceleration and is unlikely to contain any instantaneous flow reversals which might cause erroneous readings. Specifically, the following five situations are used:

Situation A	x/d = 0	Nonswirling laminar region
Situation B	x/d = 3	Nonswirling turbulent region
Situation C	x/d = 10	Nonswirling turbulent region

Situation D	x/d = 0	Swirling turbulent region with swirl vane angle 45 degrees
Situation E	x/d = 0	Swirling turbulent region with swirl vane angle 70 degrees

These locations are illustrated in Figures 8 and 9. It will be seen later that the sensitivity analysis assures users that knowledge of local configuration of probe versus flow direction is not required a priori, and useful results are forthcoming and relatively insensitive to specific configurations.

4.1 Coordinate Transformation

4.1.1 Rotational Matrices

To investigate the shifting of the dominant flow direction, the probe holder versus local time-mean flow vector configuration is varied through five different cases of interest. To relate probe coordinate data back to the facility coordinate system, use is made of Eulerian rotational matrices. These make it possible to relate all time-mean velocities and the full Reynolds stress tensor back to the facility coordinate system after any axis rotation.

Any (x,y,z)-cartesian coordinate axes may be rotated about the x, y, or z axis, respectively, by an angle θ, with corresponding coordinate transformation matrices:

$$R_{x\theta} = \begin{bmatrix} 1 & 0 & 0 \\ 0 & \cos\theta & -\sin\theta \\ 0 & \sin\theta & \cos\theta \end{bmatrix}$$

$$R_{y\theta} = \begin{bmatrix} \cos\theta & 0 & \sin\theta \\ 0 & 1 & 0 \\ -\sin\theta & 0 & \cos\theta \end{bmatrix}$$

$$R_{z\theta} = \begin{bmatrix} \cos\theta & -\sin\theta & 0 \\ \sin\theta & \cos\theta & 0 \\ 0 & 0 & 1 \end{bmatrix}$$

For example, a rotation about the z-axis by angle θ results in old (x, y, z) coordinates of a point being related to its new (X, Y, Z) coordinates via:

$$[x\ y\ z]^T = R_{z\theta}\ [X\ Y\ Z]^T$$

Similarly, velocity components (u, v, w) are related to (U, V, W) via

$$[u\ v\ w]^T = R_{z\theta}\ [U\ V\ W]^T$$

In the notation of Figure 1 with velocity components

u, v, w	in	x, r, θ	facility coordinates
$\tilde{u}, \tilde{v}, \tilde{w}$	in	x, y, z	probe Case 1 coordinates
$\hat{u}, \hat{v}, \hat{w}$	in	$\hat{x}, \hat{y}, \hat{z}$	probe Case 2 and 4 coordinates
$\hat{\hat{u}}, \hat{\hat{v}}, \hat{\hat{w}}$	in	$\hat{\hat{x}}, \hat{\hat{y}}, \hat{\hat{z}}$	probe Case 3 and 5 coordinates

the following relationships prevail.

4.1.2 Case 1

The facility and probe Case 1 coordinates are coincident and

$$[u\ v\ w]^T = [\tilde{u}\ \tilde{v}\ \tilde{w}]^T$$

4.1.3 Cases 2 and 4

In this case, a rotation of θ degree is applied about the z-axis, resulting in

$$[u \; v \; w]^T = R_{z\theta} \; [\hat{u} \; \hat{v} \; \hat{w}]^T$$

which leads to

$$\begin{bmatrix} u \\ v \\ w \end{bmatrix} = \begin{bmatrix} \hat{u} \cos \theta - \hat{v} \sin \theta \\ \hat{u} \sin \theta + \hat{v} \cos \theta \\ \hat{w} \end{bmatrix}$$

From this the directional time-mean velocities in facility coordinates can easily be inferred. The angle terms in the relationships are, in fact, the directional cosines [69], which can be used to determine the stress transformations in terms of facility coordinates. The directional cosines between any new coordinate axes, for example, x, y, and z, and the original coordinate axes $\hat{x}$, $\hat{y}$, and $\hat{z}$ can be conveniently tabulated as follows:

	x	y	z
$\hat{x}$	ℓ_1	m_1	n_1
$\hat{y}$	ℓ_2	m_2	n_2
$\hat{z}$	ℓ_3	m_3	n_3

These directional cosines (ℓ_i, m_i, n_i for i = 1, 2, and 3) can be used in the general three-dimensional stress equations governing the transformation of coordinates via [68].

$$\tau_{xx} = \ell_1^2 \tau_{\hat{x}\hat{x}} + m_1^2 \tau_{\hat{y}\hat{y}} + n_1^2 \tau_{\hat{z}\hat{z}} + 2\ell_1 m_1 \tau_{\hat{x}\hat{y}} + 2m_1 n_1 \tau_{\hat{y}\hat{z}} + 2n_1 \ell_1 \tau_{\hat{z}\hat{x}}$$

$$\tau_{yy} = \text{as above with subscript 1 replaced by 2}$$

$$\tau_{zz} = \text{as above with subscript 1 replaced by 3}$$

$$\tau_{xy} = \ell_1\ell_2\tau_{\hat{x}\hat{x}} + m_1m_2\tau_{\hat{y}\hat{y}} + n_1n_2\tau_{\hat{z}\hat{z}} + (\ell_1m_2 + \ell_2m_1)\tau_{\hat{x}\hat{y}}$$
$$+ (m_1n_2 + m_2n_1)\tau_{\hat{y}\hat{z}} + (n_1\ell_2 + n_2\ell_1)\tau_{\hat{z}\hat{x}}$$

$$\tau_{yz} = \text{as above with subscripts (1, 2) replaced by (2, 3)}$$

$$\tau_{zx} = \text{as above with subscripts (1, 2) replaced by (3, 1).}$$

These relationships lead to evaluation of all the stress components in facility coordinates, from corresponding data originally reduced in probe coordinates.

4.1.4 Cases 3 and 5

To go from Cases 2 and 4 to Cases 3 and 5, a rotation of ϕ degrees is applied about the new $\hat{x}$-axis, resulting in

$$[\hat{u}\ \hat{v}\ \hat{w}]^T = R_{\hat{x}\phi}\ [\hat{\hat{u}}\ \hat{\hat{v}}\ \hat{\hat{w}}]^T$$

and

$$[u\ v\ w]^T = R_{z\theta}R_{\hat{x}\phi}\ [\hat{\hat{u}}\ \hat{\hat{v}}\ \hat{\hat{w}}]^T$$

which is

$$\begin{bmatrix} u \\ v \\ w \end{bmatrix} = \begin{bmatrix} \cos\theta - \sin\theta\cos\phi & + \sin\theta\sin\phi \\ \sin\theta + \cos\theta\cos\phi & - \cos\theta\sin\phi \\ 0 \qquad \sin\phi & \qquad \cos\phi \end{bmatrix} \begin{bmatrix} \hat{\hat{u}} \\ \hat{\hat{v}} \\ \hat{\hat{w}} \end{bmatrix}$$

Again, this relationship permits time-mean velocity components to be converted back into facility coordinates. The coefficient matrix defined the directional cosines relating the two coordinate systems; these can be used for normal and shear stress transformations in the manner described in section 4.1.3.

CHAPTER V

EXPERIMENTAL FACILITY

5.1 Calibration Equipment

A small axisymmetric free jet is used for the static calibration of the hot-wire. The calibration jet facility, shown in Figure 10, consists of a seamless contoured nozzle geometrically similar to that of the flowfield facility. A settling chamber and turbulence management section consisting of packed straws is just upstream of the contoured nozzle. The nozzle itself has a throat diameter of 34 mm and is capable of producing Reynolds numbers up to 6×10^5 (based on throat diameter). The air is delivered by a thermally stabilized compressed air generator and produces air at ±0.5°C to that of the wind tunnel. The air is controlled to the nozzle by means of a diaphragm valve and a Fisher and Porter model 10A1735A rotameter. This arrangement allows 30 calibration points to be read over a wide range of known velocities (found by independent pitot probe measurements).

It is necessary to calibrate the hot-wire in a flowfield of known properties. The one-dimensional low turbulence level (essentially laminar) potential core of the free jet was utilized for this calibration. The hot-wire is calibrated for three different flow direction, u, v, and w, as shown in Figure 5. Each of the three calibration curves are obtained with zero velocity in the other two directions. The calibration curves demonstrate that the hot-wire is most efficiently cooled when the

flow is in the direction of the u component, whereas the wire is most inefficiently cooled when the flow is in the direction of the w component. The three orientations of the probe were made possible by use of a rotary table and DISA 55H151 and 55H153 mounting tubes.

The familiar King's law relationship

$$E^2 = A + BZ^n \tag{5.1}$$

which is employed as a calibration curve in most conventional hot-wire anemometry applications has considerable limitations. Perry and Morrison [69] have shown that this relationship is only satisfactory for mean velocities over a limited range. These researchers illustrated by dynamic calibration that this form of relationship is only suitable for flows with low turbulence levels. Typically, linearizers are used which apply the relationship of Equation (5.1) to the hot-wire output signal. The values of A, B, and n are variable to suit individual wires. The limited range of application of such an expression and its restriction to low turbulence levels makes the use of linearizers very undesirable in highly turbulent flows since it could lead to considerable errors.

Dvorak and Syred [46] found that the expression

$$E^2 = A + BZ^{1/2} + CZ \tag{5.2}$$

gave an excellent fit to obtained calibration data with a very small standard deviation being obtained over a large velocity range (1 to 60 m/s). Such a curve fit is a more realistic approach since the conventional relationship of Equation (5.1) is based on the steady flow heat transfer relationship and thus may well not provide an accurate description of the behavior of individual wires. A relationship of the form of Equation (5.2) is used to fit a curve fit to the whole calibration curve

using a least squares curve fitting technique. This curve thus allows the instantaneous velocity to wander over the entire range from zero up to the maximum value seen in the flow without distortion.

A hot-wire does not record a true zero velocity voltage while under calibration because of the thermal convection velocity induced by the bouyancy arising from the wire's own heat. Thus the zero velocity voltage obtained during calibration is spurious and is not included in the points used to obtain the curve fit.

A further point in favor of Equation (5.2) is made by Dvorak and Syred [46]. They showed that a curve fit of this form from static calibration data fitted very well the dynamic calibration data of Perry and Morrison [69] and thus stated that dynamic calibration is probably unnecessary. This is to be expected, as the diameter of the hot-wire is very small (usually 5 μm); therefore, the flow in the vicinity of the wire may be considered laminar. Thus the hot-wire sees a time-varying laminar flow in the turbulent flow whereas in the calibration rig it sees a time-steady laminar flow. This also explains the good approximation achieved by the expression in Equation (5.1) despite its having been based on laminar heat transfer analysis.

5.2 Confined Jet Facility

The swirling confined jet test facility is shown schematically in Figure 3. Air flows through an axial flow fan whose speed can be adjusted by means of a U.S. varidrive motor. The range of speed of the fan is then 1100 to 3100 rpm. The air then enters a flow straightener and turbulence management section, consisting of mesh screens and packed straws. Next is the contoured nozzle leading to the test section. This

axisymmetric nozzle was designed by the method of Morel to produce a minimum adverse pressure gradient in the boundary layer to avoid the flow unsteadiness phenomenon associated with local separation regions. The throat of this contoured nozzle is 15 cm onto which an annular vane swirler may be fitted. The swirler consists of ten blades which may be individually set to any angle of interest. A solid hub of 4 cm diameter is located at the center of the swirler with a streamlined nose facing upstream. The downstream end is simply a flat face, simulating the geometric shape of a typical fuel spray nozzle. More detailed information concerning the swirler can be found elsewhere [13].

The test section itself consists of a 90 degree expansion block of diameter 30 cm and width 3.2 cm, giving an expansion ratio of 2. A 125 cm plexiglass tube is then placed over the expansion block to provide the main body of the test section. In addition, another plexiglass tube of similar legnth but 15 cm diameter is used to provide an expansion ratio of unity. The substantial size of the test model provides excellent probe resolution for the hot-wire measurements.

The test section has the option of being equipped with a strong contraction nozzle of area ratio 4. This nozzle has a 45 degree slope facing upstream and can be located at any axial location. Alignment of the contraction nozzle and test section with the wind tunnel is obtained with the use of a laser beam.

A manual traversing mechanism can be attached to the test section as shown in Figure 11. This mechanism is equipped with a linear vernier scale which is accurately readable to within ±0.25 mm. This allows a probe to be accurately traversed across the chamber radius with the capability of manually rotating a probe about its axis to an accuracy of

±0.2 degree. A more detailed description of the confined swirling jet facility at Oklahoma State University can be found in Reference [15].

5.3 Hot-Wire Instrumentation

As mentioned previously, the six-orientation single-wire technique employs standard electronic equipment for the determination of the time-mean and turbulent stresses in the flowfield. The sensor used in this study is a normal hot-wire probe, DISA type 55P01. This probe has two prongs set 3 mm apart which support a 5 um diameter tungsten wire. This wire is gold plated near the prongs to reduce end effects and strengthen the wire. A DISA 5 m cable connects the probe support to the main bridge unit. The anemometer used is a DISA type 55M01, constant temperature standard bridge. The mean voltage across the hot-wire is measured using a Hickok Digital Systems, model DP100, integrating voltmeter with the root-mean-square component of the voltage being measured using a Hewlett Packard, model 400 HR, AC voltmeter.

To measure the eddy dissipation rate and hence the dissipation length scale, a special electronic analog device was constructed to time-differentiate the fluctuating electronic signal. This device was assembled using a 741 operational amplifier and various capacitors and resistors. A schematic of the differentiator is shown in Figure 12a. For the device to effectively differentiate at the required frequencies, the break frequency of the instrument must be approximately ten times that of the differentiating frequency. The plot of gain versus frequency in Figure 12b shows that the cutoff frequency is not reached until after 20 kHz. The calculated break point of the system is at a gain of 100; in addition, a gain of unity was obtained from the differentiator at a

frequency of 1.5 kHz. This is well within the range of frequencies to be differentiated. The output voltage from the anemometer was first passed through a DISA 55D25 filter before analog differentiation. The cutoff frequency setting for the wire is critical, since too high settings would include undesirable amounts of electronic noise and too low settings would suppress high frequency components of the signal. The settings were determined at typical locations in the flowfield by using a Hewlett Packard 3580A spectrum analyzer to identify regions of high noise. A unity gain follower was placed before the differentiator to prevent any high impedance loading of the differentiator.

The mean square of the differentiated signal was measured using Thermal Systems Inc. true rms voltmeter, model 1076. This instrument has a 1MΩ input resistance to attenuate the low frequency signals.

CHAPTER VI

RESULTS AND DISCUSSION

Nonswirling and swirling nonreacting flows are investigated in an axisymmetric test section with expansion ratio D/d = 2, which may be equipped with a strong contraction nozzle of area ratio 4 located at L/D = 2. This nozzle has a 45 degree upstream facing slope as described earlier [10]. Measurements have also been made in a nonexpanding test section with expansion ratio D/d = 1. The nozzle inlet velocities and Reynolds numbers employed in this investigation are high enough to ensure that the flowfields studied are under conditions independent of Reynolds number variation. They correspond approximately to conditions reported in associated studies [10]. In each case, radial profiles of interesting properties at six axial locations are presented. All properties shown are normalized with respect to the swirler inlet uniform axial velocity U_o deduced independently from a measurement upstream of the swirler. Finally, an accuracy and directional sensitivity analysis involving the time-mean and turbulent properties of a round free jet has been performed. Percentage changes of some of the important input parameters and their effect on the calculated output quantities have been studied. Five probe-jet axis orientations have also been used to simulate the shifting of the dominant flow direction and consequently the effectiveness of the hot-wire technique to measure the properties of a strongly swirling flow whose local flow direction is unknown.

Deduced results from the measured hot-wire signals are presented in Tables I through XXIII.

6.1 Effect of Swirl

6.1.1 Nonswirling Flows (D/d = 2)

Figure 13 shows time-mean and turbulence data for the nonswirling flow. A nearly-flat axial velocity profile is seen in the entrance region of the test section. As expected, there is no measurable swirl velocity and only a small radial velocity. Although a corner recirculation zone (CRZ) is present, there is no evidence of a central toroidal recirculation zone (CTRZ). Indeed, there is no swirl-induced centrifugal force to encourage its formation. The hot-wire anemometer cannot sense flow direction; however, directional properties of the flow can be inferred from earlier five-hole pitot probe data [10], and flow visualization photography [9]. Nevertheless, the author has retained the positive values on all figures wherever possible uncertainties might exist. The time-mean data show good agreement, within 5 percent, with that found by Chaturvedi [17] in a similar test section, and with that found by Yoon and Lilley [10] using a five-hole pitot probe in the same test facility with identical flow conditions.

The maximum values of normal stresses appear on the shear layer with the axial fluctuation component dominating. Earlier results [17] indicated that the axial turbulence intensity was larger than the other two components and that the radial turbulence intensity was approximately equal to the tangential turbulence intensity. This is confirmed in the present study.

The six-orientation technique produces positive values of shear stress. However, in certain locations in the vicinity of recirculation zones, the radial gradient of the axial velocity is predominately positive which is associated with negative values of $\overline{u'v'}$. Nevertheless, all shear stress values in this document are plotted as positive. Because of the absence of velocity gradients in the x- and θ-directions, only one shear stress (the xr-component) is significant in the nonswirling case. This shear stress, plotted in Figure 13, tends to be lower than the earlier study [17]. It should be noted, however, that the shear stresses are the most difficult turbulent quantities to measure accurately in a complex flowfield. Uncertainties in measurements of time-mean velocities and turbulence intensities are increased in the determination of shear stresses.

6.1.2 Moderate Swirl (D/d = 2)

In confined swirling jet flows the axial and tangential time-mean velocities dominate, as can be seen from Figures 14 and 15. The corner recirculation zone can be seen clearly at the expansion plane of the test section. The CRZ is not seen at any other axial location, indicating that the swirling flow greatly reduces the length of the CRZ. Swirling flow produces a central toroidal recirculation zone which can also be seen in the figures. The CTRZ appears to have a length of approximately 1.5 D. Downstream of this point on the jet axis, indication is given of a precessing vortex core (PVC) extending to the exit plane of the test section. The PVC is defined as a region of low axial velocity and high almost solid body rotation swirl along the axis, and is found to be present in the swirling flows considered. Yoon and Lilley [10]

also measured the time-mean swirling flowfield using a five-hole pitot probe, and the present data are found to be in good agreement. The PVC is most clearly observed in flow visualization studies using still photography [8, 10] and videotape recordings [9].

The three normal turbulent stresses appear to be fairly isotropic at all locations in the test chamber with maximum values occurring in regions of recirculation and regions of high shear. It was found that large-scale turbulence with big eddies occurs in recirculation regions and that small-scale turbulence with small eddies occurs in regions of peak velocities. In the downstream regions of the test chamber, the turbulence levels are low, with a more uniform radial profile, indicating a more developed nature of the flow.

It can also be seen that all three shear stress components are significant in swirling flows, as expected. The maximum values of shear stress occur in the thin shear layer regions but quickly dissipate in the downstream direction as the shear layer broadens. The stresses $\overline{u'v'}/u_o^2$ and $\overline{u'w'}/u_o^2$ are found to have large values close to the wall, because of the steep axial and swirl velocity gradients.

6.1.3 Strong Swirl (D/d = 2)

Time-mean velocity profiles for the strongest swirl cases considered are shown in Figures 16 and 17. Almost all of the flow leaves the swirler near the outer edge, producing steep velocity gradients in this vicinity. High velocity gradients can also be seen near the wall, especially at x/D = 0.5. The strong centrifugal forces present in the incoming flow produce rapid outflow to the confining boundary. Both central and corner recirculation zones can be seen clearly from the time-

mean plots. However, it appears that the CTRZ is shorter for this strong degree of swirl as compared to the moderate swirl case. In contrast, the PVC gets wider as the swirl strength increases, as also found in five-hole pitot probe data [10].

The normal turbulent stresses have increased in magnitude, consistent with the increase in swirl strength, and still a good degree of isotropy is observed throughout the entire flowfield. The highest turbulence levels again occur in regions of recirculation and on the shear layers. It can also be seen that high turbulence levels are found in the PVC.

The most dramatic effect of the increase of swirl is the large increase crease in all three shear stress values. It can be seen that very high values of shear stress occur in the shear layers and near the walls. The PVC also contains high values of shear stresses and turbulence levels. Overall, the values of shear stresses are higher than in other swirl strengths considered.

6.2 Effect of Strong Contraction Nozzle

6.2.1 Nonswirling Flows

Time-mean and turbulence characteristics for the nonswirling flow with a strong contraction nozzle at L/D = 2 are presented in Figure 18. The plots show that results vary only slightly from that of the corresponding flowfield without a contraction nozzle (see Figure 13). The major difference appears to be a slight reduction in the length of the CRZ. The measured time-mean flowfield compares favorably with previous data [10].

6.2.2 Moderate Swirl

The effects of the contraction nozzle on the moderately swirling flow with ϕ = 45 degrees are shown in Figure 19. The presence of the contraction nozzle accelerates the flow and produces a strong favorable pressure gradient over the entire flowfield of interest. This pressure gradient conflicts with the adverse pressure gradient inherent in swirling flows (associated with recirculation zones). Regions of positive axial velocity occur near the centerline at all axial locations. The central recirculation zone is now located in annular region around the jet axis and is much smaller than in the corresponding open flowfield of Figure 15. A narrow central core region is observed to extend throughout the length of the test section with strong solid body rotation. Positive axial velocities now occur in this region, as opposed to negative ones in the corresponding open-ended flow case; this and other time-mean data are in excellent agreement with earlier experimental [10] and prediction [4, 16] studies.

The directional turbulence intensities do not show any significant increase in magnitude compared to the open-ended swirling flow. However, the turbulent shear stresses are found to increase near the jet axis as the contraction nozzle exit is approached. This is because of the fairly high turbulence levels in this region and the effect of strong velocity gradients with which these stresses are associated.

6.2.3 Strong Swirl

For swirl vane angle ϕ = 70 degrees, measurements are given in Figure 20 with the strong contraction blockage located at L/D = 2. The axial velocity near the axis is positive, though less so than in the 45

degree case of Figure 19, since the favorable pressure gradient has now to overcome an even stronger unfavorable pressure gradient. The central recirculation region is now very small, extending in an annular region to less than x/D = 1.0, considerably less than the no-blockage case of Figure 17. At the axial station x/D = 1.0, forward flow occurs across the whole test section. Very strong swirl velocity magnitudes and gradients are seen, which contrast sharply with the corresponding open-ended flow situation. A wide core region is again noticed along the jet axis containing strong solid body rotation; movie photography reveals the precessing nature of this phenomenon. Again, time-mean data compare very well with previous work [10].

The normal components of the Reynolds stress tensor show an increase in turbulence along the jet axis as the contraction is approached--more so than in the 45 degree swirl case of Figure 19, but similar to those found in the open-ended case of Figure 17. Now, larger values are found near the axis, associated with the strong vortex core region. Shear stress levels at the entrance to the test section tend to be slightly lower for the blockage case. But the levels are an order of magnitude higher in the core region near the contraction nozzle. Again, this is because of the strong time-mean velocity gradients in this area.

6.3 Effect of Expansion Ratio

6.3.1 Nonswirling Flow (D/d = 1)

Figure 21 shows the very flat axial time-mean velocity profiles associated with a one-dimensional flow. The flowfield is seen to be homogeneous throughout the whole test section. This is because of pressure losses due to abrupt expansions being absent in the nonexpanding

confined jet. Radial velocities are found to be present across the whole test section. This was not to be expected as there is no expansion of the flow in this case. These velocities are assumed to be an error of the six-orientation technique which is discussed later in this chapter. No recirculation zones are evident at any section of the flowfield, as expected.

The successful design of the wind tunnel and contraction nozzle is evident by the low levels of turbulence intensity measured. The absence of time-mean velocity gradients and flow discontinuities also explains the fact that all components of the Reynolds stress tensor are negligible.

6.3.2 Moderate Swirl (D/d = 1)

Strong axial and tangential time-mean velocities dominate in the nonexpanding confined jet. These velocities were found to be approximately twice as large as those in the corresponding expanding flowfield (D/d = 2). A momentum balance across the test section indicates that these increases in magnitude are to be expected [70]. These results can be seen in Figure 22. This is because the wall of the test section produces a favorable pressure gradient across the entire flowfield which conflicts with the adverse pressure gradient within the swirling flow. However, a core region around the jet centerline is found to contain strong solid body rotation and positive axial velocities. Evidence can be seen from the time-mean velocity plots of the central hub of the swirler. Negative radial velocities were expected and measured in this particular flowfield.

Directional turbulence intensities are found to be similar in magnitude for this case as in the expanding flowfield (D/d = 2) except in the entrance region. This is because of the lack of regions of recirculation normally associated with high turbulence levels. The turbulence in this flowfield is primarily caused by passage of the air through the swirler and because of the velocity gradients. Because of these velocity gradients, shear stresses are significant throughout the entire flowfield. The magnitude of these stresses were found to be comparable to those in the expanding case.

6.3.3 Strong Swirl (D/d = 1)

It can be seen from Figure 23 that the tangential time-mean velocity completely dominates the flowfield. This strong swirl velocity produces a large core region with low axial velocity on the jet centerline. This is because of the centrifugal forces within the flow. Again, no recirculation zones are present within the flowfield. Radial velocities have increased due to the increase in swirl velocity.

The large gradients associated with the core region produce high levels of turbulence intensity along the jet centerline and correspondingly a large increase in all of the shear stresses in this region. Shear stresses in the entrance region of this flowfield are much lower than in the expanding case. Again, this is because of the lack of recirculation zones.

6.4 Turbulence Parameters

The eddy dissipation rate measurements have been performed in flows with two different expansion ratios with three degrees of swirl. The

levels of confinement considered are with expansion ratios of D/d = 2 and 1 with swirl strengths of nonswirling, moderate, and strong swirl. The measurements are obtained using the time differentiating technique described in Chapter III. Estimates of the different length scales of the flows can be obtained from the measurements of the dissipation rates. The eddy dissipation length scale (macroscale) is estimated via:

$$\ell = \frac{k^{3/2}}{\varepsilon}$$

the Taylor microscale is deduced from the isotropic relation:

$$\lambda = \left(15\ \nu\ \frac{k}{\varepsilon}\right)^{1/2}$$

and finally the Kolmogorov length scale is given by:

$$\eta = \left(\frac{\nu^3}{\varepsilon}\right)^{1/4}$$

The eddy dissipation, ε, has dimensions of L^2/T^3, the same as velocity cubed divided by a length scale. At any axial station, the station mean axial velocity ($= U_o\ (d/D)^2$) and chamber diameter D are used for this purpose. Accordingly, plots of

$$\frac{\varepsilon}{u_o^3\ d^2/D^3}$$

are given. The dissipation length scale is nondimensionalized with respect to the test chamber diameter D.

6.4.1 Expanding Flowfield (D/d = 2)

Measurements of the turbulent dissipation rate in a confined, expanding, nonswirling jet are shown in Table XII and Figure 24. The

plots show that most of the dissipation occurs on the thin shear layer in the entrance region. As the shear layer spreads across the entire test section, the corresponding dissipation rate follows. The dissipation rate is also seen to be high in the CRZ. As expected, the dissipation rates in the essentially laminar portion of the potential core are very low. These low dissipation rates in the laminar core region tend to cause high values of length scale, as seen in Table XIII. The length scales are largest on the jet centerline, outside the potential core, and then decrease as the test section is radially traversed. This is because the dissipation rates are low on the centerline, then increase radially; but the kinetic energy of the turbulence is somewhat constant across the test chamber.

When a moderate degree of swirl is introduced to the flow, the dissipation rate is found to increase significantly in the entrance region of the test section (Figure 24 and Table XIV). However, these values are rapidly reduced in the downstream region of the chamber. This implies that most of the production and dissipation of the turbulent energy is being performed in the entrance region of the test section where areas of recirculation and high shear dominate the flow. On the shear layer eddies are formed which contribute to the large rates of dissipation. Within the recirculation zones large scale eddies cascade energy to its smaller scales which eventually leads to its dissipation.

The measurements of dissipation rate in the entrance region of the test section must only be considered as qualitative as several sources of error may be present at these axial locations. In the recirculation zones the time-mean velocity direction is not well defined; therefore, perfect alignment of the sensor in the mean flow direction is not assured.

Two other distinct types of error were certainly present. The first was discussed by Kovasznay [71] and is the one arising of loss of response of the anemometer equipment to high frequency turbulence components. The anemometer system has a cutoff frequency of approximately 30 kHz which is below the frequencies at which turbulent dissipation occurs. The measured dissipation rate must therefore be extrapolated to its full rate by assuming a theoretical turbulence spectrum. Pao [72] suggested such a spectrum but it has yet to be conclusive in free or confined shear flows. Estimates of the Kolmogorov length scale indicate that it is much smaller than the hot-wire length. This leads to the second source of error of having to average over the hot-wire length. Wyngaard [73] has shown that the underestimation of the dissipation rate is in the order of 6 percent for the present flow conditions. As this is considered within the scatter of the data, no hot-wire length corrections to the measured data have been made.

The distribution of length scale for $\phi = 45$ degrees can be seen in Table XV. The table shows that low values of length scale can be expected for moderately swirling flows, especially in regions of high acceleration. Further downstream the length scales are close to unity, indicating that the flow is probably of a more uniform nature. The low dissipation rates at the exit of the test section also lend to this conclusion.

The effect of increasing the swirler angle to 70 degrees can be seen in Figure 24 and Table XVI. A note of interjection: the wind tunnel test facility cannot provide equal Reynolds number flows for all of the swirl strengths considered because of the blockage caused by the swirler vanes. Therefore, the nondimensionalizing inlet velocity, U_o, varies for each of the swirl strengths. As this value is raised to the

third power, this number becomes very significant and hence the change in scales of Figures 24 and 25. Nevertheless, the dissipation rates in the entrance region of the test section with 70 degrees of swirl are still higher than the corresponding cases with 45 degrees and zero swirl. Peak regions of dissipation still occur in the same regions as in the 45 degrees of swirl flowfield, but the reduction of dissipation rates across the test section is more rapid.

The dissipation length scales, shown in Table XVII, are smaller than the other flow cases considered, mainly because of the existence of larger recirculation zones and greater shear.

6.4.2 Nonexpanding Flowfield (D/d = 1)

Eddy dissipation measurements in nonexpanding confined jets are presented in Tables XVIII through XXIII and Figure 25. The same scales are kept on the axis of the plots to correspond to the expanding flowfield. As can be seen from Figure 25, the eddy dissipation rate is greatly decreased for the nonexpanding flow. This can be explained by the fact that there are no areas of recirculation present for any of the swirl strengths considered. However, on the centerline of the test section the dissipation rates are independent of expansion ratio for the swirling flows. This is because velocity gradients are present due to the tangential velocity.

The dissipation length scales in the nonexpanding flowfield tend to be generally lower than in the expanding case but more uniform across the entire test section. Table XXIII shows that these length scales are smaller than the test chamber diameter, indicating that turbulent dissipation is occurring.

6.4.3 Important Turbulence Properties

Other properties in turbulence modeling are the kinetic energy of turbulence, k, and the turbulent dissipation length model, ℓ. These are defined by

$$k = (u'^2 + v'^2 + w'^2)/2$$

$$\ell = k^{3/2}/\varepsilon$$

and can be obtained from data presented earlier, but are conveniently deduced and plotted now.

Plots of the kinetic energy of turbulence for two varieties of expanding flowfields for a range of swirl strengths are shown in Figures 26 and 27. These figures show that most of the kinetic energy of the turbulence in the nonswirling expanding flowfield is occurring in the downstream regions of the test section away from the laminar-type flows encountered in the entrance region. In the swirling flowfield high levels of kinetic energy are observed in two distinct regions. One is the entrance region where there are two thin shear layers. The other is in areas of recirculation including the PVC.

In the nonexpanding flowfield the levels of kinetic energy are very low in the nonswirling flow. This is because of the absence of any time-mean velocity gradients except very close to the confining wall boundary. In the swirling flowfields energy levels are again fairly large in the entrance regions and in the core region around the jet centerline. It can be seen from both Figures 26 and 27 that outside areas of recirculation and shear the radial profiles of the kinetic energy are fairly uniform, indicating a developed nature of the flow.

Figures 28 and 29, and Tables XII, XV, XVII, XIX, XXI, and XXII show plots of the calculated dissipation length scale, in the expanded and nonexpanded geometries, respectively. The accuracy of these plots is dependent upon the accuracy of the measuring techniques used for determining the dissipation rate and the directional turbulence intensities. In deducing the kinetic energy of turbulence the root-mean-square of the three turbulence intensities is measured. Therefore, any error in these measured quantities is compounded in the determination of the kinetic energy. In calculating the dissipation length scale the kinetic energy is raised to the power 3/2, this again magnifying any error in the measurements. Any errors likely to be found in the eddy dissipation rate measurements have been discussed previously in section 6.4.1. It is expected that the entrance region of the test section would be an area of the flow to give the least accurate measurements of the dissipation rate. It can be concluded that areas of high shear and recirculation (and hence high turbulence levels) will produce the worst estimates of dissipation length scales.

The plots presented here show that the largest dissipation length scales can be expected in the nonswirling expanding flowfield, especially in the downstream regions where the kinetic energy is high and the dissipation rate is fairly low. In the entrance region of the swirling flowfield the dissipation rates are very high with most of the turbulent dissipation quickly spreading over the entire test section. This leads to small dissipation length scales in entrance regions of the flowfield.

In the nonswirling, nonexpanding flowfield the dissipation length scales are very low across the entire test section. This is because of the very low turbulence levels throughout the flowfield. For the

swirling flows the length scales are small in the entrance region but increase in size inside the core region as the exit to the test section is approached. This is because of the large values of kinetic energy found in the core regions.

Overall, it is felt that these plots of the dissipation length scale are indicative of the levels of turbulence transport found in swirling confined flows with the downstream regions of the test section giving the more accurate quantitative data due to the inherent problems of hot-wire anemometry in the entrance region of the test chamber.

6.5 Uncertainty Analysis

The uncertainty analysis includes a determination of the sensitivity of the six-orientation hot-wire data reduction to various input parameters which have major contributions in the response equations. Pitch and yaw factors (G and K) are used in the response equations described in Chapter III in order to account for the directional sensitivity of the single hot-wire probe. Figure 6 shows the pitch and yaw factors plotted against the hot-wire mean effective voltage. Both the pitch and yaw factors are functions of the hot-wire mean effective voltage, but the yaw factor is far more sensitive. A one percent increase in the hot-wire voltage reduces the pitch factor by 1.3 percent and the yaw factor by 56 percent. For the present study the values of these factors are chosen at an average hot-wire voltage experienced in the flowfield. This was appropriate since the output quantities (u, u'_{rms}, $\overline{u'v'}$, etc.) are only weakly dependent on the value of K. This can be seen in the data of Table XXIV which summarizes an analysis performed on the data reduction program at a representative position in the flowfield.

Table XXIV demonstrates the percent change in the output quantities for a 1 percent change in most of the important input quantities. For the data presented in this table, only quantities calculated from the probe orientation combination 5, 6, and 1 are used, for simplicity. The situation is that of a moderately swirling confined flowfield from a swirl generator with vane angle of 38 degrees. In this swirling flow orientation, 6 was the minimum of the six mean effective cooling velocities. King [48] has argued that the probe orientation combination approximately centered around the minimum effective cooling velocity produces more accurate estimates of calculated turbulence quantities than do the other orientation combinations. However, all previously reported data have been obtained by averaging all the six possible combinations.

It is not unusual in hot-wire anemometry to have the mean velocity components and turbulence quantities that are measured be quite sensitive to changes in mean hot-wire voltage. For interpretive purposes, the mean hot-wire voltage variations can be thought of as being either errors in measuring the mean voltage, or shifts in the individual wire calibrations due to contamination or strain "aging" of the wire. The data of Table XXIV demonstrate that the most serious inaccuracies in the measurement and data reduction technique will be in the estimates of turbulent shear stresses, the most inaccurate output term being $\overline{u'w'}$.

As already discussed in Chapter III, an ad hoc assumption is made regarding the numerical values of the correlation coefficients used in the deduction of time-mean and turbulence quantities. The results of the uncertainty analysis (Table XXIV) show the time-mean and turbulence quantities to be relatively insensitive to variations in the correlation coefficients. Therefore, the major ad hoc assumption made in the

technique does not seem to have a great effect on the output quantities compared to the effect of other input quantities.

The accuracy of the hot-wire technique is dependent upon two types of input parameters. One set is the measured input data and the other is the assumed data of the reduction procedure. The accuracy of the resulting deduced values are from the d.c. voltages ($\bar{E}_1$, $\bar{E}_5$, $\bar{E}_6$), the rms of the fluctuating voltages ($E'_{1_{rms}}$, $E'_{5_{rms}}$, $E'_{6_{rms}}$), the pitch and yaw factors (G and K), and the correlation coefficients ($\gamma_{z_i z_j}$). Each of these quantities is not equally likely to have a 1 percent error. For example, an error of 1 percent in the mean voltage is very large and is more realistically in the order of 0.25 percent. However, it is useful to appreciate the likely error in each of the input parameters, an assessment of which is now given.

The quality of the measured input data of mean voltages and rms fluctuating voltages depends upon the instrumentation used and the complexity of the flowfield at the measuring location. In laminar stable flows, these values are likely to be very accurate (less than 0.25%), whereas in turbulent shear regions the mean voltages are measurable to 0.5 percent and the rms voltages to 1.0 percent. Pitch and yaw factors are obtained from calibration curves through a sequence of measurements made in a very stable flowfield in the potential core of the calibration jet. They are not likely to be in error by more than 0.2 percent.

The assumed input parameters of the data reduction, the correlation coefficients, could be in error by as much as 5 percent. This is because in most turbulent flows the correlation coefficients are usually not less than 0.8 and no greater than 0.9. As mentioned in Chapter III,

the correlation coefficient vlaues of 0.867 are obtained from measurements in a round free jet, a flow similar to the type being studied.

Overall, the worst possible scenario would be the cumulative effect of reinforcement of errors in these parameters as follows. In laminar regions the maximum errors are: 9 percent for time-mean velocities, 15 percent for normal stress, 22 percent for shear stresses, and 55 percent for the $x\theta$-component of the shear-stress tensor. In turbulent shear regions the maximum errors are: 18 percent for time-mean values, 24 percent for normal stresses, and 29 percent for shear stresses, except 98 percent for the $x\theta$-component.

It may also be noted that absolute accuracy of the technique depends also on the physical size of the probe interfering with the flow, the position of the wire at each of its rise orientations, and the effect of the dominant flow direction on the measured cooling velocities. These are assessed in the following section with section 6.9 concluding the discussion. On this basis, it is felt that maximum errors of 5, 10, and 15 percent are realistic deviations from the true time-mean, directional turbulence intensity, and turbulent shear-stress values over most flowfield locations.

6.6 Directional Sensitivity Analysis in Laminar Jet

The directional sensitivity of the technique is assessed at the five locations A through E (see Figures 8 and 9) corresponding to five different flow situations. The first of these is in the laminar potentional core region, at $x/d = 0$ and $r/d = 0$. Table XXV gives the results with the probe coordinates aligned with facility coordinates, as Case 1 of

Figure 7 illustrates. This is referred to as Situation A Case 1 with analogous statements later. The time-mean velocities, nondimensionalized with the jet exit velocity deduced from an independent measurement, are shown. In this one-dimensional flowfield the axial velocity is expected to be unity with the other two components of the velocity vector to be equal to zero. Results using each of the six possible combinations of three adjacent wire-orientations are presented, together with the mean of the values. The standard deviation and its ratio with the mean are also presented to show the amount of scatter in the readings. As can be seen, the error for the axial and swirl velocities are very low for each combination. The radial velocity error tends to be larger, possibly because of slight probe misalignment with the normal to the jet axis. The mean of these quantities brings the data to well within acceptable limits.

Results of the probe being rotated by 45 degrees about the z-axis (as in Case 2 with $\theta = -45°$) are shown in Table XXVI. This is Situation A Case 2. The probe coordinate system is now different from the jet coordinate system but the measured velocities can be related to the facility coordinates by use of the rotational matrices given in Chapter IV. The values given in Table XXVI and indeed all the tables are presented in terms of the facility coordinate system. The results show that this misalignment of the probe with the dominant flow direction still gives excellent values of velocities in the laboratory coordinate system with the use of any of the six possible wire combinations. Consequently, averaging of the data also gives good results.

Rotation about the z-axis by -90 degrees to obtain Case 4 results in no data being generated by the technique. This is because in a

steady one-dimensional flowfield, all the instantaneous cooling velocities acting on the hot-wire are equal for all six rotations. As the data analysis requires that their cooling velocities be subtracted from each other (see Reference [41]), all the output terms are deduced as zero.

To further investigate the shifting of the dominant flow direction, the probe was rotated twice (-45° about its z-axis, followed by -45° about its new $\hat{x}$-axis) so as to conform to Case 3. The results of these axis rotations can be seen in Table XXVII. Again the laboratory coordinate deduced values and deviations from expected values are relatively low, although not quite as good as in the previous case. The advantages of averaging can be seen in Table XXVII, where the under- and/or overestimation of the velocities for the individual positions are smoothed out after averaging.

Rotations of θ = -90 degrees and ϕ = -90 degrees were also carried out at the same flow location, thus obtaining Case 5. Table XXVIII shows the results of these rotations. Good axial and tangential velocity values can be seen but with a decrease in the accuracy of the radial velocity.

6.7 Directional Sensitivity Analysis in Turbulent Nonswirling Jet

Similar rotations of the probe about its axes have been performed on the shear layer of a free nonswirling axisymmetric jet at two axial locations, x/d = 3 and 10, referred to as Situations B and C. At these points in the flow the axial velocity dominates with a small contribution from the radial velocity. In axisymmetric jets it is well known

that the axial directional turbulence intensity is larger than its other two components [74]. The only significant shear stress in this flowfield is the rx-shear. Tables XXIX and XXX, obtained with Case 1 probe configuration in Situations B and C, confirm this. Incidentally, all the data presented in this study are a consequence of a typical set of readings obtained from the hot-wire technique. If a large amount of scatter is found in deduced results at a particular location, the problem is further investigated and/or remeasured before being accepted as valid. Data reported elsewhere [41] have been thoroughly analyzed and checked for repeatability.

Tables XXIX and XXX are used as a standard for nonswirling flowfield values at locations B and C, so as to be able to compare the results obtained from other probe configuration cases. However, the radial time-mean velocity appears to be very large for this particular flowfield and could possibly be in error. The coefficient of variation $(\sigma/\bar{x})$ is seen to be acceptable for most of the flow properties except for the shear stresses. These large variations are caused by the shear stresses being two orders of magnitudes lower than the time-mean velocities. Sometimes the data reduction will not resolve a particular parameter. This is usually the consequence of subtracting two almost equal effective cooling velocities as described earlier. If a large proportion of the data is not resolved from the different combinations of cooling velocities used, the parameter deduced is taken to be zero.

Results for probe configurations of Cases 2 and 4 for location B are given in Tables XXXI and XXXII; corresponding data for location C are given in Tables XXXIII and XXXIV. It can be seen, from Tables XXXII and XXXIV, that the Case 4 results give poor estimates of the time-mean

radial and swirl velocities and underestimates of the axial components of the velocity vector. This is expected because the time-mean velocity vector is almost parallel to the hot-wire support axis, and rotating the probe through its six orientations yields little effect on the sensed data. This also decreases values of the axial turbulence intensity but significantly increases the other two normal stress components. Acceptable values of the axial normal stress are obtained via $\theta = -45$ degrees (Case 2 probe configuration) but again the tangential and radial turbulence intensities are increased; however, not as significantly as in the previous Case 4. Shear stress values for both Cases 2 and 4 are found to be very poor with large coefficients of variation. Also, many of the turbulence quantities are not resolved.

It would appear from these results that the six-orientation hot-wire technique is a poor tool to use if the flow is dominately in the direction of the probe support, for reasons just described. If this occurs, simply reconfiguring the probe holder versus flow direction can overcome the problem.

Tables XXXV through XXXVIII correspond to the last four tables, but now probe configurations of Cases 3 and 5 are used at locations B (Tables XXXV and XXXVI) and C (Tables XXXVII and XXXVIII). Now the time-mean velocity components are seen to be in excellent agreement with the values determined from the standard configuration of Case 1. The axial normal stress tends to be underestimated at $x/d = 3$ and overestimated at $x/d = 10$, relative to the Case 1 calculations. The radial turbulence intensity is consistently overestimated for both compound configurations and both axial locations. This could infer a failing of the hot-wire technique. The tangential turbulence intensity measurements are found

to provide acceptable results. The dominant shear stress (the rx-component) in this flow is found to measure very well in the configurations of Cases 3 and 5, relative to Case 1 values. The coefficient of variation is not too large considering the magnitude of the numbers involved. The final components of the Reynolds stress tensor, although appearing to be measurable, exhibit a great deal of scatter, perhaps indicating that these values are close to zero.

6.8 Directional Sensitivity Analysis in Turbulent Swirling Jet

Two free swirling jets were considered for further assessment of the hot-wire technique. The air flow exiting from an axisymmetric nozzle of a wind tunnel passes through a vane swirler with 10 adjustable flat blades. The test facility and time-mean performance of the swirler are described at length elsewhere [13]. For the present study the subsequent large chamber confinement was removed and the free jet flow alone was studied, with swirl vane angles of 45 and 70 degrees being used. Figure 9 gives the specific measurement locations D and E used for measuring the 45 and 70 degree swirl situations, respectively. These locations are in the high shear region of the flow close to the swirler exit. They were chosen since it was expected that all six components of the stress tensor would be significant, thereby providing a good test of the technique for their measurement. The hot-wire was also placed well away from the edge of the recirculation zone, so as to avoid any instantaneous flow reversal on the wire. Rotations of the probe axes have been performed conforming to Cases 4 and 5 only, for both of the swirl strengths.

The standard six-orientation technique in the configuration of Case 1 produces the properties of both swirling jets as given in Tables XXXIX and XL. As can be seen, all components of the time-mean flow and the Reynolds stress tensor are evaluated. The two sets of results are not quite at the same flowfield location because of the change in size and shape of the recirculation zone as swirl strength increases. However, the increase in the turbulent properties of the flow are clearly evident.

Rotation about the z-axis by -90 degrees to Case 4 probe configuration causes a deterioration in the accuracy of the results obtained from the technique, as inspection of Tables XLI and XLII for 45 and 70 degrees, respectively, shows. The axial and swirl time-mean velocities are still fairly accurate for both flows but the radial velocity has suffered a large increase (or decrease) relative to its measurement with Case 1. The normal stresses deduced after the rotation appear to be reasonable except for the radial and swirl components in the strong swirl flow of Situation E. These two components are greatly overestimated with a great deal of scatter in the results. It is again felt that these poor results are because of the technique's inability to measure accurately flow properties when the dominant flow direction is in the direction of the probe holder. That is, when a large velocity is approximately normal to the wire in each of the six measuring orientations, insensitivity results as discussed earlier. Correspondingly, the shear stresses also show a reduction in accuracy, with all three components either over- or underpredicting the Case 1 values.

The results of the compound angle of Case 5 are presented in Tables XLIII and XLIV, respectively, for the 45 and 70 degree swirl cases. The axial time-mean velocity is seen to be good when compared to the standard

case, but the other two components show a reduction in accuracy in these highly turbulent flowfields. The inaccuracy of the radial velocity has been discussed earlier. The three components of the turbulence intensity appear to be fairly good with reasonable values deduced compared to the standard Case 1 values. Again, however, the radial and tangential components are less than desirable for the strongly swirling flowfield. The shear stresses for the 45 degree swirl situation D are considered good except for the $\overline{u'w'}$ term. This component is subject to great inaccuracies for only slight errors in these input data, as described earlier in section 6.5. For the strongly swirling flow (Situation E) the measured stresses are not so good when compared with the standard Case 1 measurements. As these tables indicate, the time-mean velocities and normal stresses are subject to error which is magnified in the determination of the shear stresses.

6.9 Assessment of the Technique

General results of the present and previous studies are now assessed in connection with the applicability, accuracy, and directional sensitivity of the six-orientation single normal hot-wire technique.

Previously, in his measurements of strongly swirling vortex flows, King [48] compared his time-mean velocity and normal stress measurements with corresponding measurements obtained using a Laser Doppler Velocimeter. He found excellent agreement indicating the validity of the method. He was not able to compare shear stress measurements in his swirl flow; however, he was unable to use his LDV for this purpose. In fact, despite the existence of advanced multicolor LDV systems and their use for shear stress measurement, no one has yet reported them in highly

swirling flow situations, certainly not one over a range of swirl strengths as reported in this thesis.

The present measurements have been compared with previously available data whenever possible. In the nonswirling confined jet case, results for time-mean velocities u and v, normal stresses u'_{rms} and v'_{rms}, and shear stresses $\overline{u'v'}$ compare very favorably (see Reference [41], Figures 7 and 8) with those of Chaturvedi [17]. He used a cross-wire probe for the shear stress measurements. So also did McKillop [12] for nonswirling confined flow in the same facility as the present research. Results, with and without exit nozzles, are in good agreement for the above quantities (see also Reference [12], Figures 21 through 28). The largest errors of approximately 15 percent occurred with the shear stresses in regions of high gradients.

In the swirling confined jet case, comparison with Janjua and McLaughlin [75] for a moderate swirl strength in an identical facility has been possible. They made triple-wire hot-wire measurements in a flow with an inlet swirl vane angle ϕ = 38 degrees, using analog-to-digital signal conversion and computer data reduction. For this purpose it was necessary to know in advance the local time-mean velocity vector direction; the data of Yoon and Lilley [10] were used for this purpose. Their measurements [75] of time-mean velocity compare very well, within 5 percent, with those of Reference [10] and hence of Reference [41]. Their measurements [75] of the three normal Reynolds stresses and the three shear Reynolds stresses are compared to x/D = 0.5, 1,0, and 1.5 with the six-orientation single-wire measurements of Reference [41]. There is excellent agreement, with a maximum discrepancy of 8 percent (see Reference [75], Figures 10 through 18), indicating again the validity of the

present measurement technique. It appears to be an extremely viable, cost-effective technique for turbulent flows of unknown dominant direction, requiring only accessibility to the measurement location. Probe interference appears not to be a major problem.

For the present study, Figures 26 through 30 summarize measured values for the five situations A through E, respectively. Each figure presents facility coordinate time-mean velocity, normal and shear stress values obtained with each of the five probe holder versus facility configuration possibilities of Cases 1 through 5. A remarkable observation is that, in general, the configuration is of little importance; results appear quite constant across the five cases.

On the other hand, present production run results have used the Case 1 configuration exclusively. In those results, generally, ensemble average of deduced results from each of the six possible combinations of three adjacent wire orientations has been used. This was because of lack of local flow directional knowledge--if this knowledge is available, it is expected [48] that the combination with minimum cooling velocity in the central of the three wire orientations used will produce more accurate estimates of deduced flow quantities. From results of the present study for Situations A through E, Table XLV confirms this, especially for time-mean values. In any case, the appropriate choice of wire orientation for minimum cooling velocity is not known a priori. The values given in this table could only be determined after the measurement. However, for turbulence quantities and in the 45 and 70 degree situations, more confidence may be placed in the average of all possible wire combinations. This smoothing has been used exclusively in the present study.

CHAPTER VII

CLOSURE

7.1 Conclusions

The present research is concerned with the time-mean and turbulence properties of a low speed, nonreacting, swirling flowfield. The measurements have been performed in a model of an axisymmetric gas turbine combustor with varying degrees of swirl and geometry. The six-orientation, single hot-wire technique has been used to produce measurements of the time-mean velocities and complete Reynolds stress tensor in all of the flowfields of interest. The turbulent eddy dissipation rate and hence the dissipation length scale have been deduced for selected flowfields via time differentiation of the fluctuating hot-wire signal.

The existence, size, and shape of both the corner recirculation zone and the central toroidal recirculation zone are affected by the degree of swirl. Measurements show that increasing the swirl strength from zero to medium swirl produces shortened corner regions and the generation of a central bubble extending to approximately 1.5 chamber diameters downstream of the jet exit. In addition, a precessing vortex core is observed on the jet centerline which stretches to the exit of the test section. Increasing the swirl strength enlarges the central zone and vortex core with negligible effect on the corner region.

The introduction of swirl to the confined, expanding jet flowfield greatly increases the turbulence properties of the flow. High levels of

normal and shear stresses are found on the two shear layers in the entrance region of the test section. Dissipation rates are also found to be large in the high shear regions of the flow. These rates reduce and spread over most of the flowfield as the exit to the test section is approached.

Placement of a strong contraction nozzle at L/D = 2 with an area reduction of 4 causes a significant effect on the time-mean swirling flowfield. Central recirculation zones are shortened and axial velocities along the entire jet axis become positive. The core regions become narrow with strong swirl velocities and gradients. Turbulence levels and shear stresses are found to increase along the jet centerline near the exit of the contraction nozzle but decrease slightly at the jet exit.

No recirculation zones are found to be present in the nonexpanding flowfield with uniform velocity profiles across the entire test section. The swirling flowfields exhibit strong tangential velocities compared with the corresponding expanding flow. A core region is still evident with almost solid body rotation along the axis. Turbulence levels are found to be low for this flow except near the jet centerline where strong velocity gradients are present.

The accuracy and directional sensitivity of the six-orientation hot-wire technique has been performed in axisymmetric and swirling free jets. Variation of input parameters and their effect on the output data has shown that the least accurate output quantities are the shear stresses, in particular the θ-component.

The directional sensitivity analysis has shown that the technique adequately measures the properties of a flowfield independent of the dominant flow direction except when the flow is predominately in the

direction of the probe holder, with the six-orientations of the probe creating insignificant changes in hot-wire response. The analysis shows that this component of time-mean velocity is inadequately deduced. Only reconfiguration of the probe can overcome this problem a posteriori.

7.2 Recommendations for Further Work

Fundamental research work should be continued in swirling flows in several areas. First, the introduction of a round nonswirling jet into the existing flowfield should be studied to enable a greater understanding of the performance of a gas turbine combustor. This would involve measurements of the time-mean and turbulence properties of the resulting flowfield. Second, the turbulent dissipation rate would have to be determined in such a flowfield before successful modeling of combustors could be achieved. This may involve improving the existing technique to account for the high frequency turbulence components and the averaging over the hot-wire length.

REFERENCES

[1] Lefebvre, A. H. Gas Turbine Combustion. New York: McGraw-Hill, 1983.

[2] Gerstein, M. (Ed.). "Fundamentals of Gas Turbine Combustion." NASA-CP-2087, 1979. Workshop held at NASA Lewis Research Center, Cleveland, Ohio, Feb. 6-7, 1979.

[3] Lilley, D. G. "Flowfield Modeling in Practical Combustors: A Review." Journal of Energy, Vol. 3, No. 4 (1979), pp. 193-210.

[4] Abujelala, M. T., and D. G. Lilley. "Confined Swirling Flow Predictions." Paper AIAA-83-0316. Reno, Nev., Jan. 10-13, 1983.

[5] Owen, F. K. "Laser Velocimeter Measurements of a Confined Turbulent Diffusion Flame Burner." Paper AIAA-76-33. Washington, D.C., Jan. 26-28, 1976.

[6] Hutchinson, P., E. E. Khalil, and J. H. Whitelaw. "Measurement and Calculation of Furnace-Flow Properties." Paper AIAA-77-50. Los Angeles, Calif., Jan. 24-26, 1977.

[7] Baker, R. J., P. Hutchinson, and J. H. Whitelaw. "Velocity Measurements in the Recirculation Region of an Industrial Flame by Laser Anemometry With Light Frequency Shifting." Combustion and Flame, Vol. 23 (1974), pp. 57-72.

[8] Rhode, D. L., D. G. Lilley, and D. K. McLaughlin. "Mean Flowfields in Axisymmetric Combustor Geometries With Swirl." Paper AIAA 82-0177, 1982. AIAA Journal (in press).

[9] Lilley, D. G. "Turbulent Combustor Flowfield Investigation." Combustion Fundamentals Research Conference, held at NASA Lewis Research Center, Cleveland, Ohio, Oct. 21-22, 1982, pp. 152-168.

[10] Yoon, H. K., and D. G. Lilley. "Five-Hole Pitot Probe Time-Mean Velocity Measurements in Confined Swirling Flows." Paper AIAA-83-0315, Reno, Nev., Jan. 10-13, 1983.

[11] Janjua, S. I. "Turbulence Measurements in a Complex Flowfield Using a Six-Orientation Hot-Wire Probe Technique." (M.S. thesis, Oklahoma State University, Dec., 1981.)

[12] McKillop, B. E. "Turbulence Measurements in a Complex Flowfield Using a Crossed Hot-Wire." (M.S. thesis, Oklahoma State University, May, 1983.)

[13] Sander, G. F., and D. G. Lilley. "The Performance of an Annular Vane Swirler." Paper AIAA-83-1326. Seattle, Wash., June 27-29, 1983.

[14] Lilley, D. G., and D. L. Rhode. A Computer Code for Swirling Turbulent Axisymmetric Recirculation Flows in Practical Isothermal Combustor Geometries." NASA CR-3442, Feb., 1982.

[15] Rhode, D. L. "Predictions and Measurements of Isothermal Flowfields in Axisymmetric Combustor Geometries." (Ph.D. thesis, Oklahoma State University, Dec., 1981.)

[16] Rhode, D. L., D. G. Lilley, and D. K. McLaughlin. "On the Prediction of Swirling Flowfields Found in Axisymmetric Combustor Geometries." ASME Journal of Fluids Engineering, Vol. 104 (1982), pp. 378-384.

[17] Chaturvedi, M. C. "Characteristics of Axisymmetric Expansions." Proceedings, Journal of the Hydraulics Division, ASCE, Vol. 89, No. HY3 (1963), pp. 61-92.

[18] Krall, K. M., and E. M. Sparrow. "Turbulent Heat Transfer in the Separated, Reattached and Redevelopment Regions of a Circular Tube." Journal of Heat Transfer (Feb., 1966), pp. 131-136.

[19] Phaneuf, J. T., and D. W. Netzer. Flow Characteristics in Solid Fuel Ramjets. Report NPS-57Nt74081. Prepared for the Naval Weapons Center by the Naval Postgraduate School, July, 1974.

[20] Back, L. H., and E. J. Roschke. "Shear Layer Flow Regimes and Wave Instabilities and Reattachment Lengths Downstream of an Abrupt Circular Channel Expansion." Journal of Applied Mechanics (Sept., 1972), pp. 677-681.

[21] Roschke, E. J., and L. H. Back. "The Influence of Upstream Conditions on Flow Reattachment Lengths Downstream of an Abrupt Circular Channel Expansion." Journal of Biomechanics, Vol. 9 (1976), pp. 481-483.

[22] Ha Minh, H., and P. Chassaing. "Perturbations of Turbulent Pipe Flow." Proceedings, Symposium on Turbulent Shear Flows. Pennsylvania State University, April, 1977, pp. 13.9-13.17.

[23] Moon, L. F., and E. Rudinger. "Velocity Distribution in an Abruptly Expanding Circular Duct." Journal of Fluids Engineering (March, 1977), pp. 226-230.

[24] Johnson, B. V., and J. C. Bennett. "Velocity and Concentration Characteristics and Their Cross Correlations for Coaxial Jets

in a Confined Sudden Expansion; Part 1: Experiments." Proceedings, ASME Symposium of Fluid Mechanics of Combustion Systems. Boulder, Colo., June, 1981, pp. 145-160.

[25] Rose, W. G. "A Swirling Round Turbulent Jet." Journal of Applied Mechanics (Dec., 1962), pp. 615-625.

[26] Chigier, N. A., and J. M. Beer. "Velocity and Static-Pressure Distributions in Swirling Air Jets Issuing From Annular and Divergent Nozzles." ASME Journal of Basic Engineering, Vol. 82 (Dec., 1964), pp. 788-796.

[27] Kerr, N. M., and D. Fraser. "Swirl-Effect on Axisymmetric Turbulent Jets." Journal of the Institute of Fuel, Vol. 38 (Dec., 1965), pp. 519-526.

[28] Chigier, N. A., and A. Chervinsky. Experimental and Theoretical Study of Turbulent Swirling Jets Issuing From a Round Orifice. T.A.E. Report 46, Nov., 1965.

[29] Pratte, B. D., and L. R. Keffer. "The Swirling Turbulent Jet." Journal of Basic Engineering, Vol. 94 (Dec., 1972), pp. 739-748.

[30] Mathur, M. L., and N. R. L. MacCollum. "Swirling Air Jets Issuing From Vane Swirlers. Part 1: Free Jets." Journal of the Institution of Fuel, Vol. 40 (May, 1976), pp. 214-224.

[31] Syred, N., J. M. Beer, and N. A. Chigier. "Turbulence Measurements in Swirling Recirculating Flows." Proceedings, Salford Symposium on Internal Flows. London, England: Institution of Mechanical Engineering, 1971, pp. B27-B36.

[32] Claypole, T. C., and N. Syred. "The Effect of Combustion on the Aerodynamics of Swirling Jets." Proceedings, Symposium on the Fluid Mechanics of Combustion Systems. Joint ASME/ASCE Fluid Engineering and Applied Mechanics Conference, Boulder, Colo., June 22-24, 1981, pp. 137-143.

[33] Beer, J. M., and N. A. Chigier. Combustion Aerodynamics, Applied Science. New York: Wiley, 1972. (Reprinted by Krieger, Melbourne, Fla., 1983.)

[34] Mathur, M. L., and N. R. L. MacCollum. "Swirling Air Jets Issuing From Vane Swirlers; Part 2: Enclosed Jets." Journal of the Institution of Fuel, Vol. 40 (June, 1967), pp. 238-245.

[35] Beltagui, S. A., and N. R. L. MacCollum. "Aerodynamics of Vane-Swirled Flames in Furnaces." Journal of the Institution of Fuel, Vol. 49 (Dec., 1979), pp. 193-200.

[36] Syred, N., and K. R. Dahman. "Effects of High Levels of Confinement Upon the Aerodynamics of Swirl Burners." Journal of Energy, Vol. 2 (Jan., 1978), pp. 8-15.

[37] Habib, M. A., and J. H. Whitelaw. "Velocity Characteristics of Confined Coaxial Jets With and Without Swirl." Paper ASME 79-WA/FE-21. New York, N.Y., Dec. 2-7, 1979.

[38] Vu, B. T., and F. C. Gouldin. "Flow Measurements in a Model Swirl Combustor." AIAA Journal, Vol. 20, No. 5 (May, 1982), pp. 642-651.

[39] Gouldin, F. C., J. S. Depsky, and S. L. Lee. "Velocity Field Characteristics of a Swirling Flow Combustor." Paper AIAA-83-0314. Reno, Nev., Jan. 10-13, 1983.

[40] Brum, R. D., and G. S. Samuelsen. "Assessment of a Dilute Swirl Combustor as a Bench Scale, Complex Flow Test Used for Modeling, Diagnostics, and Fuel Effects Studies." Paper AIAA-82-1263. Cleveland, Ohio, June 21-23, 1982.

[41] Janjua, S. I., D. K. McLaughlin, T. W. Jackson, and D. G. Lilley. "Turbulence Measurements in a Confined Jet Using a Six-Orientation Hot-Wire Probe Technique." AIAA Journal, 1983 (in press).

[42] Sommer, H. T. "Swirling Flow in a Research Combustor." Paper AIAA-83-0313. Reno, Nev., Jan. 10-13, 1983.

[43] Bradshaw, P. An Introduction to Turbulence and Its Measurement. New York: Pergamon Press, 1971.

[44] Perry, A. E. Hot-Wire Anemometry. New York: Oxford Press, 1982.

[45] Wygnanski, I., and H. Fiedler. "Some Measurements in the Self-Preserving Jet." Journal of Fluid Mechanics, Vol. 38 (1969), p. 577.

[46] Dvorak, K., and N. Syred. "The Statistical Analysis of Hot Wire Anemometer Signals in Complex Flowfields." DISA Conference, University of Leicester, England, 1972.

[47] Jorgensen, F. E. "Directional Sensitivity of Wire and Fiber Film Probes." DISA Information No. 11. Franklin Lakes, N.J., May, 1971, pp. 31-37.

[48] King, C. F. "Some Studies of Vortex Devices--Vortex Amplifier Performance Behaviour." (Ph.D. thesis, University College of Wales, Cardiff, Wales, 1978.)

[49] Hinze, J. O. Turbulence. 2nd edition. New York: McGraw-Hill, 1975.

[50] Lawn, D. J. "The Determination of the Rate of Dissipation in Turbulent Pipe Flow." Journal of Fluid Mechanics, Vol. 48 (1971), pp. 477-505.

[51] Heskestad, G. "A Generalized Taylor Hypothesis With Application for High Reynolds Number Turbulent Shear Flows." Journal of Applied Mechanics, Vol. 32 (1965), pp. 735-739.

[52] Antonia, R. A., B. R. Salyaprakash, and A. K. M. F. Hussein. "Measurements of Dissipation Rate and Some Other Characteristics of Turbulent Plane and Circular Jets." Physics of Fluids, Vol. 23, No. 4 (1980), pp. 695-700.

[53] Laufer, J. The Structure of Turbulence in Fully Developed Pipe Flow. NACA Technical Report 1209, 1956.

[54] Habib, M. A., and J. H. Whitelaw. "Velocity Characteristics of a Confined Coaxial Jet." Journal of Fluids Engineering, Vol. 101 (1979), pp. 521-529.

[55] Gosman, A. D., and F. J. K. Ideriah. TEACH-T: A General Computer Program for Two-Dimensional, Turbulent, Recirculating Flows. London, England: Imperial College, Dept. of Mechanical Engineering, 1976.

[56] Lilley, D. G. "Nonisotropic Turbulence in Swirling Flow." Acta Astronautica, Vol. 3 (1977), pp. 919-933.

[57] Launder, B. E., A. Morse, W. Rodi, and D. B. Spalding. "The Prediction of Free Shear Flows--A Comparison of the Performance of Six Turbulence Models." Proceedings, NASA Conference on Free Shear Flows. Hampton, Va.: NASA Langley Research Center, 1972.

[58] Lilley, D. G. "Prospects for Computer Modeling in Ramjet Combustors." Paper AIAA-80-1139. Hartford, Conn., June 30-July 2, 1980.

[59] Lilley, D. G. "Swirl Flows in Combustion: A Review." AIAA Journal, Vol. 15 (Aug., 1977), pp. 1063-1078.

[60] Tennankore, K. N., and F. R. Steward. "Comparison of Several Turbulence Models for Predicting Flow Patterns Within Confined Jets." Proceedings, ASME/Pennsylvania State University Symposium on Turbulent Shear Flows. University Park, Penn, April 18-20, 1977.

[61] Murthy, S. N. B. (Ed.). Turbulent Mixing in Nonreactive and Reactive Flow (A Project SQUID Workshop). New York: Plenum Press, 1975.

[62] Combustion Institute/Central States Section, Fluid Mechanics of Combustion Processes. Meeting held at NASA Lewis Research Center, Cleveland, Ohio, March 28-30, 1977.

[63] Harsha, P. T. "Kinetic Energy Methods." Handbook of Turbulence. W. Frost and T. Moulden, Eds. New York: Plenum Press, 1977.

[64] Harsha, P. T. A General Analysis of Free Turbulent Mixing. TR-73-177. Arnold Engineering Development Center, 1974.

[65] Harsha, P. T., and R. B. Edelman. "Application of Modular Modeling to Ramjet Performance Prediction." AIAA Paper 78-944. Las Vegas, Nev., July 25-27, 1978.

[66] Rodi, W. "The Prediction of Free Turbulent Boundary Layers by Use of a Two-Equation Model of Turbulence." (Ph.D. thesis, Imperial College, University of London, Dec., 1972.)

[67] Abujelala, M. A. "Turbulent Swirling Recirculating Flow Predictions." (Ph.D. thesis, Oklahoma State University, in preparation.)

[68] Yuan, S. W. Foundations of Fluid Mechanics. Englewood Cliffs, N.J.: Prentice-Hall, 1967.

[69] Perry, A. E., and G. L. Morrison. "Static and Dynamic Calibrations of Constant Temperature Hot Wire Systems." Journal of Fluid Mechanics, Vol. 47 (1971), pp. 765-777.

[70] Gupta, A. K., D. G. Lilley, and N. Syred. Swirl Flows. Tunbridge Wells, England: Abacus Press, 1983 (in press).

[71] Kovasznay, L. G. "Development of Turbulence-Measuring Equipment." NACA TN 2839, 1959.

[72] Pao, Y-H. "Structure of Turbulent Velocity and Scalar Fields at Large Wavenumbers." Physics of Fluids, Vol. 8 (1965), pp. 1063-1075.

[73] Wyngaard, J. C. "Measurement of Small-Scale Turbulence Structure With Hot Wires." Journal of Scientific Instruments, Vol. 1 (1968), pp. 1105-1108.

[74] Corrsin, S., and M. S. Uberoi. Spectrums and Diffusion in a Round Turbulent Jet. NACA Report No. 1040, 1949.

[75] Janjua, S. I., and D. K. McLaughlin. Turbulence Measurements in a Swirling Confined Jet Flowfield Using a Triple Hot-Wire Probe. Report DT-8178-02 from Dynamics Technology to NASA Lewis Research Center, Cleveland, Ohio, Nov., 1982.

TABLE I

TIME-MEAN AND TURBULENCE DATA FOR NONSWIRLING FLOW $\phi = 0°$, $D/d = 2$

R/D	X/D 0.0	0.5	1.0	1.5	2.0	2.5
0.40000	-0.04120	-0.05665	-0.08630	-0.11760	0.18523	0.13361
0.37500	-0.00807	-0.06053	-0.13375	-0.18646	0.20850	0.17099
0.35000	-0.02879	-0.06898	0.17894	0.18061	0.21762	0.22129
0.32500	-0.03216	-0.09422	0.19646	0.26519	0.25098	0.23756
0.30000	-0.02682	0.14110	0.33527	0.31599	0.28590	0.26850
0.27500	-0.02451	0.32602	0.42445	0.41726	0.31662	0.30702
0.25000	-0.01829	0.53788	0.51717	0.49678	0.35362	0.35040
0.22500	0.95514	0.70587	0.67720	0.53040	0.37038	0.40075
0.20000	0.95599	0.87940	0.79454	0.60121	0.42989	0.42899
0.17500	0.96512	0.90634	0.90023	0.68197	0.43902	0.46936
0.15000	0.96192	0.92113	0.94158	0.76173	0.46490	0.52001
0.12500	0.96147	0.91264	0.96732	0.83215	0.48785	0.55015
0.10000	0.95858	0.91700	0.96891	0.85549	0.51549	0.56495
0.07500	0.96192	0.92100	0.96640	0.87509	0.57158	0.59977
0.05000	0.96192	0.93355	0.97271	0.89259	0.58651	0.62587
0.02500	0.96335	0.94240	0.96928	0.89265	0.61281	0.66329
0.00000	0.97234	0.94179	0.95616	0.91932	0.61995	0.67988

(a) u/u_o

TABLE I (Continued)

R/D	X/D 0.0	0.5	1.0	1.5	2.0	2.5
0.40000	-0.07864	-0.05966	-0.11148	-0.12362	0.14392	0.14364
0.37500	-0.05863	-0.04275	-0.12106	-0.11812	0.14646	0.14685
0.35000	-0.07595	-0.06827	0.15144	0.15057	0.16151	0.13247
0.32500	-0.06917	-0.08026	0.17166	0.16863	0.17150	0.18654
0.30000	-0.08301	0.10777	0.15497	0.19999	0.18363	0.18779
0.27500	-0.06340	0.20263	0.24739	0.18071	0.16843	0.19778
0.25000	-0.05633	0.21505	0.25799	0.19960	0.18566	0.17347
0.22500	0.19589	0.31158	0.30888	0.21143	0.20412	0.14897
0.20000	0.18993	0.22749	0.21401	0.24971	0.15327	0.19888
0.17500	0.19685	0.21339	0.20226	0.16997	0.20958	0.15780
0.15000	0.21653	0.21237	0.19555	0.23395	0.17030	0.18115
0.12500	0.17614	0.14243	0.21905	0.19582	0.26100	0.20461
0.10000	0.17779	0.20777	0.20995	0.16003	0.26965	0.24674
0.07500	0.21651	0.21283	0.20366	0.20992	0.24025	0.25314
0.05000	0.21643	0.21818	0.22371	0.19892	0.24137	0.19346
0.02500	0.20459	0.19310	0.17020	0.20357	0.20504	0.22033
0.00000	0.20845	0.19783	0.20190	0.17162	0.19932	0.28668

(b) v/u_o

TABLE I (Continued)

R/D	X/D 0.0	0.5	1.0	1.5	2.0	2.5
0.40000	0.02307	0.04654	0.10300	0.10351	0.11961	0.10868
0.37500	0.03105	0.06077	0.10640	0.11172	0.13357	0.12518
0.35000	0.02495	0.06598	0.11819	0.13584	0.13463	0.13632
0.32500	0.02848	0.08685	0.14979	0.15739	0.16383	0.15317
0.30000	0.03499	0.12564	0.17327	0.17679	0.17883	0.16688
0.27500	0.03287	0.16069	0.18787	0.19802	0.18729	0.18030
0.25000	0.03997	0.18028	0.19491	0.19438	0.19987	0.19790
0.22500	0.01222	0.14801	0.18412	0.19756	0.21876	0.20189
0.20000	0.01241	0.05712	0.15078	0.19168	0.23061	0.20843
0.17500	0.01051	0.02970	0.11240	0.17782	0.22168	0.21202
0.15000	0.01126	0.02217	0.05974	0.15815	0.22853	0.22502
0.12500	0.01177	0.05843	0.05080	0.13227	0.24353	0.22692
0.10000	0.01162	0.01915	0.03736	0.10524	0.25402	0.23245
0.07500	0.01083	0.01604	0.03534	0.08149	0.25626	0.23286
0.05000	0.01123	0.01480	0.02860	0.08955	0.25274	0.22900
0.02500	0.01177	0.01498	0.02742	0.08768	0.25322	0.24319
0.00000	0.01148	0.01812	0.02590	0.07200	0.25415	0.23883

(c) u'_{rms}/u_o

TABLE I (Continued)

R/D	X/D 0.0	0.5	1.0	1.5	2.0	2.5
0.40000	0.03044	0.03089	0.04749	0.06306	0.07566	0.07340
0.37500	0.02836	0.02738	0.06228	0.05784	0.08237	0.05996
0.35000	0.02828	0.03689	0.06927	0.06364	0.07737	0.07490
0.32500	0.03193	0.04749	0.06413	0.08348	0.08933	0.08047
0.30000	0.03074	0.06127	0.08016	0.07653	0.08670	0.09422
0.27500	0.02119	0.09000	0.09123	0.08612	0.07138	0.08811
0.25000	0.02695	0.05708	0.06441	0.06842	0.10133	0.09215
0.22500	0.01143	0.05303	0.09093	0.08827	0.08453	0.10195
0.20000	0.01506	0.03948	0.10683	0.07593	0.10943	0.08620
0.17500	0.00650	0.03175	0.08676	0.08864	0.06652	0.10371
0.15000	0.00699	0.01442	0.06158	0.05036	0.09157	0.08293
0.12500	0.01623	0.09086	0.04744	0.05279	0.09494	0.06611
0.10000	0.01041	0.01528	0.03960	0.09742	0.10000	0.08679
0.07500	0.00809	0.01125	0.03632	0.04995	0.10600	0.09130
0.05000	0.00739	0.01074	0.02307	0.08673	0.09967	0.09621
0.02500	0.00637	0.01696	0.03818	0.07333	0.11692	0.08624
0.00000	0.00707	0.05211	0.02881	0.07911	0.10616	0.10725

(d) v'_{rms}/u_o

TABLE I (Continued)

R/D	X/D 0.0	0.5	1.0	1.5	2.0	2.5
0.40000	0.03862	0.03700	0.08976	0.08466	0.07949	0.07482
0.37500	0.04623	0.06875	0.07642	0.11720	0.08857	0.08710
0.35000	0.04496	0.06014	0.08814	0.09847	0.09465	0.09530
0.32500	0.04575	0.07635	0.11893	0.10153	0.12266	0.09617
0.30000	0.05361	0.06710	0.11085	0.11076	0.12741	0.10008
0.27500	0.05933	0.06234	0.10679	0.12757	0.13170	0.11186
0.25000	0.06549	0.11196	0.12794	0.12859	0.12616	0.12665
0.22500	0.00776	0.08444	0.10320	0.11133	0.14130	0.12771
0.20000	0.00737	0.03872	0.10066	0.10991	0.14175	0.13352
0.17500	0.00648	0.02487	0.07150	0.11170	0.14362	0.13730
0.15000	0.00710	0.01390	0.04043	0.09860	0.15187	0.12721
0.12500	0.00726	0.05623	0.03260	0.07596	0.14693	0.13665
0.10000	0.00614	0.01105	0.02535	0.07147	0.13771	0.13317
0.07500	0.00749	0.01017	0.02278	0.06014	0.15101	0.14646
0.05000	0.00714	0.00944	0.01989	0.06383	0.15219	0.14258
0.02500	0.00684	0.00970	0.01862	0.05928	0.15145	0.15658
0.00000	0.00665	0.01579	0.01676	0.04525	0.15325	0.13340

(e) w'_{rms}/u_o

TABLE I (Continued)

R/D	X/D 0.0	0.5	1.0	1.5	2.0	2.5
0.40000	0.00022	0.00051	0.00118	0.00254	0.00220	0.00196
0.37500	0.00028	0.00095	0.00179	0.01423	0.00353	0.00322
0.35000	0.00136	0.00108	0.00240	0.00353	0.00424	0.00427
0.32500	0.00023	0.00220	0.00429	0.00579	0.00491	0.00617
0.30000	0.00018	0.00000	0.00756	0.00648	0.00538	0.00754
0.27500	0.00050	0.00542	0.00611	0.01097	0.00726	0.00833
0.25000	0.00408	0.00692	0.00857	0.00782	0.00865	0.00875
0.22500	0.00002	0.00312	0.00649	0.00660	0.00822	0.00879
0.20000	0.00003	0.00056	0.00645	0.00626	0.01281	0.01744
0.17500	0.00002	0.00066	0.00260	0.00520	0.00955	0.00910
0.15000	0.00002	0.00009	0.00072	0.00436	0.01168	0.00966
0.12500	0.00001	0.00111	0.00065	0.00256	0.01299	0.01285
0.10000	0.00001	0.00007	0.00043	0.00178	0.01014	0.02194
0.07500	0.00003	0.00006	0.00024	0.00141	0.01873	0.02125
0.05000	0.00001	0.00006	0.00034	0.00200	0.04148	0.00963
0.02500	0.00001	0.00007	0.00025	0.00149	0.05488	0.02475
0.00000	0.00001	0.00005	0.00020	0.00232	0.01791	0.00848

(f) $\overline{u'v'}/u_o^2$

TABLE II

TIME-MEAN AND TURBULENCE DATA FOR SWIRLING FLOW $\phi = 38°$, $D/d = 2$

R/D	X/D 0.0	0.5	1.0	1.5	2.0	2.5
0.42500	-0.09896	1.29901	0.0	0.0	0.23554	0.28080
0.40000	-0.06402	0.99311	0.47175	0.0	0.24366	0.28807
0.37500	-0.03444	0.61711	0.38518	0.28842	0.26952	0.28854
0.35000	-0.03201	0.33441	0.27417	0.29341	0.27658	0.29332
0.32500	-0.03470	0.09991	0.19904	0.26796	0.28392	0.29281
0.30000	-0.04897	0.20141	0.12943	0.26607	0.28925	0.28803
0.27500	0.06426	0.29761	0.07652	0.25064	0.28203	0.28164
0.25000	0.24930	0.36071	0.04110	0.23349	0.27660	0.27092
0.22500	1.54394	0.41241	0.02750	0.21037	0.24222	0.25357
0.20000	1.56952	0.43431	-0.02572	0.19908	0.24093	0.22902
0.17500	1.15646	0.46031	-0.05791	0.17567	0.20173	0.20317
0.15000	0.67001	0.46361	-0.07525	0.16260	0.17914	0.17685
0.12500	0.24673	0.45831	-0.10618	0.13817	0.14764	0.13290
0.10000	-0.35617	0.44721	-0.12423	0.11900	0.11110	0.12529
0.07500	-0.12849	0.45411	-0.14824	0.08808	0.07297	0.10702
0.05000	-0.11848	0.45051	-0.14382	0.06710	-0.04146	-0.07223
0.02500	-0.13463	0.39271	-0.15786	0.04314	-0.11932	-0.08350
0.0	-0.12521	0.41641	-0.15402	0.03198	-0.13218	-0.05500

(a) u/u_o

TABLE II (Continued)

R/D	X/D 0.0	0.5	1.0	1.5	2.0	2.5
0.42500	-0.28259	0.25271	0.0	0.0	-0.10496	-0.08450
0.40000	-0.28021	0.22282	-0.17032	0.0	-0.15080	-0.07630
0.37500	-0.29243	0.18441	-0.19285	-0.15013	-0.11943	-0.10231
0.35000	-0.27253	0.16271	-0.20972	-0.15979	-0.13052	-0.07770
0.32500	-0.23813	0.14411	-0.24235	-0.15042	-0.14261	-0.07878
0.30000	-0.24081	0.14031	-0.20547	-0.17471	-0.16681	-0.11525
0.27500	0.18620	0.12111	-0.21380	-0.15213	-0.15502	-0.08418
0.25000	0.32966	0.12801	-0.19269	-0.14711	-0.15111	-0.08581
0.22500	0.45828	0.09671	-0.19407	-0.13006	-0.17335	-0.13550
0.20000	0.35722	0.12231	-0.20767	-0.12129	-0.16096	-0.10419
0.17500	0.48012	0.09911	-0.18994	-0.13549	-0.19630	-0.12409
0.15000	0.40593	0.08271	-0.19563	-0.16225	-0.17415	-0.14581
0.12500	0.23262	0.10071	-0.20737	-0.17400	-0.19436	-0.13964
0.10000	-0.10040	0.10911	-0.19467	-0.17072	-0.19954	-0.15806
0.07500	-0.09772	0.08921	-0.17873	-0.14587	-0.20515	-0.14006
0.05000	-0.09310	0.09401	-0.20325	-0.14616	-0.21271	-0.17425
0.02500	-0.08803	0.10931	-0.18629	-0.14551	-0.20156	-0.15470
0.0	-0.07267	0.11461	-0.17983	-0.15610	-0.16447	-0.16890

(b) v/u_o

TABLE II (Continued)

R/D	X/D 0.0	0.5	1.0	1.5	2.0	2.5
0.42500	0.32569	0.50041	0.0	0.0	0.46967	0.42511
0.40000	0.34760	0.40771	0.28667	0.0	0.46850	0.43713
0.37500	0.40632	0.30481	0.29970	0.33627	0.47880	0.43752
0.35000	0.40586	0.29361	0.30815	0.34015	0.48655	0.43528
0.32500	0.41543	0.30471	0.31835	0.35642	0.48016	0.44576
0.30000	0.40764	0.29571	0.34602	0.35379	0.49103	0.44807
0.27500	0.41725	0.36191	0.33110	0.37685	0.49511	0.45260
0.25000	0.46361	0.36641	0.34464	0.37453	0.50562	0.45695
0.22500	0.93520	0.37431	0.35583	0.38196	0.51561	0.44722
0.20000	1.00616	0.38501	0.34293	0.38646	0.51334	0.45626
0.17500	0.72846	0.37141	0.36453	0.40357	0.49938	0.45077
0.15000	0.38984	0.36441	0.34991	0.40259	0.49120	0.42848
0.12500	0.16201	0.32061	0.33325	0.39341	0.45391	0.40656
0.10000	0.09622	0.30101	0.33820	0.37762	0.39828	0.37506
0.07500	0.04377	0.20681	0.31151	0.36621	0.36393	0.33064
0.05000	0.05049	0.16361	0.26691	0.33293	0.29074	0.28173
0.02500	0.02438	0.12961	0.20502	0.27875	0.27436	0.20343
0.0	0.01578	0.04361	0.13233	0.25226	0.13257	0.20192

(c) w/u_o

TABLE II (Continued)

R/D	X/D 0.0	0.5	1.0	1.5	2.0	2.5
0.42500	0.12225	0.51771	0.0	0.0	0.08954	0.06675
0.40000	0.10583	0.52811	0.20142	0.0	0.08484	0.06554
0.37500	0.09571	0.44351	0.19113	0.11708	0.09623	0.06502
0.35000	0.09982	0.36311	0.16907	0.12779	0.09537	0.06322
0.32500	0.09121	0.31261	0.15325	0.10378	0.09810	0.06944
0.30000	0.09692	0.26221	0.13952	0.10983	0.09628	0.06911
0.27500	0.07959	0.22611	0.12708	0.11593	0.09854	0.07023
0.25000	0.18487	0.21681	0.12204	0.11628	0.10230	0.07430
0.22500	0.11312	0.22551	0.12037	0.10909	0.10661	0.08408
0.20000	0.09921	0.20651	0.11662	0.10741	0.11384	0.07755
0.17500	0.24096	0.23351	0.11197	0.11186	0.10807	0.08675
0.15000	0.24756	0.23951	0.10478	0.11111	0.10589	0.08004
0.12500	0.16943	0.24221	0.10702	0.10028	0.10587	0.07777
0.10000	0.09981	0.24091	0.11019	0.10279	0.11527	0.08336
0.07500	0.08535	0.27201	0.11192	0.10861	0.12519	0.09934
0.05000	0.07591	0.26791	0.12434	0.10777	0.11009	0.09219
0.02500	0.07113	0.24111	0.11852	0.10666	0.13067	0.12482
0.0	0.06095	0.25511	0.14957	0.08329	0.14067	0.13742

(d) u'_{rms}/u_o

TABLE II (Continued)

R/D	X/D 0.0	0.5	1.0	1.5	2.0	2.5
0.42500	0.11226	0.09941	0.0	0.0	0.07623	0.07697
0.40000	0.12405	0.09101	0.11290	0.0	0.07700	0.05517
0.37500	0.11057	0.09151	0.10898	0.07483	0.08247	0.06503
0.35000	0.10485	0.10221	0.10258	0.06542	0.07833	0.06604
0.32500	0.10730	0.06971	0.11015	0.09740	0.09194	0.05524
0.30000	0.08612	0.06941	0.10410	0.08881	0.09209	0.06632
0.27500	0.07732	0.06081	0.11466	0.09483	0.10100	0.07254
0.25000	0.12949	0.05971	0.09537	0.08868	0.09927	0.07905
0.22500	0.13031	0.05411	0.09312	0.08538	0.09029	0.06890
0.20000	0.12399	0.04891	0.09903	0.08951	0.08428	0.07965
0.17500	0.14685	0.06511	0.09933	0.08201	0.08508	0.06235
0.15000	0.13129	0.05781	0.10346	0.07913	0.10023	0.09256
0.12500	0.09130	0.04951	0.10067	0.07737	0.11710	0.08363
0.10000	0.05977	0.04801	0.09377	0.08481	0.10285	0.07879
0.07500	0.05011	0.05391	0.09264	0.07247	0.09787	0.09043
0.05000	0.05114	0.05081	0.10375	0.07393	0.10178	0.08103
0.02500	0.04115	0.04871	0.09924	0.07173	0.12085	0.08228
0.0	0.03370	0.05761	0.08281	0.06955	0.08635	0.06516

(e) v'_{rms}/u_o

TABLE II (Continued)

R/D	X/D 0.0	0.5	1.0	1.5	2.0	2.5
0.42500	0.12401	0.35591	0.0	0.0	0.09822	0.06947
0.40000	0.11973	0.39861	0.15799	0.0	0.10320	0.07357
0.37500	0.12192	0.38481	0.16007	0.11872	0.09997	0.07462
0.35000	0.12372	0.34221	0.17029	0.11587	0.10079	0.07264
0.32500	0.12005	0.28961	0.16537	0.10932	0.10300	0.07530
0.30000	0.11699	0.25821	0.16592	0.11521	0.10330	0.08047
0.27500	0.12222	0.22511	0.16113	0.11544	0.10722	0.07701
0.25000	0.22843	0.21571	0.15773	0.11819	0.11438	0.08383
0.22500	0.09894	0.20341	0.15960	0.12062	0.11692	0.08737
0.20000	0.08407	0.18591	0.14796	0.11969	0.11845	0.08785
0.17500	0.23118	0.19731	0.15540	0.12243	0.12256	0.09307
0.15000	0.24359	0.20341	0.14450	0.12933	0.13073	0.09102
0.12500	0.16144	0.19971	0.14555	0.12396	0.12900	0.10263
0.10000	0.11343	0.19961	0.14786	0.13093	0.13262	0.10503
0.07500	0.05966	0.19511	0.14190	0.13841	0.15084	0.12029
0.05000	0.05345	0.18171	0.13714	0.13987	0.13692	0.12525
0.02500	0.04430	0.17021	0.13012	0.13936	0.11639	0.13390
0.0	0.04382	0.16351	0.14091	0.15338	0.17164	0.14215

(f) w'_{rms}/u_o

TABLE II (Continued)

R/D	X/D 0.0	0.5	1.0	1.5	2.0	2.5
0.42500	0.00613	0.02141	0.0	0.0	0.00448	0.00173
0.40000	0.00549	0.02271	0.01192	0.0	0.00342	0.00305
0.37500	0.00380	0.01771	0.01652	0.00906	0.00991	0.00187
0.35000	0.00410	0.00981	0.00697	0.01529	0.00761	0.00243
0.32500	0.00485	0.01151	0.00637	0.00558	0.00520	0.00246
0.30000	0.00449	0.00511	0.00711	0.00519	0.00492	0.00271
0.27500	0.00137	0.00461	0.00633	0.00600	0.00874	0.00388
0.25000	0.01012	0.00501	0.00376	0.00551	0.00568	0.00358
0.22500	0.00915	0.00461	0.0	0.00644	0.00689	0.00362
0.20000	0.00391	0.00521	0.0	0.00714	0.00870	0.00386
0.17500	0.01165	0.00381	0.00438	0.00529	0.00536	0.00405
0.15000	0.01634	0.00411	0.00572	0.00347	0.00522	0.00354
0.12500	0.00568	0.00481	0.00252	0.00494	0.00319	0.00162
0.10000	0.00169	0.00611	0.00253	0.02970	0.00630	0.00236
0.07500	0.00108	0.00541	0.00221	0.00309	0.00169	0.00161
0.05000	0.00109	0.00571	0.00110	0.00346	0.00064	0.00149
0.02500	0.00115	0.00441	0.0	0.00295	0.00001	0.00250
0.0	0.00082	0.00721	0.00139	0.0	0.00548	0.00783

(g) $\overline{u'v'}/u_o^2$

TABLE II (Continued)

R/D	X/D 0.0	0.5	1.0	1.5	2.0	2.5
0.42500	0.00378	0.07711	0.0	0.0	0.00290	0.00133
0.40000	0.00403	0.06791	0.01047	0.0	0.00331	0.00154
0.37500	0.00355	0.04971	0.01378	0.00755	0.00289	0.00172
0.35000	0.00293	0.04311	0.00761	0.00641	0.00297	0.00244
0.32500	0.00182	0.01761	0.00790	0.00576	0.00332	0.00178
0.30000	0.00098	0.01931	0.00771	0.00568	0.00363	0.00299
0.27500	0.00124	0.01331	0.00665	0.00495	0.00445	0.00219
0.25000	0.01261	0.01651	0.00703	0.00407	0.00396	0.00232
0.22500	0.00384	0.01601	0.00923	0.00387	0.00359	0.00339
0.20000	0.00303	0.01331	0.00012	0.00477	0.00422	0.00290
0.17500	0.02108	0.01601	0.00213	0.00410	0.00414	0.00268
0.15000	0.01943	0.01691	0.00473	0.00474	0.00436	0.00284
0.12500	0.01146	0.02061	0.00479	0.00348	0.00521	0.00250
0.10000	0.00170	0.02011	0.00473	0.00332	0.00523	0.00204
0.07500	0.00208	0.02011	0.00672	0.00344	0.00411	0.00295
0.05000	0.00239	0.03391	0.00550	0.00656	0.00485	0.00346
0.02500	0.00141	0.01961	0.00487	0.00583	0.00402	0.00683
0.0	0.00035	0.01221	0.00507	0.00312	0.00739	0.00437

(h) $\overline{u'w'}/u_o^2$

TABLE II (Continued)

R/D	X/D 0.0	0.5	1.0	1.5	2.0	2.5
0.42500	0.00190	0.02071	0.0	0.0	0.00263	0.00254
0.40000	0.00142	0.01331	0.01039	0.0	0.00472	0.00243
0.37500	0.00216	0.00841	0.00482	0.00485	0.00459	0.00211
0.35000	0.00356	0.01121	0.00508	0.00406	0.00406	0.00278
0.32500	0.00359	0.00901	0.00711	0.00427	0.00531	0.00224
0.30000	0.00250	0.00451	0.00441	0.00538	0.00366	0.00307
0.27500	0.00349	0.00461	0.00397	0.00430	0.00587	0.00330
0.25000	0.00961	0.00401	0.00463	0.00316	0.00513	0.00306
0.22500	0.00631	0.00351	0.00451	0.00417	0.00446	0.17921
0.20000	0.00836	0.00371	0.00349	0.00347	0.00362	0.00323
0.17500	0.01734	0.00571	0.00485	0.00312	0.00405	0.00250
0.15000	0.01808	0.00431	0.00419	0.00357	0.00469	0.00418
0.12500	0.00589	0.00481	0.00367	0.00364	0.00404	0.00270
0.10000	0.00503	0.00331	0.00402	0.00403	0.00374	0.00347
0.07500	0.00117	0.00681	0.00438	0.00428	0.00534	0.00345
0.05000	0.00027	0.00441	0.00546	0.00463	0.00412	0.00363
0.02500	0.00047	0.00141	0.00305	0.00345	0.00297	0.00347
0.0	0.00031	0.01191	0.01091	0.00367	0.0	0.00430

(i) $\overline{v'w'}/u_o^2$

TABLE III

TIME-MEAN AND TURBULENCE DATA FOR SWIRLING FLOW $\phi = 45°$, $D/d = 2$

R/D	X/D 0.0	0.5	1.0	1.5	2.0	2.5
0.40000	-0.03688	0.67746	0.33174	0.0	0.22437	0.27278
0.37500	-0.03734	0.59195	0.26744	0.26181	0.23188	0.27463
0.35000	-0.04436	0.45220	0.20450	0.25418	0.23650	0.27462
0.32500	-0.02354	0.26989	0.14989	0.24821	0.25272	0.27221
0.30000	-0.01796	0.41712	0.08997	0.23086	0.24627	0.26419
0.27500	-0.01173	-0.10746	0.04988	0.20515	0.24259	0.25081
0.25000	0.15958	-0.20271	0.02710	0.19525	0.24476	0.23579
0.22500	1.31853	-0.23869	-0.02299	0.18805	0.25329	0.20934
0.20000	1.23248	-0.26459	-0.02384	0.17073	0.25017	0.18730
0.17500	1.04948	-0.29657	-0.04025	0.15493	0.21802	0.15018
0.15000	0.58556	-0.31015	-0.05518	0.14690	0.18995	0.11435
0.12500	0.37335	-0.31837	-0.07169	0.12194	0.18466	0.08715
0.10000	0.18504	-0.31803	-0.08169	0.11658	0.16152	0.05600
0.07500	-0.17245	-0.33078	-0.08774	0.08779	-0.14732	0.02467
0.05000	-0.16577	-0.32824	-0.10845	0.06769	-0.13151	-0.01697
0.02500	-0.18066	-0.34165	-0.09243	0.04824	-0.11288	-0.03239
0.0	-0.17783	-0.33121	-0.11555	0.02889	-0.13105	-0.06285

(a) u/u_o

TABLE III (Continued)

R/D	X/D 0.0	0.5	1.0	1.5	2.0	2.5
0.40000	-0.13018	0.36951	-0.20535	0.0	-0.09570	-0.10748
0.37500	-0.13370	0.33663	-0.21453	-0.15360	-0.09131	-0.11806
0.35000	-0.13120	0.33785	-0.20700	-0.16056	-0.10332	-0.12345
0.32500	-0.14734	0.27977	-0.20459	-0.14247	-0.09451	-0.11625
0.30000	-0.13355	0.14941	-0.23474	-0.12576	-0.11669	-0.11391
0.27500	0.10811	0.22244	-0.20205	-0.14650	-0.10293	-0.12266
0.25000	0.19280	0.21498	-0.18764	-0.17251	-0.11748	-0.12792
0.22500	0.15782	0.18968	-0.17636	-0.17136	-0.10558	-0.08062
0.20000	0.27848	0.17971	-0.17910	-0.15628	-0.12730	-0.10454
0.17500	0.31614	0.15147	-0.17470	-0.13042	-0.12148	-0.13229
0.15000	0.27452	0.15867	-0.20389	-0.13030	-0.14033	-0.11165
0.12500	0.27716	-0.14719	-0.17081	-0.15377	-0.11489	-0.12914
0.10000	0.19978	-0.15531	-0.16576	-0.15871	-0.11663	-0.14543
0.07500	-0.08661	-0.15495	-0.18164	-0.15990	-0.12366	-0.13458
0.05000	-0.11661	-0.17545	-0.16251	-0.13066	-0.13668	-0.15933
0.02500	-0.09726	-0.14726	-0.17427	-0.14348	-0.14111	-0.18209
0.0	-0.11389	-0.16758	-0.15342	-0.13390	-0.12394	-0.16990

(b) v/u_o

TABLE III (Continued)

R/D	X/D 0.0	0.5	1.0	1.5	2.0	2.5
0.40000	0.25314	0.33848	0.21098	0.0	0.29266	0.41400
0.37500	0.27503	0.30430	0.23050	0.28680	0.28853	0.41971
0.35000	0.28635	0.26401	0.25155	0.29984	0.29169	0.42706
0.32500	0.30199	0.14910	0.25301	0.31564	0.29597	0.43340
0.30000	0.32754	0.88451	0.25728	0.32413	0.29055	0.44111
0.27500	0.32600	0.19286	0.26954	0.32627	0.29603	0.44539
0.25000	0.34159	0.19631	0.27022	0.31315	0.30273	0.45438
0.22500	0.82527	0.20539	0.27689	0.32712	0.30099	0.45974
0.20000	0.80192	0.21758	0.27895	0.33541	0.33413	0.45665
0.17500	0.78580	0.21184	0.28018	0.33859	0.29509	0.45752
0.15000	0.35588	0.20645	0.27493	0.34573	0.27795	0.45003
0.12500	0.19200	0.18035	0.24762	0.33285	0.27216	0.41799
0.10000	0.11309	0.16649	0.24213	0.32130	0.26712	0.38725
0.07500	0.26359	0.14067	0.18999	0.28345	0.24521	0.33495
0.05000	0.06941	0.08292	0.14821	0.26216	0.20097	0.26311
0.02500	0.05474	0.03348	0.10317	0.20864	0.15522	0.18475
0.0	0.03534	0.02926	0.08459	0.16708	0.14715	0.13029

(c) w/u_o

TABLE III (Continued)

R/D	X/D 0.0	0.5	1.0	1.5	2.0	2.5
0.40000	0.07608	0.30153	0.16484	0.0	0.06277	0.05669
0.37500	0.07609	0.31191	0.15003	0.10880	0.06431	0.05664
0.35000	0.07485	0.29965	0.13979	0.10594	0.06420	0.05769
0.32500	0.06867	0.25786	0.13161	0.10244	0.06972	0.05881
0.30000	0.07268	0.29756	0.11314	0.09901	0.06862	0.05664
0.27500	0.07924	0.19640	0.10585	0.09546	0.06797	0.06668
0.25000	0.13268	0.14867	0.09913	0.09188	0.07030	0.06204
0.22500	0.11027	0.13640	0.09961	0.09335	0.07831	0.05908
0.20000	0.13949	0.13174	0.09489	0.09436	0.08369	0.06140
0.17500	0.19274	0.12619	0.08646	0.09380	0.08469	0.05584
0.15000	0.19439	0.12491	0.08807	0.09450	0.08394	0.05260
0.12500	0.19027	0.12799	0.09195	0.08832	0.08934	0.05940
0.10000	0.17666	0.13304	0.08502	0.09724	0.08853	0.05893
0.07500	0.18419	0.13925	0.09252	0.09431	0.08971	0.07011
0.05000	0.10875	0.13634	0.10126	0.09690	0.09573	0.08180
0.02500	0.09030	0.13936	0.11831	0.09343	0.10568	0.11003
0.0	0.08533	0.14643	0.13925	0.10232	0.12027	0.14820

(d) u'_{rms}/u_o

TABLE III (Continued)

R/D	X/D 0.0	0.5	1.0	1.5	2.0	2.5
0.40000	0.07746	0.17362	0.11263	0.0	0.04447	0.05672
0.37500	0.07538	0.15874	0.10566	0.07473	0.06803	0.03744
0.35000	0.07359	0.15854	0.10751	0.07694	0.06083	0.04693
0.32500	0.07258	0.13908	0.09708	0.08188	0.06729	0.04724
0.30000	0.06216	0.13565	0.10635	0.08440	0.06244	0.05099
0.27500	0.06380	0.11951	0.09461	0.08424	0.07452	0.04691
0.25000	0.09489	0.10357	0.09442	0.07022	0.07615	0.04290
0.22500	0.10735	0.09730	0.08816	0.06649	0.07940	0.07188
0.20000	0.12066	0.08806	0.07999	0.07667	0.07248	0.07511
0.17500	0.13332	0.08881	0.09036	0.07896	0.07107	0.06029
0.15000	0.14147	0.08302	0.08877	0.07750	0.06280	0.06589
0.12500	0.11666	0.08109	0.08708	0.07793	0.06981	0.06423
0.10000	0.08643	0.07780	0.08793	0.06545	0.06853	0.06369
0.07500	0.04930	0.08782	0.08728	0.06323	0.06870	0.07803
0.05000	0.06155	0.07287	0.09186	0.06368	0.06718	0.06986
0.02500	0.05529	0.08423	0.08226	0.06795	0.06127	0.07651
0.0	0.05126	0.07698	0.08008	0.06821	0.05756	0.08720

(e) v'_{rms}/u_o

TABLE III (Continued)

R/D	X/D 0.0	0.5	1.0	1.5	2.0	2.5
0.40000	0.10110	0.22339	0.13562	0.0	0.06432	0.05790
0.37500	0.10056	0.24663	0.13596	0.09977	0.06450	0.06128
0.35000	0.10100	0.25936	0.13228	0.09825	0.06752	0.05816
0.32500	0.10465	0.20752	0.12992	0.09724	0.06875	0.05979
0.30000	0.11243	0.36332	0.13390	0.09742	0.06747	0.06106
0.27500	0.11870	0.17235	0.13002	0.09796	0.06923	0.06199
0.25000	0.15056	0.14152	0.12609	0.09310	0.07366	0.06584
0.22500	0.07939	0.12988	0.12381	0.10103	0.07790	0.06580
0.20000	0.11322	0.12245	0.12389	0.10598	0.08604	0.06908
0.17500	0.17957	0.11046	0.12543	0.10726	0.08103	0.06771
0.15000	0.16740	0.10675	0.12766	0.11086	0.08655	0.07620
0.12500	0.15836	0.10156	0.12424	0.11602	0.08967	0.08214
0.10000	0.15091	0.10756	0.12418	0.12116	0.09319	0.08921
0.07500	0.17150	0.10873	0.12017	0.12154	0.09733	0.10196
0.05000	0.08218	0.09088	0.11077	0.13040	0.10254	0.10740
0.02500	0.06987	0.09572	0.11215	0.12103	0.10774	0.10649
0.0	0.05778	0.09495	0.13293	0.11863	0.11504	0.13608

(f) w'_{rms}/u_o

TABLE III (Continued)

R/D	X/D 0.0	0.5	1.0	1.5	2.0	2.5
0.40000	0.00185	0.02248	0.00648	0.0	0.00238	0.00191
0.37500	0.00111	0.02587	0.00777	0.00263	0.00182	0.01245
0.35000	0.00174	0.01419	0.00477	0.00274	0.00161	0.00141
0.32500	0.00162	0.01260	0.00583	0.00438	0.00158	0.00282
0.30000	0.00402	0.01092	0.00504	0.00380	0.00120	0.00231
0.27500	0.00241	0.00539	0.00358	0.00435	0.00130	0.00170
0.25000	0.00595	0.00304	0.00407	0.00329	0.00163	0.00210
0.22500	0.00323	0.00383	0.00271	0.00380	0.00147	0.00147
0.20000	0.01016	0.00493	0.00343	0.00333	0.00286	0.00156
0.17500	0.01136	0.00397	0.00294	0.00455	0.00312	0.00171
0.15000	0.00947	0.00450	0.00504	0.00462	0.00253	0.00159
0.12500	0.00766	0.00504	0.00232	0.00560	0.00318	0.00091
0.10000	0.00416	0.00351	0.00303	0.00254	0.00297	0.00281
0.07500	0.02915	0.00382	0.00217	0.00621	0.00246	0.00172
0.05000	0.00157	0.00425	0.00168	0.00154	0.00209	0.00027
0.02500	0.00176	0.00481	0.0	0.00188	0.00160	0.00142
0.0	0.00160	0.00507	0.00356	0.00155	0.01461	0.00172

(g) $\overline{u'v'}/u_o^2$

TABLE III (Continued)

R/D	X/D 0.0	0.5	1.0	1.5	2.0	2.5
0.40000	0.00218	0.03438	0.01013	0.0	0.00160	0.00110
0.37500	0.00207	0.02593	0.00598	0.00451	0.00149	0.00123
0.35000	0.00120	0.04575	0.00504	0.00387	0.00176	0.00127
0.32500	0.00227	0.02389	0.00488	0.00335	0.00169	0.00109
0.30000	0.00181	0.00546	0.00563	0.00318	0.00183	0.00119
0.27500	0.00218	0.00842	0.00330	0.00264	0.00147	0.00194
0.25000	0.00436	0.00491	0.00203	0.00287	0.00245	0.00179
0.22500	0.00490	0.00487	0.00396	0.00292	0.00192	0.00155
0.20000	0.00918	0.00380	0.00180	0.00308	0.00258	0.00142
0.17500	0.01518	0.00421	0.00339	0.00275	0.00261	0.00115
0.15000	0.01345	0.00348	0.00374	0.00328	0.00206	0.00106
0.12500	0.01064	0.00477	0.00426	0.00379	0.00251	0.00132
0.10000	0.01247	0.00355	0.00540	0.00357	0.00247	0.00142
0.07500	0.01363	0.00507	0.00454	0.00340	0.00240	0.00161
0.05000	0.00446	0.00302	0.00540	0.00488	0.00269	0.00138
0.02500	0.00106	0.00295	0.00449	0.00340	0.00188	0.00284
0.0	0.00160	0.00252	0.00180	0.00180	0.00431	0.00473

(h) $\overline{u'w'}/u_o^2$

TABLE III (Continued)

R/D	X/D 0.0	0.5	1.0	1.5	2.0	2.5
0.40000	0.00202	0.01514	0.00849	0.0	0.00200	0.00228
0.37500	0.00225	0.01246	0.00466	0.00325	0.00219	0.00172
0.35000	0.00210	0.01070	0.00398	0.00272	0.00169	0.00166
0.32500	0.00302	0.00569	0.00360	0.00289	0.00181	0.00167
0.30000	0.00270	0.00656	0.00449	0.00326	0.00199	0.00203
0.27500	0.00357	0.01617	0.00376	0.00231	0.00202	0.00158
0.25000	0.00724	0.00285	0.00297	0.00263	0.00235	0.00191
0.22500	0.00250	0.00284	0.00310	0.00316	0.00177	0.00194
0.20000	0.00463	0.00255	0.00339	0.00246	0.00390	0.00169
0.17500	0.01232	0.00242	0.00354	0.00254	0.00298	0.00111
0.15000	0.00964	0.00380	0.00367	0.00317	0.00222	0.00174
0.12500	0.00380	0.00386	0.00309	0.00358	0.00233	0.00170
0.10000	0.00362	0.00455	0.00297	0.00312	0.00222	0.00251
0.07500	0.03110	0.00281	0.00244	0.00265	0.00236	0.00304
0.05000	0.00144	0.00167	0.00296	0.00371	0.00229	0.00183
0.02500	0.00116	0.00400	0.00441	0.00229	0.00213	0.00127
0.0	0.00069	0.0	0.00364	0.00282	0.05537	0.00451

(i) $\overline{v'w'}/u_o^2$

TABLE IV

TIME-MEAN AND TURBULENCE DATA FOR SWIRLING FLOW $\phi = 60°$, $D/d = 2$

R/D	X/D 0.0	0.5	1.0	1.5	2.0	2.5
0.40000	0.0	0.49217	0.31133	0.31486	0.30659	0.28807
0.37500	-0.07333	0.39919	0.27156	0.30938	0.29750	0.28146
0.35000	-0.06606	0.22536	0.22515	0.30762	0.27598	0.26689
0.32500	-0.06850	0.10189	0.19773	0.28816	0.26942	0.25158
0.30000	-0.15799	-0.08607	0.16693	0.27487	0.24347	0.23387
0.27500	-0.18802	-0.13285	0.14474	0.25138	0.21352	0.21084
0.25000	0.36777	-0.21157	0.12313	0.23724	0.17886	0.17719
0.22500	2.38754	-0.24909	0.09666	0.19489	0.14388	0.13774
0.20000	2.07039	-0.27121	0.07737	0.14217	0.10083	0.10595
0.17500	0.86021	-0.29642	0.03795	0.10575	0.06282	0.05640
0.15000	0.12166	-0.28989	-0.02106	0.04347	0.01489	0.01524
0.12500	-0.12345	-0.27268	-0.05842	0.01781	-0.04219	-0.02332
0.10000	-0.07132	-0.26371	-0.12231	-0.05131	-0.07042	-0.07316
0.07500	-0.06638	-0.22285	-0.14538	-0.08968	-0.10964	-0.10975
0.05000	-0.03364	-0.20452	-0.14232	-0.12130	-0.14402	-0.12116
0.02500	-0.03369	-0.19160	-0.15569	-0.10532	-0.14467	-0.11812
0.0	-0.08577	-0.17385	-0.21657	-0.20524	-0.12334	-0.15047

(a) u/u_o

TABLE IV (Continued)

R/D	X/D 0.0	0.5	1.0	1.5	2.0	2.5
0.40000	0.0	0.40117	-0.20301	-0.13247	-0.09679	-0.06435
0.37500	-0.47440	0.37669	-0.24575	-0.13983	-0.09029	-0.09356
0.35000	-0.49696	0.37707	-0.20859	-0.12404	-0.09980	-0.10336
0.32500	-0.42889	-0.38516	-0.19945	-0.15612	-0.09210	-0.06987
0.30000	-0.36638	-0.34229	-0.25987	-0.15070	-0.07028	-0.08612
0.27500	-0.30747	-0.33499	-0.25231	-0.12714	-0.08429	-0.09180
0.25000	-0.37316	-0.30463	-0.25906	-0.13314	-0.15497	-0.09048
0.22500	0.39624	-0.28266	-0.27575	-0.16065	-0.08364	-0.12971
0.20000	0.58957	-0.25957	-0.22052	-0.14981	-0.12052	-0.15798
0.17500	0.48978	-0.25101	-0.21957	-0.15444	-0.13965	-0.10483
0.15000	0.30864	-0.23483	-0.25594	-0.15327	-0.11854	-0.10368
0.12500	0.22688	-0.28077	-0.23706	-0.15995	-0.12352	-0.13598
0.10000	-0.21001	-0.26225	-0.16987	-0.17681	-0.12640	-0.13221
0.07500	-0.19132	-0.22878	-0.23615	-0.13468	-0.16040	-0.18576
0.05000	-0.14624	-0.21247	-0.25093	-0.16738	-0.20132	-0.18451
0.02500	-0.13764	-0.20313	-0.21668	-0.20604	-0.21453	-0.22260
0.0	-0.11428	-0.21680	-0.18964	-0.18555	-0.16929	-0.19026

(b) v/u_o

TABLE IV (Continued)

R/D	X/D 0.0	0.5	1.0	1.5	2.0	2.5
0.40000	0.0	0.62032	0.78571	0.72571	0.68974	0.67590
0.37500	0.77779	0.62865	0.78354	0.73595	0.69982	0.69853
0.35000	0.82904	0.60704	0.79273	0.75148	0.71597	0.70718
0.32500	0.88902	0.57609	0.81206	0.76649	0.73401	0.72687
0.30000	0.89920	0.59359	0.83000	0.77983	0.75163	0.74568
0.27500	0.90031	0.60729	0.84125	0.80646	0.76465	0.76138
0.25000	0.90597	0.63210	0.86395	0.80806	0.77182	0.77447
0.22500	1.81744	0.65221	0.87015	0.81257	0.78470	0.77055
0.20000	1.37634	0.68063	0.87945	0.81358	0.77796	0.75960
0.17500	0.73194	0.68143	0.87849	0.80341	0.75380	0.74574
0.15000	0.36400	0.67493	0.86993	0.77698	0.70959	0.70763
0.12500	0.24824	0.62792	0.79790	0.71831	0.64630	0.63058
0.10000	0.23219	0.55336	0.72146	0.63894	0.55689	0.55852
0.07500	0.16426	0.42916	0.60333	0.54874	0.45578	0.47810
0.05000	0.21831	0.28836	0.45262	0.42982	0.33845	0.31846
0.02500	0.13103	0.14917	0.30243	0.30347	0.19823	0.17268
0.0	0.16717	0.03460	0.24621	0.21345	0.15795	0.22857

(c) w/u_o

TABLE IV (Continued)

R/D	X/D 0.0	0.5	1.0	1.5	2.0	2.5
0.40000	0.0	0.31420	0.15848	0.08846	0.05910	0.05509
0.37500	0.15709	0.31168	0.14773	0.08357	0.05420	0.06136
0.35000	0.13380	0.26033	0.13614	0.08432	0.05805	0.05778
0.32500	0.14174	0.23011	0.12884	0.08656	0.05592	0.05495
0.30000	0.13261	0.19168	0.11798	0.08521	0.05716	0.05689
0.27500	0.14067	0.16509	0.12170	0.07953	0.05308	0.05657
0.25000	0.21790	0.16750	0.12266	0.07964	0.04960	0.05205
0.22500	0.23132	0.15180	0.12447	0.07108	0.05105	0.04523
0.20000	0.39060	0.14695	0.12741	0.07052	0.05024	0.05116
0.17500	0.38505	0.14400	0.13415	0.07879	0.05697	0.05481
0.15000	0.18932	0.14337	0.13168	0.07262	0.06253	0.06089
0.12500	0.15641	0.15609	0.14123	0.08226	0.07469	0.07010
0.10000	0.15527	0.16321	0.13300	0.08013	0.07158	0.07729
0.07500	0.12686	0.17429	0.12786	0.08802	0.08653	0.09202
0.05000	0.10248	0.17922	0.14409	0.11059	0.10377	0.10519
0.02500	0.13948	0.16132	0.15399	0.11987	0.14918	0.14356
0.0	0.10965	0.18792	0.22186	0.19364	0.21146	0.21023

(d) u'_{rms}/u_o

TABLE IV (Continued)

R/D	X/D 0.0	0.5	1.0	1.5	2.0	2.5
0.40000	0.0	0.18459	0.13106	0.08725	0.06338	0.05050
0.37500	0.19498	0.21049	0.14515	0.07996	0.05175	0.05502
0.35000	0.18869	0.20541	0.15709	0.10415	0.07363	0.07253
0.32500	0.17652	0.19361	0.14964	0.09366	0.09249	0.06790
0.30000	0.16862	0.17402	0.13838	0.10419	0.09530	0.08188
0.27500	0.18195	0.17998	0.14997	0.09865	0.07912	0.08845
0.25000	0.17170	0.15439	0.14558	0.10788	0.11929	0.15799
0.22500	0.24317	0.15551	0.13397	0.08874	0.09452	0.09137
0.20000	0.19194	0.14783	0.15776	0.11790	0.06969	0.06090
0.17500	0.22563	0.14909	0.16372	0.13257	0.07247	0.06572
0.15000	0.15880	0.14380	0.13930	0.10550	0.06173	0.07608
0.12500	0.12637	0.11547	0.14711	0.07596	0.05616	0.08183
0.10000	0.09561	0.12628	0.16167	0.08392	0.08344	0.09120
0.07500	0.10227	0.10857	0.12668	0.09071	0.07473	0.09966
0.05000	0.08342	0.10834	0.11537	0.09223	0.10133	0.10277
0.02500	0.07027	0.09922	0.10299	0.11091	0.09540	0.11136
0.0	0.07477	0.11478	0.11096	0.09629	0.08045	0.10685

(e) v'_{rms}/u_o

TABLE IV (Continued)

R/D	X/D 0.0	0.5	1.0	1.5	2.0	2.5
0.40000	0.0	0.30197	0.17085	0.09984	0.06877	0.07470
0.37500	0.16802	0.30459	0.16973	0.09325	0.07188	0.08126
0.35000	0.16253	0.28992	0.15996	0.09393	0.07001	0.08361
0.32500	0.17745	0.27379	0.15816	0.09650	0.06992	0.08393
0.30000	0.19060	0.25009	0.15686	0.09641	0.07174	0.08376
0.27500	0.20104	0.22422	0.15953	0.10141	0.07158	0.08662
0.25000	0.30603	0.21656	0.16244	0.09238	0.07086	0.08542
0.22500	0.16825	0.19624	0.16581	0.10151	0.07543	0.08815
0.20000	0.26093	0.18683	0.16761	0.09414	0.07017	0.07343
0.17500	0.33162	0.18263	0.18030	0.09528	0.07901	0.07390
0.15000	0.23155	0.18428	0.18967	0.09977	0.08994	0.08517
0.12500	0.19283	0.19901	0.19832	0.10912	0.10375	0.10597
0.10000	0.17558	0.20249	0.19702	0.11387	0.10939	0.11615
0.07500	0.16273	0.20588	0.19767	0.12491	0.11935	0.13588
0.05000	0.14615	0.18398	0.20042	0.14168	0.12718	0.12742
0.02500	0.16732	0.17897	0.18058	0.14494	0.14747	0.13802
0.0	0.11369	0.15687	0.15485	0.18117	0.19234	0.18786

(f) w'_{rms}/u_o

TABLE IV (Continued)

R/D	X/D 0.0	0.5	1.0	1.5	2.0	2.5
0.40000	0.0	0.02321	0.02249	0.00612	0.00327	0.00203
0.37500	0.01356	0.02585	0.01654	0.01052	0.00305	0.00200
0.35000	0.01397	0.02748	0.01186	0.00691	0.00261	0.00275
0.32500	0.01195	0.01998	0.00919	0.00383	0.00398	0.00257
0.30000	0.01010	0.00755	0.00828	0.00466	0.00215	0.00295
0.27500	0.00738	0.01163	0.01239	0.00465	0.00124	0.00345
0.25000	0.04842	0.00489	0.00944	0.00706	0.00065	0.00043
0.22500	0.02500	0.00897	0.41637	0.00150	0.00353	0.00046
0.20000	0.04222	0.00809	0.01272	0.00311	0.00095	0.00009
0.17500	1.35934	0.00655	0.01513	0.01170	0.00059	0.00155
0.15000	0.01076	0.00981	0.01048	0.00402	0.00188	0.00195
0.12500	0.01107	0.01033	0.00820	0.00495	0.00210	0.00273
0.10000	0.00515	0.01263	0.00705	0.00189	0.00452	0.00321
0.07500	0.00507	0.00819	0.00857	0.00348	0.00121	0.00425
0.05000	0.00267	0.00499	0.00988	0.00430	0.00635	0.00496
0.02500	0.00549	0.00869	0.00621	0.00638	0.00390	0.00342
0.0	0.00181	0.00542	0.01012	0.01334	0.02982	0.02595

(g) $\overline{u'v'}/u_o^2$

TABLE IV (Continued)

R/D	X/D 0.0	0.5	1.0	1.5	2.0	2.5
0.40000	0.0	0.02285	0.00820	0.00300	0.00136	0.00209
0.37500	0.00533	0.03086	0.00842	0.00240	0.00205	0.00218
0.35000	0.00783	0.02649	0.00561	0.00301	0.00147	0.00227
0.32500	0.00042	0.01490	0.00546	0.00321	0.00145	0.00154
0.30000	0.00459	0.00948	0.00451	0.00300	0.00139	0.00131
0.27500	0.00656	0.00882	0.00619	0.00298	0.00114	0.00158
0.25000	0.02562	0.00817	0.00614	0.00248	0.00126	0.00122
0.22500	0.02307	0.00609	0.00641	0.00266	0.00095	0.00076
0.20000	0.05639	0.00782	0.00559	0.00192	0.00079	0.00087
0.17500	0.04885	0.00639	0.00720	0.00293	0.00110	0.00103
0.15000	0.01190	0.00634	0.00578	0.00139	0.00201	0.00128
0.12500	0.01808	0.01020	0.00049	0.00077	0.00048	0.00053
0.10000	0.00792	0.01074	0.00303	0.00059	0.00089	0.00122
0.07500	0.00911	0.00981	0.00491	0.00172	0.00269	0.00352
0.05000	0.00782	0.01013	0.01030	0.00340	0.00422	0.00438
0.02500	0.01029	0.00750	0.01141	0.00393	0.00725	0.00521
0.0	0.00610	0.01438	0.02966	0.02802	0.01916	0.01533

(h) $\overline{u'w'}/u_o^2$

TABLE IV (Continued)

R/D	X/D 0.0	0.5	1.0	1.5	2.0	2.5
0.40000	0.0	0.01929	0.00971	0.00292	0.00161	0.00134
0.37500	0.00708	0.01711	0.00831	0.00338	0.00129	0.00253
0.35000	0.01087	0.01454	0.00787	0.00283	0.00163	0.00186
0.32500	0.00666	0.01029	0.00808	0.00261	0.00240	0.00249
0.30000	0.01082	0.00971	0.00881	0.00356	0.00405	0.00381
0.27500	0.01238	0.01121	0.00936	0.00387	0.00233	0.00485
0.25000	0.02179	0.01238	0.00989	0.00459	0.00327	0.00539
0.22500	0.01306	0.00865	0.00997	0.00522	0.00451	0.00394
0.20000	0.02572	0.00814	0.00998	0.00576	0.00270	0.00185
0.17500	0.02231	0.00977	0.01238	0.00329	0.00193	0.00188
0.15000	0.00564	0.00737	0.01304	0.00299	0.00254	0.00257
0.12500	0.00311	0.00730	0.01277	0.00283	0.00382	0.00246
0.10000	0.00348	0.00936	0.00927	0.00427	0.00342	0.00358
0.07500	0.00270	0.00858	0.00842	0.00419	0.00369	0.00531
0.05000	0.00266	0.00608	0.00833	0.00529	0.00580	0.00376
0.02500	0.01572	0.00306	0.00559	0.00696	0.00222	0.00033
0.0	0.00316	0.00403	0.00812	0.04593	0.00508	0.01914

(i) $\overline{v'w'}/u_o^2$

TABLE V

TIME-MEAN AND TURBULENCE DATA FOR SWIRLING
FLOW $\phi = 70°$, $D/d = 2$

R/D	X/D 0.0	0.5	1.0	1.5	2.0	2.5
0.42500	-0.04027	0.41394	0.42729	0.33326	0.39612	0.33870
0.40000	-0.13648	0.23164	0.41282	0.30621	0.36734	0.32245
0.37500	-0.20328	0.05252	0.38130	0.27842	0.36187	0.29925
0.35000	-0.23359	0.06638	0.37646	0.24554	0.29978	0.27150
0.32500	-0.31535	-0.13707	0.33254	0.19764	0.26890	0.22739
0.30000	-0.35734	-0.19018	0.31811	0.14411	0.22220	0.19620
0.27500	1.69614	-0.22151	0.26312	0.09574	0.17705	0.15123
0.25000	2.56019	-0.21819	0.20954	0.02685	0.11855	0.10562
0.22500	1.61275	-0.21877	0.13258	-0.03401	0.07681	0.04350
0.17500	0.48988	-0.23856	0.05496	-0.07837	-0.04660	-0.04984
0.15000	-0.26577	-0.24173	-0.04233	-0.13452	-0.10426	-0.09747
0.12500	-0.36368	-0.24526	-0.08835	-0.16801	-0.14492	-0.14329
0.10000	-0.22628	-0.22790	-0.11946	-0.19412	-0.18376	-0.17067
0.07500	-0.14030	-0.19700	-0.12570	-0.19520	-0.21318	-0.22030
0.05000	-0.08045	-0.15834	-0.12037	-0.19283	-0.20407	-0.21236
0.02500	-0.09295	-0.11113	-0.10564	-0.14595	-0.20353	-0.25129
0.0	-0.16564	-0.23115	-0.17708	-0.36971	-0.22437	-0.30015

(a) u/u_o

TABLE V (Continued)

R/D	X/D 0.0	0.5	1.0	1.5	2.0	2.5
0.42500	-0.65966	-0.38704	-0.18698	-0.17373	-0.10534	-0.08377
0.40000	-0.65199	-0.39642	-0.23884	-0.14996	-0.13783	-0.08500
0.37500	-0.62437	-0.32962	-0.21115	-0.10220	-0.15136	-0.08056
0.35000	-0.56639	-0.35485	-0.26376	-0.14755	-0.05590	-0.08213
0.32500	-0.48143	-0.33787	-0.30948	-0.10932	-0.10759	-0.15065
0.30000	0.44870	-0.32779	-0.28377	-0.07996	-0.08060	-0.13703
0.27500	0.99340	-0.27447	-0.23457	-0.09643	-0.12352	-0.09438
0.25000	0.66344	-0.28585	-0.22794	-0.13628	-0.16646	-0.14599
0.22500	-0.88255	-0.23114	-0.24385	-0.13746	-0.18227	-0.17462
0.17500	-0.53970	-0.26696	-0.20855	-0.18099	-0.20092	-0.27808
0.15000	-0.39923	-0.25751	-0.28683	-0.11611	-0.18631	-0.22729
0.12500	-0.22723	-0.25186	-0.28413	-0.15304	-0.24007	-0.25800
0.10000	-0.26130	-0.25124	-0.20174	-0.18000	-0.18233	-0.26063
0.07500	-0.27350	-0.20743	-0.27587	-0.20159	-0.22836	-0.26783
0.05000	-0.23679	-0.19307	-0.27353	-0.20278	-0.24429	-0.25425
0.02500	-0.21598	-0.20331	-0.23849	-0.25400	-0.27159	-0.30877
0.0	-0.15380	-0.17331	-0.25637	-0.13685	-0.28910	-0.29648

(b) v/u_o

TABLE V (Continued)

R/D	X/D 0.0	0.5	1.0	1.5	2.0	2.5
0.42500	1.21798	0.88511	0.99699	0.98193	0.97912	0.90624
0.40000	1.32426	0.87413	1.01112	1.01589	1.00843	0.95507
0.37500	1.36037	0.89104	1.05917	1.03127	1.04351	1.00359
0.35000	1.42685	0.92783	1.10100	1.05402	1.06422	1.04439
0.32500	1.46821	0.95297	1.11879	1.06620	1.10339	1.06379
0.30000	1.51944	0.99488	1.13925	1.08849	1.13328	1.10695
0.27500	1.79081	1.04911	1.17221	1.11163	1.14924	1.13271
0.25000	2.01401	1.06285	1.18384	1.10745	1.17806	1.12370
0.22500	1.60458	1.09651	1.18166	1.11306	1.18009	1.11619
0.17500	1.05564	1.05360	1.15216	1.05061	1.08417	1.01850
0.15000	0.72605	0.99358	1.06461	0.96910	1.00262	0.93756
0.12500	0.59387	0.90242	0.94252	0.86021	0.88072	0.85746
0.10000	0.42971	0.76588	0.83664	0.72547	0.75090	0.71930
0.07500	0.33390	0.61675	0.69038	0.58152	0.60755	0.56275
0.05000	0.29886	0.44241	0.46709	0.45296	0.43106	0.40367
0.02500	0.21110	0.24257	0.28730	0.26301	0.22962	0.18013
0.0	0.15458	0.16940	0.27046	0.47091	0.13236	0.17801

(c) w/u_o

TABLE V (Continued)

R/D	X/D 0.0	0.5	1.0	1.5	2.0	2.5
0.42500	0.20164	0.28235	0.17063	0.08539	0.07526	0.10962
0.40000	0.18665	0.23429	0.16855	0.07902	0.06449	0.09120
0.37500	0.17839	0.20737	0.17187	0.07504	0.07868	0.09611
0.35000	0.16212	0.18021	0.16134	0.07140	0.08193	0.09254
0.32500	0.15624	0.16439	0.15084	0.07106	0.08024	0.08684
0.30000	0.19091	0.15056	0.14907	0.08531	0.08176	0.08728
0.27500	0.48071	0.14310	0.14916	0.08280	0.07169	0.10965
0.25000	0.43451	0.12425	0.14048	0.08579	0.07782	0.08827
0.22500	0.51638	0.13521	0.14031	0.07999	0.08545	0.08781
0.17500	0.40006	0.14211	0.14525	0.08954	0.07878	0.07619
0.15000	0.22058	0.14403	0.13444	0.08806	0.08630	0.08436
0.12500	0.21905	0.14685	0.13116	0.08896	0.09625	0.09791
0.10000	0.18227	0.15188	0.12804	0.09544	0.12113	0.12689
0.07500	0.14890	0.16060	0.12964	0.12090	0.14076	0.15439
0.05000	0.13921	0.15900	0.13115	0.14754	0.15784	0.18821
0.02500	0.14528	0.15419	0.17191	0.17066	0.18383	0.22296
0.0	0.17621	0.18415	0.19784	0.33382	0.24565	0.28911

(d) u'_{rms}/u_o

TABLE V (Continued)

R/D	x/D 0.0	0.5	1.0	1.5	2.0	2.5
0.42500	0.26339	0.20877	0.15655	0.08136	0.08406	0.13974
0.40000	0.26226	0.21123	0.17533	0.06374	0.08243	0.12017
0.37500	0.25064	0.20768	0.17839	0.08131	0.08745	0.10782
0.35000	0.24732	0.18762	0.13923	0.08460	0.12935	0.14202
0.32500	0.23453	0.17925	0.16676	0.10783	0.11293	0.15764
0.30000	0.22809	0.18555	0.17618	0.15133	0.10633	0.09631
0.27500	0.38379	0.19917	0.18712	0.08315	0.10482	0.11814
0.25000	0.48827	0.18160	0.18532	0.11520	0.08827	0.13606
0.22500	0.40225	0.18530	0.16900	0.06598	0.09322	0.08633
0.17500	0.26863	0.17553	0.16353	0.08344	0.09699	0.11116
0.15000	0.15938	0.15328	0.14090	0.12246	0.10135	0.14004
0.12500	0.17672	0.14209	0.12458	0.12392	0.10957	0.13039
0.10000	0.14218	0.12399	0.12800	0.10829	0.12244	0.13357
0.07500	0.13980	0.11247	0.12313	0.09833	0.12005	0.12290
0.05000	0.13443	0.11085	0.12704	0.11076	0.13680	0.15799
0.02500	0.11939	0.11231	0.11698	0.12361	0.13634	0.14016
0.0	0.06196	0.11950	0.13196	0.06982	0.16225	0.18426

(e) v'_{rms}/u_o

TABLE V (Continued)

R/D	X/D 0.0	0.5	1.0	1.5	2.0	2.5
0.42500	0.24652	0.31910	0.18919	0.10281	0.10594	0.16125
0.40000	0.22684	0.31239	0.18260	0.10807	0.10476	0.15208
0.37500	0.22741	0.28878	0.18129	0.10885	0.11373	0.17196
0.35000	0.22737	0.25454	0.18512	0.11032	0.12759	0.17784
0.32500	0.23633	0.23907	0.18264	0.11094	0.13549	0.20060
0.30000	0.29694	0.20285	0.18905	0.11317	0.14119	0.20762
0.27500	0.44099	0.20115	0.18649	0.12509	0.14225	0.19316
0.25000	0.40131	0.19033	0.18618	0.10720	0.14130	0.16813
0.22500	0.49142	0.19567	0.18661	0.10837	0.12409	0.12711
0.17500	0.45087	0.19066	0.19197	0.12262	0.11830	0.11098
0.15000	0.27464	0.20589	0.18183	0.12476	0.12770	0.10417
0.12500	0.22188	0.20612	0.18646	0.13572	0.15955	0.16192
0.10000	0.20220	0.21664	0.19011	0.14942	0.17335	0.19834
0.07500	0.19510	0.21093	0.19938	0.15881	0.19878	0.22810
0.05000	0.18017	0.19345	0.18729	0.17696	0.21533	0.24740
0.02500	0.17676	0.17093	0.19417	0.17697	0.21313	0.25002
0.0	0.21950	0.16230	0.14449	0.30600	0.17862	0.24953

(f) w'_{rms}/u_o

TABLE V (Continued)

R/D	X/D 0.0	0.5	1.0	1.5	2.0	2.5
0.42500	0.01333	0.04025	0.02251	0.00833	0.00325	0.00563
0.40000	0.01181	0.05410	0.01969	0.00498	0.00399	0.00689
0.37500	0.01532	0.01591	0.02221	0.00205	0.00368	0.02793
0.35000	0.00961	0.0	0.02247	0.00011	0.00600	0.00618
0.32500	0.00594	0.00779	0.01789	0.00146	0.00235	0.00339
0.30000	0.03483	0.01527	0.01000	0.00364	0.01387	0.00762
0.27500	0.06356	0.01299	0.01425	0.00802	0.00704	0.04053
0.25000	0.08769	0.00832	0.00860	0.00444	0.02280	0.00312
0.22500	0.07422	0.00642	0.00981	0.0	0.00535	0.00538
0.17500	0.01187	0.00268	0.02786	0.00568	0.00925	0.00599
0.15000	0.01390	0.00328	0.0	0.00206	0.00312	0.00579
0.12500	0.01694	0.00461	0.00968	0.00145	0.01413	0.00902
0.10000	0.01008	0.00358	0.00984	0.00198	0.00575	0.00558
0.07500	0.00522	0.01131	0.00840	0.00431	0.01207	0.01003
0.05000,	0.00266	0.00584	0.00519	0.00567	0.00849	0.00926
0.02500	0.00263	0.00847	0.00902	0.00409	0.00459	0.00771
0.0	0.02465	0.02312	0.00535	0.00998	0.00403	0.00203

(g) $\overline{u'v'}/u_o^2$

TABLE V (Continued)

R/D	X/D 0.0	0.5	1.0	1.5	2.0	2.5
0.42500	0.01409	0.02760	0.01102	0.00371	0.00353	0.00488
0.40000	0.00682	0.01776	0.01088	0.00304	0.00303	0.00630
0.37500	0.00737	0.00811	0.01046	0.00252	0.00442	0.00870
0.35000	0.01418	0.00034	0.00871	0.00200	0.00458	0.00807
0.32500	0.00490	0.00489	0.00823	0.00188	0.00440	0.00647
0.30000	0.02234	0.00412	0.00965	0.00296	0.00331	0.00481
0.27500	0.01719	0.00608	0.00784	0.00237	0.00118	0.00200
0.25000	0.07886	0.00618	0.00818	0.00196	0.00130	0.00059
0.22500	0.05419	0.00471	0.00731	0.00230	0.00126	0.00105
0.17500	0.05391	0.00440	0.00757	0.00066	0.00042	0.00040
0.15000	0.01125	0.00545	0.0	0.00094	0.00053	0.00120
0.12500	0.01861	0.00753	0.00097	0.00197	0.00306	0.00159
0.10000	0.01191	0.01038	0.00604	0.00303	0.00493	0.00443
0.07500	0.00933	0.01080	0.00741	0.00413	0.01113	0.01195
0.05000	0.00882	0.00746	0.00784	0.00664	0.01768	0.02562
0.02500	0.00902	0.01063	0.00834	0.00909	0.01450	0.02918
0.0	0.01690	0.01904	0.00918	0.00169	0.02117	0.03000

(h) $\overline{u'w'}/u_o^2$

TABLE V (Continued)

R/D	X/D 0.0	0.5	1.0	1.5	2.0	2.5
0.42500	0.01604	0.01818	0.01208	0.01004	0.00422	0.00264
0.40000	0.01580	0.02237	0.01159	0.00872	0.00411	0.00713
0.37500	0.01288	0.01911	0.01059	0.00843	0.02242	0.01736
0.35000	0.01950	0.01673	0.00933	0.01148	0.00826	0.01860
0.32500	0.01704	0.01716	0.00958	0.00637	0.00705	0.01429
0.30000	0.03463	0.01166	0.01188	0.00742	0.00914	0.01442
0.27500	0.06580	0.01468	0.01656	0.00685	0.00780	0.01262
0.25000	0.08242	0.01235	0.01919	0.00630	0.01087	0.00907
0.22500	0.09286	0.01603	0.01300	0.00647	0.00497	0.00931
0.17500	0.03862	0.00959	0.01444	0.00472	0.00404	0.00557
0.15000	0.01535	0.01344	0.01090	0.00469	0.00476	0.00705
0.12500	0.01206	0.01107	0.00990	0.00832	0.00712	0.00925
0.10000	0.00767	0.01339	0.01080	0.00760	0.00858	0.01145
0.07500	0.03990	0.00891	0.01030	0.00549	0.01048	0.01257
0.05000	0.00397	0.00655	0.00630	0.00752	0.01087	0.01298
0.02500	0.00615	0.00422	0.00630	0.00415	0.00506	0.00119
0.0	0.01556	0.08634	0.01480	0.00142	0.00614	0.00765

(i) $\overline{v'w'}/u_o^2$

TABLE VI

TIME-MEAN AND TURBULENCE DATA FOR NONSWIRLING FLOW $\phi = 0°$, $D/d = 2$, WITH CONTRACTION NOZZLE AT $L/D = 2$

R/D	X/D 0.0	0.5	1.0	1.5	2.0
0.40000	0.00000	-0.04970	-0.09439	0.11410	0.08509
0.37500	0.00000	-0.05885	-0.07255	0.08016	0.11457
0.35000	-0.00696	-0.05772	0.14327	0.18748	0.14335
0.32500	-0.00465	-0.05786	0.21259	0.21179	0.20170
0.30000	-0.00723	0.12951	0.29238	0.28887	0.24429
0.27500	-0.00834	0.25667	0.38693	0.35524	0.30961
0.25000	0.01195	0.47596	0.47558	0.45492	0.36377
0.22500	0.90434	0.69004	0.60736	0.57005	0.47949
0.20000	0.90683	0.86864	0.70071	0.69624	0.53578
0.17500	0.91783	0.89361	0.79163	0.77728	0.60296
0.15000	0.91782	0.90368	0.84767	0.85634	0.66423
0.12500	0.91603	0.91059	0.88421	0.90837	0.74082
0.10000	0.92350	0.91064	0.89256	0.93550	0.77872
0.07500	0.93125	0.91061	0.89283	0.94571	0.83534
0.05000	0.93278	0.92273	0.89278	0.95827	0.84848
0.02500	0.94394	0.90873	0.89277	0.96606	0.86975
0.00000	0.95407	0.91861	0.88379	0.96366	0.89484

(a) u/u_o

TABLE VI (Continued)

R/D	X/D 0.0	0.5	1.0	1.5	2.0
0.40000	0.00000	-0.04547	0.12270	0.12671	0.11051
0.37500	0.00000	-0.05038	0.14682	0.14398	0.12102
0.35000	-0.04011	-0.05990	0.16119	0.15001	0.12424
0.32500	-0.03826	-0.06912	0.14304	0.16066	0.17491
0.30000	-0.03211	0.11358	0.17898	0.16165	0.18650
0.27500	-0.04019	0.14873	0.17523	0.21174	0.20309
0.25000	0.03868	0.22172	0.21082	0.17771	0.19836
0.22500	0.12379	0.23772	0.22144	0.19748	0.20221
0.20000	0.10230	0.22650	0.25502	0.24826	0.17270
0.17500	0.12948	0.22999	0.25758	0.18533	0.16898
0.15000	0.07727	0.20089	0.23644	0.19443	0.25873
0.12500	0.09039	0.19161	0.18665	0.20221	0.20272
0.10000	0.11210	0.21731	0.18803	0.18571	0.22430
0.07500	0.13147	0.21736	0.18774	0.18600	0.19712
0.05000	0.10460	0.17611	0.18777	0.16644	0.24159
0.02500	0.09543	0.22309	0.18812	0.21548	0.24430
0.00000	0.13728	0.19955	0.19440	0.23677	0.25231

(b) v/u_o

TABLE VI (Continued)

R/D	X/D 0.0	0.5	1.0	1.5	2.0
0.40000	0.00000	0.04841	0.09728	0.11330	0.10344
0.37500	0.00000	0.04979	0.11811	0.14394	0.12596
0.35000	0.02279	0.06135	0.12283	0.12974	0.13598
0.32500	0.02231	0.08779	0.15566	0.13635	0.14295
0.30000	0.02190	0.10941	0.15509	0.16579	0.15657
0.27500	0.01936	0.14284	0.18393	0.18150	0.17278
0.25000	0.02510	0.16332	0.18777	0.20566	0.19646
0.22500	0.01535	0.14464	0.16620	0.21885	0.19939
0.20000	0.01638	0.08102	0.17222	0.21287	0.19225
0.17500	0.01481	0.03943	0.09233	0.19452	0.21271
0.15000	0.01491	0.02811	0.06735	0.15951	0.17325
0.12500	0.01590	0.02170	0.04657	0.12574	0.17168
0.10000	0.01513	0.01814	0.03900	0.26336	0.15349
0.07500	0.01438	0.01673	0.03260	0.07624	0.14147
0.05000	0.01485	0.01666	0.02959	0.06806	0.11700
0.02500	0.01469	0.01551	0.02916	0.06027	0.09653
0.00000	0.01413	0.01530	0.02906	0.06052	0.09585

(c) u'_{rms}/u_o

TABLE VI (Continued)

R/D	X/D 0.0	0.5	1.0	1.5	2.0
0.40000	0.00000	0.02975	0.05959	0.05347	0.05629
0.37500	0.00000	0.02392	0.07421	0.06926	0.06022
0.35000	0.02165	0.03382	0.07830	0.05713	0.06883
0.32500	0.02295	0.03368	0.07063	0.07004	0.07468
0.30000	0.02044	0.04451	0.07144	0.08026	0.08193
0.27500	0.01940	0.05095	0.09154	0.08657	0.07896
0.25000	0.02080	0.06427	0.08246	0.09362	0.08776
0.22500	0.01758	0.05446	0.05813	0.07158	0.09627
0.20000	0.02537	0.03991	0.06436	0.05932	0.07575
0.17500	0.01157	0.02000	0.03779	0.09755	0.10136
0.15000	0.02340	0.02459	0.03184	0.05581	0.06998
0.12500	0.02259	0.01430	0.03193	0.04038	0.10053
0.10000	0.01789	0.00894	0.03339	0.09272	0.07099
0.07500	0.01093	0.00756	0.02722	0.06584	0.07325
0.05000	0.01976	0.01869	0.02764	0.06365	0.05580
0.02500	0.02132	0.00733	0.02719	0.03929	0.07194
0.00000	0.01197	0.01361	0.02715	0.02474	0.05881

(d) v'_{rms}/u_o

TABLE VI (Continued)

R/D	X/D 0.0	0.5	1.0	1.5	2.0
0.40000	0.00000	0.04511	0.07355	0.08682	0.09939
0.37500	0.00000	0.04315	0.07523	0.10368	0.11186
0.35000	0.03137	0.05325	0.08014	0.11080	0.13062
0.32500	0.03125	0.06745	0.08830	0.11270	0.11211
0.30000	0.03695	0.07851	0.09703	0.11344	0.11596
0.27500	0.03960	0.09724	0.12374	0.12035	0.12321
0.25000	0.03550	0.10676	0.12384	0.13352	0.14194
0.22500	0.00784	0.09175	0.10982	0.12787	0.12546
0.20000	0.00851	0.05312	0.08880	0.12967	0.11580
0.17500	0.00839	0.02539	0.07091	0.11929	0.13664
0.15000	0.00839	0.01730	0.04652	0.09720	0.10957
0.12500	0.00893	0.01296	0.03021	0.06880	0.10037
0.10000	0.00856	0.01138	0.02528	0.06321	0.09743
0.07500	0.00808	0.01026	0.02155	0.05167	0.08749
0.05000	0.00749	0.00995	0.01987	0.04506	0.08954
0.02500	0.00821	0.00918	0.01963	0.03908	0.08126
0.00000	0.00792	0.00958	0.01976	0.03958	0.06619

(e) w'_{rms}/u_o

TABLE VI (Continued)

R/D	X/D 0.0	0.5	1.0	1.5	2.0
0.40000	0.00000	0.00044	0.00060	0.00144	0.00094
0.37500	0.00000	0.00038	0.00182	0.00006	0.00210
0.35000	0.00003	0.00061	0.00187	0.00292	0.00718
0.32500	0.00011	0.00147	0.00334	0.00396	0.00311
0.30000	0.00002	0.00117	0.00554	0.00672	0.00441
0.27500	0.00000	0.00252	0.00616	0.00806	0.00552
0.25000	0.00026	0.00563	0.00892	0.00737	0.00858
0.22500	0.00006	0.00380	0.00440	0.00898	0.00687
0.20000	0.00004	0.00141	0.00387	0.00637	0.00829
0.17500	0.00002	0.00030	0.00080	0.00593	0.00991
0.15000	0.00001	0.00011	0.00115	0.00372	0.00729
0.12500	0.00002	0.00006	0.00040	0.00860	0.00680
0.10000	0.00003	0.00005	0.00019	0.00092	0.00519
0.07500	0.00001	0.00003	0.00010	0.00097	0.00383
0.05000	0.00001	0.00003	0.00010	0.00087	0.00403
0.02500	0.00001	0.00003	0.00011	0.00100	0.00507
0.00000	0.00001	0.00002	0.00009	0.00050	0.00336

(f) $\overline{u'v'}/u_o^2$

TABLE VII

TIME-MEAN AND TURBULENCE DATA FOR SWIRLING FLOW $\phi = 45°$, D/d = 2, WITH CONTRACTION NOZZLE AT L/D = .2

R/D	X/D 0.0	0.5	1.0	1.5	2.0
0.40000	0.00000	0.42561	0.24801	0.12393	0.07270
0.37500	-0.12226	0.31929	0.21806	0.14442	0.08043
0.35000	-0.07221	0.11425	0.16135	0.15661	0.10763
0.32500	-0.03677	-0.07813	0.12351	0.16307	0.14662
0.30000	-0.02125	-0.17716	0.08992	0.18722	0.18782
0.27500	-0.04911	-0.22492	0.07458	0.21352	0.23966
0.25000	-0.09842	-0.27500	0.04413	0.23014	0.28450
0.22500	1.24277	-0.30150	0.05413	0.25252	0.33350
0.20000	1.45896	-0.28622	0.04817	0.27508	0.38776
0.17500	1.58500	-0.25213	0.07603	0.29773	0.45446
0.15000	1.16454	-0.20605	0.10792	0.34184	0.52150
0.12500	0.26514	-0.11827	0.19007	0.40068	0.60074
0.10000	0.04634	-0.03713	0.32247	0.52869	0.71788
0.07500	0.05948	0.15273	0.48458	0.69637	0.86708
0.05000	0.13250	0.28492	0.69349	0.85020	1.01395
0.02500	0.17967	0.40450	0.76821	0.93271	1.12060
0.00000	0.20763	0.36991	0.77649	0.88484	1.07042

(a) u/u_o

TABLE VII (Continued

R/D	X/D 0.0	0.5	1.0	1.5	2.0
0.40000	0.00000	0.36778	-0.28033	0.19289	0.14559
0.37500	-0.36666	0.33599	-0.24671	0.19461	0.17198
0.35000	-0.36116	0.35940	-0.26561	0.19987	0.18926
0.32500	-0.35745	0.33637	-0.27591	-0.18159	0.21616
0.30000	-0.31724	0.28699	-0.26635	-0.17742	0.22894
0.27500	-0.26576	-0.26613	-0.26344	-0.24298	-0.21595
0.25000	0.23174	-0.25644	-0.27733	-0.24302	-0.25469
0.22500	0.37325	-0.24920	-0.30302	-0.25841	-0.25045
0.20000	0.46237	-0.28738	-0.25839	-0.26215	-0.30618
0.17500	0.49022	-0.32627	-0.28955	-0.32023	-0.27790
0.15000	0.40088	-0.29947	-0.34714	-0.26842	-0.28766
0.12500	0.26000	-0.33800	-0.43615	-0.37144	-0.34083
0.10000	0.24048	-0.37047	-0.49054	-0.37756	-0.46190
0.07500	0.22495	-0.43738	-0.61020	-0.51660	-0.42491
0.05000	0.25343	-0.45263	-0.68326	-0.49914	-0.50249
0.02500	0.20608	-0.42549	-0.71520	-0.56333	-0.40979
0.00000	0.24016	-0.44969	-0.68424	-0.49251	-0.57365

(b) v/u_o

TABLE VII (Continued)

R/D	X/D 0.0	0.5	1.0	1.5	2.0
0.40000	0.00000	0.39434	0.52072	0.59830	0.62745
0.37500	0.55072	0.36346	0.55194	0.60413	0.64800
0.35000	0.61137	0.33510	0.56353	0.62524	0.68226
0.32500	0.62426	0.35044	0.56526	0.64953	0.70651
0.30000	0.65199	0.39277	0.59074	0.69278	0.74207
0.27500	0.65162	0.41528	0.62826	0.70526	0.77787
0.25000	0.64888	0.44636	0.63162	0.75810	0.80100
0.22500	1.00212	0.49356	0.68399	0.80077	0.85857
0.20000	1.19580	0.52602	0.74992	0.86395	0.90030
0.17500	1.30912	0.59971	0.79922	0.90531	0.97339
0.15000	0.96492	0.63651	0.87868	0.99991	1.05204
0.12500	0.36278	0.65844	0.94789	1.06409	1.13199
0.10000	0.30355	0.63146	0.95472	1.12393	1.17860
0.07500	0.28984	0.49823	0.86416	1.02243	1.19136
0.05000	0.17791	0.39482	0.60534	0.73723	0.99389
0.02500	0.20856	0.20362	0.23990	0.33687	0.62539
0.00000	0.17941	0.03144	0.18316	0.14124	0.08428

(c) w/u_o

TABLE VII (Continued)

R/D	X/D 0.0	0.5	1.0	1.5	2.0
0.40000	0.00000	0.28419	0.14854	0.06933	0.04510
0.37500	0.13396	0.28402	0.14442	0.07288	0.04430
0.35000	0.12891	0.23389	0.13597	0.07356	0.04506
0.32500	0.11804	0.18407	0.12569	0.07495	0.04528
0.30000	0.11198	0.17358	0.11712	0.07491	0.04501
0.27500	0.11493	0.15902	0.12259	0.07771	0.04760
0.25000	0.11957	0.14618	0.12081	0.07830	0.05191
0.22500	0.27612	0.14295	0.11988	0.08471	0.05824
0.20000	0.17747	0.14579	0.12607	0.08874	0.06147
0.17500	0.14070	0.14948	0.13908	0.09114	0.07237
0.15000	0.32411	0.14968	0.14984	0.12677	0.07721
0.12500	0.19202	0.16568	0.15679	0.12219	0.09289
0.10000	0.11923	0.18234	0.18358	0.13633	0.10511
0.07500	0.12654	0.20303	0.20780	0.15026	0.10930
0.05000	0.18758	0.20495	0.25275	0.17556	0.17950
0.02500	0.19025	0.21996	0.25423	0.21848	0.28673
0.00000	0.23061	0.24524	0.24778	0.20835	0.32274

(d) u'_{rms}/u_o

TABLE VII (Continued)

R/D	X/D 0.0	0.5	1.0	1.5	2.0
0.40000	0.00000	0.15290	0.13758	0.09167	0.07937
0.37500	0.13309	0.13285	0.14047	0.09023	0.07742
0.35000	0.13963	0.18110	0.13895	0.09178	0.08159
0.32500	0.13391	0.15740	0.14117	0.10239	0.08459
0.30000	0.13718	0.12871	0.15047	0.11505	0.09428
0.27500	0.12154	0.12760	0.13680	0.09343	0.10403
0.25000	0.10438	0.13433	0.12844	0.09653	0.09414
0.22500	0.26477	0.13615	0.12563	0.10198	0.09905
0.20000	0.15577	0.14210	0.13974	0.11257	0.07635
0.17500	0.14936	0.14143	0.14696	0.10661	0.09576
0.15000	0.14248	0.16309	0.15335	0.12088	0.10505
0.12500	0.14376	0.16766	0.16541	0.14802	0.11288
0.10000	0.10976	0.18800	0.23642	0.17472	0.10388
0.07500	0.12040	0.19107	0.27389	0.18069	0.17943
0.05000	0.10888	0.19352	0.28226	0.26458	0.20489
0.02500	0.09697	0.19559	0.30346	0.24377	0.24884
0.00000	0.11332	0.20458	0.30158	0.26334	0.23194

(e) v'_{rms}/u_o

TABLE VII (Continued)

R/D	X/D 0.0	0.5	1.0	1.5	2.0
0.40000	0.00000	0.26578	0.15693	0.08627	0.05232
0.37500	0.15594	0.25628	0.15655	0.08533	0.05269
0.35000	0.15529	0.25774	0.15223	0.08724	0.05094
0.32500	0.15478	0.21607	0.14658	0.09015	0.05353
0.30000	0.15893	0.20206	0.14505	0.09263	0.05434
0.27500	0.16898	0.19350	0.15187	0.09404	0.05644
0.25000	0.19446	0.18004	0.15690	0.10271	0.06259
0.22500	0.25282	0.17056	0.16624	0.10748	0.06799
0.20000	0.15886	0.17529	0.17758	0.11379	0.07994
0.17500	0.12083	0.19110	0.18653	0.11774	0.08966
0.15000	0.26169	0.20225	0.20597	0.14473	0.09492
0.12500	0.17628	0.20722	0.20648	0.13524	0.11018
0.10000	0.15475	0.21432	0.20323	0.14700	0.11630
0.07500	0.16324	0.22238	0.21255	0.15685	0.12193
0.05000	0.21034	0.21840	0.23823	0.18130	0.18536
0.02500	0.24490	0.21192	0.26134	0.23588	0.26644
0.00000	0.20938	0.22658	0.24990	0.19947	0.24578

(f) w'_{rms}/u_o

TABLE VII (Continued)

R/D	X/D 0.0	0.5	1.0	1.5	2.0
0.40000	0.00000	0.02134	0.00975	0.00184	0.00084
0.37500	0.00458	0.02058	0.01048	0.00184	0.00078
0.35000	0.00642	0.01652	0.00821	0.00207	0.00086
0.32500	0.00418	0.00559	0.00985	0.00208	0.00074
0.30000	0.00000	0.01034	0.01021	0.00319	0.00170
0.27500	0.00240	0.00964	0.00974	0.00246	0.00092
0.25000	0.00418	0.00926	0.00699	0.00336	0.00144
0.22500	0.02134	0.01025	0.00621	0.00273	0.00198
0.20000	0.00998	0.00721	0.00674	0.00557	0.00249
0.17500	0.01117	0.02064	0.00947	0.00451	0.00335
0.15000	0.01531	0.00855	0.01203	0.00708	0.00275
0.12500	0.01166	0.01829	0.01489	0.00702	0.00539
0.10000	0.00000	0.00327	0.01439	0.00990	0.00443
0.07500	0.00644	0.00852	0.02000	0.01323	0.00719
0.05000	0.01704	0.00962	0.02190	0.01720	0.01104
0.02500	0.03102	0.00901	0.00507	0.01955	0.02560
0.00000	0.01351	0.00870	0.00879	0.02486	0.02389

(g) $\overline{u'v'}/u_o^2$

TABLE VII (Continued)

R/D	X/D 0.0	0.5	1.0	1.5	2.0
0.40000	0.00000	0.01924	0.00566	0.00135	0.00020
0.37500	0.00706	0.01815	0.00580	0.00130	0.00021
0.35000	0.00613	0.02628	0.00502	0.00143	0.00034
0.32500	0.00370	0.00751	0.00353	0.00161	0.00036
0.30000	0.00524	0.00690	0.00577	0.00168	0.00033
0.27500	0.00328	0.01044	0.00563	0.00205	0.00049
0.25000	0.00233	0.00898	0.00273	0.00252	0.00081
0.22500	0.02236	0.00680	0.00380	0.00178	0.00129
0.20000	0.01138	0.00732	0.00317	0.00249	0.00223
0.17500	0.00527	0.00753	0.00603	0.00223	0.00229
0.15000	0.03142	0.00589	0.00528	0.00683	0.00258
0.12500	0.01291	0.00704	0.00668	0.00396	0.00364
0.10000	0.00440	0.01139	0.00887	0.00640	0.00500
0.07500	0.00527	0.00768	0.00638	0.01234	0.00484
0.05000	0.01512	0.01352	0.01907	0.01156	0.01218
0.02500	0.00941	0.01112	0.01818	0.01425	0.03462
0.00000	0.00206	0.01608	0.01698	0.00874	0.01608

(h) $\overline{u'w'}/u_o^2$

TABLE VII (Continued)

R/D	X/D 0.0	0.5	1.0	1.5	2.0
0.40000	0.00000	0.00909	0.00832	0.00295	0.00143
0.37500	0.00604	0.01075	0.00698	0.00394	0.00147
0.35000	0.00881	0.00276	0.00688	0.00296	0.00169
0.32500	0.00650	0.00535	0.00813	0.00308	0.00113
0.30000	0.00750	0.00988	0.00594	0.00280	0.00140
0.27500	0.00797	0.01144	0.00565	0.00297	0.00162
0.25000	0.00917	0.01128	0.00701	0.00354	0.00163
0.22500	0.01674	0.01163	0.00829	0.00342	0.00154
0.20000	0.00750	0.01056	0.00883	0.00460	0.00189
0.17500	0.00476	0.00929	0.01069	0.00395	0.00256
0.15000	0.01365	0.00844	0.01278	0.00259	0.00378
0.12500	0.00922	0.01033	0.01376	0.00710	0.00384
0.10000	0.00382	0.00963	0.01096	0.00946	0.00738
0.07500	0.00475	0.00853	0.01662	0.01448	0.00674
0.05000	0.00585	0.00941	0.01379	0.00974	0.00900
0.02500	0.00782	0.01000	0.02331	0.02971	0.03363
0.00000	0.02215	0.01146	0.02074	0.02447	0.06575

(i) $\overline{v'w'}/u_o^2$

TABLE VIII

TIME-MEAN AND TURBULENCE DATA FOR SWIRLING FLOW ϕ = 70°, D/d = 2, WITH CONTRACTION NOZZLE AT L/D = 2

R/D	X/D 0.0	0.5	1.0	1.5	2.0
0.42500	0.00000	0.22830	0.00000	0.18076	0.34424
0.40000	-0.02807	0.13741	0.20679	0.14233	0.34133
0.37500	-0.07091	0.03600	0.17987	0.10312	0.32466
0.35000	-0.05704	-0.05162	0.17728	0.07521	0.32662
0.32500	-0.03613	-0.04366	0.14952	0.03979	0.36077
0.30000	0.12974	-0.13449	0.12264	0.04443	0.35727
0.27500	1.67413	-0.06708	0.11241	0.07212	0.41261
0.25000	2.32211	-0.06559	0.12785	0.08962	0.50742
0.22500	1.77876	-0.10316	0.11396	0.11997	0.54987
0.20000	0.92559	-0.04439	0.15261	0.18482	0.56821
0.17500	-0.08335	0.05297	0.21385	0.22081	0.57793
0.15000	-0.33973	0.17205	0.30250	0.24584	0.60591
0.12500	-0.35188	0.24328	0.34406	0.27629	0.54886
0.10000	-0.18670	0.32868	0.38178	0.27934	0.59902
0.07500	0.10389	0.34384	0.35052	0.30007	0.54211
0.05000	0.30619	0.35272	0.37285	0.32678	0.39648
0.00000	0.42242	0.32736	0.33767	0.45736	0.35764

(a) u/u_o

TABLE VIII (Continued)

R/D	X/D 0.0	0.5	1.0	1.5	2.0
0.42500	0.00000	0.36362	0.00000	0.30316	0.33237
0.40000	-0.32856	0.36999	-0.25894	-0.24726	0.31595
0.37500	-0.36667	0.33034	-0.27522	-0.29958	-0.36865
0.35000	-0.44379	0.40754	-0.29810	-0.35925	-0.42876
0.32500	-0.42146	0.17503	-0.28436	-0.32845	-0.35257
0.30000	0.53087	-0.37889	-0.34601	-0.31155	-0.35304
0.27500	0.64536	-0.17020	-0.36993	-0.37450	-0.42610
0.25000	0.77652	-0.17169	-0.39628	-0.42774	-0.49919
0.22500	0.71315	-0.34337	-0.47798	-0.43118	-0.43894
0.20000	0.67117	-0.43427	-0.36822	-0.54012	-0.49197
0.17500	0.57221	-0.42074	-0.41772	-0.47652	-0.48248
0.15000	0.56541	-0.48988	-0.45402	-0.53539	-0.58432
0.12500	0.51857	-0.46236	-0.44922	-0.51827	-0.64213
0.10000	0.50837	-0.41656	-0.32535	-0.56273	-0.59646
0.07500	0.56046	-0.32507	-0.35135	-0.50814	-0.58887
0.05000	0.64651	-0.45904	-0.32376	-0.62108	-0.66869
0.00000	0.75908	-0.37863	-0.36557	-0.64922	-0.46462

(b) v/u_o

TABLE VIII (Continued)

R/D	X/D 0.0	0.5	1.0	1.5	2.0
0.42500	0.00000	1.09010	0.00000	1.21292	1.11118
0.40000	1.37914	1.11337	1.21259	1.28333	1.19952
0.37500	1.45528	1.11623	1.25771	1.33233	1.24624
0.35000	1.67982	1.13448	1.28502	1.37921	1.33772
0.32500	1.81400	0.55463	1.33736	1.48143	1.46639
0.30000	1.89632	1.29662	1.38881	1.58595	1.57527
0.27500	1.87882	0.62919	1.56277	1.70555	1.67880
0.25000	2.58376	0.68851	1.72509	1.83314	1.79217
0.22500	1.89310	1.64183	1.86771	1.84029	1.86455
0.20000	1.66374	1.78448	1.83756	1.93058	1.91182
0.17500	1.54915	1.95647	1.94731	2.09516	1.95736
0.15000	1.46043	1.94696	2.00751	2.07505	2.01846
0.12500	1.44988	2.03124	1.87411	1.85871	1.99352
0.10000	1.38590	1.72405	1.54657	1.42112	1.69915
0.07500	1.24122	1.31257	1.06093	1.03470	1.19964
0.05000	0.96980	0.75400	0.60336	0.64874	0.72726
0.00000	0.49947	0.33221	0.16693	0.31227	0.44627

(c) w/u_o

TABLE VIII (Continued)

R/D	X/D 0.0	0.5	1.0	1.5	2.0
0.42500	0.00000	0.19069	0.00000	0.06448	0.05281
0.40000	0.12229	0.17002	0.10665	0.06016	0.06350
0.37500	0.11662	0.16912	0.10731	0.06286	0.05467
0.35000	0.12445	0.15835	0.10738	0.05907	0.05506
0.32500	0.12918	0.06546	0.09972	0.06489	0.05751
0.30000	0.13835	0.13740	0.10784	0.05611	0.05781
0.27500	0.47325	0.06167	0.10110	0.07713	0.07507
0.25000	0.30314	0.06184	0.10363	0.07148	0.08669
0.22500	0.32031	0.13997	0.10358	0.07735	0.10618
0.20000	0.38331	0.14789	0.08764	0.08964	0.14249
0.17500	0.30034	0.13601	0.09206	0.09442	0.17523
0.15000	0.25202	0.17328	0.08721	0.10103	0.19309
0.12500	0.23300	0.16888	0.12366	0.15580	0.22343
0.10000	0.22355	0.19305	0.15863	0.17390	0.27490
0.07500	0.24063	0.21848	0.19409	0.20758	0.32792
0.05000	0.28726	0.24522	0.25011	0.29106	0.37399
0.00000	0.42737	0.27720	0.27156	0.35148	0.54286

(d) u'_{rms}/u_o

TABLE VIII (Continued)

R/D	X/D 0.0	0.5	1.0	1.5	2.0
0.42500	0.00000	0.22069	0.00000	0.08717	0.10198
0.40000	0.15720	0.16967	0.16322	0.11059	0.11134
0.37500	0.16166	0.19388	0.16210	0.08596	0.09533
0.35000	0.17413	0.14120	0.15896	0.05786	0.08609
0.32500	0.19129	0.06991	0.14895	0.07563	0.13336
0.30000	0.13448	0.14524	0.11013	0.03749	0.12633
0.27500	0.37350	0.06100	0.12684	0.11462	0.16173
0.25000	0.36390	0.08317	0.10222	0.07262	0.13291
0.22500	0.30969	0.18987	0.11130	0.10062	0.19028
0.20000	0.31356	0.16624	0.10884	0.11763	0.19575
0.17500	0.32454	0.15881	0.10477	0.16153	0.25331
0.15000	0.23507	0.19973	0.13741	0.18945	0.22446
0.12500	0.22582	0.18239	0.14795	0.18900	0.28378
0.10000	0.27068	0.23084	0.18212	0.19041	0.31977
0.07500	0.26682	0.24707	0.18813	0.23130	0.29017
0.05000	0.26173	0.20085	0.14663	0.22607	0.27756
0.00000	0.29642	0.18277	0.16106	0.25919	0.26320

(e) v'_{rms}/u_o

TABLE VIII (Continued)

R/D	X/D 0.0	0.5	1.0	1.5	2.0
0.42500	0.00000	0.23815	0.00000	0.08044	0.07797
0.40000	0.18888	0.23011	0.13845	0.07506	0.07090
0.37500	0.18576	0.22009	0.14180	0.07606	0.06655
0.35000	0.18543	0.20970	0.13389	0.08438	0.07221
0.32500	0.20367	0.08622	0.13616	0.08393	0.08073
0.30000	0.22612	0.18248	0.14200	0.09444	0.07817
0.27500	0.47924	0.08233	0.13073	0.09279	0.09334
0.25000	0.39397	0.08187	0.13771	0.09791	0.09429
0.22500	0.39264	0.18810	0.13368	0.09731	0.12141
0.20000	0.44370	0.18941	0.12344	0.10787	0.16564
0.17500	0.42210	0.21581	0.13544	0.11989	0.21735
0.15000	0.32956	0.19603	0.12544	0.14631	0.23101
0.12500	0.30991	0.23969	0.18926	0.24020	0.27282
0.10000	0.28829	0.28423	0.26096	0.24514	0.37576
0.07500	0.29553	0.31817	0.25798	0.24732	0.41956
0.05000	0.39346	0.27914	0.25812	0.30483	0.41102
0.00000	0.43432	0.24771	0.22985	0.35146	0.56138

(f) w'_{rms}/u_o

TABLE VIII (Continued)

R/D	X/D 0.0	0.5	1.0	1.5	2.0
0.42500	0.00000	0.00839	0.00000	0.00082	0.00236
0.40000	0.00959	0.01461	0.00138	0.00229	0.00555
0.37500	0.01603	0.00751	0.00262	0.00252	0.00226
0.35000	0.00653	0.01509	0.09652	0.00170	0.00094
0.32500	0.00559	0.00270	0.01087	0.00389	0.00560
0.30000	0.01035	0 00955	0.00211	0.00084	0.00183
0.27500	0.07000	0.00110	0.00709	0.00550	0.01001
0.25000	0.03172	0.00113	0.00911	0.00210	0.00478
0.22500	0.04278	0.00660	0.00023	0.00248	0.00761
0.20000	0.06653	0.01294	0.00239	0.00491	0.03912
0.17500	0.00566	0.01149	0.00307	0.00639	0.02410
0.15000	0.01425	0.00130	0.00450	0.00807	0.02167
0.12500	0.01947	0.00278	0.01083	0.04147	0.02811
0.10000	0.04314	0.01024	0.01502	0.00761	0.02306
0.07500	0.03166	0.01771	0.01596	0.01688	0.02697
0.05000	0.02475	0.01800	0.01548	0.02925	0.03048
0.00000	0.01424	0.01140	0.00923	0.01063	0.06862

(g) $\overline{u'v'}/u_o^2$

TABLE VIII (Continued)

R/D	X/D 0.0	0.5	1.0	1.5	2.0
0.42500	0.00000	0.01553	0.00000	0.00189	0.00189
0.40000	0.00099	0.00571	0.00623	0.00134	0.00186
0.37500	0.00354	0.00376	0.00578	0.00098	0.00090
0.35000	0.00255	0.00290	0.00348	0.00107	0.00078
0.32500	0.00386	0.00037	0.00377	0.00085	0.00140
0.30000	0.00532	0.00237	0.00491	0.00108	0.00153
0.27500	0.09874	0.00065	0.00434	0.00291	0.00511
0.25000	0.05532	0.00047	0.00215	0.00174	0.00336
0.22500	0.09032	0.00231	0.00170	0.00162	0.00548
0.20000	0.04700	0.00278	0.00180	0.00360	0.00862
0.17500	0.02589	0.00446	0.00280	0.00258	0.01432
0.15000	0.01966	0.00089	0.00284	0.00357	0.01561
0.12500	0.02367	0.00522	0.00454	0.00893	0.01724
0.10000	0.02208	0.00901	0.01106	0.01556	0.01772
0.07500	0.01832	0.01732	0.01458	0.01021	0.03515
0.05000	0.04631	0.02709	0.02406	0.00727	0.03792
0.00000	0.08151	0.01914	0.01990	0.02101	0.04905

(h) $\overline{u'w'}/u_o^2$

TABLE VIII (Continued)

R/D	X/D 0.0	0.5	1.0	1.5	2.0
0.42500	0.00000	0.01117	0.00000	0.00365	0.00344
0.40000	0.00824	0.01476	0.00910	0.00223	0.00227
0.37500	0.01002	0.01196	0.00960	0.00603	0.00198
0.35000	0.01109	0.01054	0.00940	0.00183	0.00190
0.32500	0.01340	0.00259	0.00827	0.00419	0.00382
0.30000	0.01254	0.00904	0.00628	0.00198	0.00286
0.27500	0.05393	0.00199	0.00447	0.00310	0.00530
0.25000	0.06650	0.00186	0.00425	0.00330	0.00483
0.22500	0.05991	0.00941	0.00556	0.00455	0.01007
0.20000	0.06670	0.00794	0.00510	0.00455	0.01376
0.17500	0.04181	0.01007	0.00418	0.00928	0.01958
0.15000	0.02552	0.00214	0.00603	0.00983	0.02605
0.12500	0.02118	0.01764	0.00945	0.02116	0.02718
0.10000	0.02449	0.01999	0.01750	0.01903	0.03637
0.07500	0.02136	0.02473	0.01206	0.01576	0.03909
0.05000	0.03301	0.06839	0.01353	0.01866	0.02735
0.00000	0.01435	0.01158	0.00987	0.00975	0.08561

(i) $\overline{v'w'}/u_o^2$

TABLE IX

TIME-MEAN AND TURBULENCE DATA FOR NONSWIRLING FLOW $\phi = 0°$, $D/d = 1$

R/D	X/D 0.0	0.5	1.0	1.5	2.0	2.5
0.40000	0.95691	0.96237	0.97277	0.98534	0.97740	0.97020
0.35000	0.95635	0.96568	0.98597	0.98450	0.99022	0.98496
0.30000	0.95691	0.96621	0.98450	0.98617	0.98329	0.97782
0.25000	0.95744	0.96390	0.98290	0.99310	0.98718	0.98544
0.20000	0.94775	0.97164	0.98439	0.99249	0.98391	0.98339
0.15000	0.94961	0.96623	0.98300	0.98767	0.98568	0.98554
0.10000	0.97350	0.95846	0.98290	0.98634	0.98401	0.98495
0.05000	0.97189	0.95344	0.98488	0.99133	0.98718	0.97842
0.00000	0.98321	0.94699	0.98300	0.98299	0.98559	0.98544

(a) u/u_o

TABLE IX (Continued)

R/D	X/D 0.0	0.5	1.0	1.5	2.0	2.5
0.40000	0.18739	0.25598	0.20737	0.19801	0.22136	0.20864
0.35000	0.19032	0.20588	0.19848	0.20586	0.17671	0.20532
0.30000	0.18710	0.23001	0.20590	0.21324	0.20709	0.21944
0.25000	0.18354	0.21519	0.21360	0.21235	0.20641	0.20263
0.20000	0.18434	0.20085	0.20606	0.21560	0.20930	0.21212
0.15000	0.20579	0.22989	0.21326	0.20296	0.21633	0.20264
0.10000	0.18949	0.24273	0.21335	0.23165	0.20928	0.20537
0.05000	0.20439	0.22491	0.20323	0.22109	0.20645	0.21626
0.00000	0.19351	0.25228	0.21338	0.21226	0.19784	0.20240

(b) v/u_o

TABLE IX (Continued)

R/D	X/D 0.0	0.5	1.0	1.5	2.0	2.5
0.40000	0.01040	0.01065	0.01149	0.01096	0.00984	0.01151
0.35000	0.01032	0.01033	0.01160	0.01097	0.01113	0.01049
0.30000	0.01022	0.01027	0.01093	0.01089	0.01037	0.00996
0.25000	0.00975	0.01026	0.01102	0.01048	0.01091	0.01100
0.20000	0.00947	0.01062	0.01142	0.01059	0.01077	0.01068
0.15000	0.00889	0.01149	0.01125	0.01068	0.01108	0.01074
0.10000	0.00909	0.00972	0.01152	0.01090	0.01081	0.01029
0.05000	0.00897	0.00978	0.01158	0.01018	0.01086	0.01037
0.00000	0.00910	0.01030	0.01138	0.01042	0.01026	0.01114

(c) u'_{rms}/u_o

TABLE IX (Continued)

R/D	X/D 0.0	0.5	1.0	1.5	2.0	2.5
0.40000	0.01305	0.00616	0.01160	0.01168	0.00576	0.01069
0.35000	0.01305	0.00704	0.01221	0.01097	0.01930	0.01019
0.30000	0.01395	0.00480	0.01058	0.01043	0.01049	0.00593
0.25000	0.01480	0.00583	0.01030	0.00709	0.01182	0.01114
0.20000	0.01421	0.01043	0.01214	0.00733	0.01070	0.01018
0.15000	0.00602	0.00638	0.01216	0.01183	0.01058	0.01085
0.10000	0.01130	0.00380	0.01200	0.00743	0.01101	0.00974
0.05000	0.00841	0.00479	0.01258	0.00610	0.01132	0.00662
0.00000	0.01315	0.00365	0.01153	0.00973	0.01068	0.01255

(d) v'_{rms}/u_o

TABLE IX (Continued)

R/D	X/D 0.0	0.5	1.0	1.5	2.0	2.5
0.40000	0.00584	0.00686	0.00651	0.00629	0.00596	0.00667
0.35000	0.00581	0.00588	0.00657	0.00633	0.00614	0.00621
0.30000	0.00575	0.00598	0.00638	0.00614	0.00601	0.00576
0.25000	0.00543	0.00593	0.00629	0.00601	0.00622	0.00623
0.20000	0.00549	0.00642	0.00645	0.00602	0.00614	0.00616
0.15000	0.00514	0.00653	0.00638	0.00627	0.00633	0.00609
0.10000	0.00549	0.00582	0.00645	0.00554	0.00608	0.00600
0.05000	0.00527	0.00562	0.00643	0.00592	0.00610	0.00595
0.00000	0.00518	0.00605	0.00658	0.00605	0.00610	0.00630

(e) w'_{rms}/u_o

TABLE IX (Continued)

R/D	X/D 0.0	0.5	1.0	1.5	2.0	2.5
0.40000	0.00002	0.00002	0.00002	0.00001	0.00001	0.00001
0.35000	0.00001	0.00001	0.00001	0.00001	0.00005	0.00001
0.30000	0.00001	0.00001	0.00001	0.00001	0.00001	0.00001
0.25000	0.00001	0.00001	0.00001	0.00001	0.00002	0.00001
0.20000	0.00001	0.00001	0.00001	0.00001	0.00001	0.00001
0.15000	0.00001	0.00002	0.00002	0.00001	0.00002	0.00001
0.10000	0.00001	0.00001	0.00002	0.00001	0.00001	0.00001
0.05000	0.00001	0.00001	0.00002	0.00001	0.00001	0.00001
0.00000	0.00001	0.00001	0.00002	0.00001	0.00001	0.00002

(f) $\overline{u'v'}/u_o^2$

TABLE X

TIME-MEAN AND TURBULENCE DATA FOR SWIRLING FLOW $\phi = 45°$, $D/d = 1$

R/D	X/D 0.0	0.5	1.0	1.5	2.0	2.5
0.40000	1.18549	1.00735	1.06299	1.03988	1.08904	1.05625
0.35000	1.13369	1.18345	1.08473	1.11666	1.12213	1.08154
0.30000	0.90400	1.19202	1.11702	1.08744	1.11471	1.07422
0.25000	0.64494	1.02705	1.00901	0.99255	1.06866	0.98362
0.20000	0.65108	0.73032	0.80941	0.81242	0.88494	0.80682
0.15000	0.94149	0.56437	0.64497	0.66163	0.71642	0.65760
0.10000	0.88221	0.69893	0.64975	0.63718	0.62408	0.57497
0.05000	0.69509	0.80690	0.61296	0.60459	0.54871	0.53031
0.00000	0.45368	0.48991	0.60383	0.48669	0.42516	0.44334

(a) u/u_o

TABLE X (Continued)

R/D	X/D 0.0	0.5	1.0	1.5	2.0	2.5
0.40000	-0.35796	-0.39705	-0.32888	-0.37152	-0.29429	-0.32840
0.35000	-0.44089	-0.44469	-0.38894	-0.36172	-0.30857	-0.35767
0.30000	-0.43907	-0.51899	-0.43738	-0.39130	-0.35244	-0.35134
0.25000	-0.35738	-0.47963	-0.40294	-0.43076	-0.37362	-0.31067
0.20000	-0.37322	-0.41710	-0.30511	-0.35882	-0.35204	-0.33478
0.15000	-0.38264	-0.42676	-0.28449	-0.27685	-0.25490	-0.24257
0.10000	-0.38156	-0.43182	-0.23326	-0.23832	-0.23953	-0.28309
0.05000	-0.31287	-0.50141	-0.26397	-0.24474	-0.22955	-0.16186
0.00000	-0.41983	-0.57815	-0.37440	-0.35047	-0.26195	-0.20889

(b) v/u_o

TABLE X (Continued)

R/D	X/D 0.0	0.5	1.0	1.5	2.0	2.5
0.40000	1.62370	1.10494	1.16475	1.10877	1.06865	1.05235
0.35000	1.84793	1.22001	1.27788	1.24079	1.18844	1.16480
0.30000	1.96662	1.38906	1.40765	1.37115	1.32513	1.31613
0.25000	1.70000	1.54840	1.51550	1.49386	1.46145	1.42993
0.20000	1.29943	1.40419	1.39789	1.37854	1.35636	1.28195
0.15000	0.90066	1.05145	0.95292	0.93625	0.94806	0.85561
0.10000	0.84431	0.71837	0.68540	0.60931	0.62430	0.52053
0.05000	0.71966	0.53579	0.57890	0.49868	0.45204	0.37528
0.00000	0.18194	0.20806	0.04266	0.21733	0.04539	0.02353

(c) w/u_o

TABLE X (Continued)

R/D	X/D 0.0	0.5	1.0	1.5	2.0	2.5
0.40000	0.12427	0.11699	0.10202	0.09109	0.07997	0.07134
0.35000	0.11187	0.12854	0.09885	0.08983	0.07119	0.06318
0.30000	0.12671	0.11573	0.14058	0.08793	0.08340	0.06187
0.25000	0.15179	0.11636	0.12337	0.09394	0.07759	0.07353
0.20000	0.16379	0.12585	0.12414	0.11004	0.09587	0.09175
0.15000	0.18181	0.09069	0.09129	0.09377	0.08920	0.07984
0.10000	0.20298	0.07945	0.07438	0.07416	0.07008	0.07120
0.05000	0.28790	0.08526	0.07985	0.07448	0.07831	0.08554
0.00000	0.26561	0.15732	0.16557	0.11273	0.11611	0.11482

(d) u'_{rms}/u_o

TABLE X (Continued)

R/D	X/D 0.0	0.5	1.0	1.5	2.0	2.5
0.40000	0.15755	0.16619	0.14470	0.11248	0.11144	0.11998
0.35000	0.08790	0.16650	0.10659	0.14325	0.10601	0.08878
0.30000	0.14918	0.14560	0.12619	0.10653	0.09618	0.08273
0.25000	0.17896	0.14253	0.12349	0.08374	0.07906	0.10626
0.20000	0.14476	0.17426	0.14952	0.07987	0.08145	0.06671
0.15000	0.16010	0.12785	0.09635	0.09318	0.11699	0.08852
0.10000	0.16806	0.11522	0.10542	0.10250	0.08419	0.07906
0.05000	0.19801	0.14065	0.09019	0.10546	0.09568	0.09635
0.00000	0.17257	0.15884	0.13266	0.11838	0.11217	0.07738

(e) v'_{rms}/u_o

TABLE X (Continued)

R/D	X/D 0.0	0.5	1.0	1.5	2.0	2.5
0.40000	0.12748	0.11103	0.08961	0.08017	0.06656	0.06416
0.35000	0.10798	0.11798	0.09672	0.08153	0.06367	0.05584
0.30000	0.14675	0.10350	0.12107	0.08109	0.08139	0.05879
0.25000	0.17727	0.11364	0.11897	0.09031	0.07459	0.07212
0.20000	0.19078	0.13182	0.13832	0.12378	0.10685	0.10810
0.15000	0.17087	0.10669	0.10816	0.11616	0.10861	0.09351
0.10000	0.18888	0.08057	0.07510	0.07050	0.07020	0.07305
0.05000	0.26716	0.08376	0.08361	0.07076	0.08052	0.08756
0.00000	0.18482	0.13600	0.14263	0.11930	0.10500	0.08839

(f) w'_{rms}/u_o

TABLE X (Continued)

R/D	X/D 0.0	0.5	1.0	1.5	2.0	2.5
0.40000	0.00753	0.01107	0.00993	0.00305	0.00265	0.00370
0.35000	0.00433	0.00791	0.00941	0.00531	0.00317	0.00172
0.30000	0.01265	0.00716	0.00636	0.00305	0.00257	0.00321
0.25000	0.02521	0.01011	0.02119	0.00449	0.00575	0.00378
0.20000	0.01149	0.00937	0.01139	0.00550	0.00497	0.00331
0.15000	0.01468	0.00478	0.00341	0.00313	0.00360	0.00264
0.10000	0.01176	0.00259	0.00206	0.00232	0.00220	0.00234
0.05000	0.02182	0.00280	0.00276	0.00311	0.00264	0.00333
0.00000	0.01327	0.00675	0.02568	0.00493	0.00432	0.00286

(g) $\overline{u'v'}/u_o^2$

TABLE X (Continued)

R/D	X/D 0.0	0.5	1.0	1.5	2.0	2.5
0.40000	0.00670	0.00378	0.00400	0.00264	0.00201	0.00170
0.35000	0.00446	0.00576	0.00423	0.00231	0.00139	0.00155
0.30000	0.00547	0.00420	0.00983	0.00278	0.00534	0.00113
0.25000	0.00831	0.00468	0.00522	0.00317	0.00210	0.00190
0.20000	0.00863	0.00558	0.00616	0.00490	0.00386	0.00354
0.15000	0.01375	0.00260	0.00311	0.00317	0.00299	0.00265
0.10000	0.01237	0.00165	0.00165	0.00170	0.00172	0.00266
0.05000	0.02829	0.00211	0.00230	0.00144	0.00243	0.00257
0.00000	0.02327	0.00572	0.00628	0.00540	0.00296	0.00131

(h) $\overline{u'w'}/u_o^2$

TABLE X (Continued)

R/D	X/D 0.0	0.5	1.0	1.5	2.0	2.5
0.40000	0.00551	0.00624	0.00556	0.00329	0.00184	0.00160
0.35000	0.00391	0.00536	0.00600	0.00303	0.00162	0.00208
0.30000	0.00741	0.00622	0.00778	0.00428	0.00378	0.00166
0.25000	0.00915	0.00683	0.00683	0.00450	0.00308	0.00164
0.20000	0.01000	0.00689	0.00640	0.00413	0.00298	0.00249
0.15000	0.00859	0.00407	0.00565	0.00463	0.00526	0.00354
0.10000	0.01041	0.00267	0.00170	0.00198	0.00197	0.00221
0.05000	0.01827	0.00330	0.00239	0.00213	0.00304	0.00423
0.00000	0.00891	0.00842	0.00720	0.00381	0.00530	0.00548

(i) $\overline{v'w'}/u_o^2$

TABLE XI

TIME-MEAN AND TURBULENCE DATA FOR SWIRLING
FLOW ϕ 70°, D/d = 1

R/D	X/D 0.0	0.5	1.0	1.5	2.0	2.5
0.40000	0.96916	1.39540	1.31862	1.54532	1.44842	1.56530
0.35000	0.68737	1.24505	1.20356	1.33750	1.25229	1.37570
0.30000	0.45968	0.95934	0.86565	0.97687	0.95379	1.05196
0.25000	0.49724	0.64804	0.53392	0.62789	0.63652	0.67435
0.20000	0.41193	0.50722	0.33662	0.46917	0.48091	0.53746
0.15000	0.43384	0.50370	0.38377	0.53126	0.54320	0.59537
0.10000	0.48320	0.62213	0.47881	0.58299	0.59273	0.62264
0.05000	0.29888	0.43734	0.31956	0.35852	0.33742	0.38893
0.00000	0.24105	0.21781	0.26216	0.50040	0.35674	0.29737

(a) u/u_o

TABLE XI (Continued)

R/D	X/D 0.0	0.5	1.0	1.5	2.0	2.5
0.40000	-0.87473	-0.85858	-0.74571	-0.65854	-0.62449	-0.59624
0.35000	-0.93201	-0.88228	-0.72452	-0.64644	-0.51469	-0.70527
0.30000	-0.95093	-0.76984	-0.66105	-0.67129	-0.63591	-0.65284
0.25000	-0.69600	-0.66485	-0.58064	-0.61537	-0.62756	-0.62817
0.20000	-0.42010	-0.57234	-0.57819	-0.50940	-0.61207	-0.54206
0.15000	-0.47944	-0.53127	-0.47535	-0.51312	-0.42770	-0.52410
0.10000	-0.47253	-0.47449	-0.44797	-0.45131	-0.39607	-0.42876
0.05000	-0.49340	-0.40731	-0.35214	-0.36155	-0.37473	-0.38378
0.00000	-0.64070	-0.55437	-0.52542	-0.36087	-0.41796	-0.48731

(b) v/u_o

TABLE XI (Continued)

R/D	X/D 0.0	0.5	1.0	1.5	2.0	2.5
0.40000	3.68524	3.29227	3.03081	2.88351	2.69193	2.60096
0.35000	3.66816	3.48987	3.21755	3.16599	2.95113	2.89234
0.30000	3.53561	3.31105	3.12769	3.08672	2.86707	2.90785
0.25000	3.06514	2.86767	2.83523	2.79280	2.62267	2.70156
0.20000	2.35935	2.58671	2.49177	2.55418	2.39492	2.46870
0.15000	1.77326	2.20931	2.13293	2.13768	2.02313	2.05116
0.10000	1.64778	1.74692	1.65754	1.61651	1.55514	1.51023
0.05000	1.30221	1.47941	1.34895	1.23680	1.16812	1.17233
0.00000	0.42987	0.39632	0.31035	0.39868	0.31932	0.45583

(c) w/u_o

TABLE XI (Continued)

R/D	X/D 0.0	0.5	1.0	1.5	2.0	2.5
0.40000	0.24056	0.16244	0.11276	0.15604	0.14081	0.15585
0.35000	0.25802	0.13878	0.11798	0.12535	0.12647	0.14460
0.30000	0.19850	0.14521	0.12165	0.11593	0.11341	0.13029
0.25000	0.19100	0.11790	0.10385	0.08622	0.08432	0.08566
0.20000	0.22368	0.09785	0.08327	0.08056	0.07198	0.07279
0.15000	0.19129	0.09789	0.08599	0.08272	0.08634	0.08459
0.10000	0.19231	0.11109	0.09591	0.09706	0.10192	0.10428
0.05000	0.24747	0.15651	0.14546	0.15378	0.15545	0.15152
0.00000	0.42688	0.40798	0.33071	0.29568	0.38963	0.41305

(d) u'_{rms}/u_o

TABLE XI (Continued)

R/D	X/D 0.0	0.5	1.0	1.5	2.0	2.5
0.40000	0.34548	0.17349	0.12829	0.13514	0.15022	0.13683
0.35000	0.36225	0.19190	0.17212	0.20558	0.16390	0.14238
0.30000	0.31337	0.22495	0.19497	0.17490	0.17640	0.20356
0.25000	0.28187	0.20545	0.17596	0.15967	0.14469	0.14249
0.20000	0.30662	0.19049	0.13811	0.16951	0.12926	0.16248
0.15000	0.22060	0.16240	0.16211	0.14883	0.17125	0.18307
0.10000	0.23246	0.13379	0.13804	0.11566	0.13724	0.11611
0.05000	0.24872	0.17155	0.19548	0.17760	0.18096	0.19824
0.00000	0.24982	0.21379	0.21542	0.22964	0.18928	0.17940

(e) v'_{rms}/u_o

TABLE XI (Continued)

R/D	X/D 0.0	0.5	1.0	1.5	2.0	2.5
0.40000	0.35450	0.17818	0.11871	0.16368	0.14099	0.15297
0.35000	0.35529	0.16645	0.12588	0.13645	0.13751	0.14237
0.30000	0.32300	0.18020	0.14690	0.13568	0.13291	0.13820
0.25000	0.31672	0.15530	0.13595	0.11736	0.10870	0.11040
0.20000	0.32553	0.15002	0.11845	0.10993	0.10215	0.09940
0.15000	0.25880	0.14961	0.12153	0.11997	0.12371	0.11864
0.10000	0.25473	0.15379	0.12938	0.12572	0.12986	0.12271
0.05000	0.33082	0.20794	0.17837	0.17077	0.18860	0.15715
0.00000	0.49734	0.41293	0.40983	0.37406	0.35371	0.41667

(f) w'_{rms}/u_o

TABLE XI (Continued)

R/D	X/D 0.0	0.5	1.0	1.5	2.0	2.5
0.40000	0.03414	0.01889	0.01161	0.01282	0.01180	0.00880
0.35000	0.01164	0.01095	0.01704	0.01448	0.02442	0.01493
0.30000	0.02185	0.01222	0.02612	0.01303	0.01869	0.01247
0.25000	0.02489	0.00985	0.04619	0.00489	0.00404	0.00632
0.20000	0.04136	0.01159	0.00378	0.00224	0.00326	0.00169
0.15000	0.01624	0.00242	0.00263	0.00343	0.00455	0.00295
0.10000	0.01119	0.00498	0.00409	0.00570	0.01691	0.00569
0.05000	0.02982	0.01204	0.00656	0.01872	0.01068	0.01635
0.00000	0.04258	0.02983	0.05754	0.02447	0.01340	0.04284

(g) $\overline{u'v'}/u_o^2$

TABLE XI (Continued)

R/D	X/D 0.0	0.5	1.0	1.5	2.0	2.5
0.40000	0.02583	0.00983	0.00423	0.00841	0.00733	0.00899
0.35000	0.02434	0.00834	0.00512	0.00518	0.00574	0.00714
0.30000	0.01128	0.00771	0.00546	0.00491	0.00481	0.00618
0.25000	0.01145	0.00450	0.00384	0.00259	0.00210	0.00212
0.20000	0.01666	0.00426	0.00166	0.00152	0.00152	0.00142
0.15000	0.01270	0.00199	0.00142	0.00094	0.00295	0.00163
0.10000	0.01425	0.00452	0.00319	0.00377	0.00485	0.00362
0.05000	0.02021	0.00859	0.00653	0.00754	0.00893	0.00644
0.00000	0.05646	0.04231	0.07119	0.03460	0.03039	0.01449

(h) $\overline{u'w'}/u_o^2$

TABLE XI (Continued)

R/D	X/D 0.0	0.5	1.0	1.5	2.0	2.5
0.40000	0.05123	0.00739	0.00682	0.00713	0.00702	0.00724
0.35000	0.04781	0.01042	0.00706	0.00749	0.00644	0.00774
0.30000	0.06877	0.01397	0.00985	0.00657	0.00670	0.00934
0.25000	0.03187	0.00962	0.00956	0.00731	0.00505	0.00587
0.20000	0.03272	0.01045	0.00650	0.00475	0.00448	0.00472
0.15000	0.01971	0.00912	0.00625	0.00961	0.00840	0.00769
0.10000	0.02207	0.00702	0.00615	0.00459	0.00664	0.00477
0.05000	0.02702	0.01331	0.01224	0.01096	0.01415	0.01085
0.00000	0.02358	0.03737	0.09601	0.04847	0.02987	0.05598

(i) $\overline{v'w'}/u_o^2$

TABLE XII

EDDY DISSIPATION RATE FOR NONSWIRLING
FLOW $\phi = 0°$, $D/d = 2$

R/D	X/D 0.0	0.5	1.0	1.5	2.0	2.5
0.40000	0.2132	0.02745	0.13813	0.20029	0.16351	0.12194
0.37500	0.1207	0.04346	0.15351	0.20255	0.18896	0.12658
0.35000	0.0959	0.06522	0.20544	0.22457	0.19727	0.12933
0.32500	0.0725	0.12932	0.19411	0.21370	0.19038	0.12628
0.30000	0.0644	0.24867	0.19490	0.20873	0.18409	0.12102
0.27500	0.0661	0.30299	0.18795	0.20389	0.17966	0.12848
0.25000	0.1956	0.25481	0.15930	0.17369	0.16384	0.11831
0.22500	0.0012	0.07538	0.11253	0.15879	0.15064	0.11276
0.20000	0.0012	0.00538	0.07366	0.12329	0.14103	0.11183
0.17500	0.0012	0.00112	0.03850	0.09268	0.12084	0.10895
0.15000	0.0012	0.00109	0.02283	0.07199	0.10207	0.10112
0.12500	0.0012	0.00109	0.00935	0.05325	0.09185	0.09075
0.10000	0.0012	0.00109	0.00611	0.03974	0.08111	0.08883
0.07500	0.0013	0.00108	0.00181	0.02980	0.06948	0.08883
0.05000	0.0013	0.00107	0.00160	0.02503	0.06281	0.08158
0.02500	0.0013	0.00107	0.00168	0.02004	0.05615	0.08088
0.00000	0.0014	0.00107	0.00164	0.01564	0.05354	0.07951

$$\frac{\varepsilon}{u_o^3 \, d^2/D^3}$$

TABLE XIII

TURBULENT DISSIPATION LENGTH SCALE FOR NON-SWIRLING FLOW $\phi = 0°$, $D/d = 2$

R/D	X/D 0.0	0.5	1.0	1.5	2.0	2.5
0.40000	0.0011	0.01550	0.03098	0.02282	0.03699	0.03992
0.37500	0.0029	0.02857	0.02811	0.03549	0.04379	0.04916
0.35000	0.0030	0.01954	0.02976	0.03638	0.04311	0.06637
0.32500	0.0048	0.02136	0.05981	0.05706	0.08272	0.08687
0.30000	0.0079	0.02120	0.07807	0.07435	0.10107	0.11809
0.27500	0.0077	0.03431	0.09711	0.10943	0.10858	0.13349
0.25000	0.0039	0.05890	0.12564	0.11669	0.14679	0.19216
0.22500	0.0076	0.10663	0.15256	0.12834	0.19270	0.21977
0.20000	0.0107	0.13215	0.17890	0.14629	0.24960	0.22772
0.17500	0.0032	0.15888	0.14758	0.18069	0.23651	0.26427
0.15000	0.0041	0.03447	0.05286	0.14134	0.33538	0.27980
0.12500	0.0116	2.34259	0.06843	0.11167	0.41507	0.31713
0.10000	0.0055	0.02522	0.05016	0.14641	0.49840	0.35550
0.07500	0.0041	0.01413	0.13379	0.06835	0.64084	0.38764
0.05000	0.0039	0.01149	0.06435	0.15522	0.67997	0.40725
0.02500	0.0036	0.01967	0.10883	0.15066	0.80523	0.48078
0.00000	0.0033	0.24863	0.06480	0.14164	0.82711	0.45121

ℓ/D

TABLE XIV

EDDY DISSIPATION RATE FOR SWIRLING FLOW $\phi = 45°$, $D/d = 2$

R/D	X/D 0.0	0.5	1.0	1.5	2.0	2.5
0.40000	0.53285	2.63818	0.66902	0.07787	0.06683	0.02181
0.37500	0.46495	2.41473	0.65175	0.07776	0.06785	0.02199
0.35000	0.39778	2.06796	0.58861	0.07678	0.07088	0.02194
0.32500	0.34589	1.83089	0.53923	0.07668	0.07587	0.02212
0.30000	0.30352	1.27736	0.47720	0.07668	0.07787	0.02238
0.27500	0.35454	0.62444	0.46133	0.07466	0.07899	0.02256
0.25000	10.69514	0.39914	0.40645	0.07466	0.08101	0.02274
0.22500	2.44690	0.33506	0.39064	0.07668	0.08321	0.02262
0.20000	3.08548	0.26991	0.35222	0.07862	0.08248	0.02232
0.17500	3.98031	0.25330	0.33235	0.08732	0.08275	0.02115
0.15000	2.28597	0.22745	0.31068	0.09800	0.15089	0.01968
0.12500	0.82920	0.23765	0.30020	0.11683	0.14740	0.01959
0.10000	0.40974	0.24724	0.29080	0.14354	0.08119	0.01930
0.07500	0.17704	0.24187	0.27973	0.15464	0.06370	0.02146
0.05000	0.09434	0.24874	0.31975	0.21786	0.06835	0.02756
0.02500	0.08100	0.23716	0.32977	0.29133	0.07839	0.04019
0.00000	0.07973	0.22470	0.38197	0.22509	0.09494	0.05688

$$\frac{\varepsilon}{u_o^3 \, d^2/D^3}$$

TABLE XV

TURBULENT DISSIPATION LENGTH SCALE FOR SWIRLING FLOW $\phi = 45°$, $D/d = 2$

R/D	X/D 0.0	0.5	1.0	1.5	2.0	2.5
0.40000	0.0190	0.03789	0.02972	0.00000	0.02133	0.06276
0.37500	0.0227	0.04597	0.02585	0.08237	0.03063	0.04921
0.35000	0.0251	0.05318	0.02574	0.08079	0.02749	0.05425
0.32500	0.0268	0.03575	0.02390	0.08026	0.03126	0.05703
0.30000	0.0295	0.12931	0.02555	0.07919	0.02742	0.05884
0.27500	0.0320	0.05373	0.02187	0.07852	0.03278	0.06734
0.25000	0.0074	0.04306	0.02243	0.06198	0.03588	0.06241
0.22500	0.0188	0.04021	0.02173	0.06577	0.04279	0.09251
0.20000	0.0041	0.04208	0.02165	0.07547	0.04727	0.10705
0.17500	0.0133	0.03816	0.02365	0.07002	0.04401	0.08071
0.15000	0.0371	0.03879	0.02598	0.06483	0.02355	0.10549
0.12500	0.0085	0.03612	0.02630	0.05471	0.02898	0.12477
0.10000	0.0054	0.03797	0.02575	0.04720	0.05384	0.14121
0.07500	0.0072	0.04490	0.02709	0.04208	0.07363	0.20626
0.05000	0.0121	0.03279	0.02410	0.03449	0.07785	0.18022
0.02500	0.0118	0.04019	0.02611	0.02274	0.07796	0.17651
0.00000	0.0118	0.04368	0.03356	0.03134	0.08135	0.26216

ℓ/D

TABLE XVI

EDDY DISSIPATION RATE FOR SWIRLING
FLOW $\phi = 70°$, $D/d = 2$

R/D	X/D 0.0	0.5	1.0	1.5	2.0	2.5
0.40000	11.1470	6.84526	1.30463	0.53967	0.37635	0.22396
0.37500	10.2957	5.81686	1.30675	0.53175	0.37071	0.20687
0.35000	10.0253	4.46902	1.30675	0.52399	0.35217	0.18750
0.32500	9.2281	3.52620	1.27500	0.49918	0.34692	0.18479
0.30000	8.7530	2.82470	1.25684	0.47504	0.34179	0.16913
0.27500	9.7939	2.22108	1.12189	0.45807	0.31905	0.16913
0.25000	244.7585	1.86164	1.08733	0.44111	0.31905	0.16913
0.22500	88.8377	1.61360	0.97354	0.40717	0.31905	0.18214
0.20000	82.5523	1.37915	0.83157	0.37869	0.31510	0.18750
0.17500	95.1438	1.28775	0.73386	0.35450	0.32983	0.19026
0.15000	31.5657	1.12745	0.56831	0.35753	0.34560	0.19596
0.12500	7.8883	0.99626	0.46715	0.35111	0.38071	0.21135
0.10000	6.4776	0.89717	0.42500	0.40029	0.42142	0.23225
0.07500	5.8435	0.82685	0.39275	0.49664	0.50546	0.28413
0.05000	4.8939	0.81994	0.43987	0.62290	0.74237	0.39283
0.02500	3.8009	0.98153	0.65454	0.93257	1.06569	0.58451
0.00000	4.1386	1.31648	1.08092	1.49088	1.58223	0.91911

$$\frac{\varepsilon}{u_o^3 \, d^2/D^3}$$

TABLE XVII

TURBULENT DISSIPATION LENGTH SCALE FOR
SWIRLING FLOW ϕ = 70°, D/d = 2

R/D	X/D 0.0	0.5	1.0	1.5	2.0	2.5
0.40000	0.0090	0.02207	0.02898	0.01004	0.01393	0.08717
0.37500	0.0084	0.02127	0.03044	0.00867	0.01239	0.06720
0.35000	0.0079	0.02209	0.03130	0.01009	0.01759	0.08543
0.32500	0.0080	0.01934	0.02495	0.01081	0.03227	0.11349
0.30000	0.0080	0.01986	0.02735	0.01469	0.03011	0.16367
0.27500	0.0107	0.01961	0.03347	0.02752	0.03274	0.12289
0.25000	0.0025	0.02424	0.03632	0.01618	0.03073	0.13314
0.22500	0.0072	0.02158	0.03840	0.02000	0.02756	0.09898
0.20000	0.0094	0.02810	0.04072	0.01260	0.02496	0.04181
0.17500	0.0043	0.02836	0.04750	0.02075	0.02184	0.03955
0.15000	0.0026	0.03198	0.04707	0.02967	0.02568	0.05257
0.12500	0.0083	0.03471	0.05308	0.03429	0.03752	0.08120
0.10000	0.0063	0.03932	0.06021	0.03168	0.04897	0.12079
0.07500	0.0055	0.04085	0.06916	0.03137	0.05602	0.13657
0.05000	0.0053	0.03542	0.05754	0.03793	0.05143	0.15264
0.02500	0.0064	0.02421	0.04975	0.03160	0.04059	0.11586
0.00000	0.0082	0.02186	0.02819	0.09125	0.03649	0.11731

ℓ/D

TABLE XVIII

EDDY DISSIPATION RATE FOR NONSWIRLING
FLOW $\phi = 0°$, $D/d = 1$

R/D	X/D 0.0	0.5	1.5	2.0	2.0
0.40000	0.0002	0.00016	0.00016	0.00016	0.00016
0.35000	0.0002	0.00015	0.00015	0.00016	0.00016
0.30000	0.0002	0.00016	0.00015	0.00016	0.00016
0.25000	0.0002	0.00016	0.00015	0.00016	0.00016
0.20000	0.0002	0.00017	0.00015	0.00017	0.00016
0.15000	0.0002	0.00017	0.00015	0.00018	0.00017
0.10000	0.0002	0.00017	0.00015	0.00018	0.00017
0.05000	0.0002	0.00018	0.00015	0.00020	0.00020
0.00000	0.0002	0.00017	0.00016	0.00020	0.00023

$$\frac{\varepsilon}{u_o^3 \, d^2/D^3}$$

TABLE XIX

TURBULENT DISSIPATION LENGTH SCALE FOR NONSWIRLING FLOW $\phi = 0°$, $D/d = 1$

R/D	X/D 0.0	0.5	1.5	2.0	2.0
0.40000	0.0123	0.00634	0.01156	0.00470	0.01109
0.35000	0.0128	0.00608	0.01085	0.02799	0.00910
0.30000	0.0140	0.00478	0.00996	0.00917	0.00492
0.25000	0.0147	0.00497	0.00634	0.01144	0.01085
0.20000	0.0134	0.00905	0.00670	0.00933	0.00912
0.15000	0.0038	0.00651	0.01152	0.00910	0.00928
0.10000	0.0085	0.00355	0.00672	0.00885	0.00750
0.05000	0.0053	0.00361	0.00535	0.00851	0.00455
0.00000	0.0103	0.00399	0.00838	0.00714	0.00886

ℓ/D

TABLE XX

EDDY DISSIPATION RATE FOR SWIRLING FLOW $\phi = 45°$, $D/d = 1$

R/D	X/D 0.0	0.5	1.5	2.0	2.5
0.40000	0.3485	0.10730	0.07017	0.04747	0.05148
0.35000	0.2766	0.11498	0.08286	0.05044	0.04685
0.30000	0.0419	0.15721	0.10236	0.04647	0.03575
0.25000	0.3184	0.17357	0.10989	0.04788	0.03146
0.20000	0.4144	0.14901	0.07216	0.03203	0.02399
0.15000	0.4956	0.08380	0.02435	0.01623	0.01434
0.10000	0.6623	0.05917	0.00859	0.00771	0.00722
0.05000	0.9433	0.08093	0.00878	0.00627	0.00819
0.00000	0.9231	0.16954	0.03547	0.04795	0.08689

$$\frac{\varepsilon}{u_o^3 \, d^2/D^3}$$

TABLE XXI

TURBULENT DISSIPATION LENGTH SCALE FOR SWIRLING FLOW $\phi = 45°$, $D/d = 1$

R/D	X/D 0.0	0.5	1.5	2.0	2.5
0.40000	0.0136	0.04093	0.02282	0.02639	0.02490
0.35000	0.0073	0.04313	0.02822	0.02036	0.01385
0.30000	0.1234	0.02169	0.01419	0.02625	0.01661
0.25000	0.0282	0.02060	0.01196	0.01759	0.03642
0.20000	0.0208	0.03804	0.03046	0.04963	0.05669
0.15000	0.0183	0.02876	0.07913	0.13321	0.08573
0.10000	0.0182	0.02516	0.12504	0.10103	0.10533
0.05000	0.0319	0.02747	0.12848	0.18111	0.16325
0.00000	0.0189	0.03737	0.08262	0.05267	0.01804

ℓ/D

TABLE XXII

EDDY DISSIPATION RATE FOR SWIRLING
FLOW $\phi = 70°$, $D/d = 1$

R/D	X/D 0.0	0.5	1.0	1.5	2.0	2.5
0.40000	2.7634	0.68206	0.30665	0.41474	0.37897	0.42545
0.35000	2.8850	0.48559	0.19261	0.27656	0.27705	0.33611
0.30000	2.4453	0.31508	0.15655	0.13285	0.14549	0.17919
0.25000	1.9826	0.23232	0.10764	0.09050	0.07013	0.05794
0.20000	1.5822	0.15386	0.05847	0.05934	0.03813	0.02884
0.15000	2.0106	0.07797	0.03140	0.02479	0.01915	0.01445
0.10000	2.0015	0.04197	0.01934	0.01468	0.01296	0.01286
0.05000	0.9741	0.05913	0.07533	0.02855	0.02701	0.04398
0.00000	1.6247	1.17237	1.63111	0.85518	0.94017	1.82331

$$\frac{\varepsilon}{u_o^3 \, d^2/D^3}$$

TABLE XXIII

TURBULENT DISSIPATION LENGTH SCALE FOR SWIRLING FLOW $\phi = 70°$, $D/d = 1$

R/D	X/D 0.0	0.5	1.0	1.5	2.0	2.5
0.40000	0.0213	0.01359	0.01038	0.01559	0.01450	0.01422
0.35000	0.0226	0.01766	0.02657	0.02710	0.01959	0.01602
0.30000	0.0172	0.03772	0.04582	0.04152	0.03719	0.04258
0.25000	0.0179	0.03458	0.04855	0.03943	0.04012	0.04851
0.20000	0.0279	0.04108	0.04845	0.06131	0.05388	0.10394
0.15000	0.0104	0.06389	0.12007	0.12886	0.21947	0.31337
0.10000	0.0109	0.10540	0.17445	0.18273	0.26994	0.21515
0.05000	0.0407	0.18111	0.12924	0.30335	0.36808	0.20613
0.00000	0.0751	0.07139	0.03993	0.06128	0.06577	0.04478

ℓ/D

TABLE XXIV

EFFECT OF INPUT PARAMETERS ON TURBULENCE QUANTITIES IN A CONFINED SWIRLING FLOW WITH SWIRL VANE ANGLE OF 38° AT A REPRESENTATIVE FLOWFIELD POSITION (x/D = 1, r/D = 0.25)

PARAMETER	% CHANGE IN PARAMETER	% CHANGE IN TIME-MEAN AND TURBULENCE QUANTITIES								
		$\bar{u}$	$\bar{v}$	$\bar{w}$	u'_{rms}	v'_{rms}	w'_{rms}	$\overline{u'v'}$	$\overline{u'w'}$	$\overline{v'w'}$
$\bar{E}_1$	+1	+16.10	+0.66	+4.98	+15.75	-2.06	+2.75	+6.0	+51.43	+11.94
$\bar{E}_5$	+1	+2.19	-2.21	+11.49	-6.50	+2.42	+12.88	+4.0	+14.29	+7.46
$\bar{E}_6$	+1	-10.59	-0.36	-8.50	-1.88	+7.07	-9.54	-6.0	-54.29	-11.94
$E'_{1_{rms}}$	+1	+0.27	-0.06	+0.14	+1.63	+0.13	+0.39	+2.0	+2.86	+1.49
$E'_{5_{rms}}$	+1	+0.05	0.0	+0.14	0.0	-0.13	+1.57	0.0	0.0	+1.49
$E'_{6_{rms}}$	+1	-0.16	+0.18	-0.14	-0.63	+1.03	-1.08	-2.0	-5.71	0.0
G	+1	-1.02	0.0	-1.01	-1.0	0.0	-0.98	-2.0	-2.86	-1.49
K	+1	+0.01	-0.04	+0.01	+0.01	0.0	+0.01	0.0	0.0	0.0
$\gamma_{Z_pZ_Q}$	+1	+0.05	0.0	+0.14	-0.13	-0.13	-1.77	0.0	-2.86	+1.49
$\gamma_{Z_QZ_R}$	+1	+0.21	+0.01	+0.05	-1.63	+0.13	-0.79	0.0	-5.71	+1.49
$\gamma_{Z_pZ_R}$	+1	-0.16	+0.18	-0.08	+0.13	0.0	+0.69	-2.0	+2.86	0.0

TABLE XXV

MEASUREMENTS FOR SITUATION A, CASE 1

Combination Used	Measured u/u_o	v/u_o	w/u_o
612	0.978	0.203	0.009
123	0.961	0.199	NR
234	0.970	0.126	0.020
345	0.968	NR*	0.013
456	0.976	0.011	0.008
561	0.967	0.197	0.017
Mean $\bar{x}$	0.970	0.147	0.013
S.D. σ	0.006	0.074	0.005
$\sigma/\bar{x}$	0.006	0.503	0.353

* Not Resolved

TABLE XXVI

MEASUREMENTS FOR SITUATION A, CASE 2

Combination Used	Measured u/u_o	v/u_o	w/u_o
612	0.978	0.031	0.035
123	0.972	0.036	0.040
234	0.990	0.056	0.015
345	0.982	0.043	0.022
456	0.988	0.024	0.049
561	0.986	0.022	0.041
Mean $\bar{x}$	0.983	0.021	0.033
S.D. σ	0.006	0.012	0.012
$\sigma/\bar{x}$	0.006	0.553	0.353

TABLE XXVII

MEASUREMENTS FOR SITUATION A, CASE 3

Combination Used	Measured u/u_o	v/u_o	w/u_o
612	0.954	-0.030	-0.008
123	0.954	-0.031	-0.008
234	0.967	-0.039	-0.051
345	0.948	-0.103	0.080
456	0.971	0.001	-0.003
561	0.951	-0.030	0.006
Mean $\bar{x}$	0.958	-0.039	0.001
S.D. σ	0.008	0.031	0.039
$\sigma/\bar{x}$	0.009	0.805	38.986

TABLE XXVIII

MEASUREMENTS FOR SITUATION A, CASE 5

Combination Used	Measured u/u_o	v/u_o	w/u_o
612	0.976	0.203	0.010
123	0.960	0.200	NR
234	0.971	0.126	0.019
345	0.968	NR	0.013
456	0.976	0.010	0.008
561	0.968	0.198	0.017
Mean $\bar{x}$	0.969	0.147	0.013
S.D. σ	0.005	0.074	0.004
$\sigma/\bar{x}$	0.006	0.503	0.317

TABLE XXIX

MEASUREMENTS FOR SITUATION B, CASE 1

Combinations Used	Measured u/u_o	v/u_o	w/u_o	u'_{rms}/u_o	v'_{rms}/u_o	w'_{rms}/u_o	$\overline{u'v'}/u_o^2$	$\overline{u'w'}/u_o^2$	$\overline{v'w'}/u_o^2$
612	0.593	0.211	0.036	0.171	0.062	0.066	0.0101	0.0019	NR
123	0.577	0.195	0.056	0.142	0.035	0.099	0.0020	0.0010	0.0037
234	0.582	0.220	0.012	0.142	0.091	0.136	0.0001	0.0029	NR
345	0.587	0.110	0.019	0.125	0.209	0.126	0.0001	0.0000	NR
456	0.616	NR	0.014	0.156	0.027	0.148	NR	NR	0.0221
561	0.602	0.207	0.042	0.157	0.079	0.056	0.0031	0.0000	NR
Mean $\bar{x}$	0.593	0.189	0.030	0.149	0.084	0.105	0.0031	0.0012	0.0129
S.D. σ	0.013	0.040	0.016	0.014	0.060	0.035	0.0037	0.0011	0.0092
$\sigma/\bar{x}$	0.022	0.212	0.537	0.098	0.718	0.330	1.1910	0.9350	0.7130

TABLE XXX

MEASUREMENTS FOR SITUATION C, CASE 1

Combination Used	Measured u/u_o	v/u_o	w/u_o	u'_{rms}/u_o	v'_{rms}/u_o	w'_{rms}/u_o	$\overline{u'v'}/u_o^2$	$\overline{u'w'}/u_o^2$	$\overline{v'w'}/u_o^2$
612	0.433	0.158	0.009	0.147	0.052	0.059	0.0077	0.0011	NR
123	0.464	0.153	0.026	0.128	0.067	0.051	0.0022	NR	NR
234	0.477	0.093	0.026	0.127	0.066	0.119	NR	NR	0.0057
345	NR								
456	0.460	0.167	0.034	0.123	0.070	0.118	0.0032	NR	0.0015
561	0.449	0.151	NR	0.124	0.056	0.070	0.0016	NR	NR
Mean $\bar{x}$	0.456	0.144	0.023	0.130	0.062	0.083	0.0038	0.0011	0.0037
S.D. σ	0.015	0.026	0.009	0.009	0.007	0.029	0.0024	0	0.0021
$\sigma/\bar{x}$	0.032	0.182	0.396	0.068	0.112	0.353	0.6468	0	0.5833

TABLE XXXI

MEASUREMENTS FOR SITUATION B, CASE 2

Combination Used	Measured u/u_o	v/u_o	w/u_o	u'_{rms}/u_o	v'_{rms}/u_o	w'_{rms}/u_o	$\overline{u'v'}/u_o^2$	$\overline{u'w'}/u_o^2$	$\overline{v'w'}/u_o^2$
612	0.552	0.039	0.043	0.133	0.133	0.174	-0.0215	-0.0039	0.0039
123	0.554	0.066	0.033	0.168	0.168	0.125	0.0126	0.0011	-0.0011
234	0.520	-0.055	0.162	0.147	0.149	0.156	-0.0058	NR	NR
345	NR	NR	0.124	0.217	0.217	0.300	0.0922	NR	NR
456	0.527	-0.033	0.081	0.137	0.142	0.164	0.0205	NR	NR
561	0.576	0.033	0.112	0.155	0.155	0.103	-0.0001	NR	NR
Mean $\bar{x}$	0.546	0.010	0.092	0.159	0.161	0.170	0.0163	-0.0014	0.0014
S.D. σ	0.020	0.046	0.045	0.028	0.027	0.063	0.0365	0.0025	0.0025
$\sigma/\bar{x}$	0.037	4.600	0.493	0.177	0.170	0.369	2.2371	1.7875	1.7875

TABLE XXXII

MEASUREMENTS FOR SITUATION B, CASE 4

Combinations Used	Measured u/u_o	v/u_o	w/u_o	u'_{rms}/u_o	v'_{rms}/u_o	w'_{rms}/u_o	$\overline{u'v'}/u_o^2$	$\overline{u'w'}/u_o^2$	$\overline{v'w'}/u_o^2$
612	0.537	0.342	0.197	0.097	0.179	0.289	0.0032	0.0003	NR
123	0.607	0.157	0.236	0.140	0.270	0.123	NR	0.0031	0.0234
234	0.501	0.379	0.023	0.071	0.245	0.198	NR	0.0031	NR
345	0.594	0.119	0.326	0.129	0.314	0.079	NR	0.0053	0.0008
456	0.484	0.065	0.408	NR	0.422	0.126	NR	0.0428	NR
561	0.568	NR	NR	0.117	0.281	0.289	NR	NR	0.0007
Mean $\bar{x}$	0.549	0.212	0.238	0.111	0.285	0.184	0.0032	0.0109	0.0083
S.D. σ	0.045	0.125	0.130	0.024	0.074	0.082	0	0.0160	0.0107
$\sigma/\bar{x}$	0.083	0.589	0.546	0.221	0.259	0.446	0	1.4700	1.2864

TABLE XXXIII

MEASUREMENTS FOR SITUATION C, CASE 2

Combination Used	Measured u/u_o	v/u_o	w/u_o	u'_{rms}/u_o	v'_{rms}/u_o	w'_{rms}/u_o	$\overline{u'v'}/u_o^2$	$\overline{u'w'}/u_o^2$	$\overline{v'w'}/u_o^2$
612	0.446	0.052	0.007	0.099	0.099	0.153	0.0090	0.0012	0.0000
123	0.447	0.076	0.050	0.123	0.123	0.096	NR	0.0000	NR
234	0.450	0.084	0.016	0.124	0.124	0.111	0.0110	NR	NR
345	0.458	-0.009	0.004	0.105	0.105	0.133	0.0230	0.0023	NR
456	0.443	0.095	0.017	0.130	0.130	0.132	0.0240	NR	NR
561	0.428	0.100	NR	0.136	0.136	0.099	0.0140	0.0016	0.0025
Mean $\bar{x}$	0.445	0.066	0.019	0.119	0.119	0.121	0.0160	0.0013	0.0012
S.D. σ	0.009	0.037	0.016	0.013	0.013	0.020	0.0062	0.0008	0.0012
$\sigma/\bar{x}$	0.020	0.561	0.862	0.111	0.111	0.169	0.3861	0.6421	1.0000

TABLE XXXIV

MEASUREMENTS FOR SITUATION C, CASE 4

Combination Used	Measured u/u_o	v/u_o	w/u_o	u'_{rms}/u_o	v'_{rms}/u_o	w'_{rms}/u_o	$\overline{u'v'}/u_o^2$	$\overline{u'w'}/u_o^2$	$\overline{v'w'}/u_o^2$
612	0.300	0.471	0.085	NR	NR	0.347	0.0262	NR	0.0779
123	0.360	0.073	0.191	.0.099	.0.285	0.210	NR	NR	NR
234	0.382	0.124	NR	0.109	0.237	0.225	NR	NR	0.0236
345	0.354	0.244	0.135	0.080	0.185	0.214	0.0036	0.0053	NR
456	0.380	0.227	0.191	0.105	0.216	0.181	NR	0.0161	NR
561	0.289	NR	0.279	NR	0.337	0.248	NR	NR	NR
Mean $\bar{x}$	0.343	0.228	0.176	0.098	0.252	0.237	0.0149	0.0107	0.0507
S.D. σ	0.037	0.137	0.065	0.011	0.053	0.053	0.0113	0.0054	0.0271
$\sigma/\bar{x}$	0.107	0.602	0.368	0.113	0.210	0.223	0.7584	0.5047	0.5355

TABLE XXXV

MEASUREMENTS FOR SITUATION B, CASE 3

Combination Used	Measured u/u_o	v/u_o	w/u_o	u'_{rms}/u_o	v'_{rms}/u_o	w'_{rms}/u_o	$\overline{u'v'}/u_o^2$	$\overline{u'w'}/u_o^2$	$\overline{v'w'}/u_o^2$
612	0.548	0.053	-0.022	0.089	0.112	0.118	-0.0015	-0.0261	-0.0272
123	0.575	0.076	-0.006	0.120	0.084	0.088	-0.0084	0.0342	-0.0073
234	0.559	0.022	-0.024	0.099	0.118	0.121	-0.0024	-0.0163	-0.0058
345	0.559	0.037	0.000	0.142	0.139	0.146	-0.0033	-0.0060	-0.0033
456	0.547	0.025	-0.019	0.118	0.159	0.162	0.0181	-0.0428	0.0181
561	0.547	0.063	-0.034	0.135	0.125	0.136	0.0112	0.0044	0.0112
Mean $\bar{x}$	0.556	0.046	-0.017	0.117	0.123	0.128	0.0031	-0.0088	-0.0024
S.D. σ	0.010	0.020	0.011	0.0186	0.023	0.023	0.0100	0.0243	0.0145
$\sigma/\bar{x}$	0.018	0.429	0.669	0.159	0.188	0.183	2.9016	2.7612	6.0300

TABLE XXXVI

MEASUREMENTS FOR SITUATION B, CASE 5

Combinations Used	Measured u/u_o	v/u_o	w/u_o	u'_{rms}/u_o	v'_{rms}/u_o	w'_{rms}/u_o	$\overline{u'v'}/u_o^2$	$\overline{u'w'}/u_o^2$	$\overline{v'w'}/u_o^2$
612	0.656	0.211	0.015	0.170	0.069	0.060	NR	0.0103	NR
123	0.579	0.188	0.043	0.161	0.114	0.031	0.0017	0.0021	0.0051
234	0.587	0.141	0.021	0.163	0.157	0.101	0.0080	NR	NR
345	0.504	0.354	0.012	0.164	0.154	0.133	NR	NR	NR
456	0.590	0.130	0.053	0.148	0.137	0.120	0.0008	NR	NR
561	0.580	0.205	0.065	0.147	0.066	0.047	NR	0.0040	0.0019
Mean $\bar{x}$	0.583	0.205	0.035	0.159	0.116	0.082	0.0035	0.0054	0.0035
S.D. σ	0.044	0.073	0.020	0.008	0.037	0.038	0.0032	0.0035	0.0016
$\sigma/\bar{x}$	0.076	0.357	0.573	0.053	0.320	0.465	0.9143	0.6490	0.4571

TABLE XXXVII

MEASUREMENTS FOR SITUATION C, CASE 3

Combination Used	Measured u/u_o	v/u_o	w/u_o	u'_{rms}/u_o	v'_{rms}/u_o	w'_{rms}/u_o	$\overline{u'v'}/u_o^2$	$\overline{u'w'}/u_o^2$	$\overline{v'w'}/u_o^2$
612	0.467	0.043	-0.057	0.073	0.090	0.092	-0.0130	-0.0146	-0.0008
123	0.451	0.066	-0.063	0.100	0.074	0.075	0.0010	0.0256	-0.0002
234	0.456	0.055	-0.063	0.085	0.106	0.108	-0.0011	0.0199	-0.0029
345	0.448	-0.017	0.002	0.111	0.080	0.114	0.0095	-0.0023	0.0088
456	0.434	0.046	-0.141	0.118	0.115	0.119	0.0188	0.0013	0.0211
561	0.418	0.097	-0.141	0.100	0.101	0.105	0.0143	-0.0032	0.0120
Mean $\bar{x}$	0.446	0.048	-0.060	0.098	0.094	0.102	0.0049	0.0044	0.0063
S.D. σ	0.158	0.034	0.042	0.015	0.014	0.015	0.0106	0.0139	0.0085
$\sigma/\bar{x}$	0.035	0.713	0.707	0.154	0.153	0.145	2.1632	3.1641	1.3516

TABLE XXXVIII

MEASUREMENTS FOR SITUATION C, CASE 5

Combination Used	u/u_o	v/u_o	w/u_o	Measured u'_{rms}/u_o	v'_{rms}/u_o	w'_{rms}/u_o	$\overline{u'v'}/u_o^2$	$\overline{u'w'}/u_o^2$	$\overline{v'w'}/u_o^2$
612	0.417	NR	0.162	0.142	0.062	0.047	0.0044	0.0068	0.0011
123	0.454	0.013	0.152	0.156	0.069	0.061	NR	0.0025	NR
234	0.473	0.024	0.075	0.154	0.147	0.032	NR	NR	0.0083
345	NR								
456	0.453	0.064	0.176	0.141	0.131	0.041	0.0041	0.0038	0.0039
561	0.431	0.014	0.168	0.141	0.038	0.054	0.0023	0.0024	NR
Mean $\bar{x}$	0.446	0.029	0.147	0.147	0.089	0.047	0.0036	0.0038	0.0044
S.D. σ	0.019	0.021	0.037	0.007	0.042	0.010	0.0009	0.0018	0.0030
$\sigma/\bar{x}$	0.044	0.717	0.249	0.046	0.473	0.214	0.2608	0.4676	0.6735

TABLE XXXIX

MEASUREMENTS FOR SITUATION D, CASE 1

Combination Used	u/u_o	v/u_o	w/u_o	Measured u'_{rms}/u_o	v'_{rms}/u_o	w'_{rms}/u_o	$\overline{u'v'}/u_o^2$	$\overline{u'w'}/u_o^2$	$\overline{v'w'}/u_o^2$
612	1.661	0.633	1.616	0.077	0.142	0.106	0.0073	0.0074	0.0056
123	1.763	0.577	1.724	0.127	0.148	0.098	0.0065	0.0120	0.0079
234	1.808	0.355	1.590	0.149	0.138	0.142	NR	0.0018	0.0127
345	1.773	0.457	1.597	0.170	0.196	0.135	NR	0.0063	NR
456	1.726	0.823	1.540	0.142	0.181	0.148	0.0075	0.0020	NR
561	1.702	0.665	1.609	0.138	0.091	0.108	0.0043	0.0045	0.0066
Mean $\bar{x}$	1.739	0.585	1.613	0.134	0.149	0.123	0.0064	0.0057	0.0082
S.D. σ	0.048	0.022	0.055	0.028	0.004	0.019	0.0013	0.0035	0.0027
$\sigma/\bar{x}$	0.029	0.038	0.034	0.213	0.225	0.158	0.1983	0.6131	0.3321

TABLE XL

MEASUREMENTS FOR SITUATION E, CASE 1

Combination Used	Measured u/u_o	v/u_o	w/u_o	u'_{rms}/u_o	v'_{rms}/u_o	w'_{rms}/u_o	$\overline{u'v'}/u_o^2$	$\overline{u'w'}/u_o^2$	$\overline{v'w'}/u_o^2$
612	0.708	0.522	0.424	0.218	0.303	0.341	0.0623	0.0057	0.0422
123	0.562	0.590	0.419	0.420	0.322	0.252	0.0298	0.0108	0.0091
234	0.752	0.269	0.338	0.487	0.129	0.433	NR	0.0020	0.3600
345	0.563	0.482	0.373	0.591	0.121	0.649	0.3900	NR	0.0475
456	0.628	0.323	0.478	0.463	0.135	0.525	0.0384	0.0411	NR
561	0.533	0.563	0.383	0.443	0.304	0.332	NR	0.0881	0.0462
Mean $\bar{x}$	0.624	0.458	0.403	0.437	0.219	0.422	0.0424	0.0295	0.0362
S.D. σ	0.081	0.120	0.044	0.112	0.091	0.133	0.01207	0.0324	0.0141
$\sigma/\bar{x}$	0.130	0.263	0.110	0.256	0.451	0.315	0.2846	1.0975	0.3903

TABLE XLI

MEASUREMENTS FOR SITUATION D, CASE 4

Combination Used	Measured u/u_o	v/u_o	w/u_o	u'_{rms}/u_o	v'_{rms}/u_o	w'_{rms}/u_o	$\overline{u'v'}/u_o^2$	$\overline{u'w'}/u_o^2$	$\overline{v'w'}/u_o^2$
612	1.640	0.806	1.556	0.126	0.112	0.100	0.0054	0.0067	NR
123	1.641	0.747	1.523	0.122	0.098	0.134	NR	0.0002	0.0033
234	1.680	0.806	1.489	0.141	0.171	0.096	0.0024	0.0028	0.0043
345	1.774	0.809	1.394	0.107	0.179	0.183	0.0045	NR	0.0023
456	1.472	1.026	1.532	0.097	0.167	0.155	0.0018	NR	0.0015
561	1.639	0.806	1.654	0.130	0.114	0.132	0.0044	NR	0.0108
Mean $\bar{x}$	1.641	0.833	1.525	0.121	0.140	0.133	0.0037	0.0032	0.0044
S.D. σ	0.089	0.051	0.078	0.015	0.033	0.030	0.0014	0.0027	0.0033
$\sigma/\bar{x}$	0.089	0.107	0.051	0.120	0.234	0.226	0.3690	0.8348	0.7578

TABLE XLII

MEASUREMENTS FOR SITUATION E, CASE 4

Combination Used	Measured u/u_o	v/u_o	w/u_o	u'_{rms}/u_o	v'_{rms}/u_o	w'_{rms}/u_o	$\overline{u'v'}/u_o^2$	$\overline{u'w'}/u_o^2$	$\overline{v'w'}/u_o^2$
612	0.320	0.347	NR	NR	0.856	NR	NR	0.0802	NR
123	0.688	0.596	0.157	0.370	0.196	0.663	0.0080	0.0192	0.0060
234	0.442	0.156	0.647	NR	0.642	0.637	0.0421	0.0309	NR
345	NR	NR	NR	NR	NR	0.914	NR	NR	NR
456	0.430	0.476	0.435	NR	0.694	0.694	0.0313	NR	0.0458
561	0.723	NR	0.289	0.375	0.418	0.613	NR	NR	0.0346
Mean $\bar{x}$	0.521	0.394	0.382	0.373	0.561	0.704	0.0271	0.0440	0.0288
S.D. σ	0.157	0.163	0.182	0.002	0.230	0.108	0.0142	0.0273	0.0167
$\sigma/\bar{x}$	0.302	0.414	0.476	0.007	0.410	0.154	0.5251	0.6197	0.0582

TABLE XLIII

MEASUREMENTS FOR SITUATION D, CASE 5

Combination Used	Measured u/u_o	v/u_o	w/u_o	u'_{rms}/u_o	v'_{rms}/u_o	w'_{rms}/u_o	$\overline{u'v'}/u_o^2$	$\overline{u'w'}/u_o^2$	$\overline{v'w'}/u_o^2$
612	1.777	0.452	1.445	0.128	0.155	0.198	0.0133	NR	0.0133
123	1.744	0.491	1.428	0.186	0.183	0.174	0.0004	NR	0.0186
234	1.703	0.310	1.603	0.196	0.202	0.178	0.0031	NR	0.0179
345	1.852	0.362	1.388	0.126	0.183	0.184	NR	0.0004	0.0215
456	1.853	0.350	1.387	0.124	0.113	0.184	0.0103	0.0009	0.0014
561	1.886	0.491	1.433	0.090	0.110	0.198	NR	NR	0.0124
Mean $\bar{x}$	1.802	0.409	1.447	0.142	0.158	0.186	0.0068	0.0007	0.0142
S.D. σ	0.066	0.072	0.073	0.037	0.035	0.009	0.0052	0.0003	0.0065
$\sigma/\bar{x}$	0.036	0.175	0.050	0.026	0.224	0.492	0.7682	0.3571	0.4571

TABLE XLIV

MEASUREMENTS FOR SITUATION E, CASE 5

Combination Used	u/u_o	v/u_o	w/u_o	Measured u'_{rms}/u_o	v'_{rms}/u_o	w'_{rms}/u_o	$\overline{u'v'}/u_o^2$	$\overline{u'w'}/u_o^2$	$\overline{v'w'}/u_o^2$
612	0.707	NR	0.547	0.318	0.447	0.316	0.0195	0.0103	0.0275
123	0.552	NR	0.613	0.624	0.338	0.356	0.0342	NR	0.0831
234	0.740	0.103	0.246	0.645	0.610	NR	0.0148	0.0086	NR
345	0.734	0.251	0.336	0.573	0.564	0.165	0.0460	NR	0.0170
456	0.435	0.225	0.695	0.546	0.363	0.319	0.0147	0.0300	NR
561	0.424	0.301	0.613	0.496	0.177	0.346	0.0175	NR	0.0284
Mean $\bar{x}$	0.599	0.220	0.508	0.534	0.416	0.300	0.0245	0.0163	0.0425
S.D. σ	0.135	0.073	0.162	0.108	0.145	0.069	0.0117	0.0097	0.0290
$\sigma/\bar{x}$	0.225	0.331	0.318	0.202	0.349	0.231	0.4773	0.5958	0.6824

TABLE XLV

COMPARISON OF AVERAGED RESULTS FROM SIX POSSIBLE WIRE COMBINATIONS WITH OPTIMAL COMBINATION

Situation		Measured u/u_o	v/u_o	w/u_o	u'_{rms}/u_o	v'_{rms}/u_o	w'_{rms}/u_o	$\overline{u'v'}/u_o^2$	$\overline{u'w'}/u_o^2$	$\overline{v'w'}/u_o^2$
A	345	0.968	NR	0.013						
	$\bar{x}$	0.970	0.147	0.013						
B	345	0.587	0.110	0.019	0.125	0.209	0.126	0.0001	0.0000	NR
	$\bar{x}$	0.593	0.189	0.030	0.157	0.084	0.105	0.0031	0.0012	0.0129
C	345	NR								
	$\bar{x}$	0.456	0.144	0.023	0.130	0.062	0.083	0.0037	0.0011	0.0036
D	561	1.702	0.665	1.609	0.138	0.091	0.108	0.0043	0.0045	0.0066
	$\bar{x}$	1.739	0.585	1.613	0.134	0.149	0.123	0.0064	0.0057	0.0082
E	561	0.628	0.323	0.478	0.463	0.135	0.525	0.0384	0.0411	NR
	$\bar{x}$	0.624	0.458	0.403	0.437	0.219	0.422	0.0424	0.0295	0.0362

APPENDIX B

FIGURES

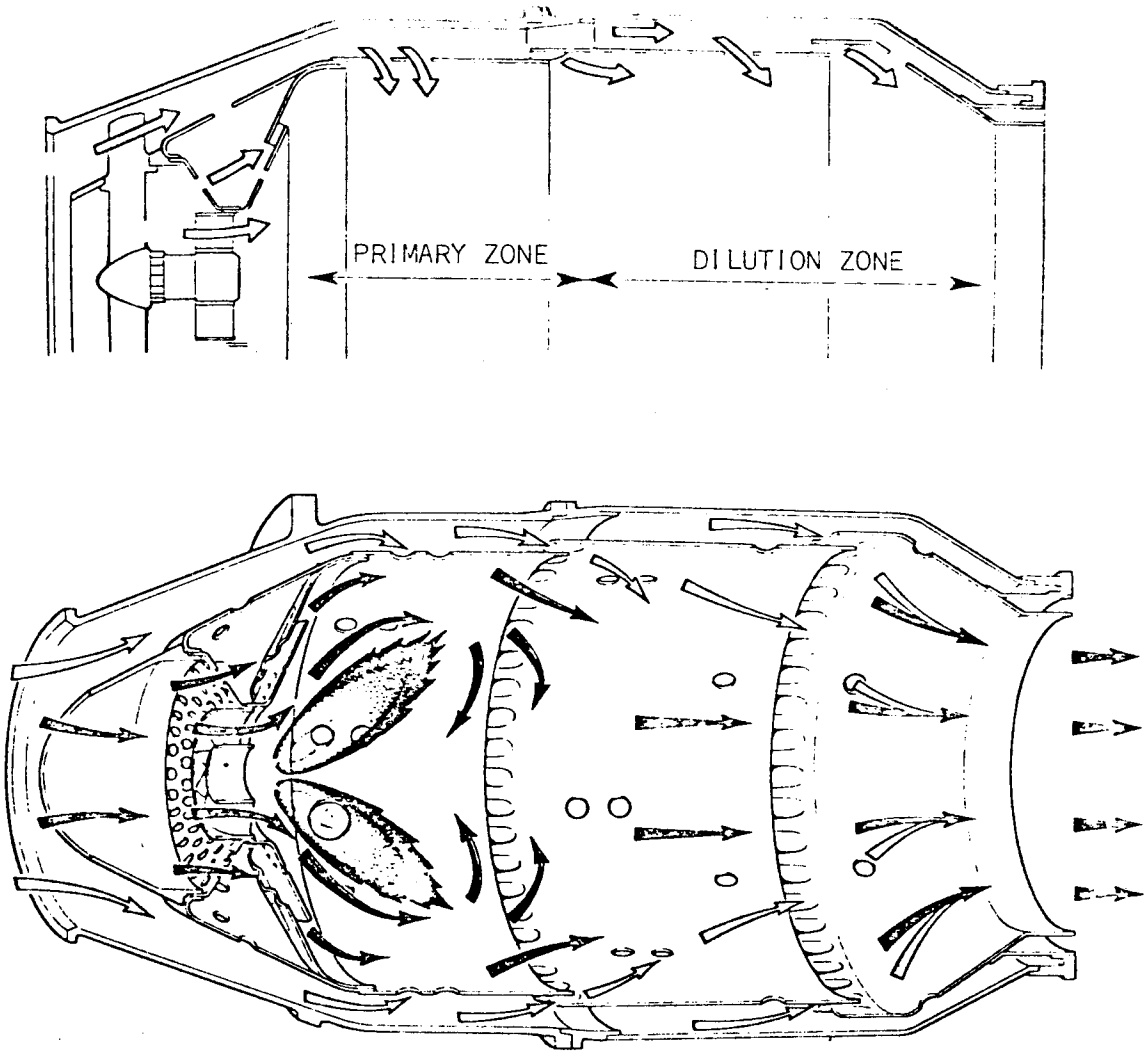

Figure 1. Typical Axisymmetric Gas Turbine Combustion Chamber

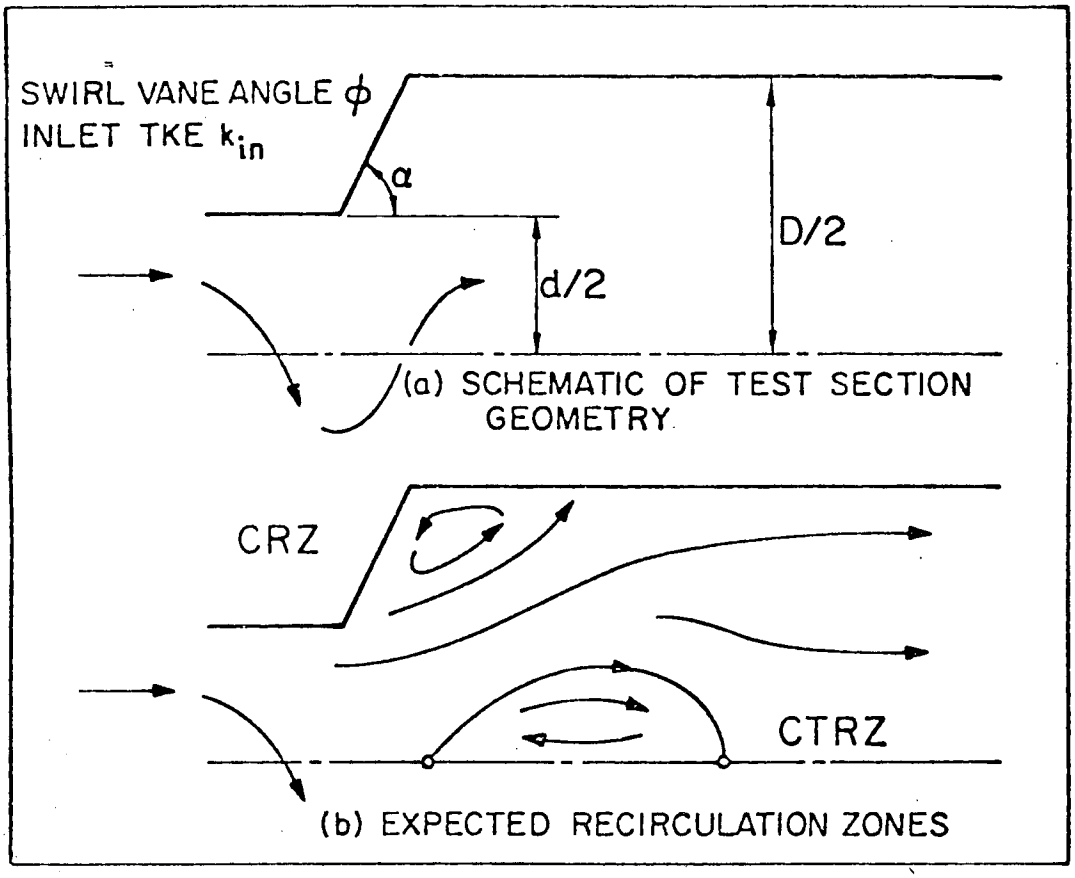

Figure 2. The Flowfield Being Investigated

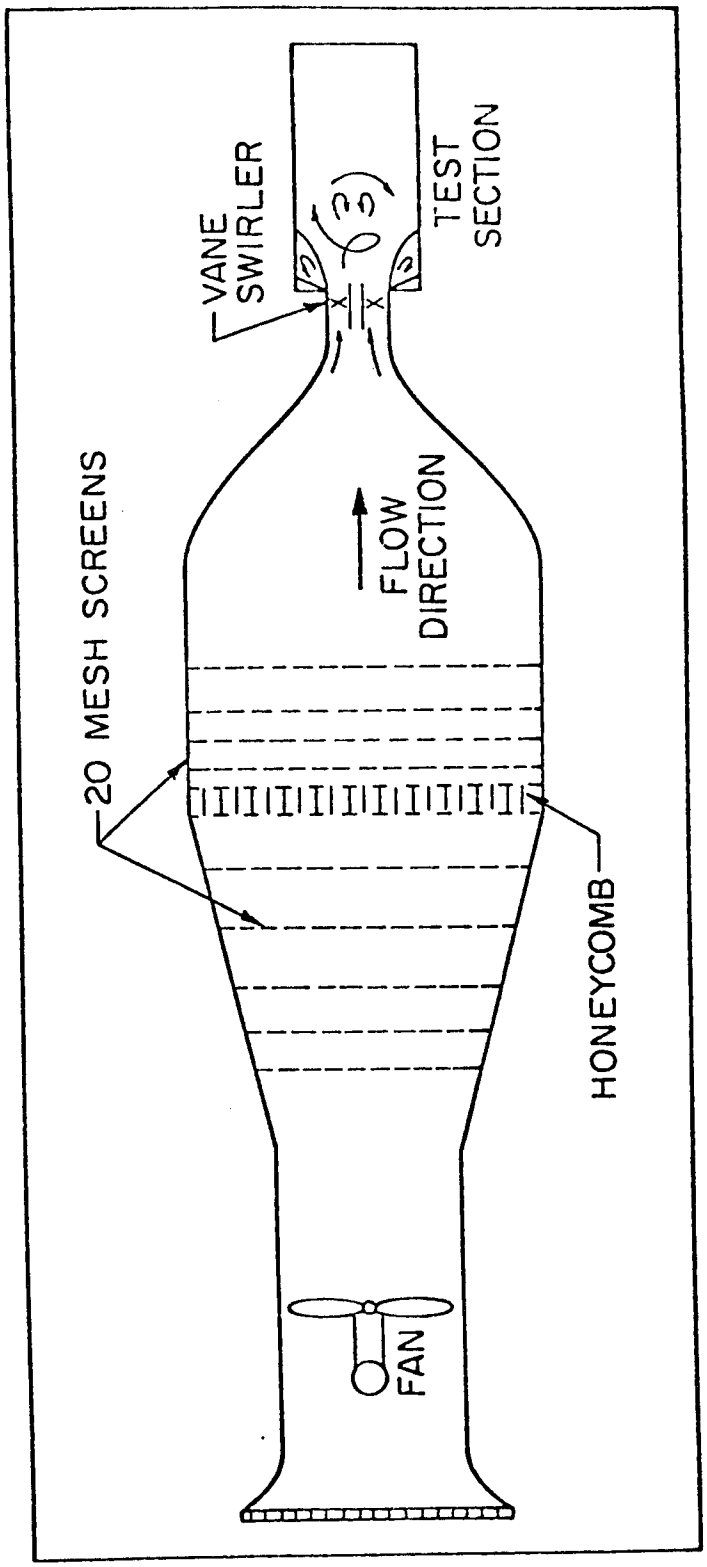

Figure 3. Schematic of Experimental Facility

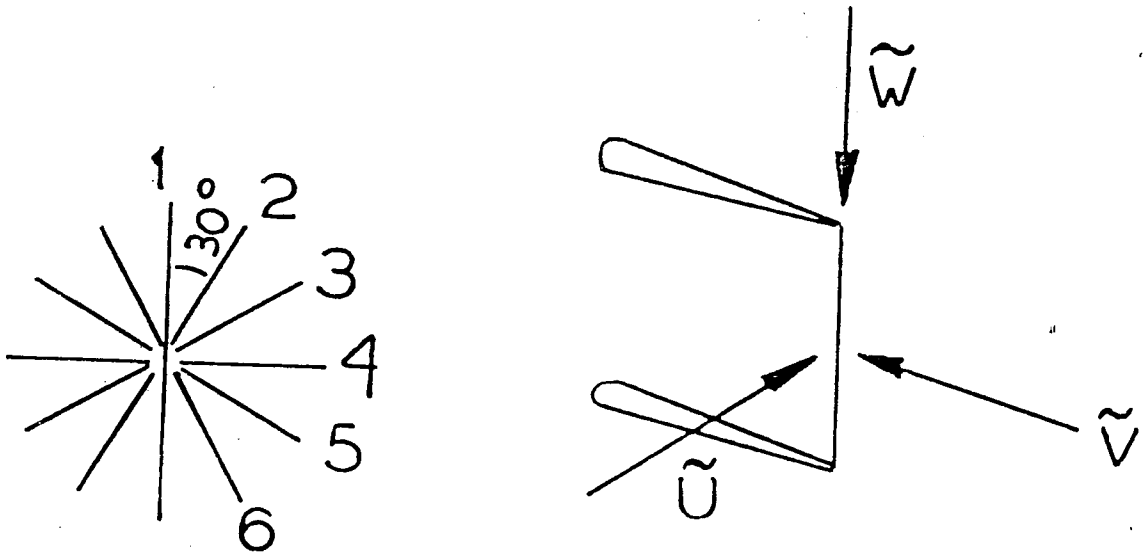

Figure 4. The Six Positions and Probe Coordinates

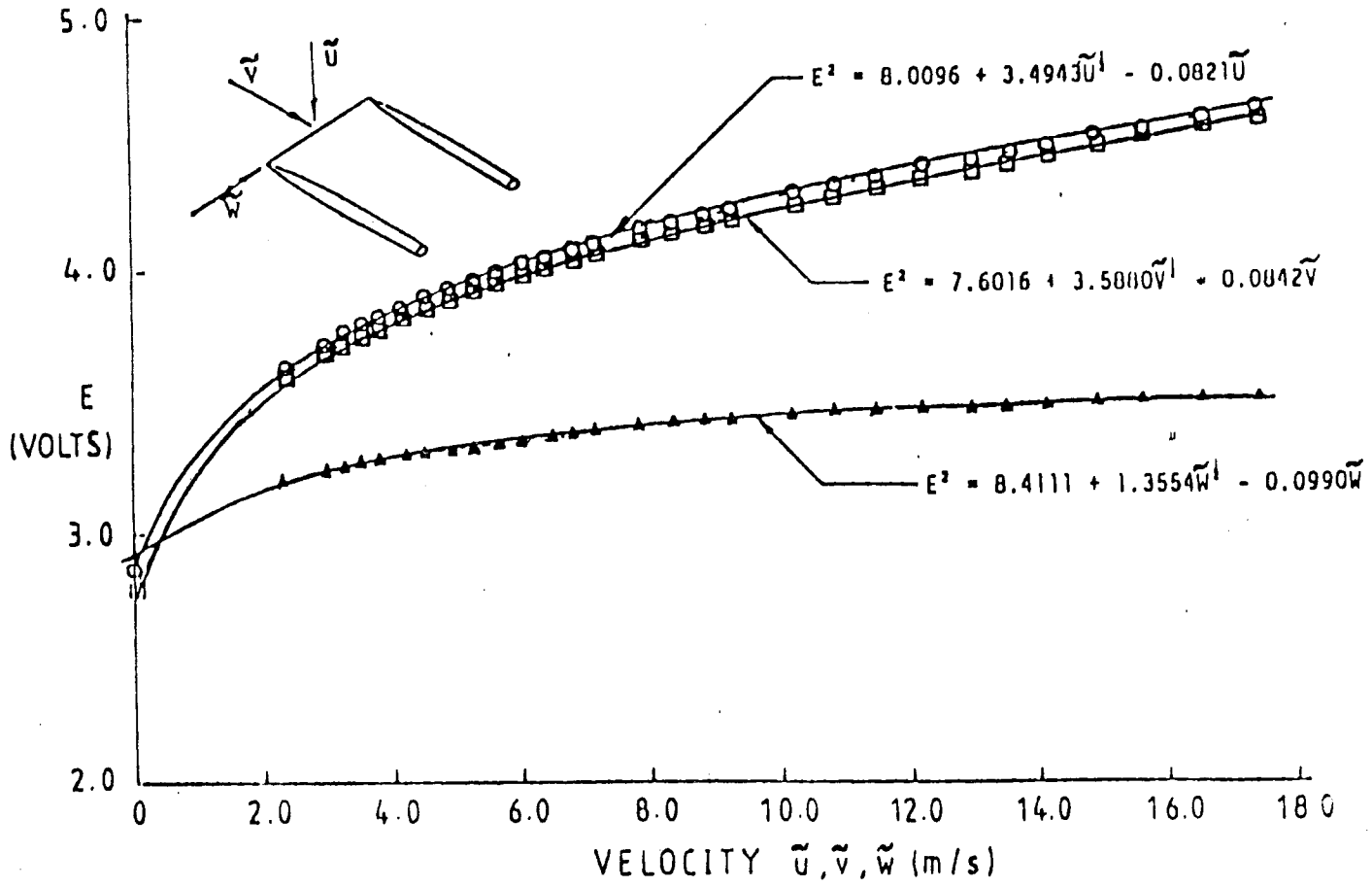

Figure 5. The Three-Directional Hot-Wire Calibration

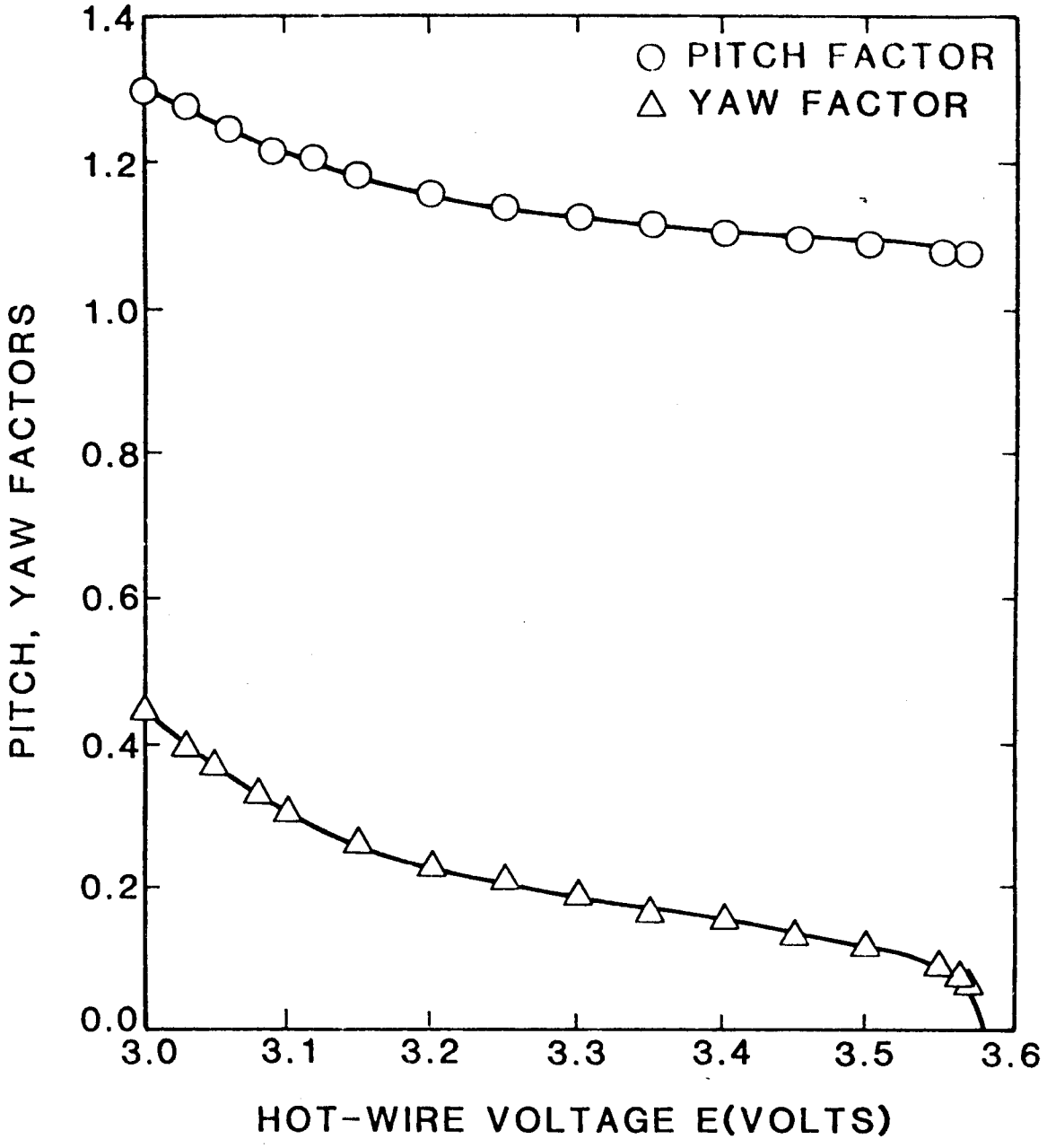

Figure 6. Pitch and Yaw Factors as a Function of Hot-Wire Mean Effective Voltage

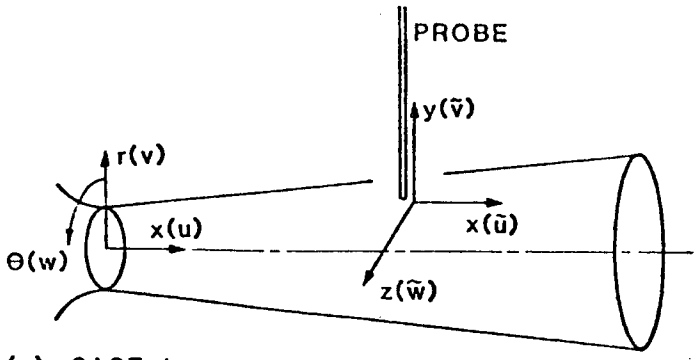

(a) CASE 1

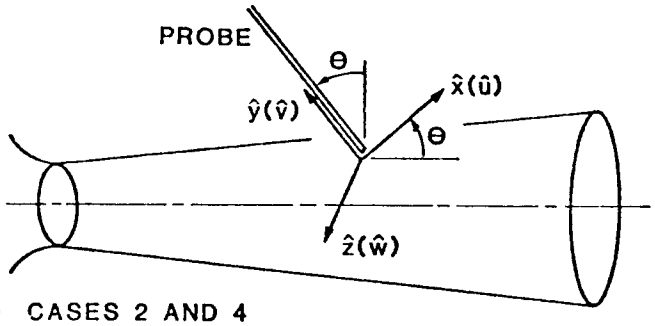

(b) CASES 2 AND 4

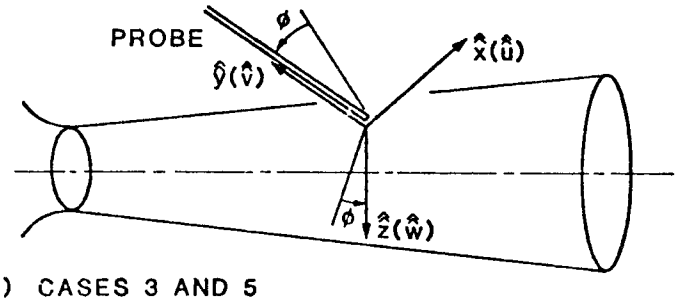

(c) CASES 3 AND 5

Figure 7. Configuration Used in the Directional Sensitivity Study

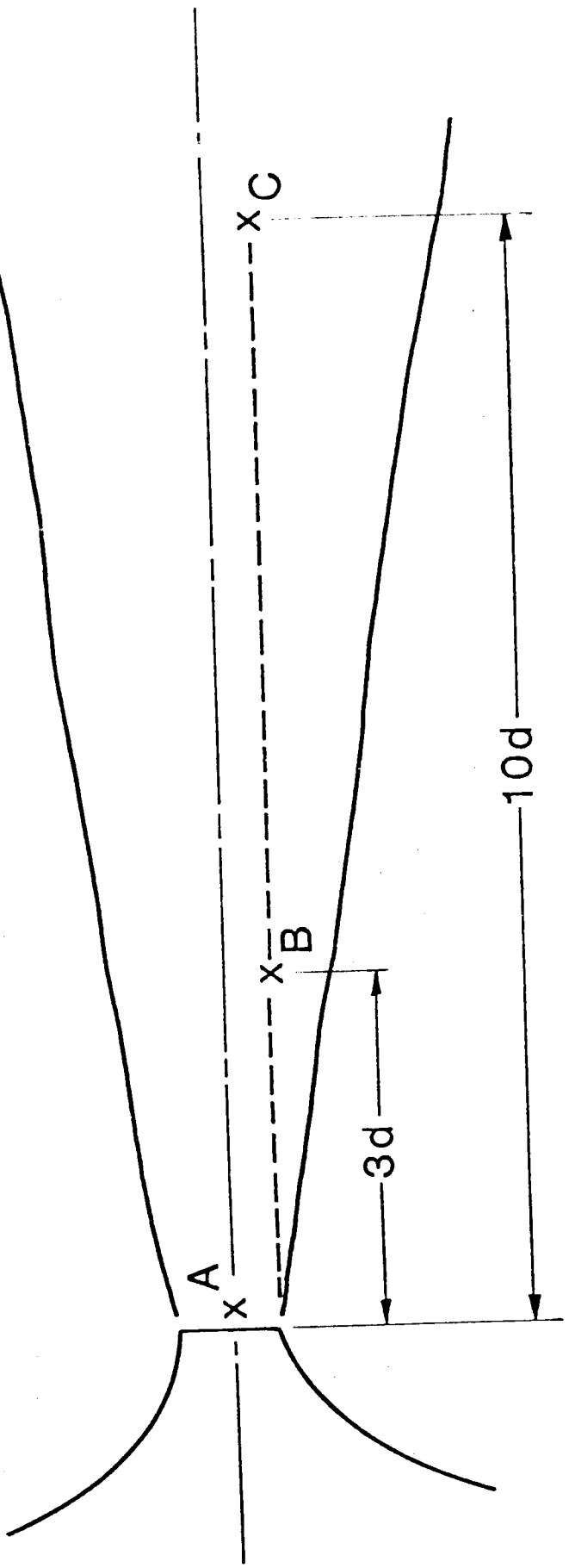

Figure 8. Free Nonswirling Jet Measurement Locations for Situations A, B, and C

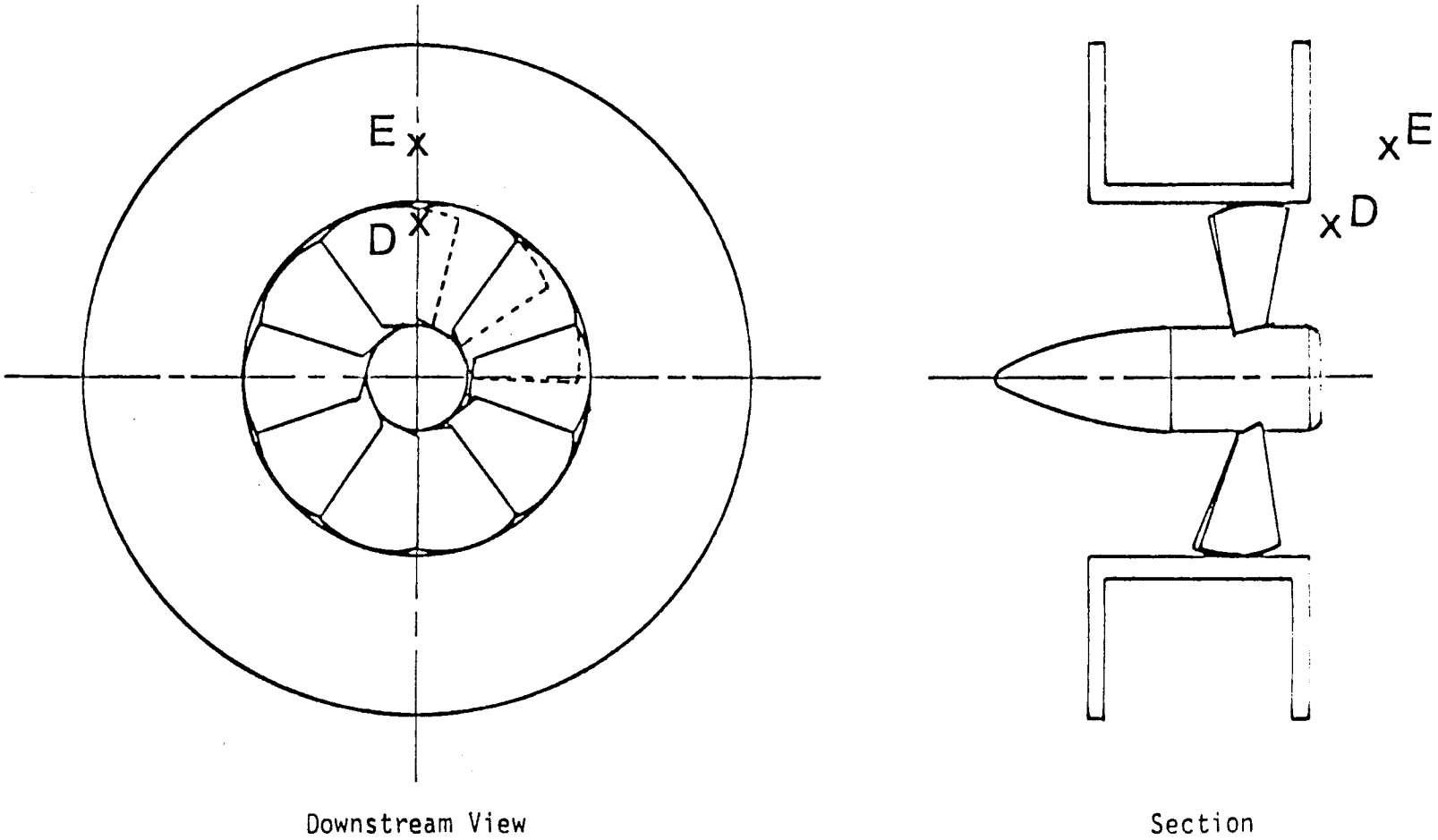

Downstream View

Section

Figure 9. Free Swirling Jet Measurement Locations for Situations D and E

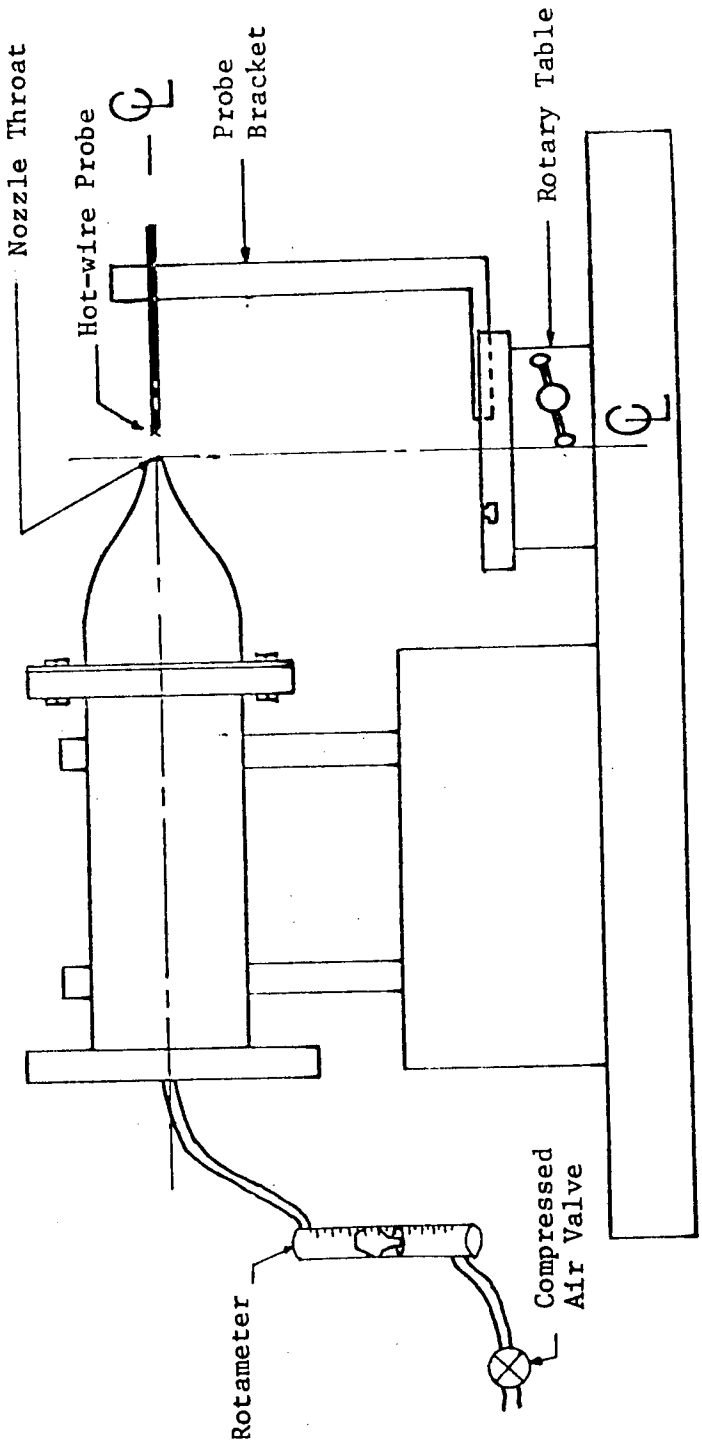

Figure 10. Free Jet Calibration Apparatus

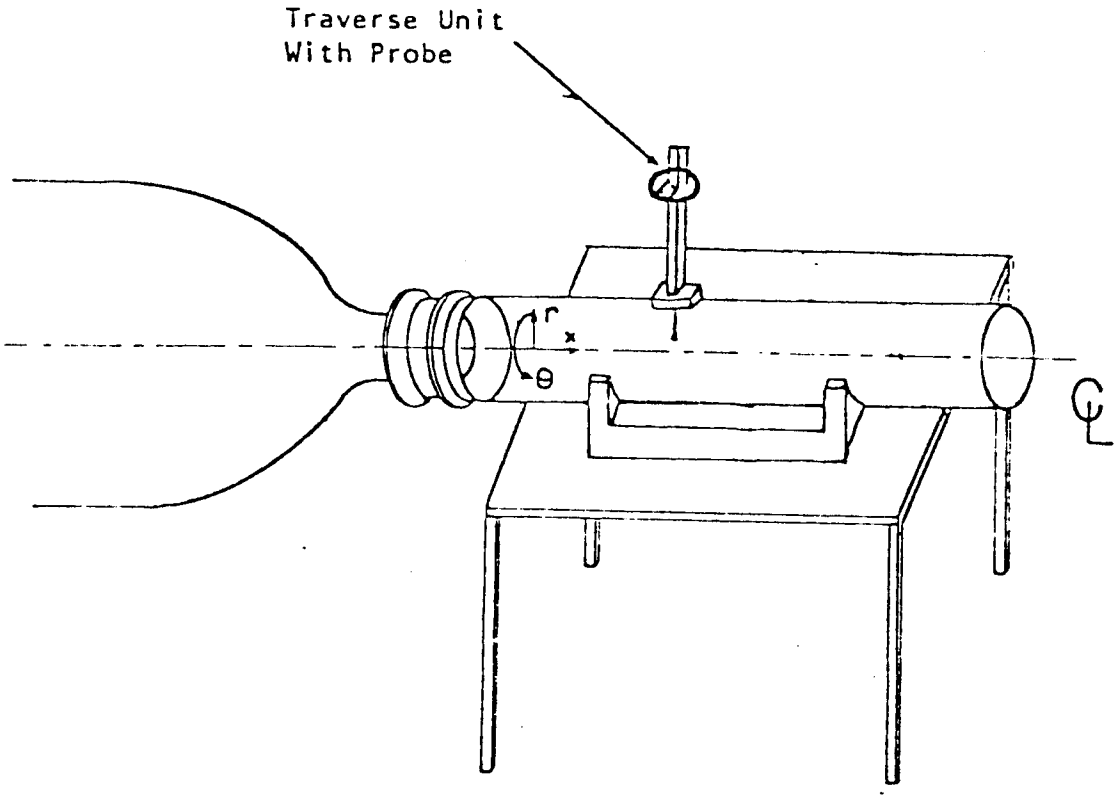

Figure 11. Hot-Wire Probe Mounted on Test Section

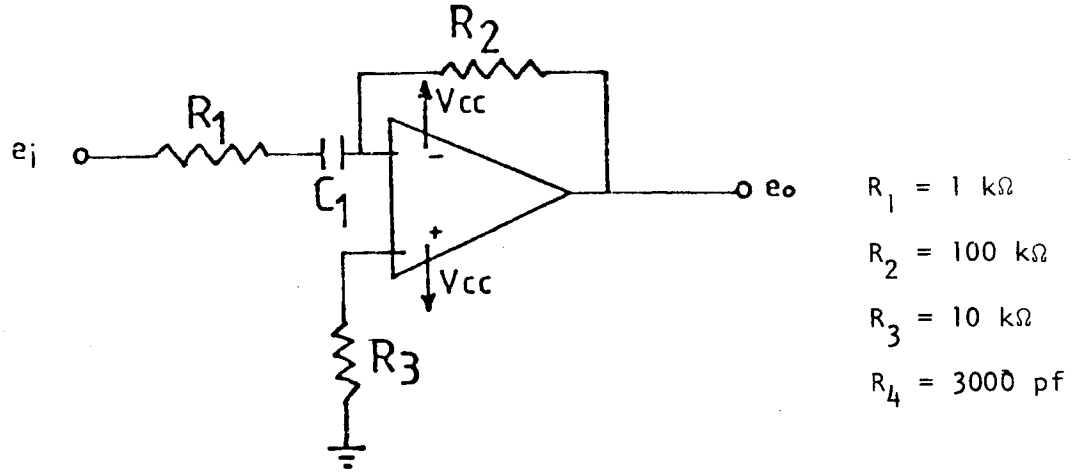

(a) Schematic of Differentiator

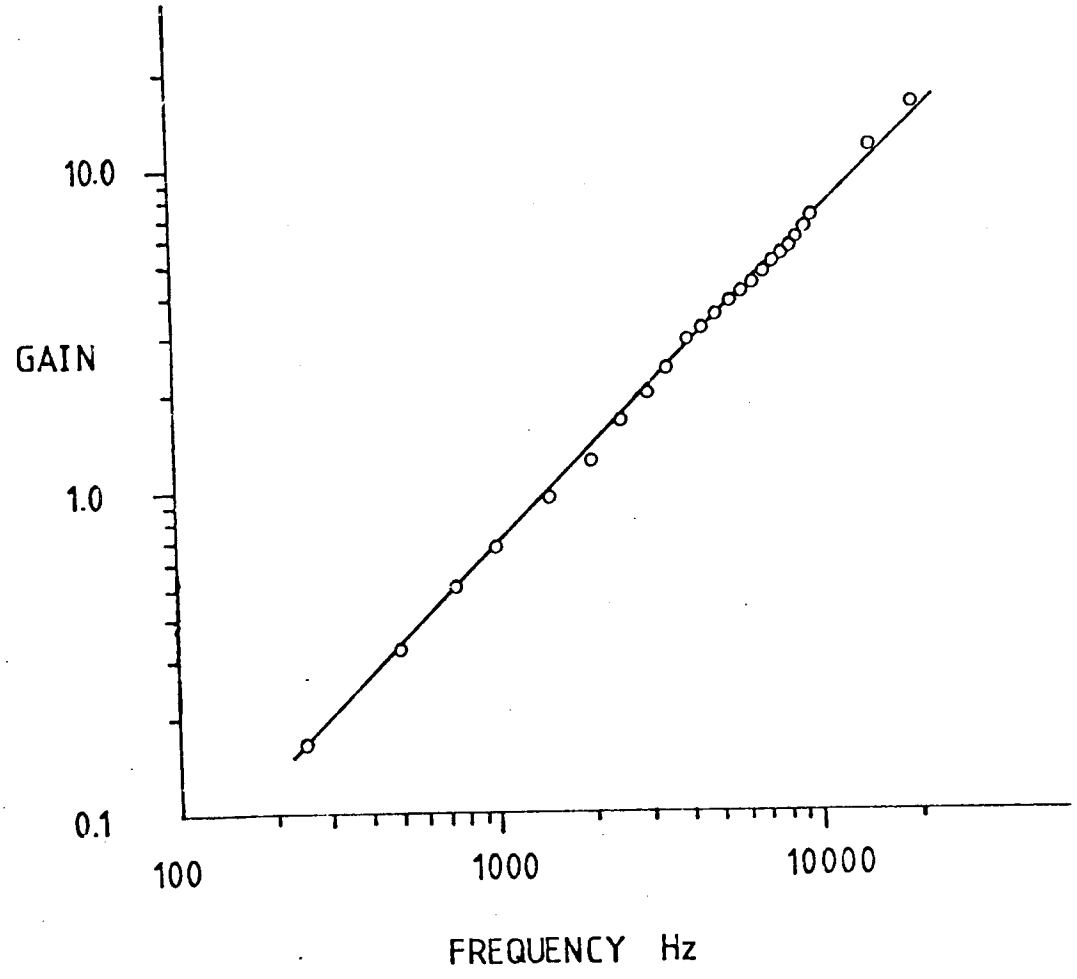

(b) Bode Plot of Differentiator

Figure 12. Schematic and Bode Plot of Differentiator

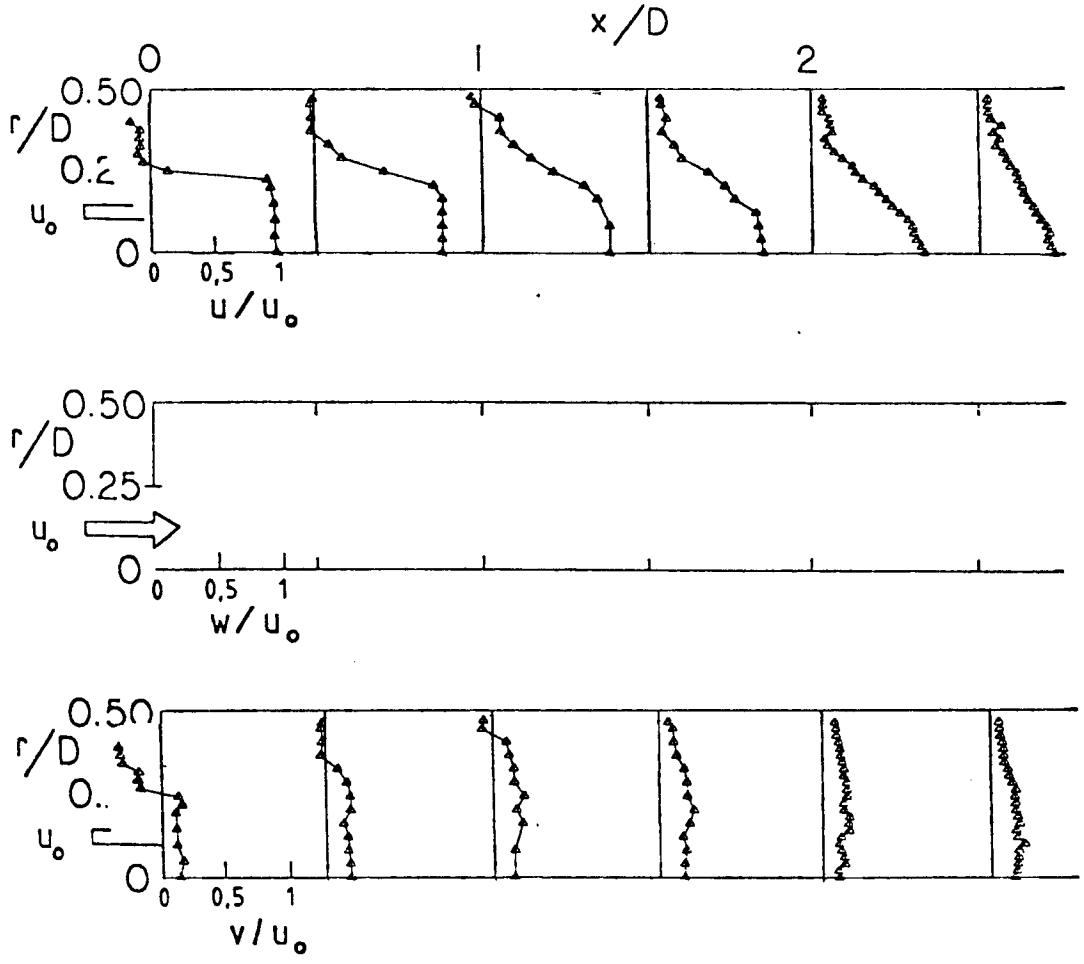

Figure 13. Time-Mean and Turbulent Flowfield ϕ = 0 Degrees (No Swirler), D/d = 2

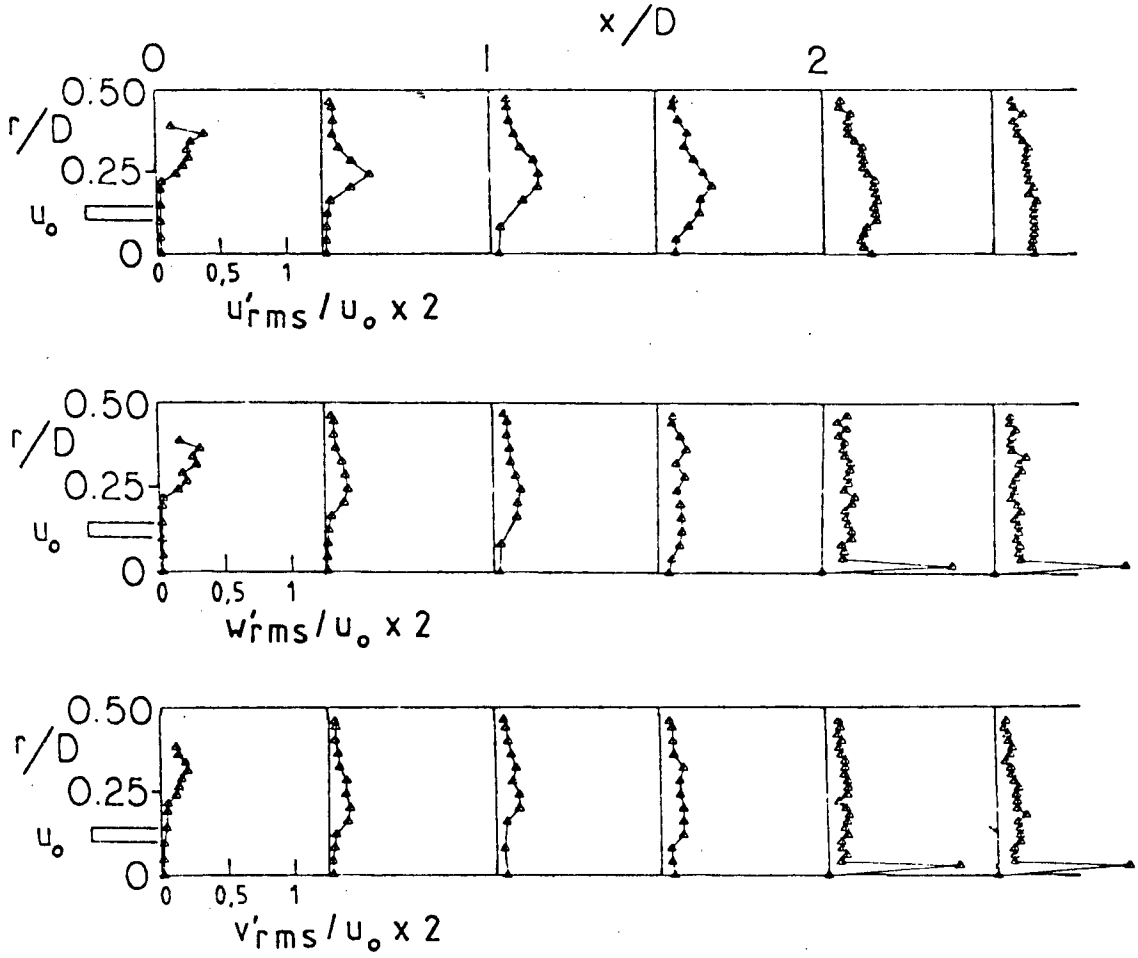

Figure 13. (Continued)

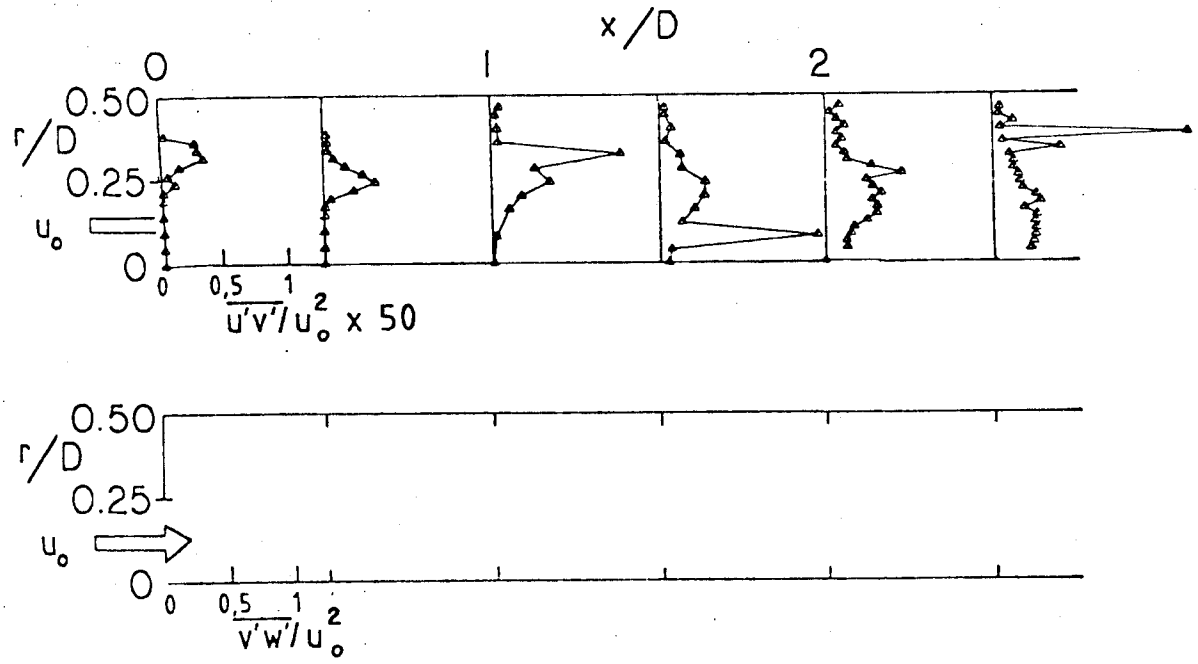

Figure 13. (Continued)

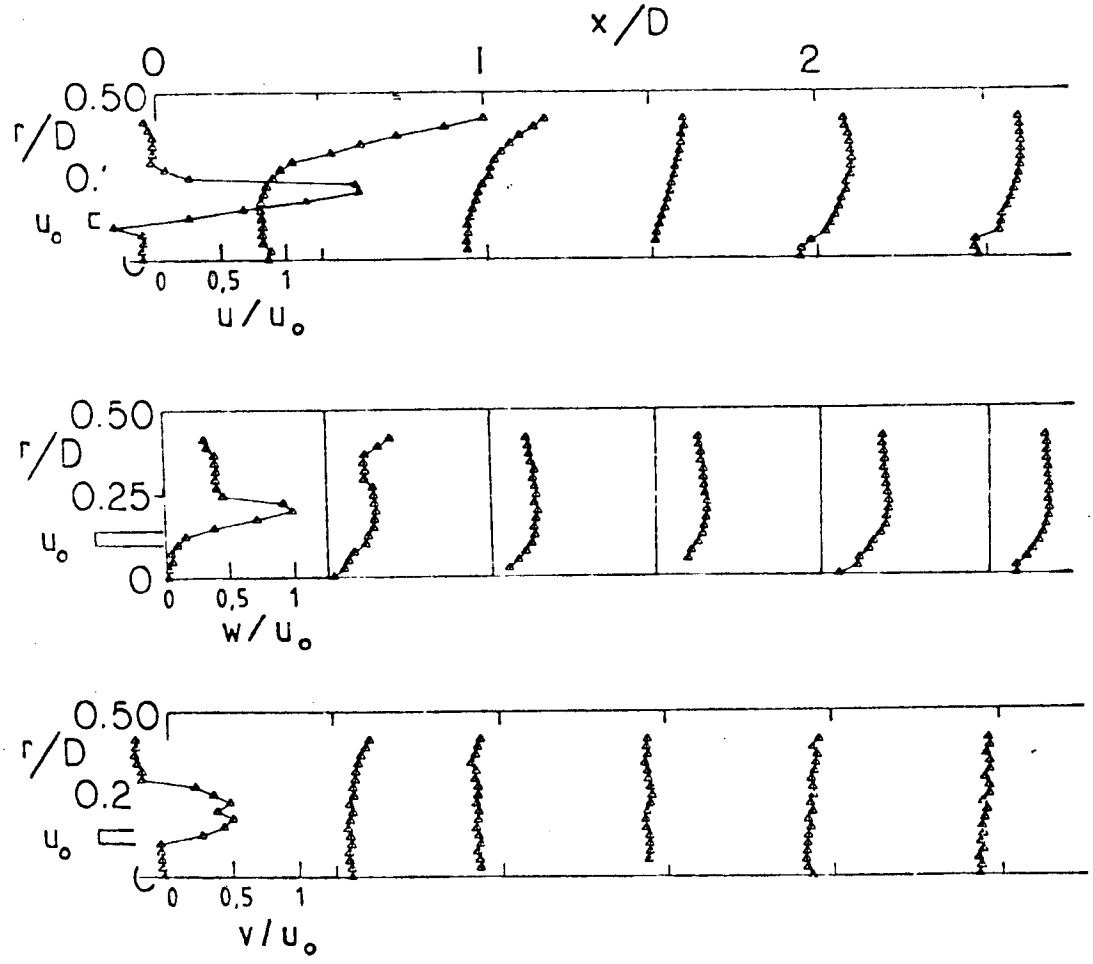

Figure 14. Time-Mean and Turbulent Flowfield ϕ = 38 Degrees, D/d = 2

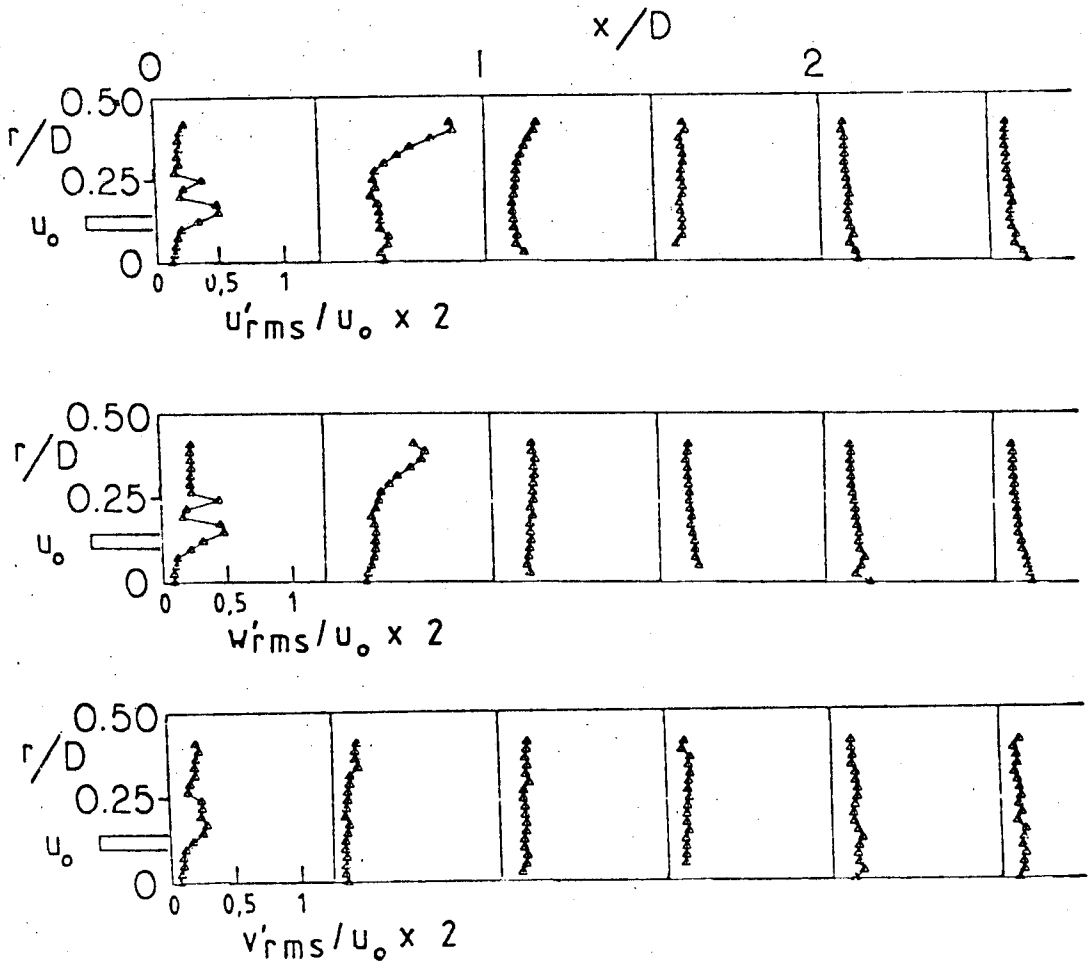

Figure 14. (Continued)

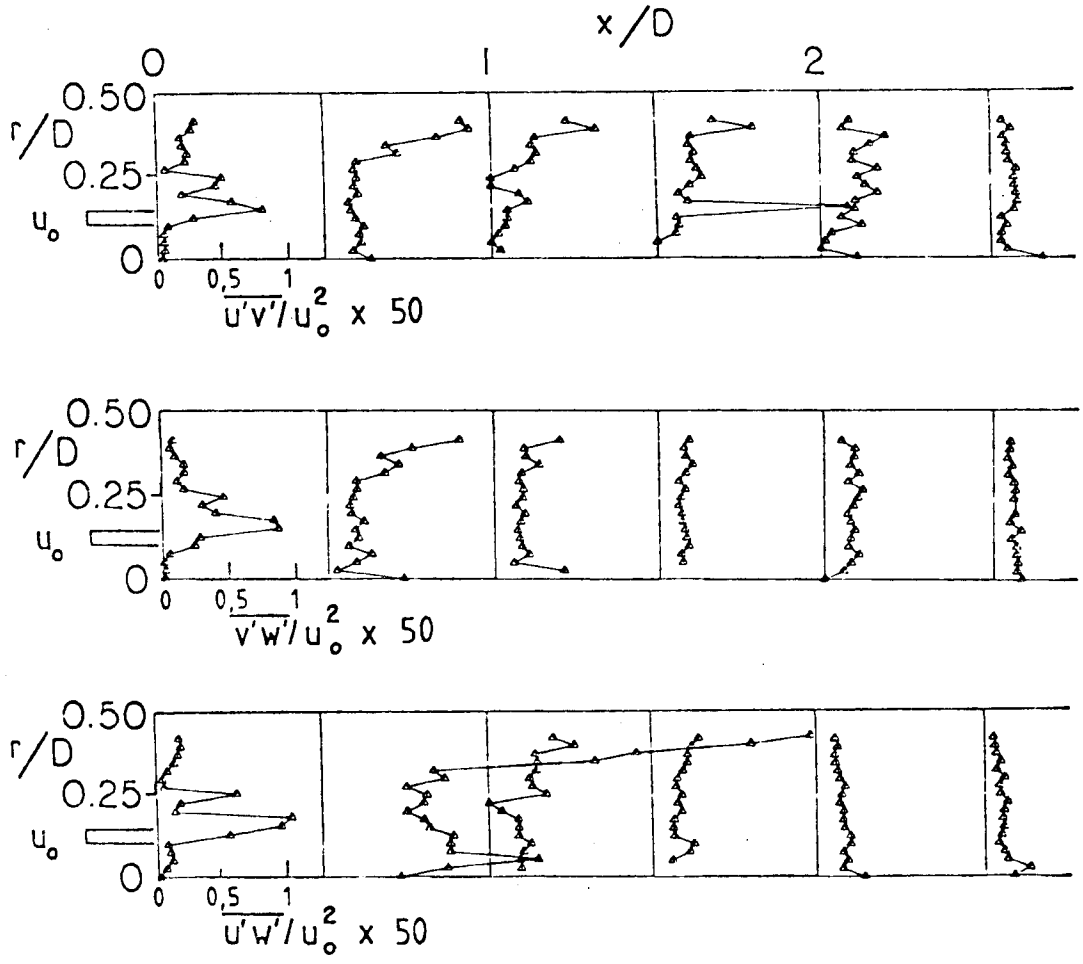

Figure 14. (Continued)

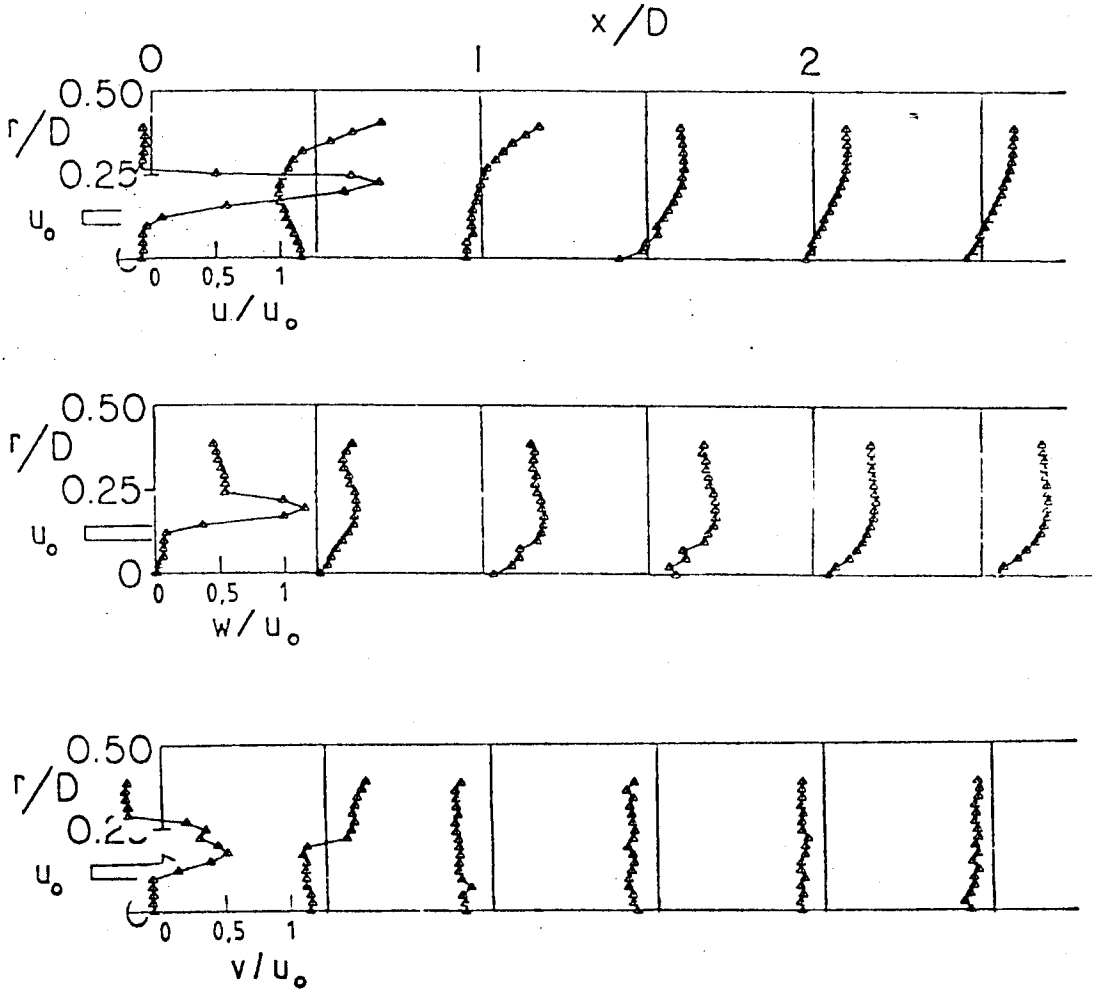

Figure 15. Time-Mean and Turbulent Flowfield ϕ = 45 Degrees, D/d = 2

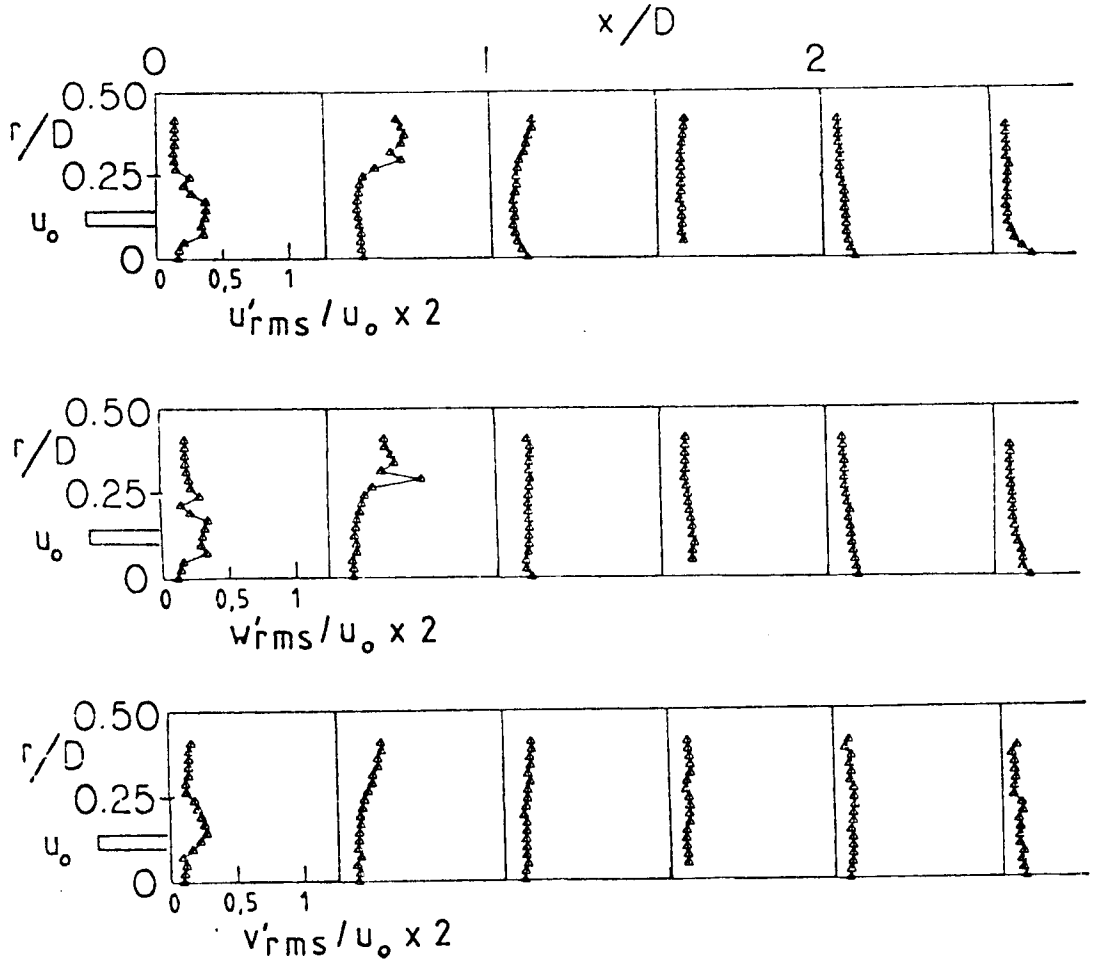

Figure 15. (Continued)

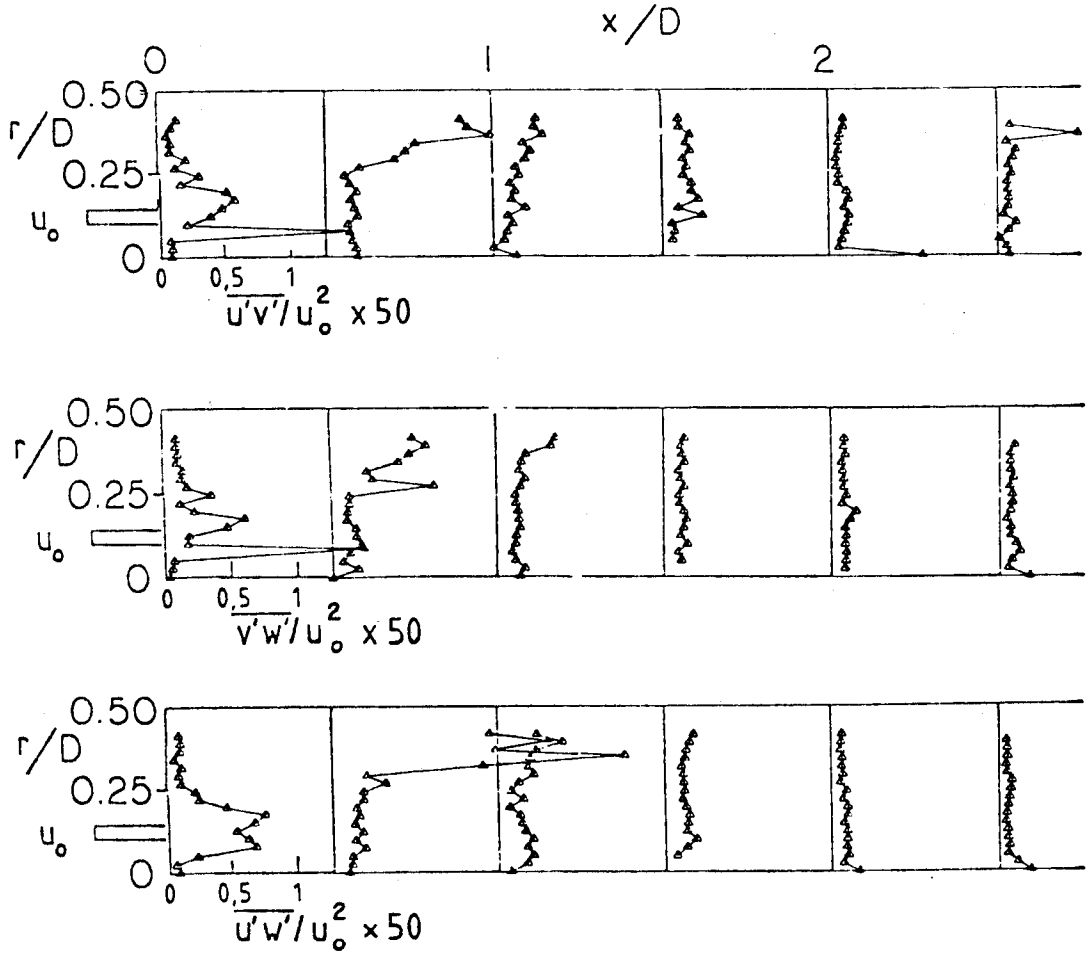

Figure 15. (Continued)

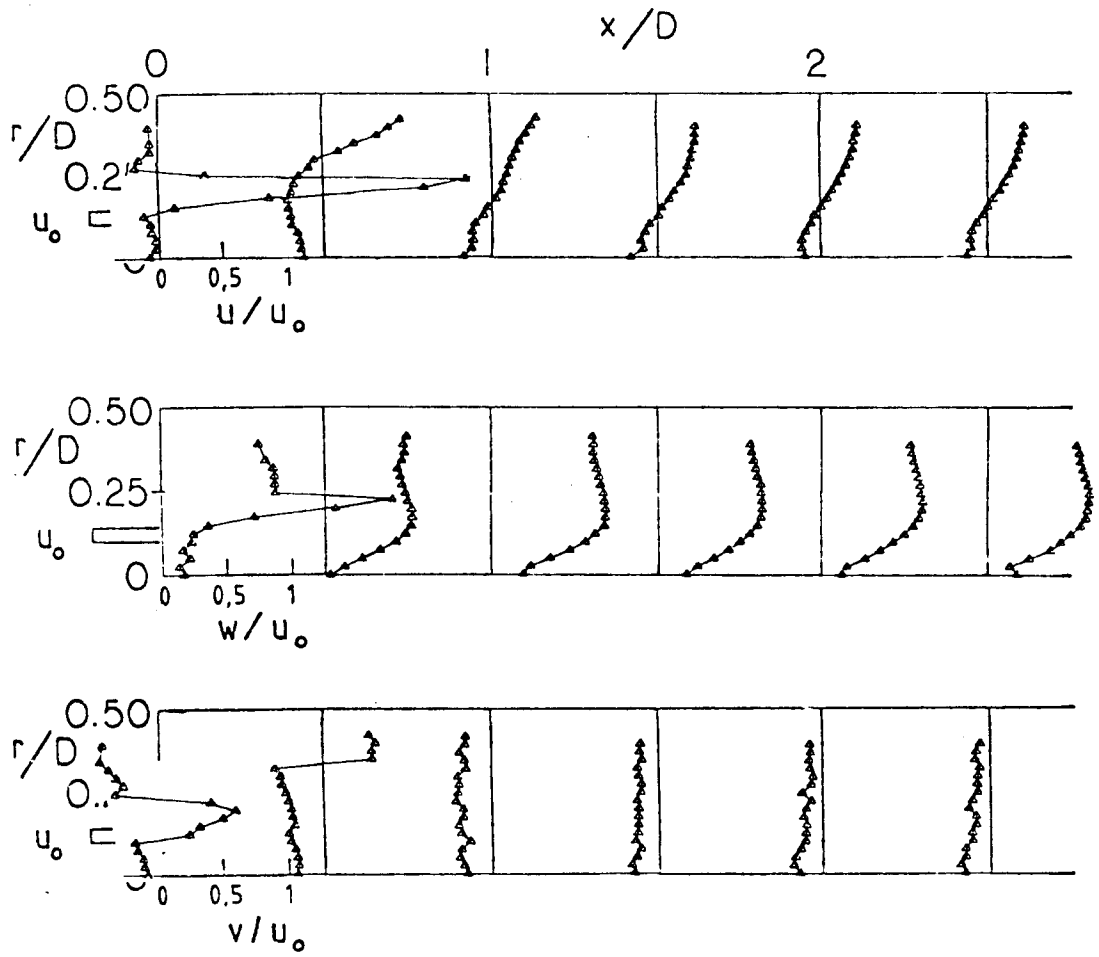

Figure 16. Time-Mean and Turbulent Flowfield ϕ = 60 Degrees, D/d = 2

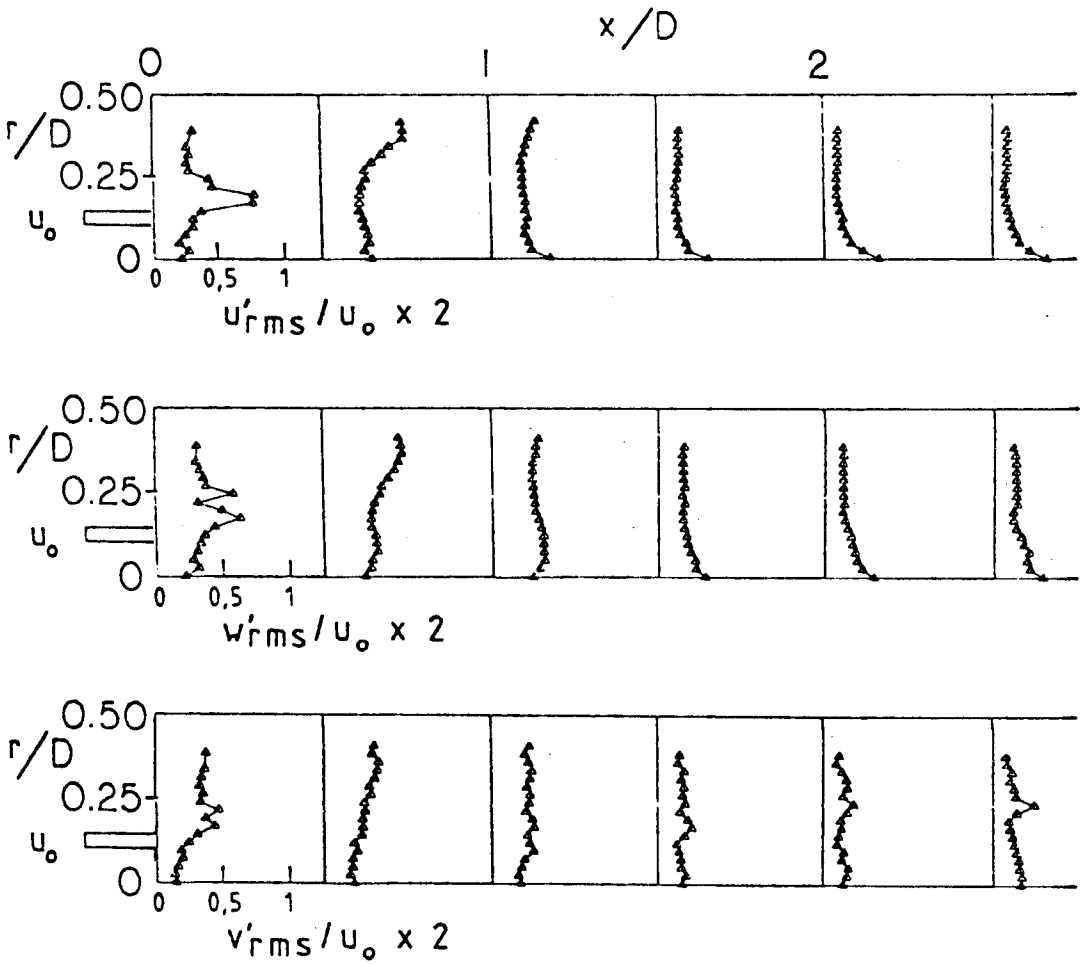

Figure 16. (Continued)

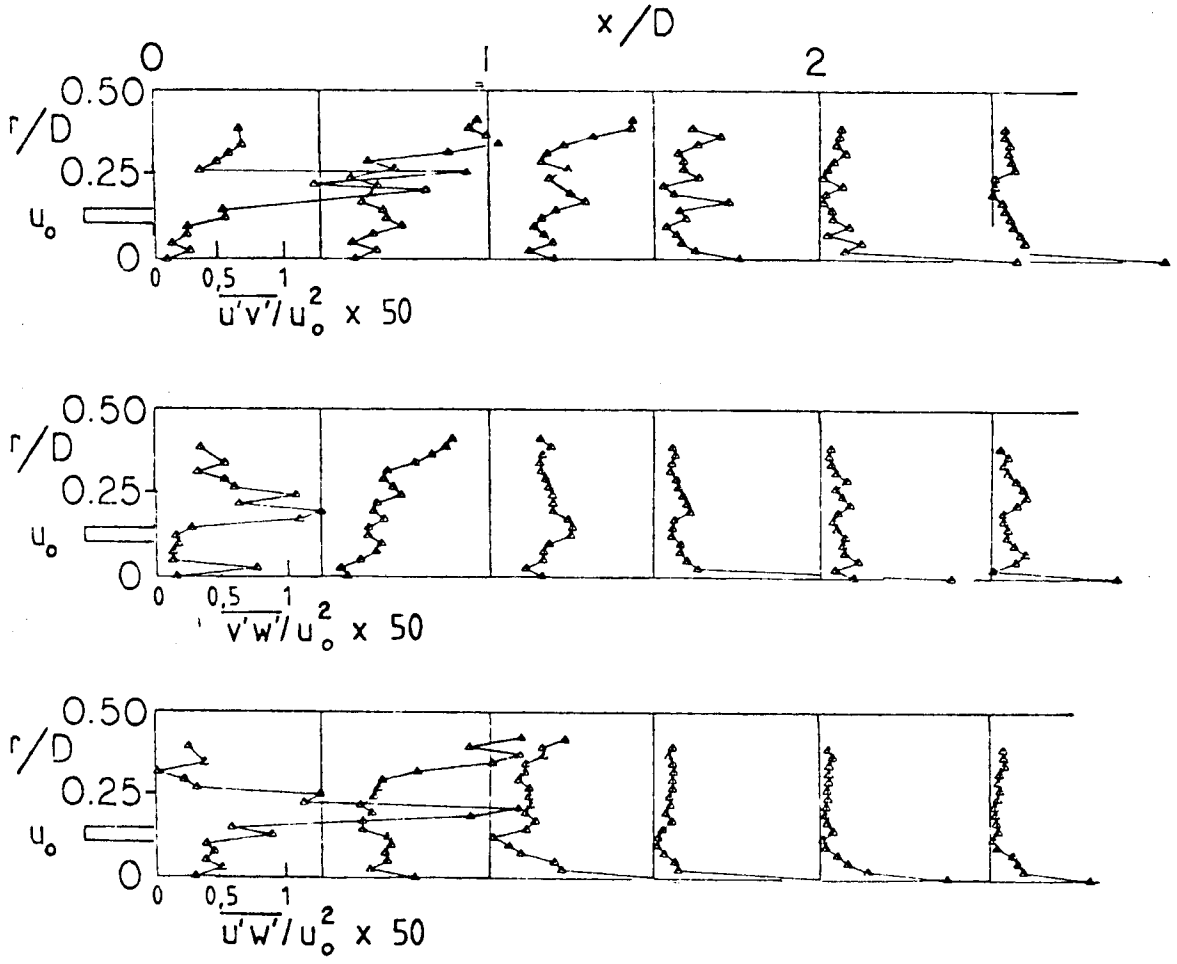

Figure 16. (Continued)

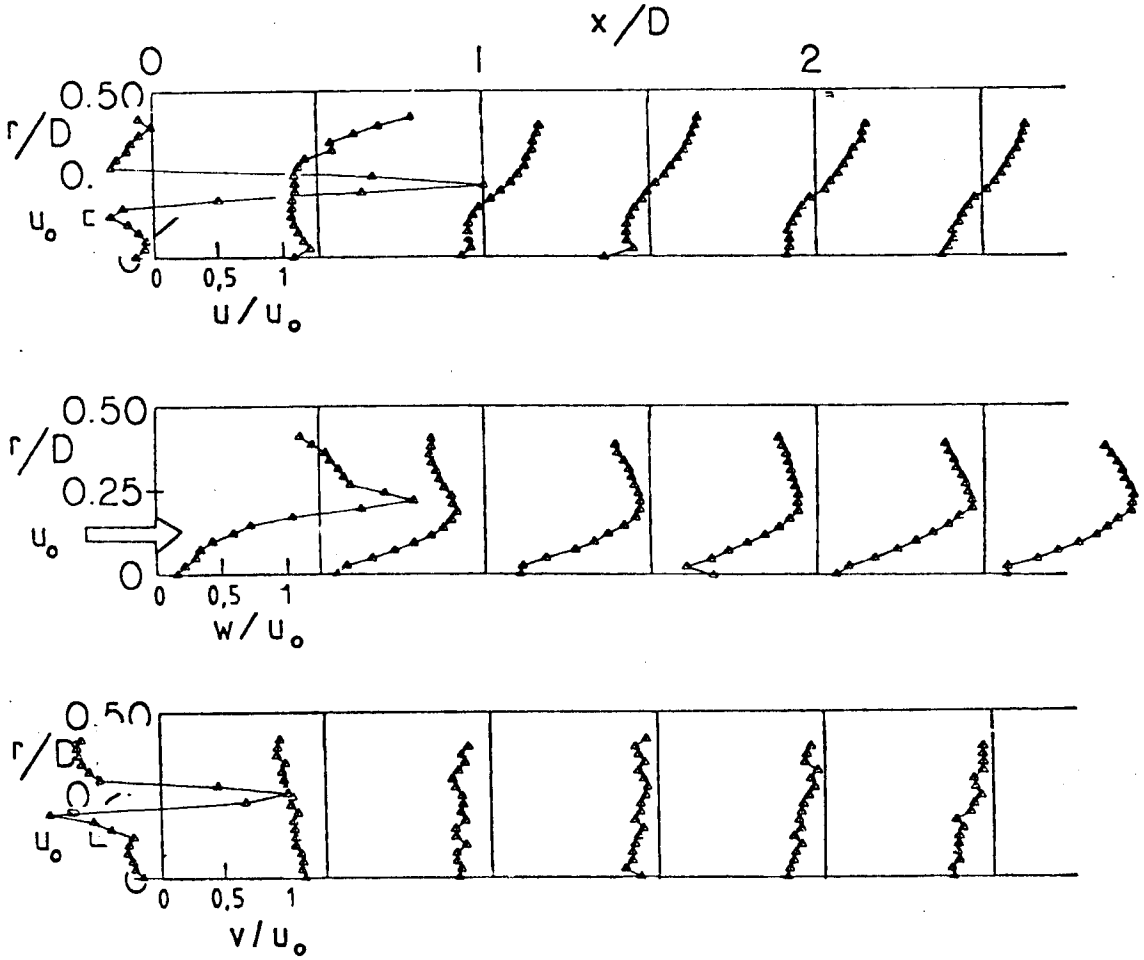

Figure 17. Time-Mean and Turbulent Flowfield ϕ = 70 Degrees, D/d = 2

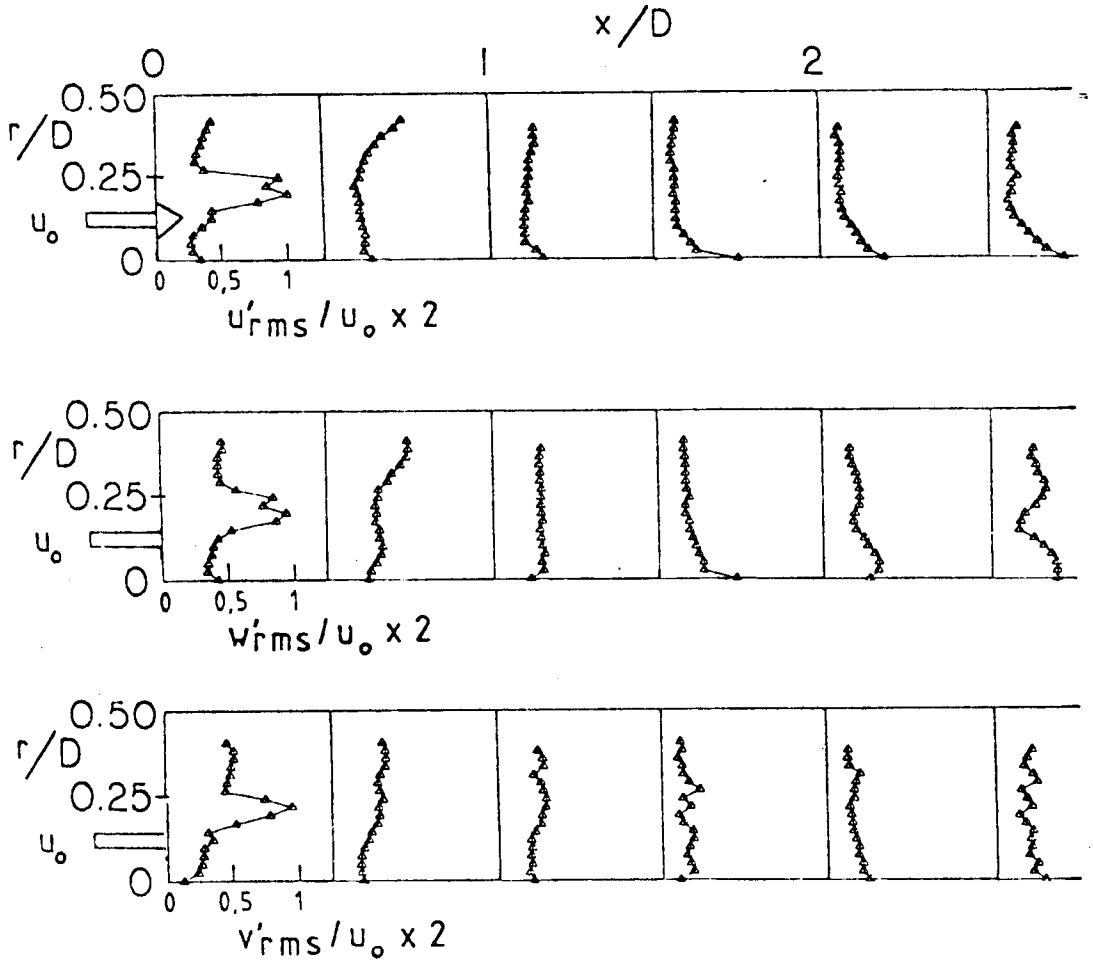

Figure 17. (Continued)

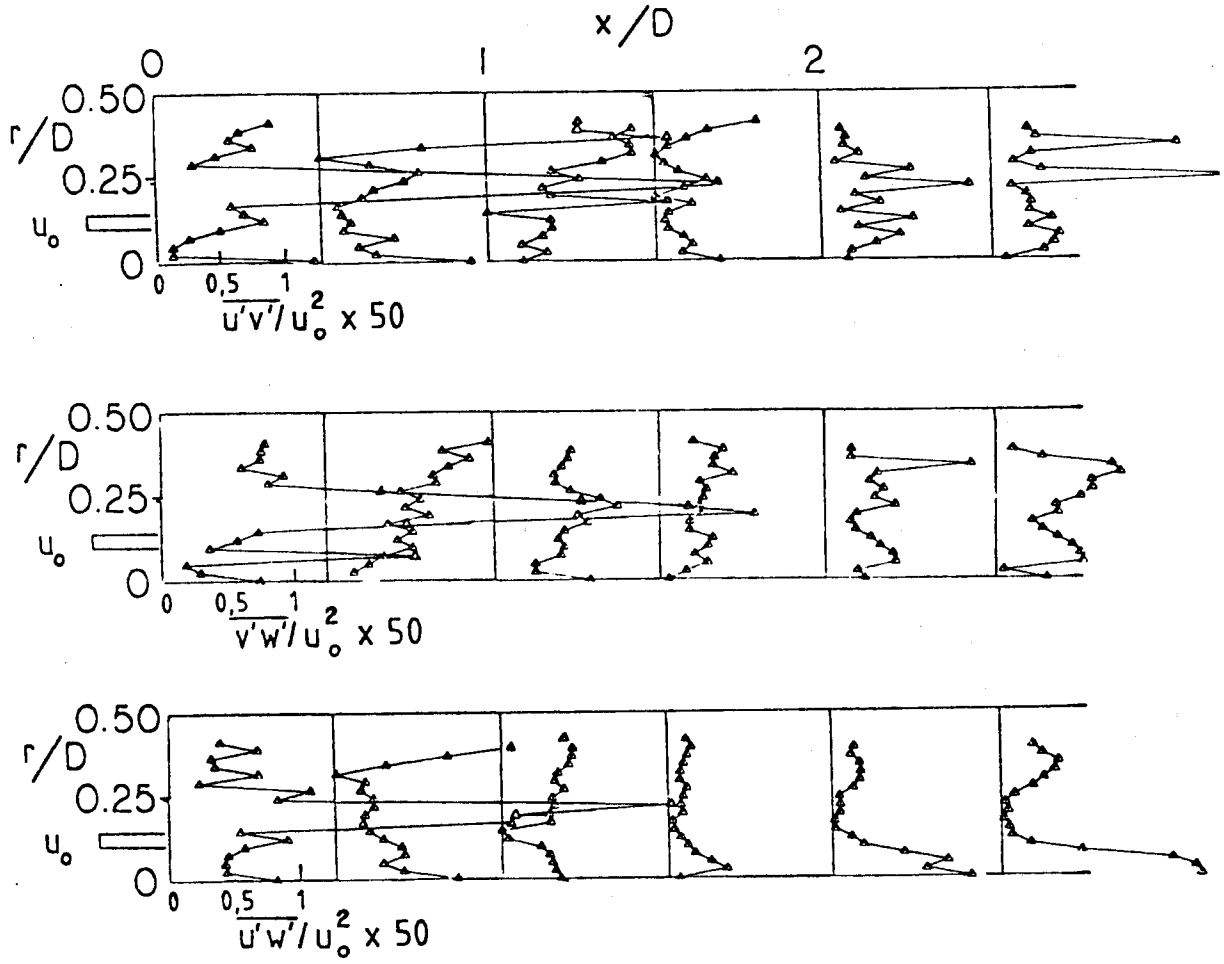

Figure 17. (Continued)

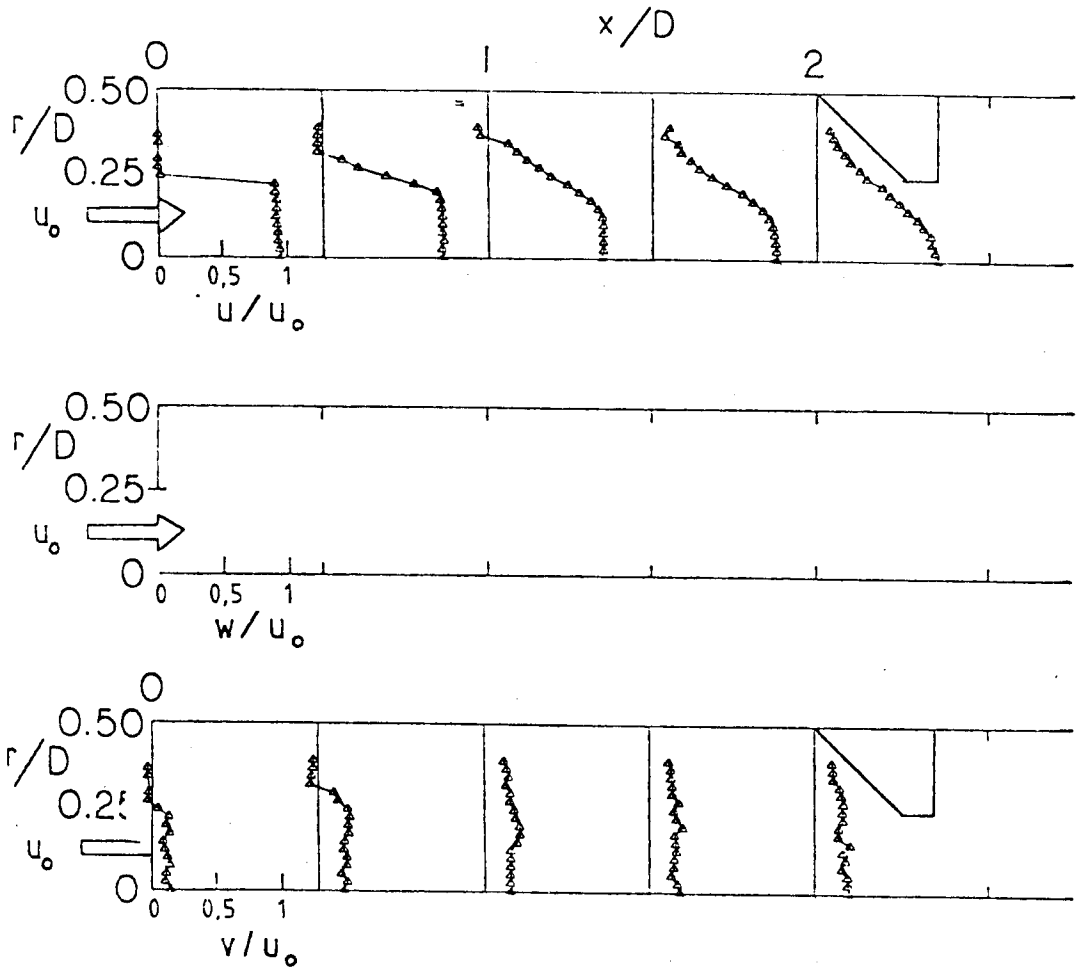

Figure 18. Time-Mean and Turbulent Flowfield ϕ = 0 Degrees (No Swirler), With Strong Contraction Nozzle at L/D = 2

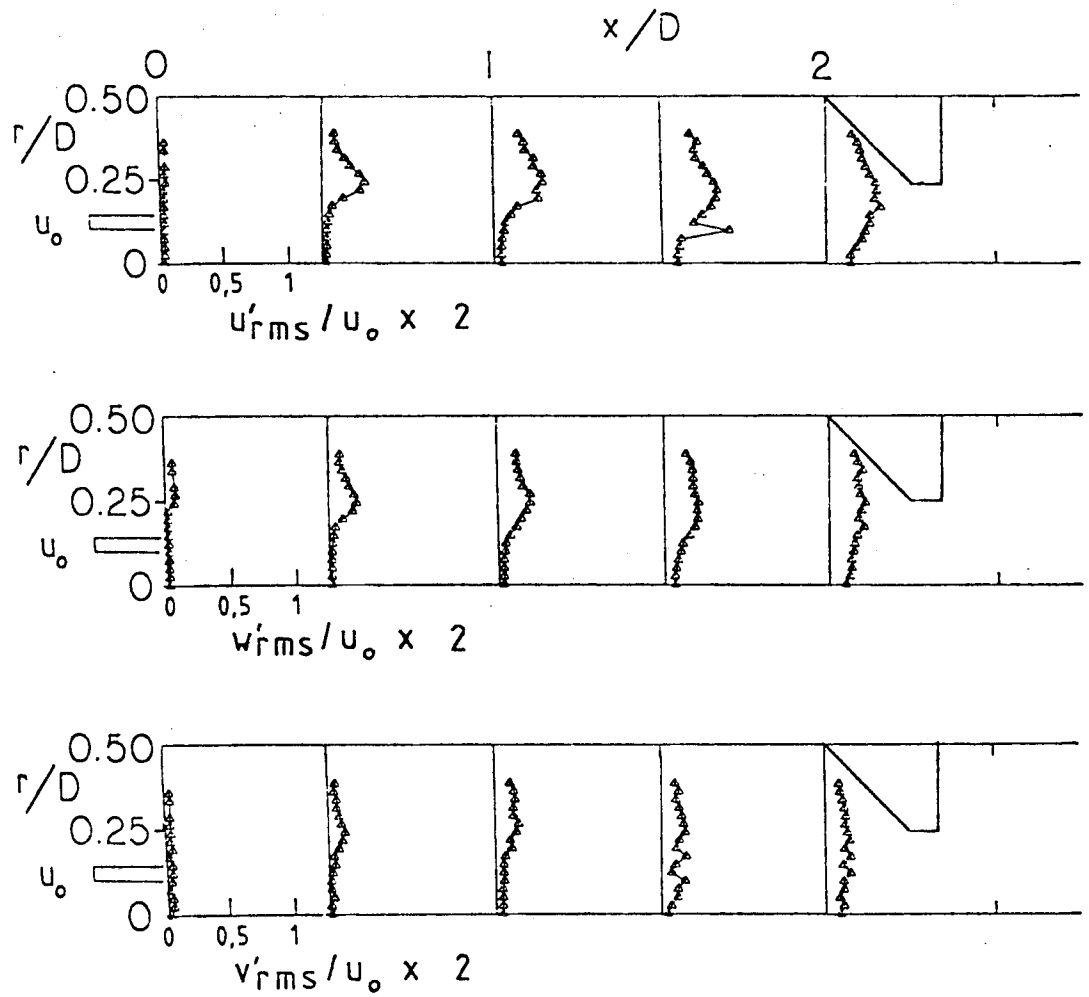

Figure 18. (Continued)

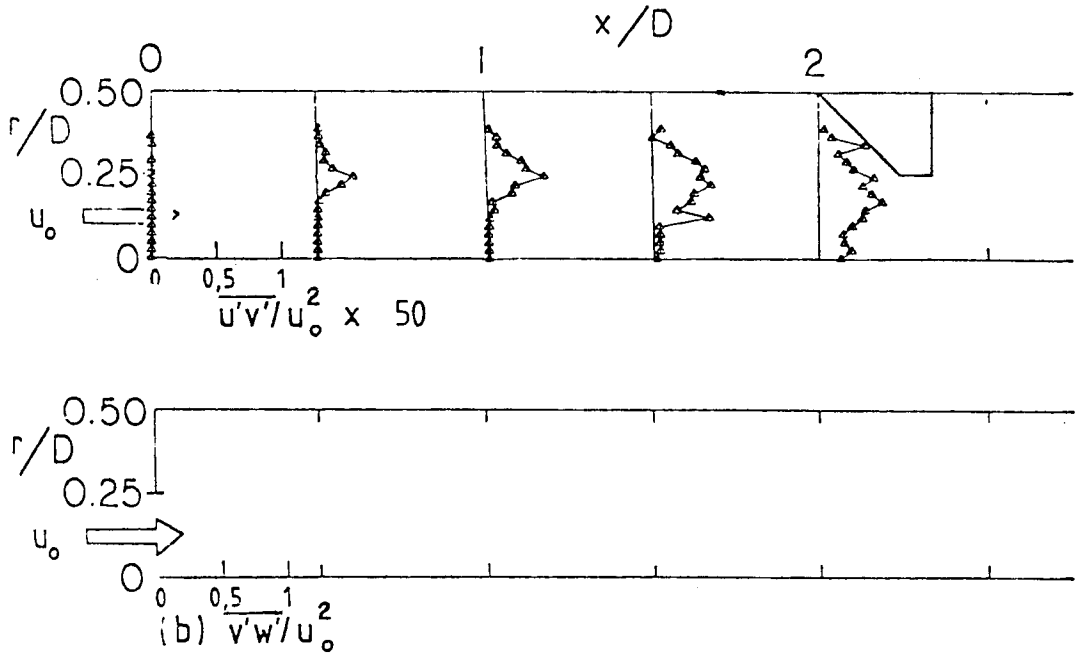

Figure 18. (Continued)

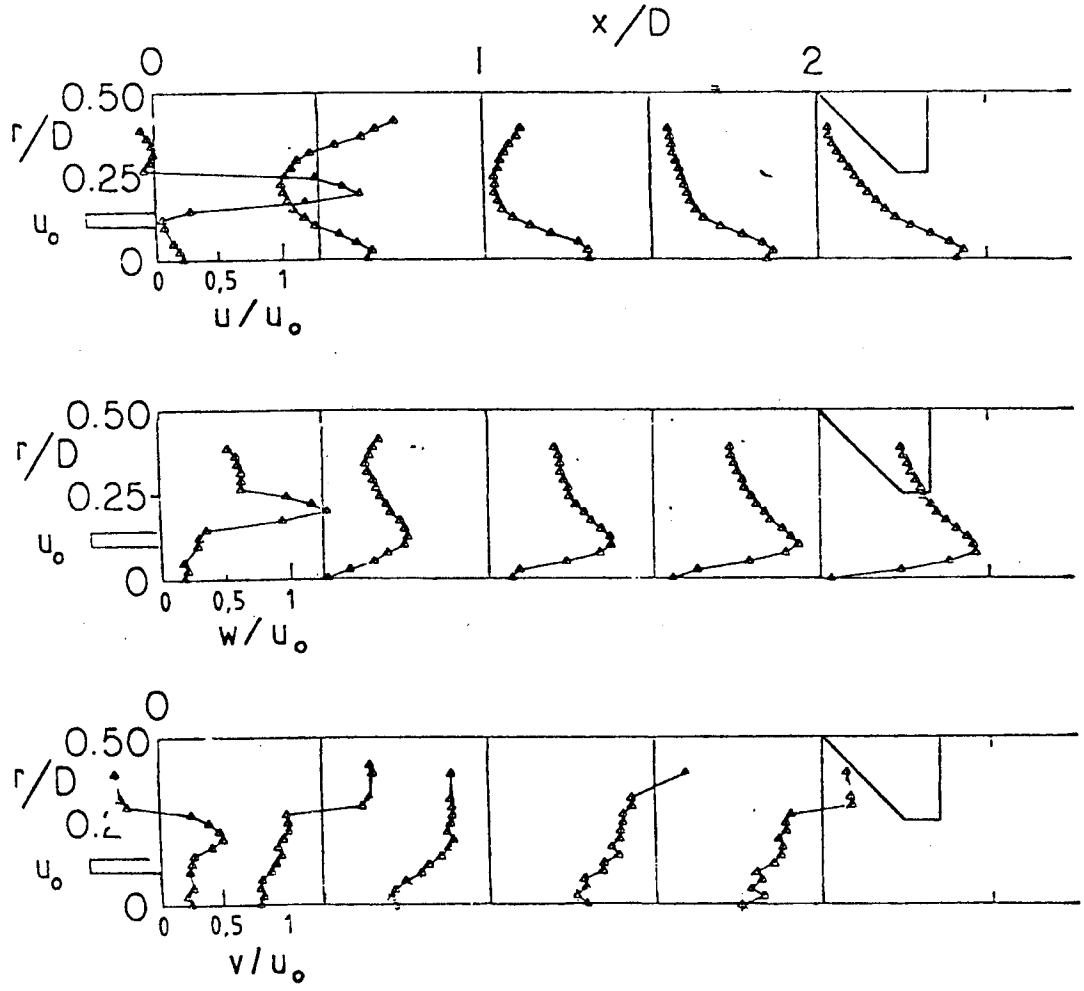

Figure 19. Time-Mean and Turbulent Flowfield ϕ = 45 Degrees With Strong Contraction Nozzle at L/D = 2

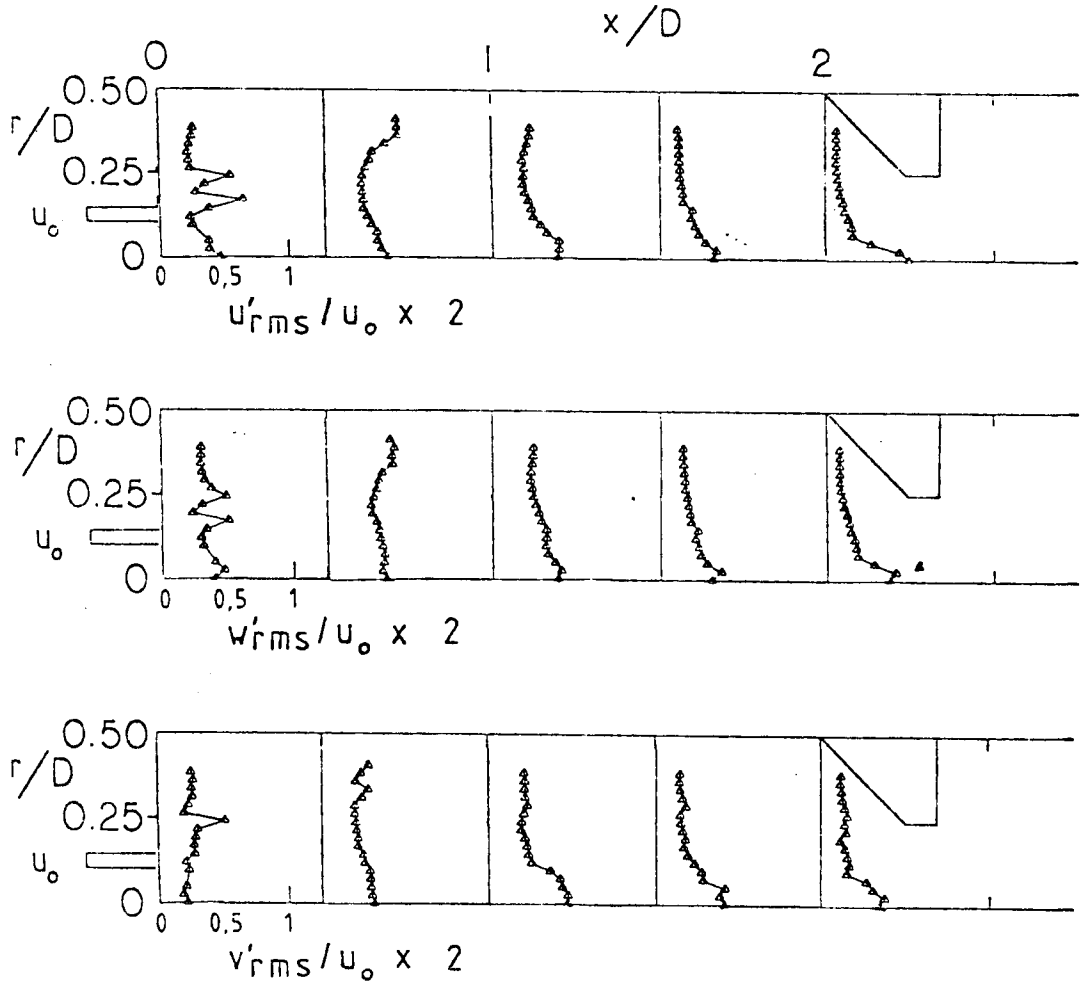

Figure 19. (Continued)

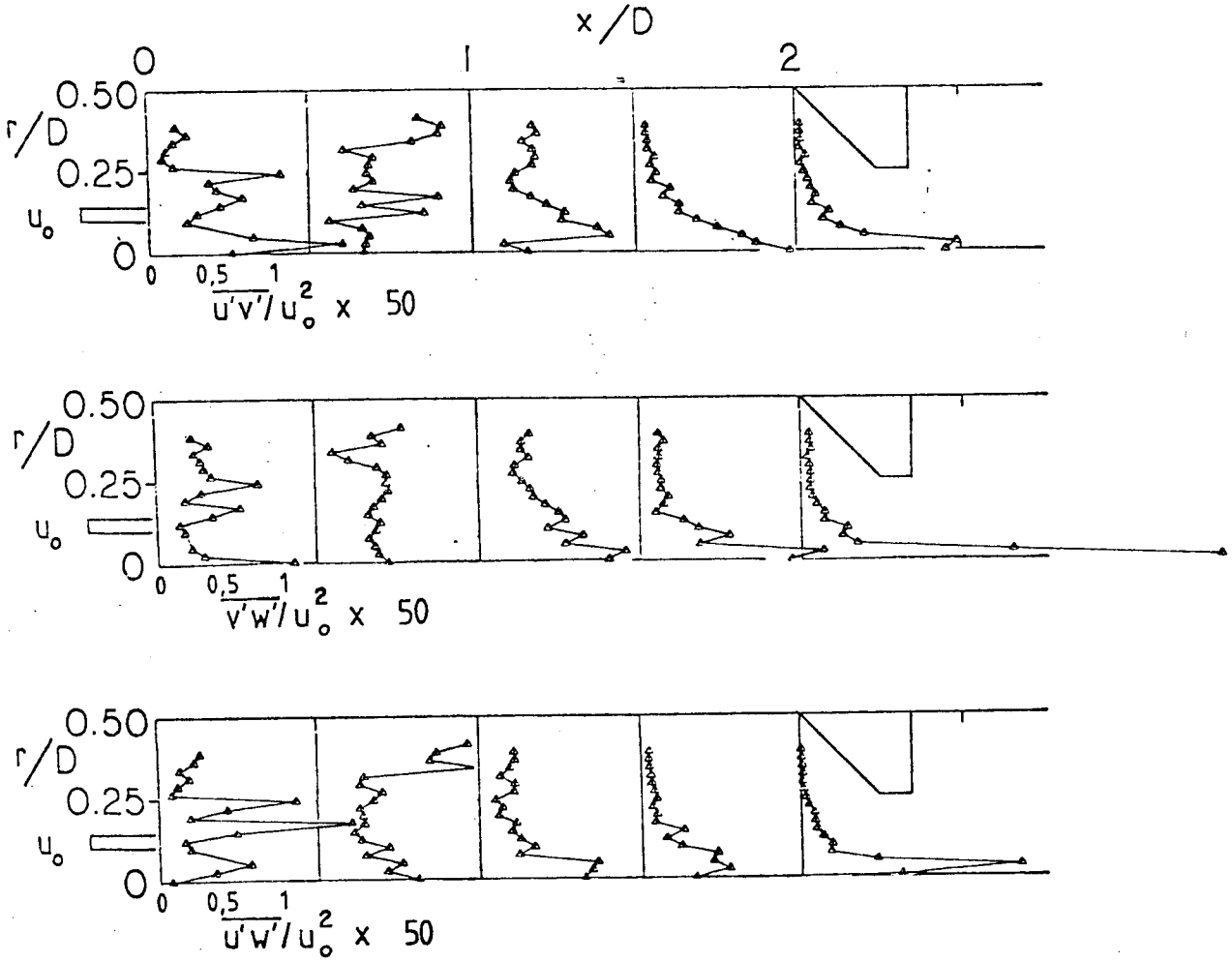

Figure 19. (Continued)

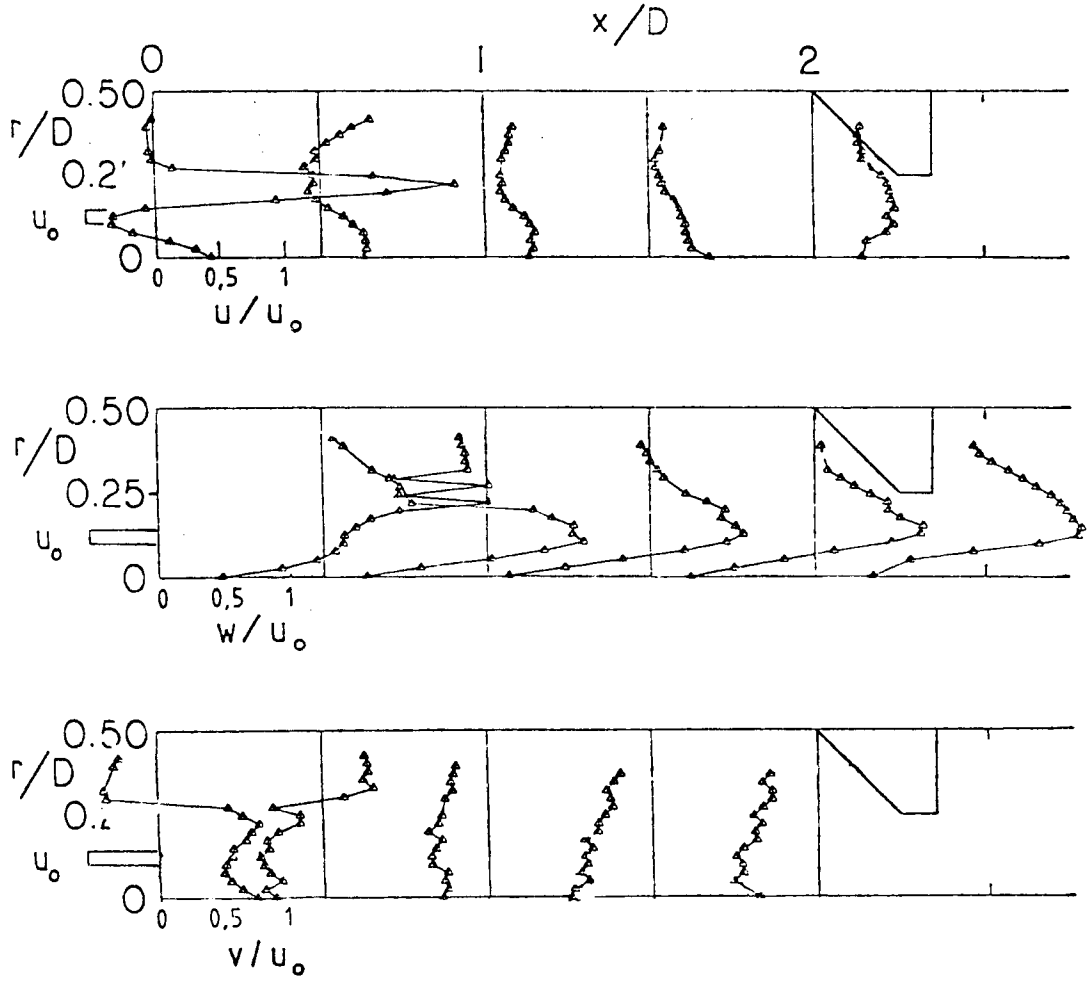

Figure 20. Time-Mean and Turbulent Flowfield ϕ = 70 Degrees, With Strong Contraction Nozzle at L/D = 2

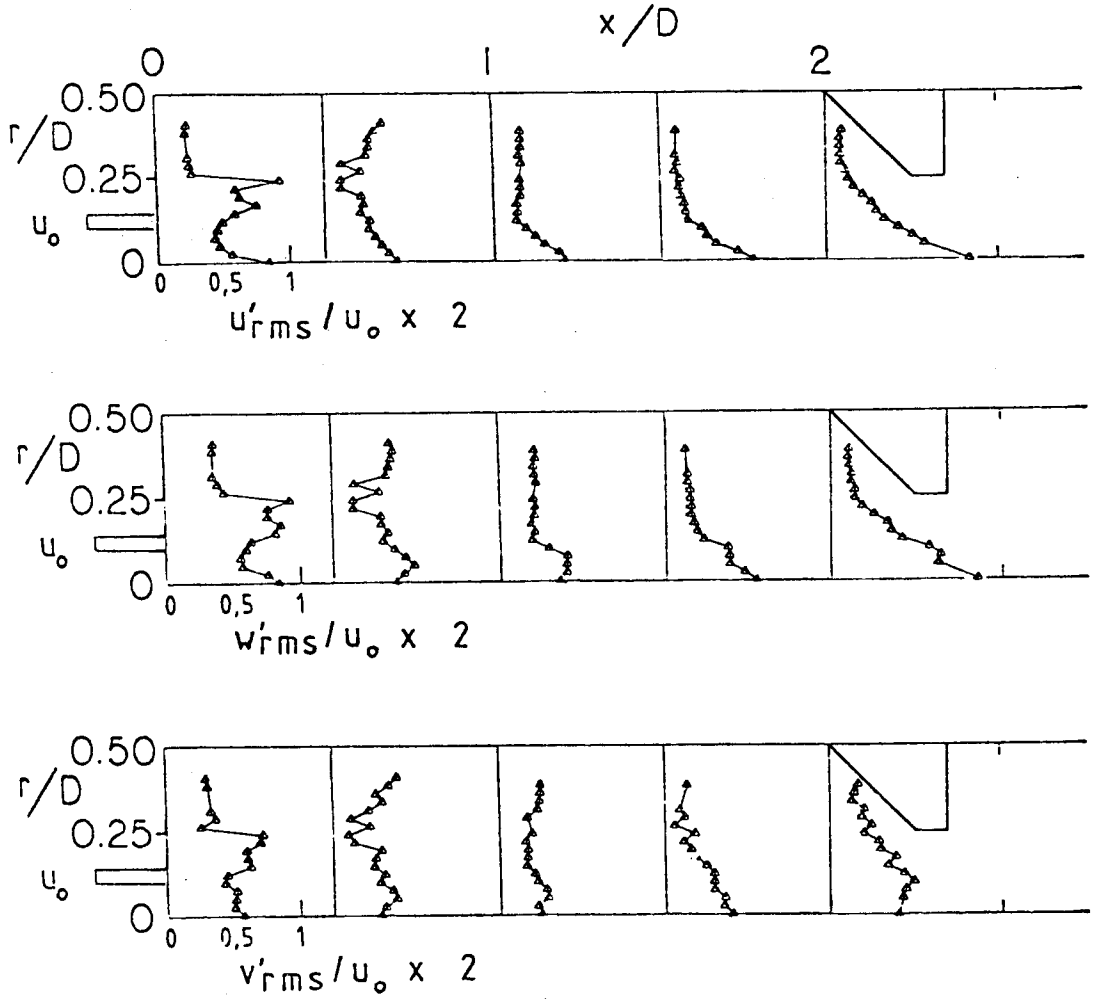

Figure 20. (Continued)

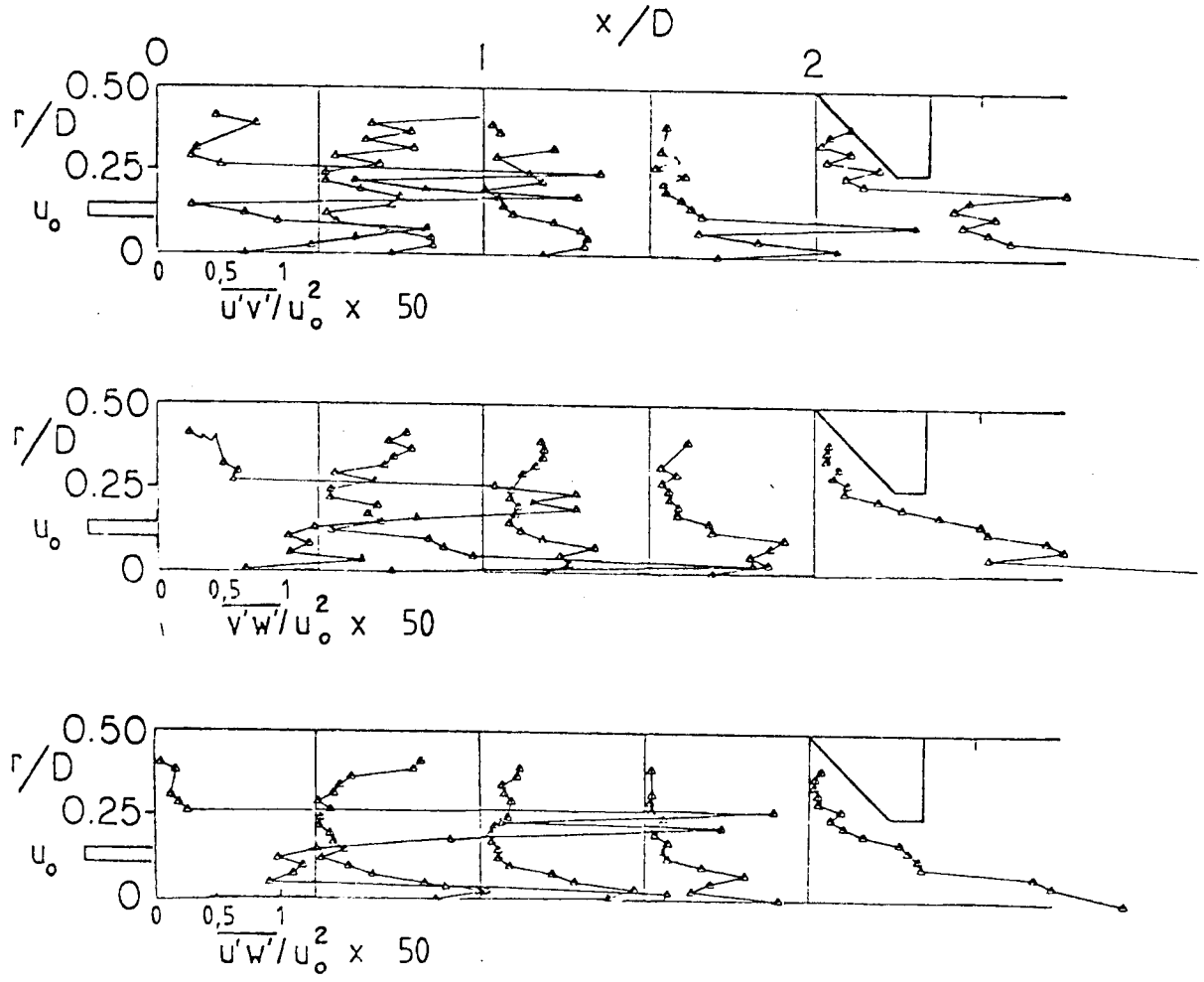

Figure 20. (Continued)

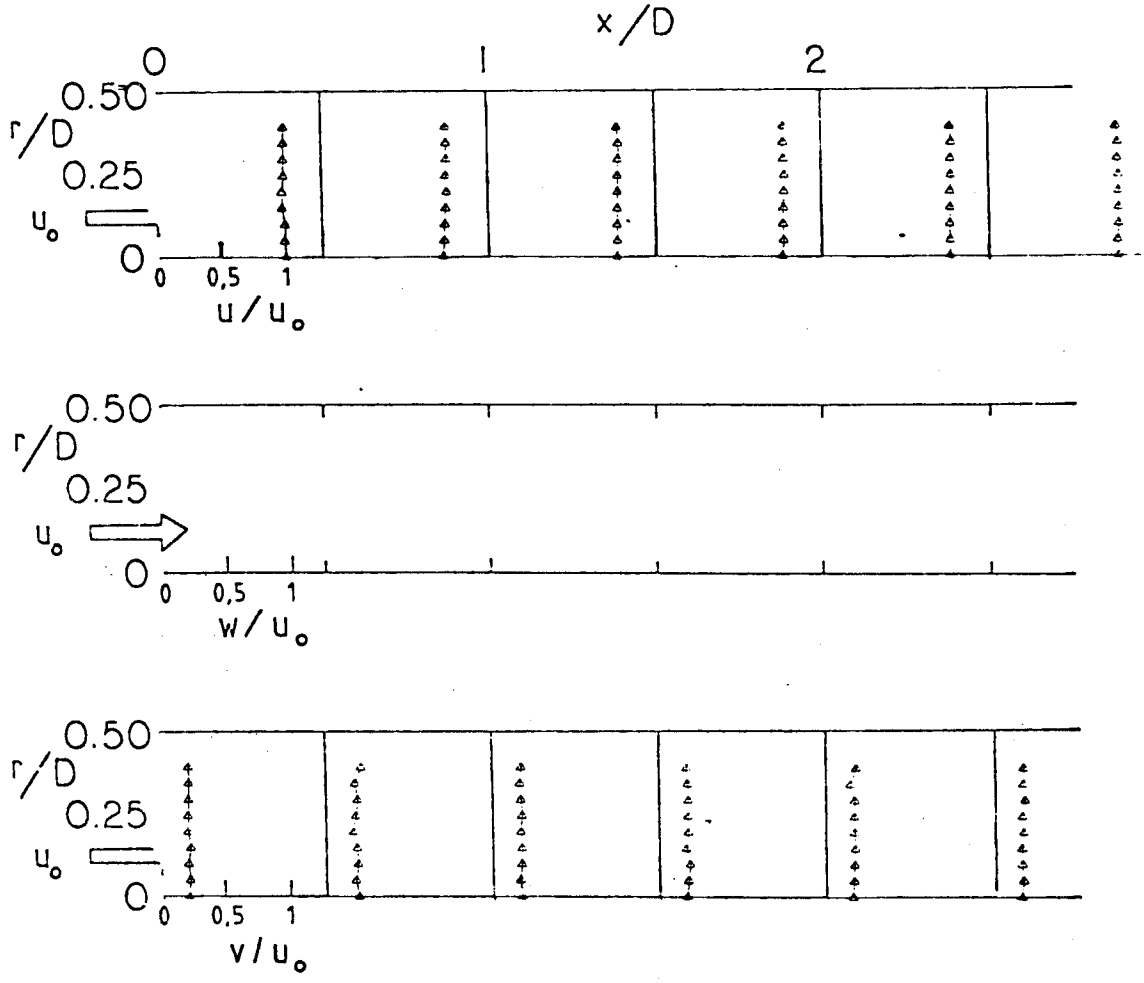

Figure 21. Time-Mean and Turbulent Flowfield ϕ = 0 Degrees, (No Swirler), D/d = 1

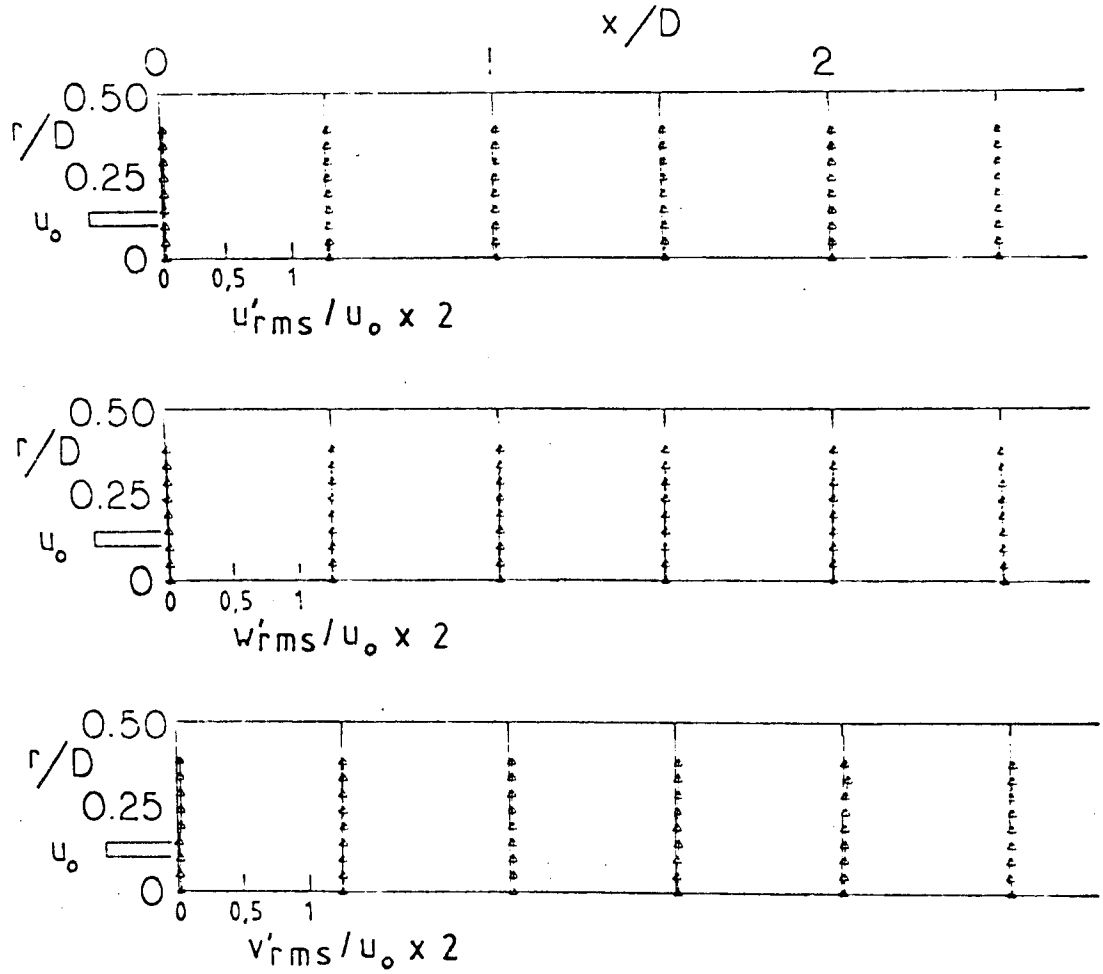

Figure 21. (Continued)

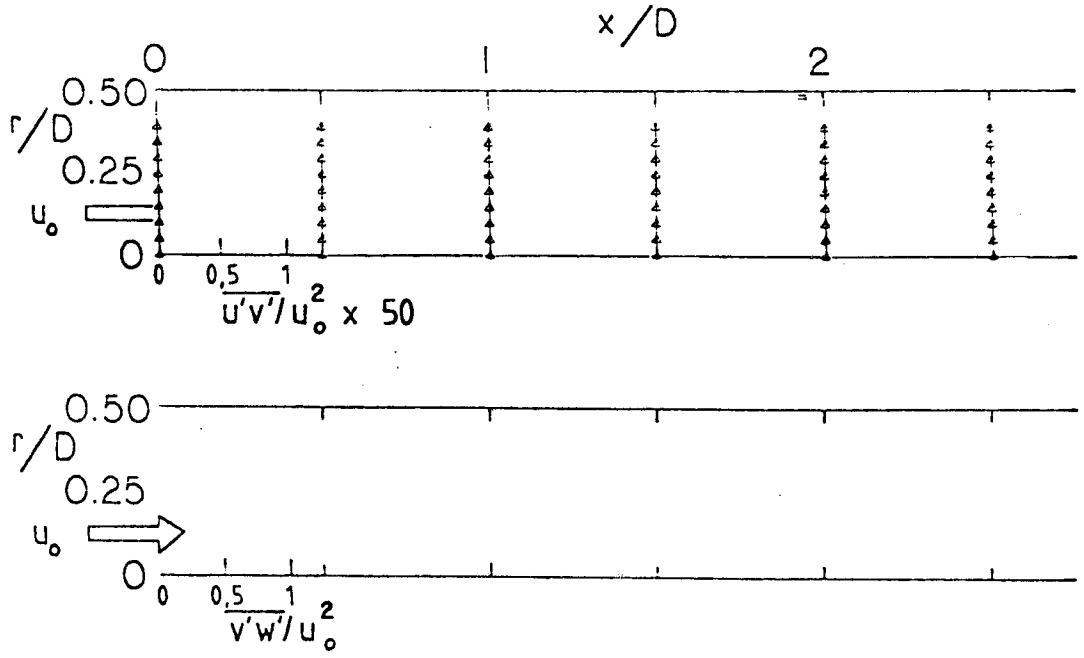

Figure 21. (Continued)

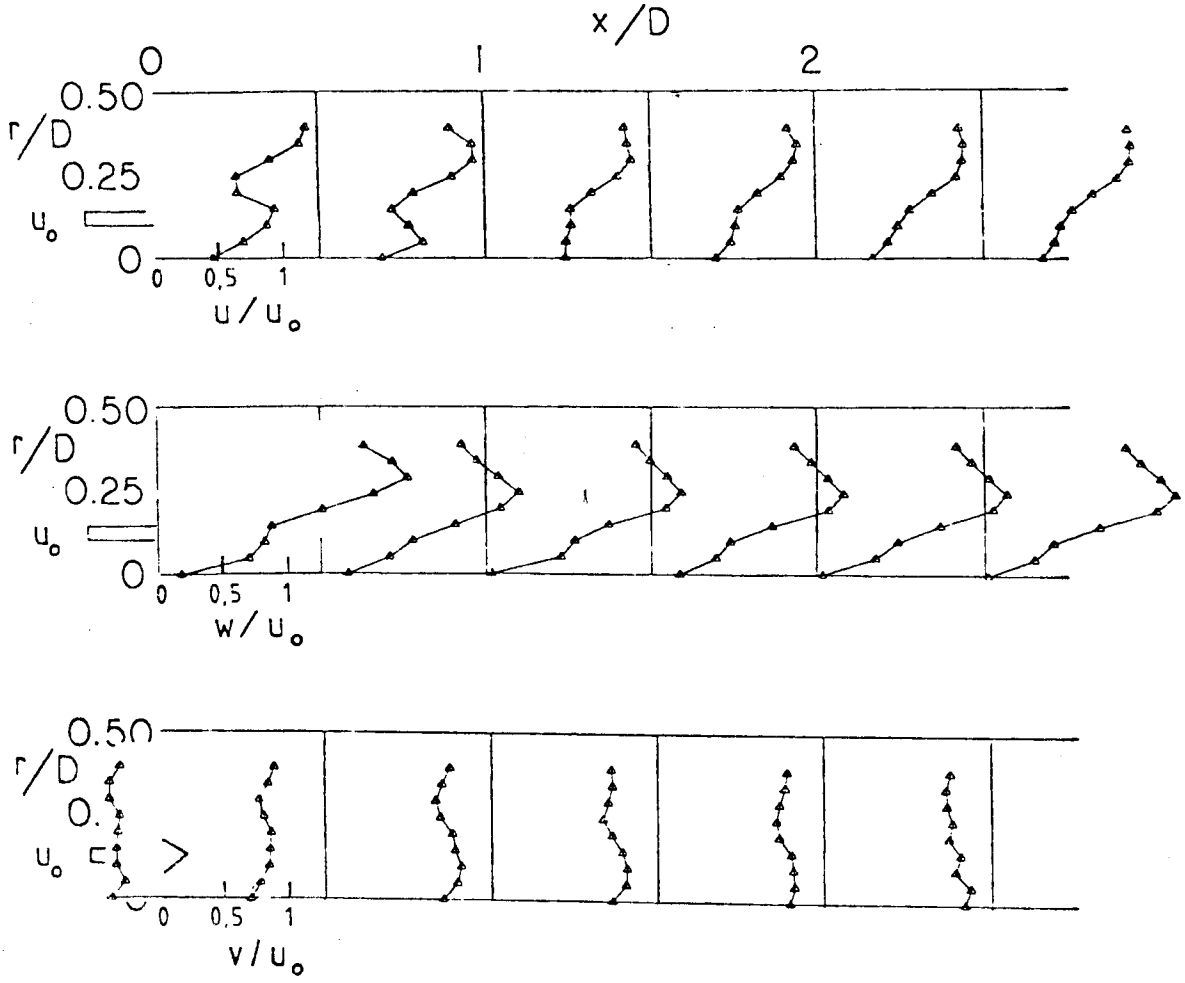

Figure 22. Time-Mean and Turbulent Flowfield ϕ = 45 Degrees, D/d = 1

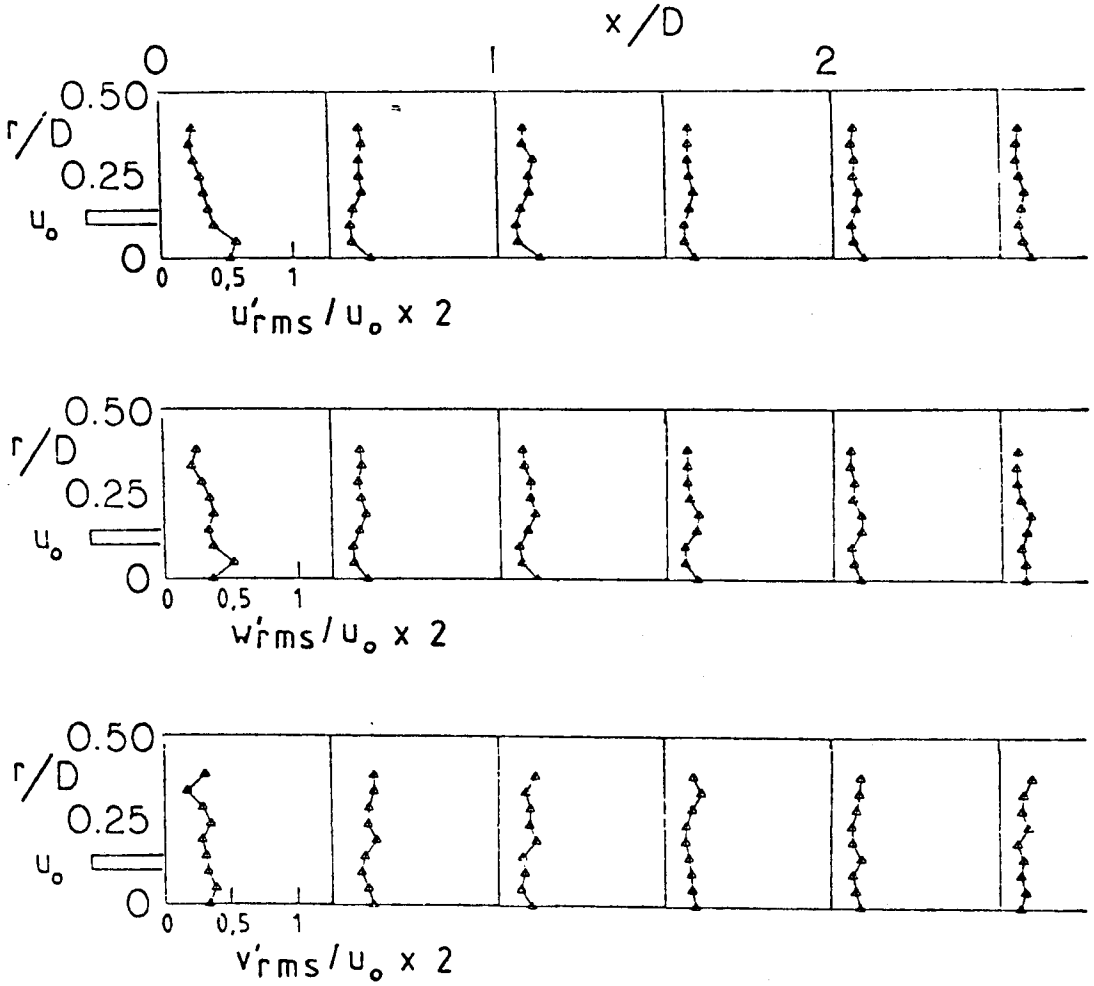

Figure 22. (Continued)

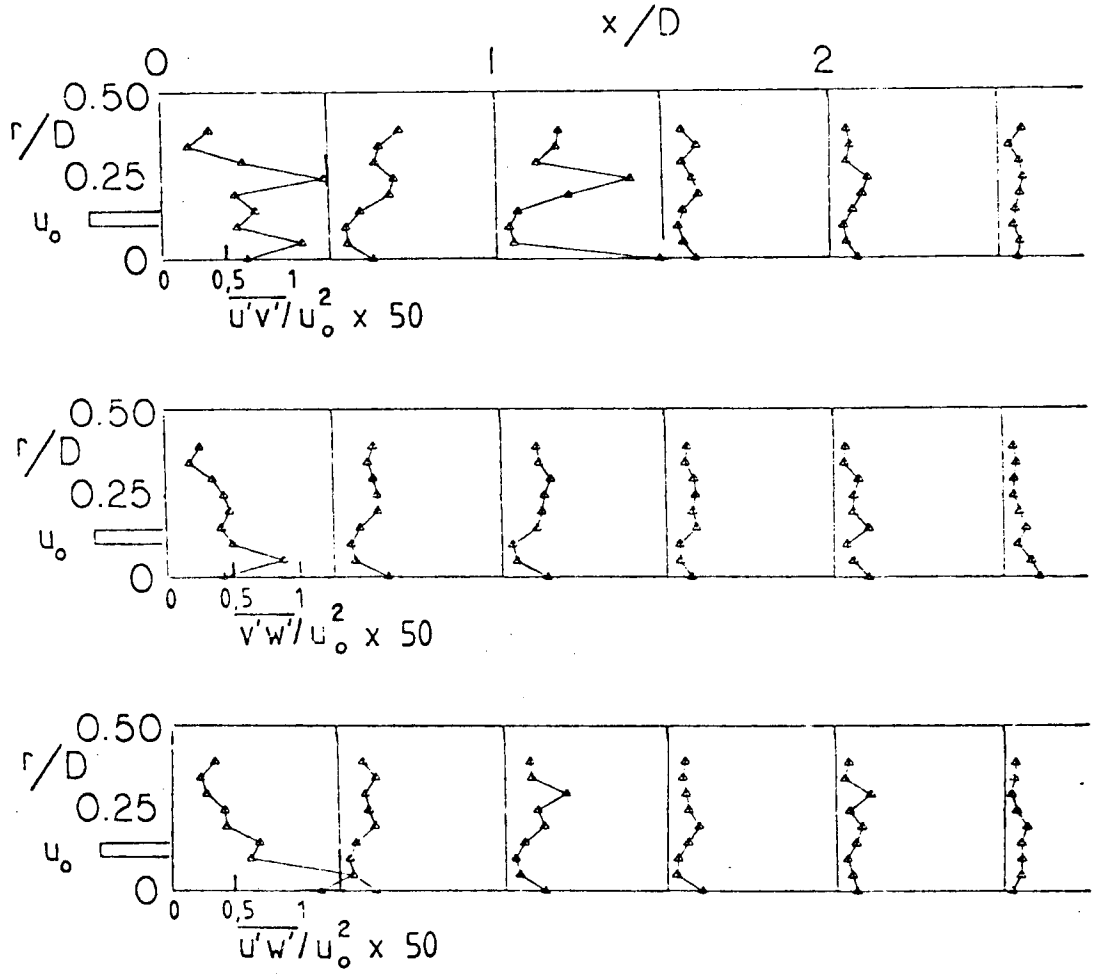

Figure 22. (Continued)

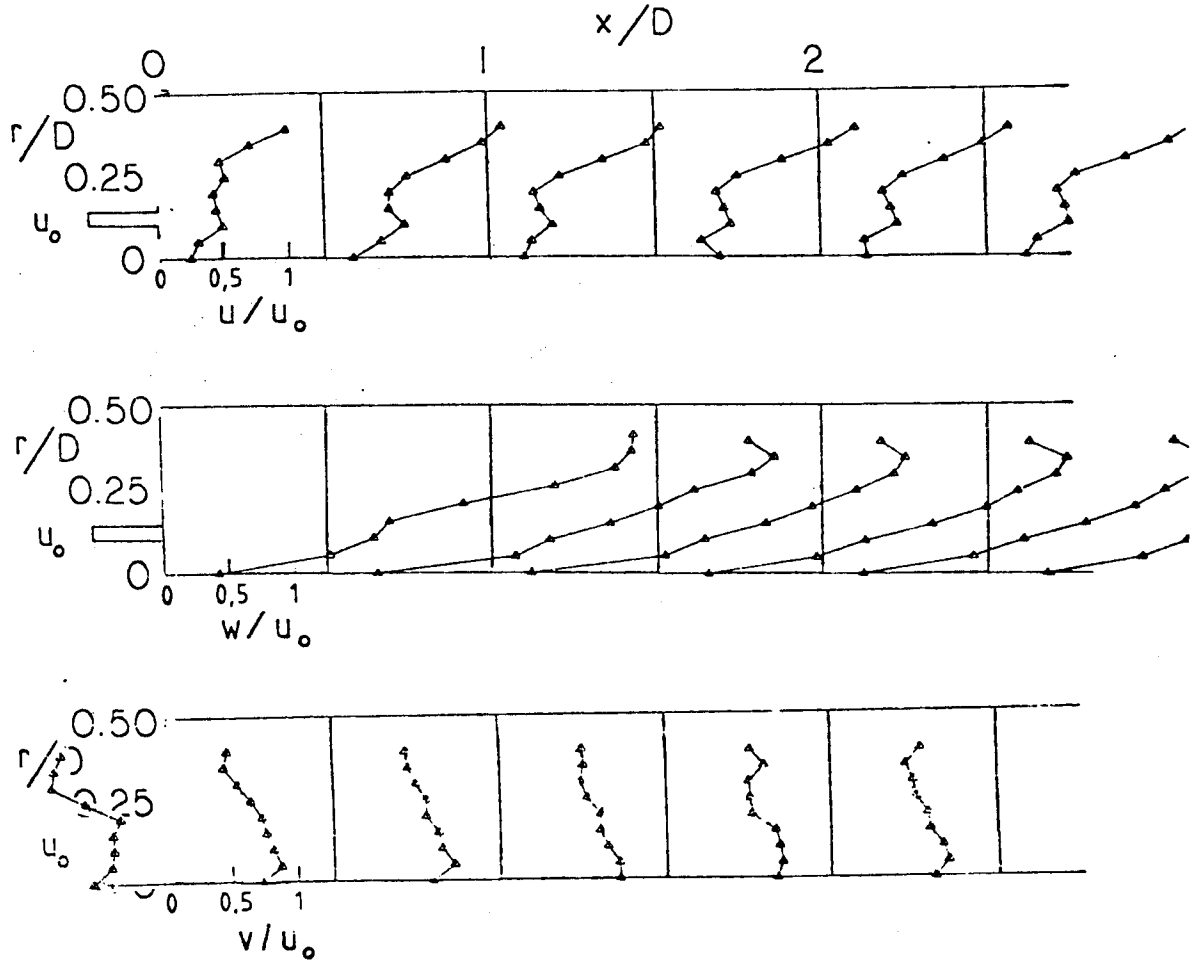

Figure 23. Time-Mean and Turbulent Flowfield ϕ = 70 Degrees, D/d = 1

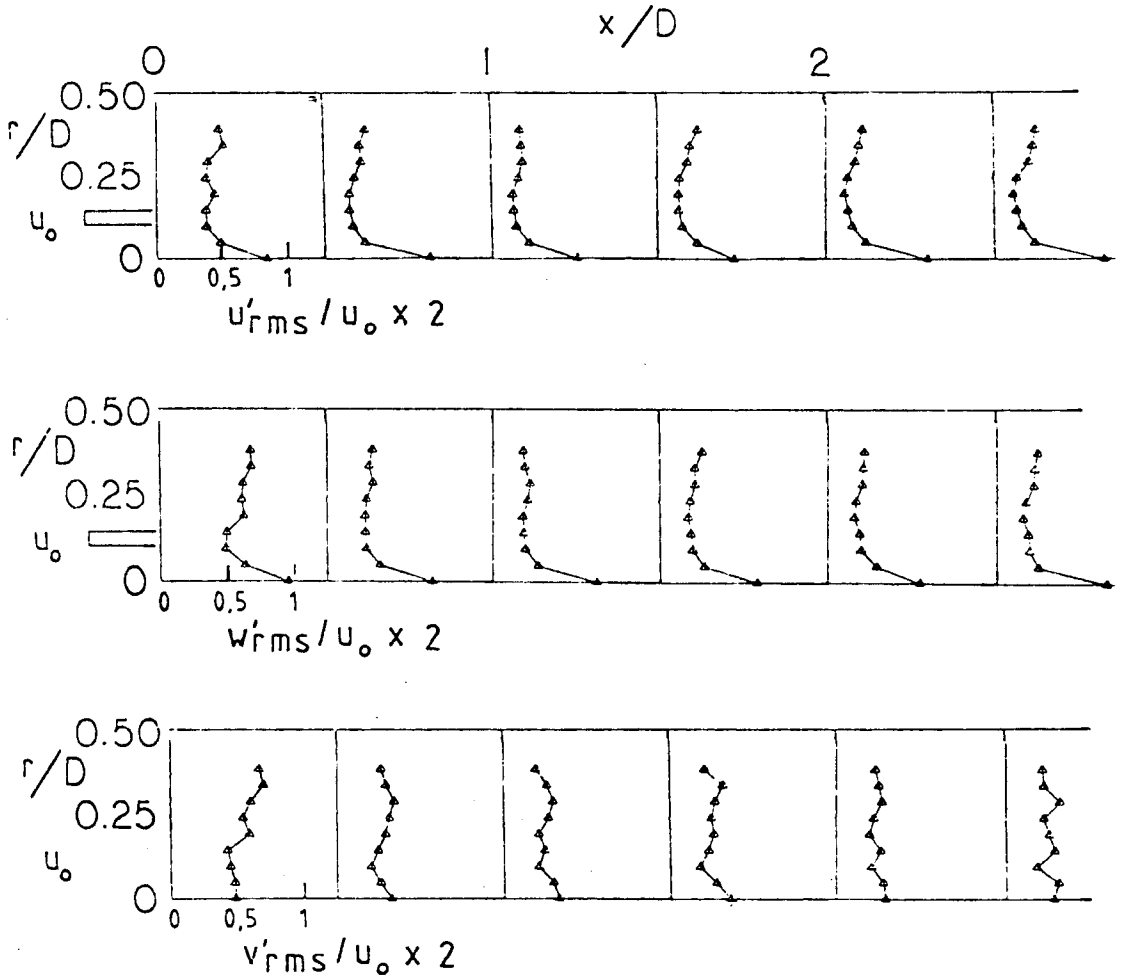

Figure 23. (Continued)

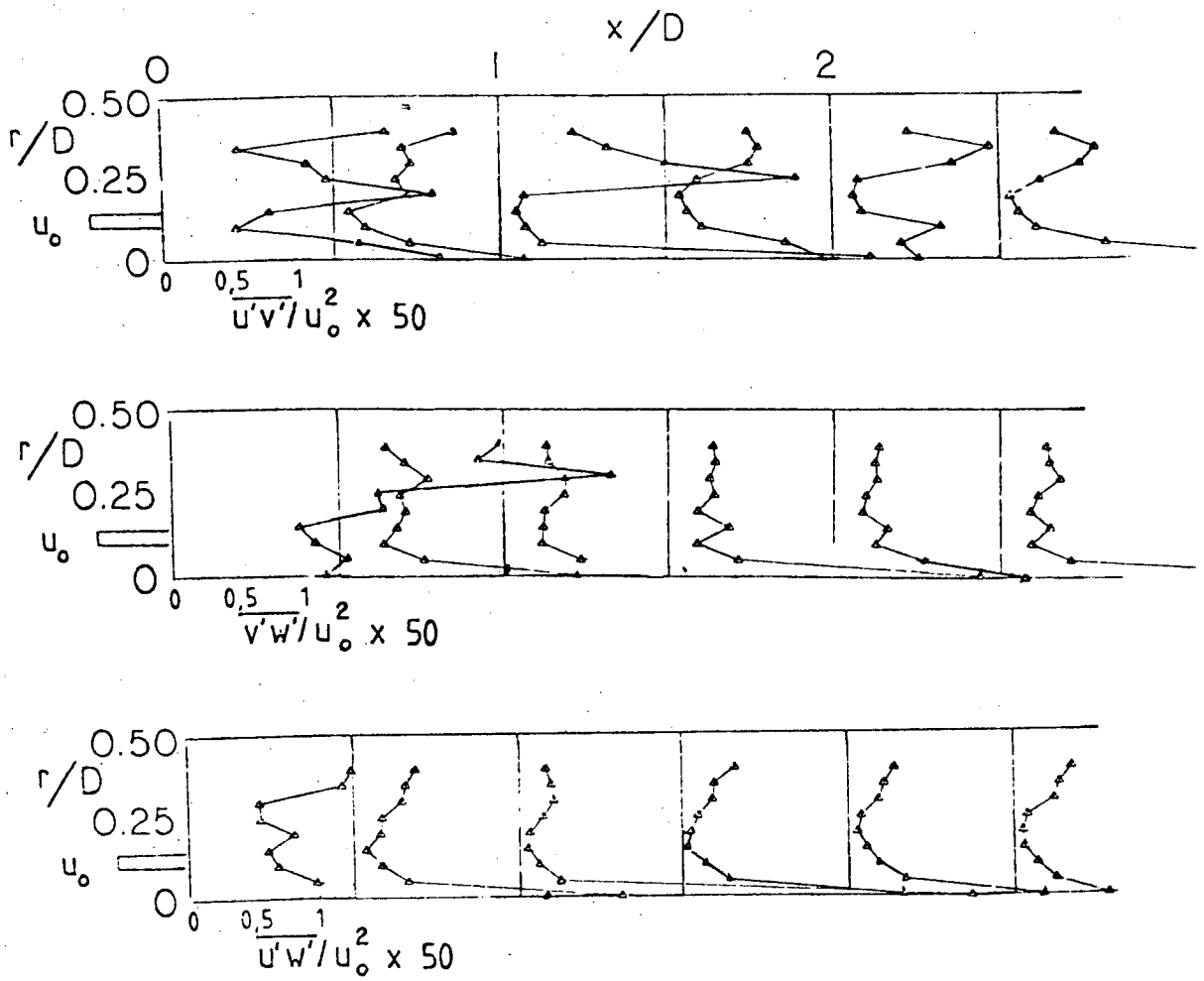

Figure 23. (Continued)

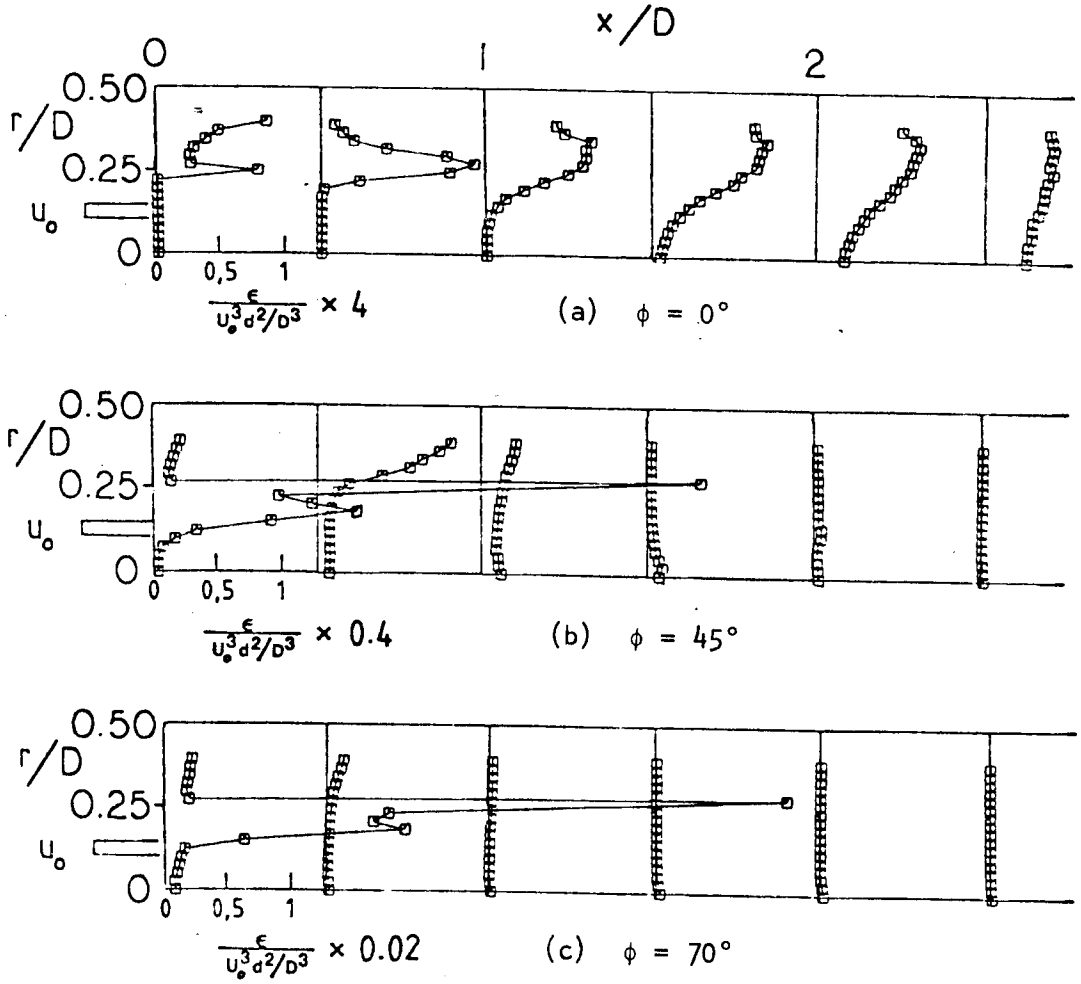

Figure 24. Eddy Dissipation Rate, D/d = 2

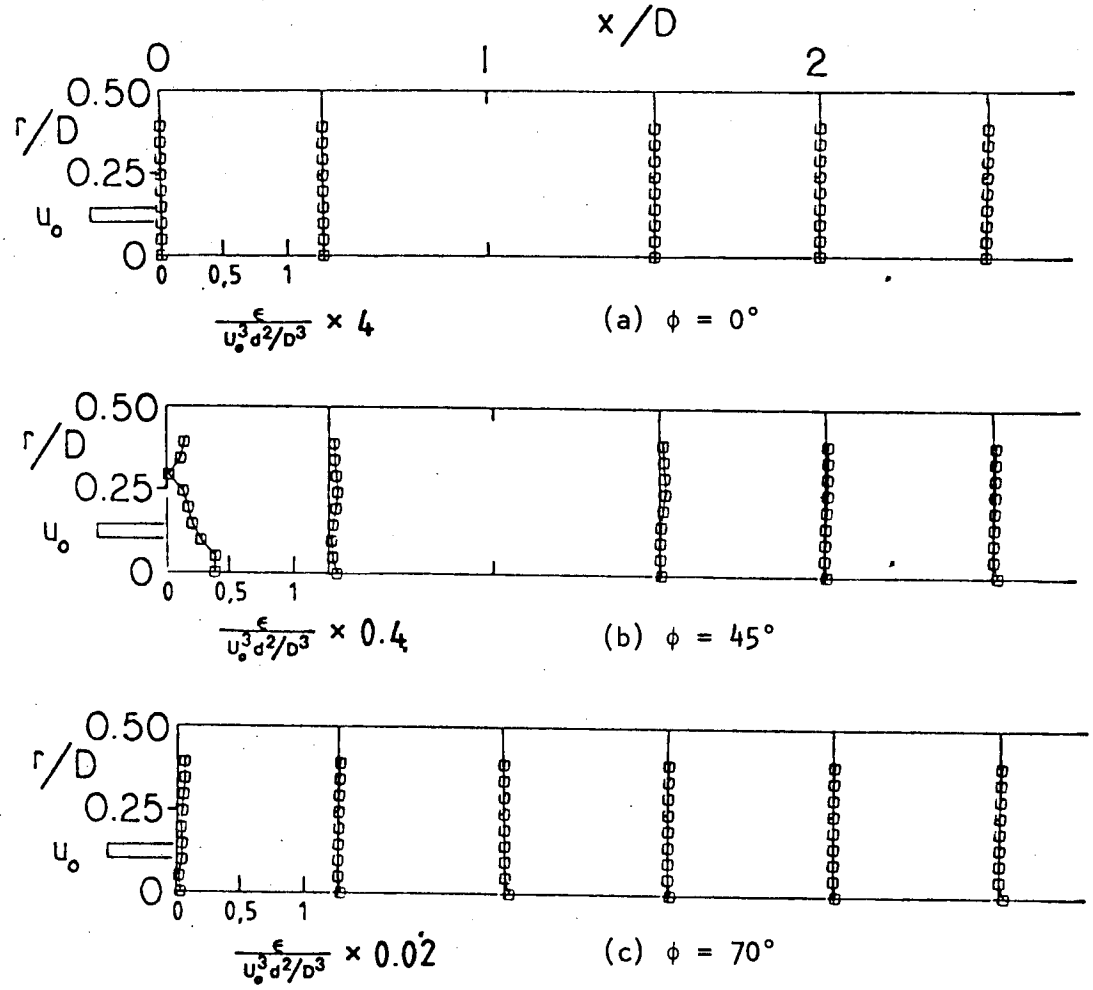

Figure 25. Eddy Dissipation Rate, D/d = 1

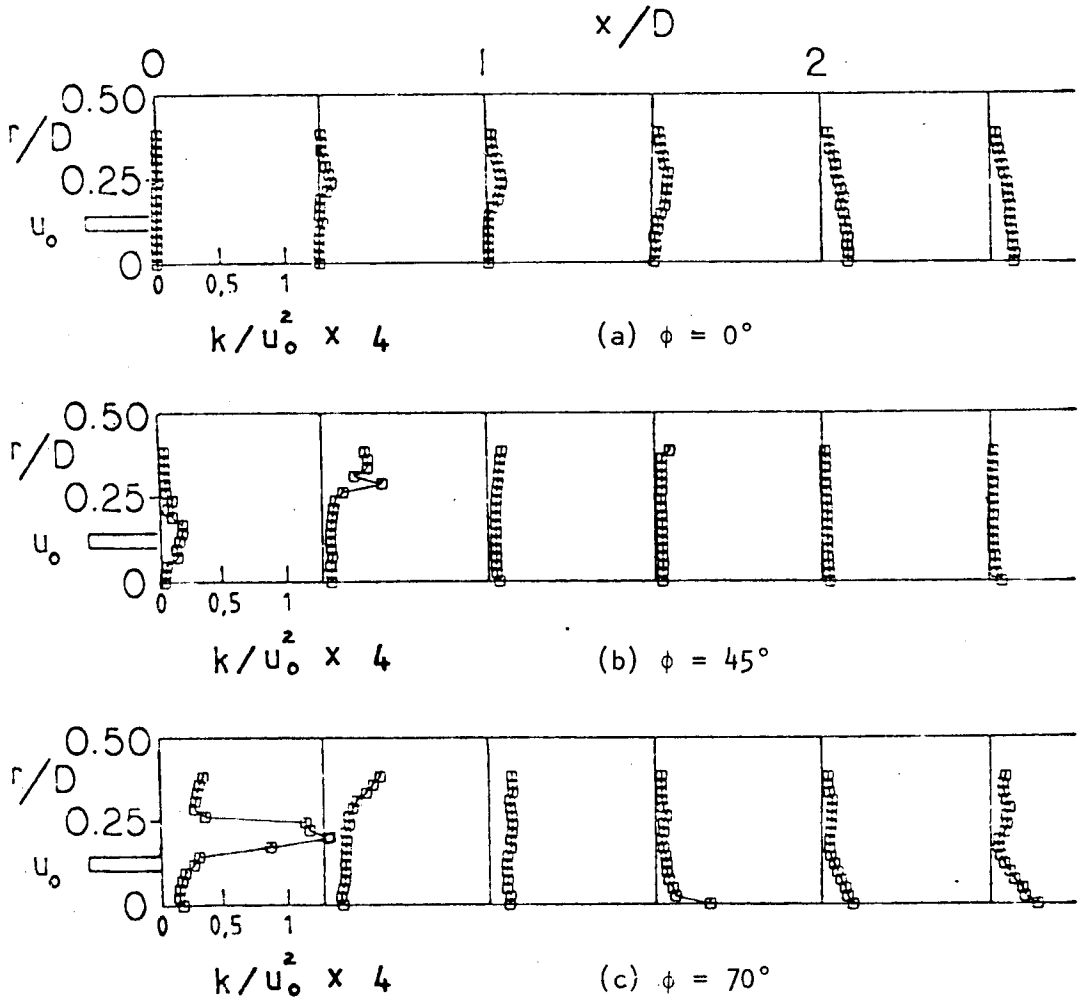

Figure 26. Kinetic Energy of Turbulence, D/d = 2

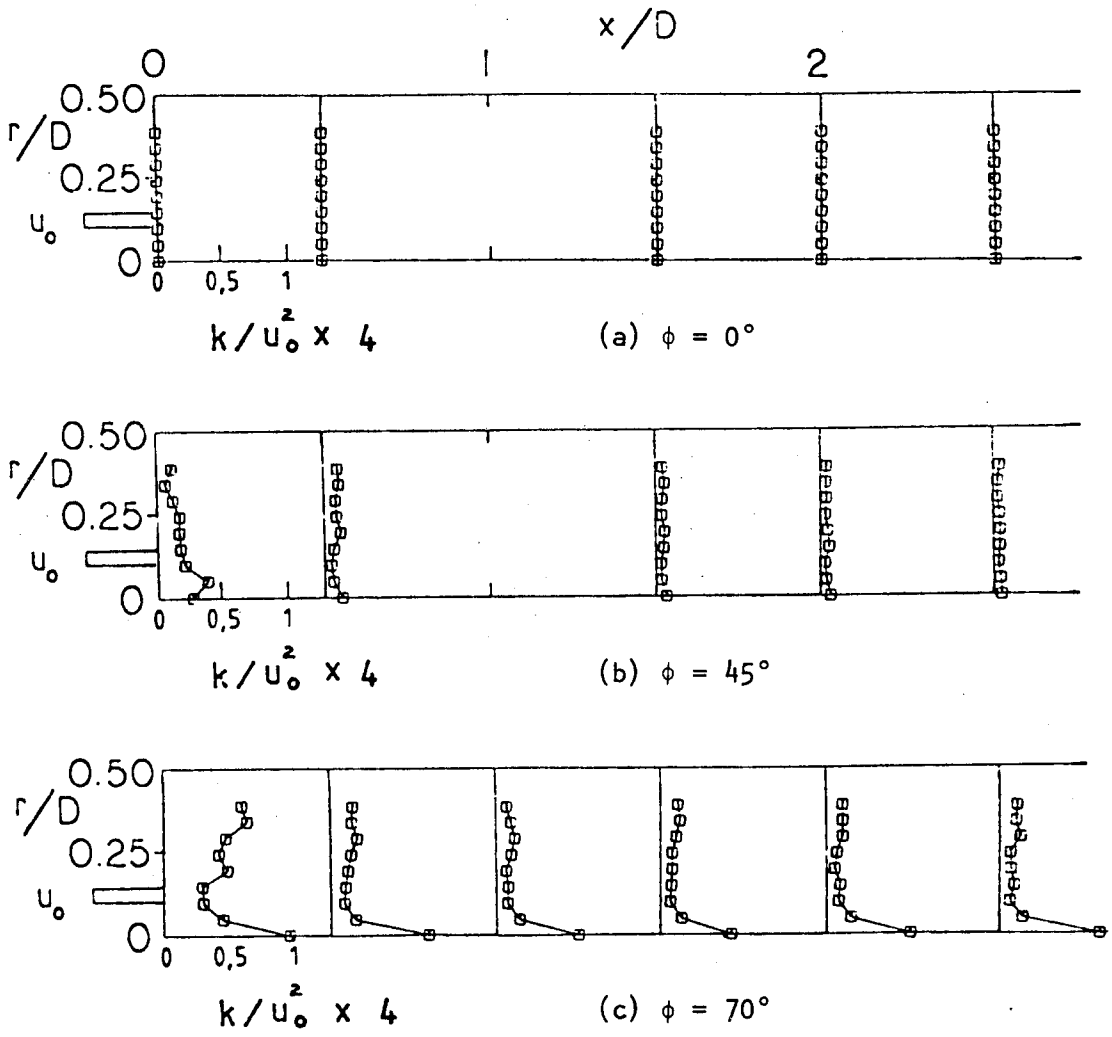

Figure 27. Kinetic Energy of Turbulence, D/d = 1

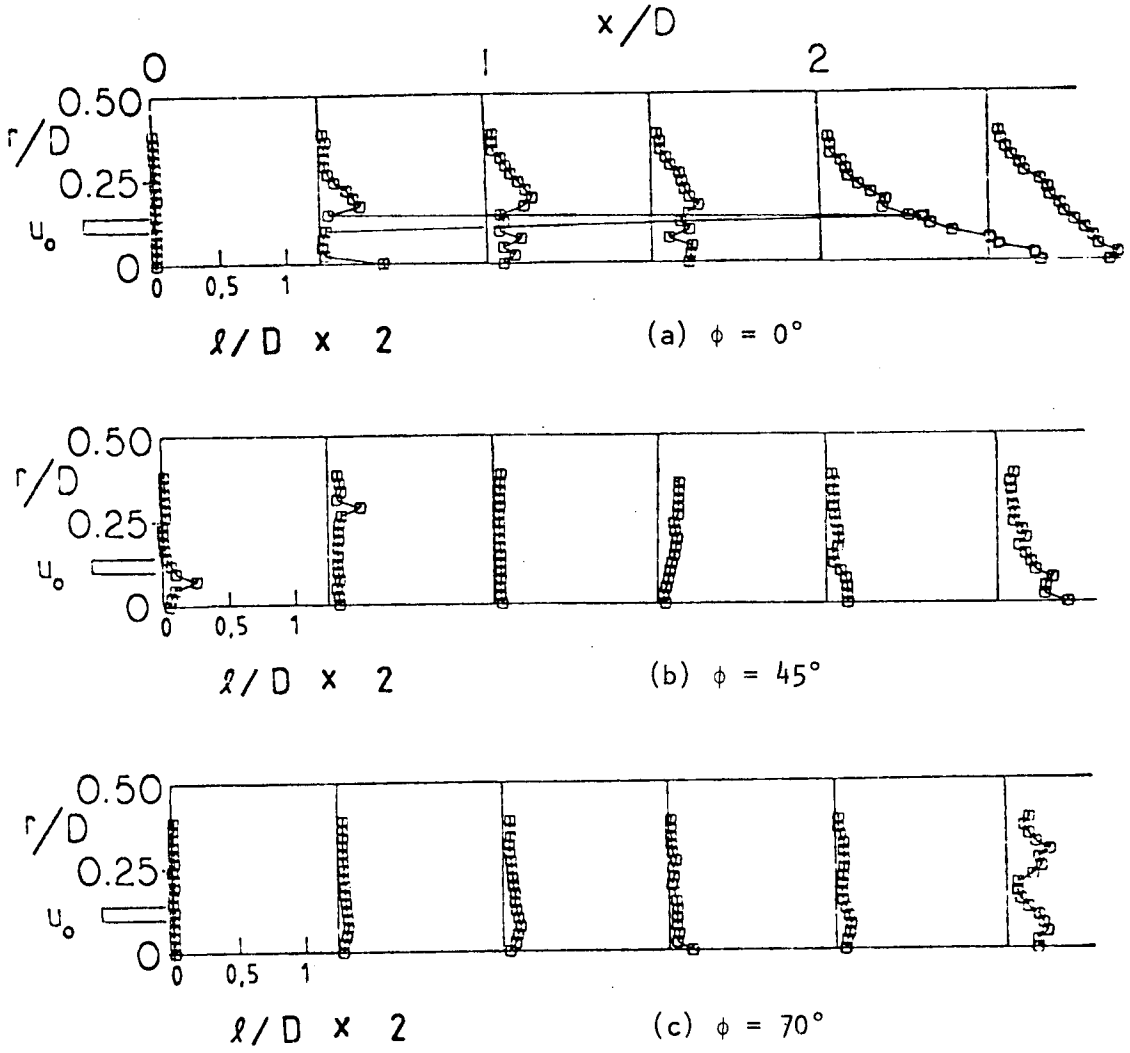

Figure 28. Turbulent Dissipation Length Scale, D/d = 2

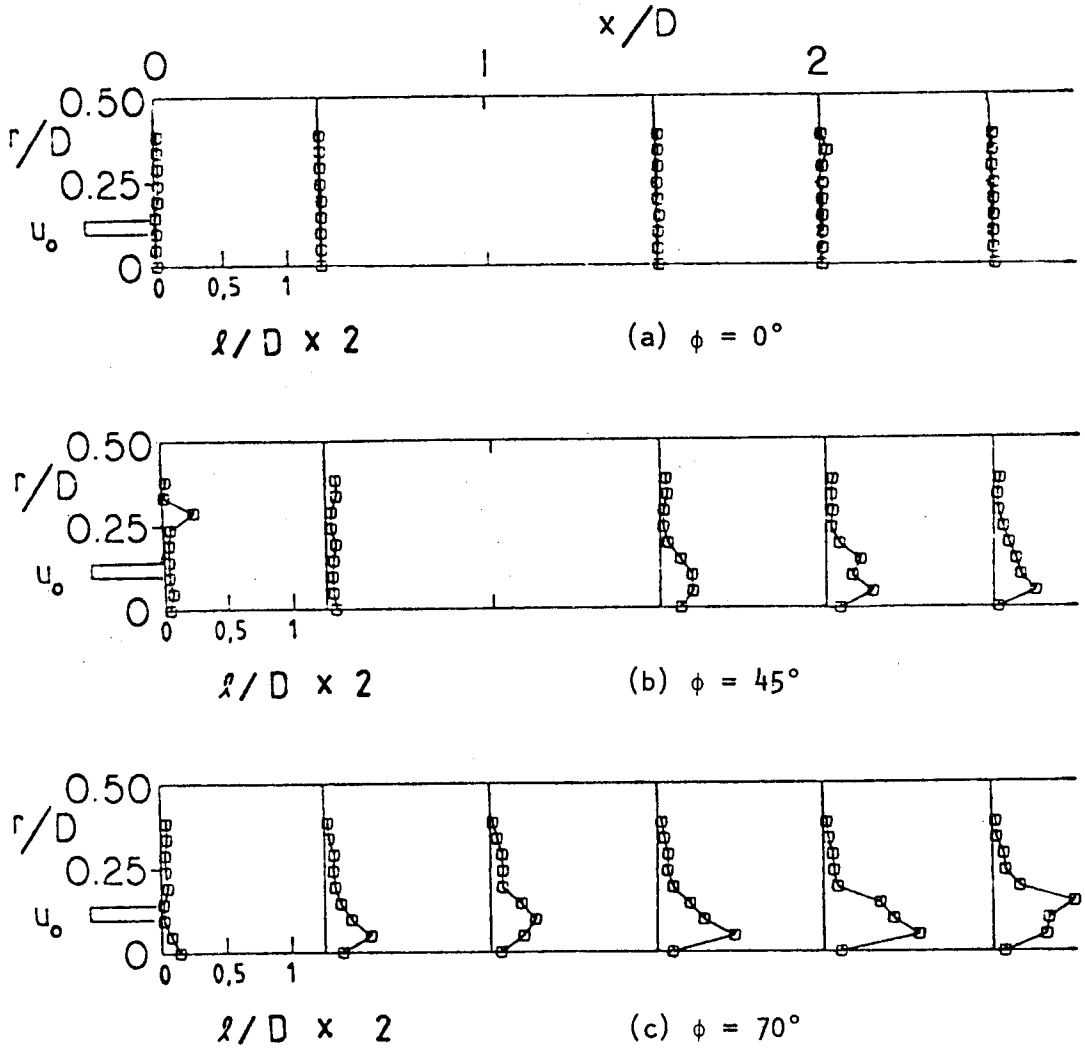

Figure 29. Turbulent Dissipation Length Scale, D/d = 1

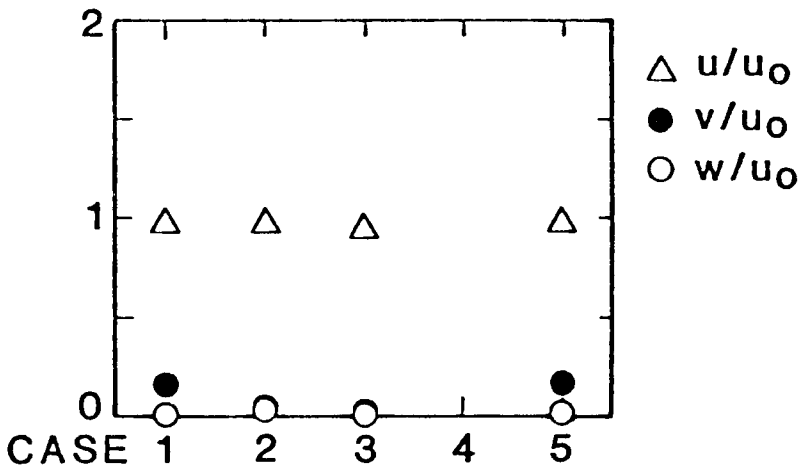

Figure 30. Measurements for Situation A With Different Probe Configuration Cases

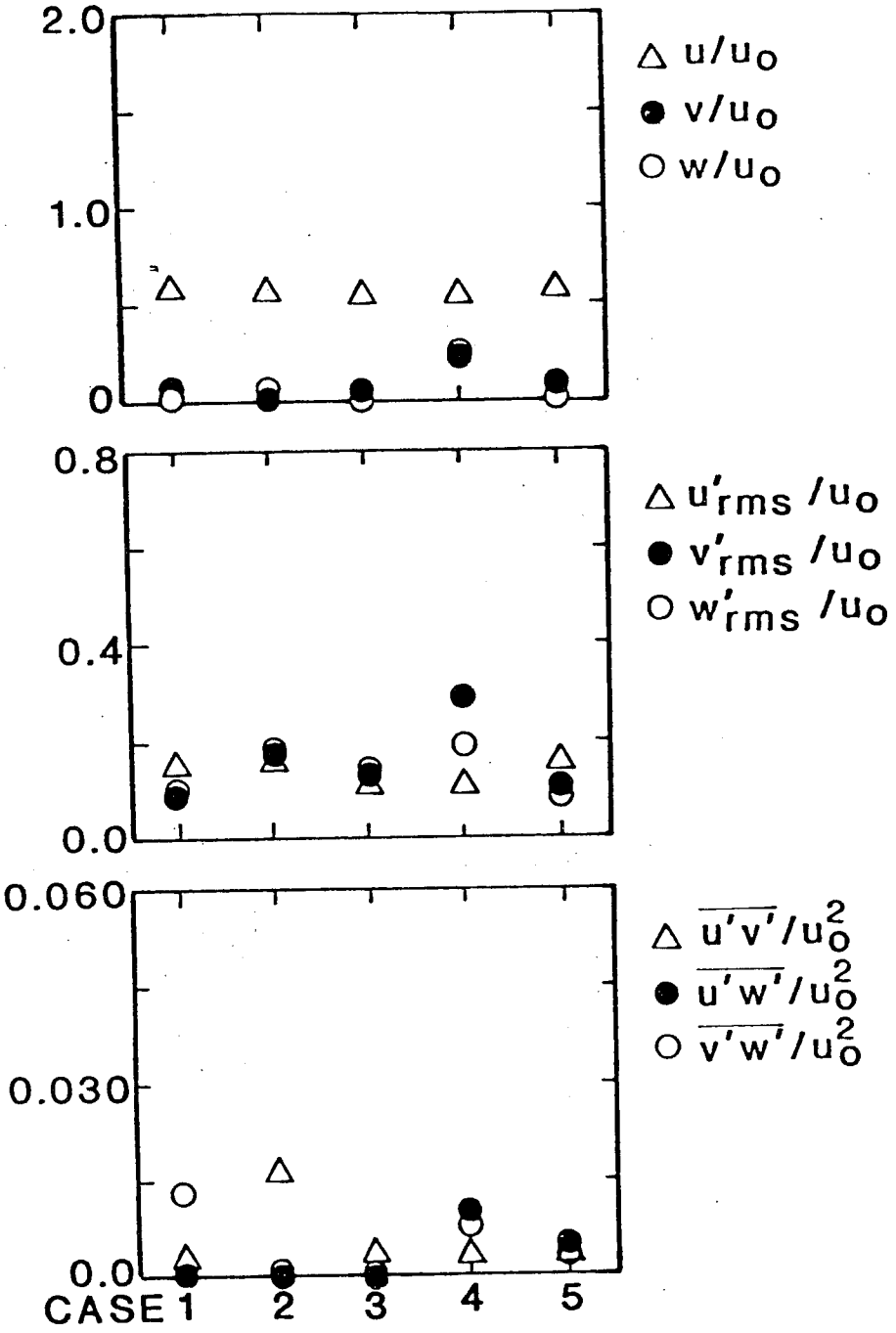

Figure 31. Measurements for Situation B With Different Probe Configuration Cases

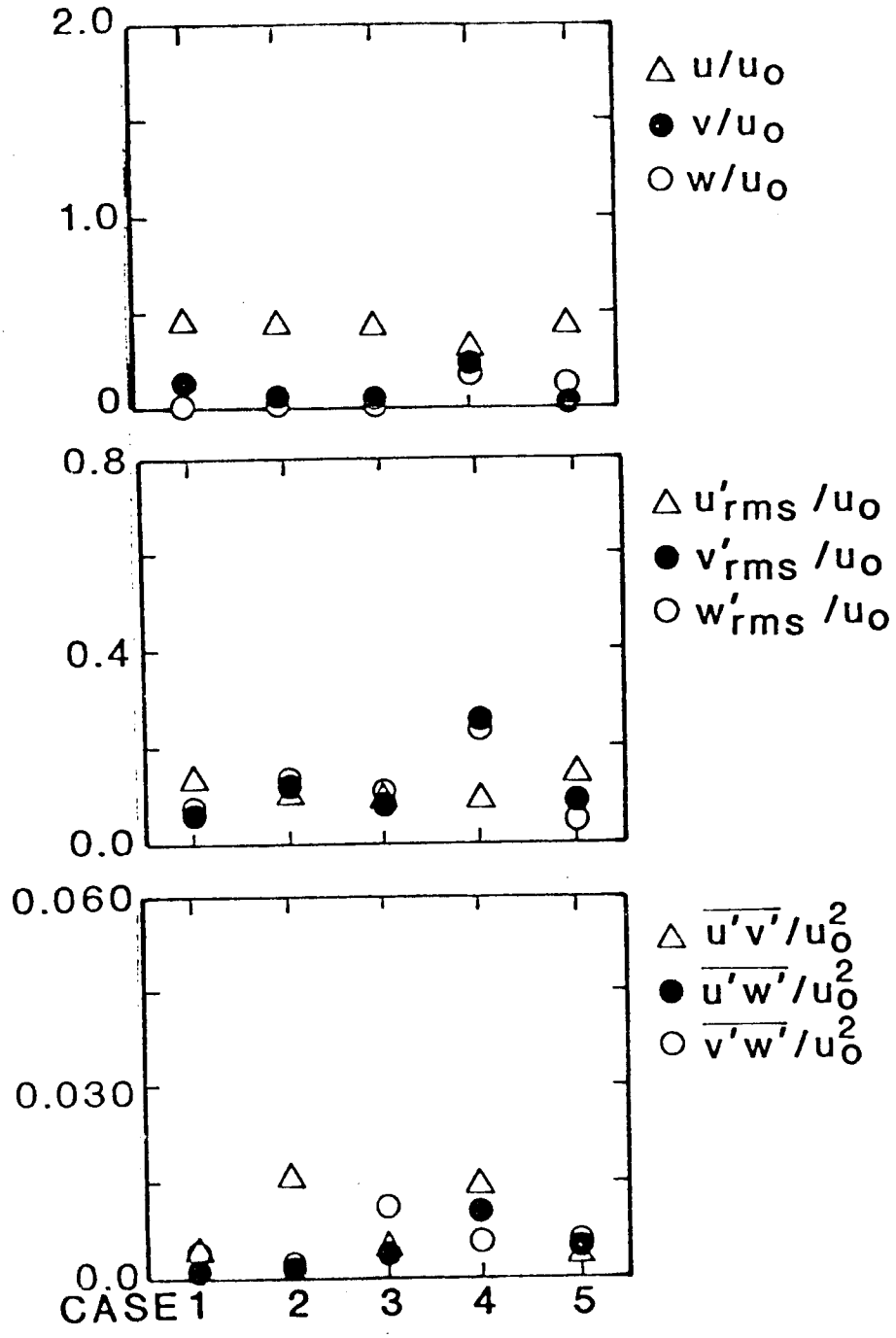

Figure 32. Measurements for Situation C With Different Probe Configuration Cases

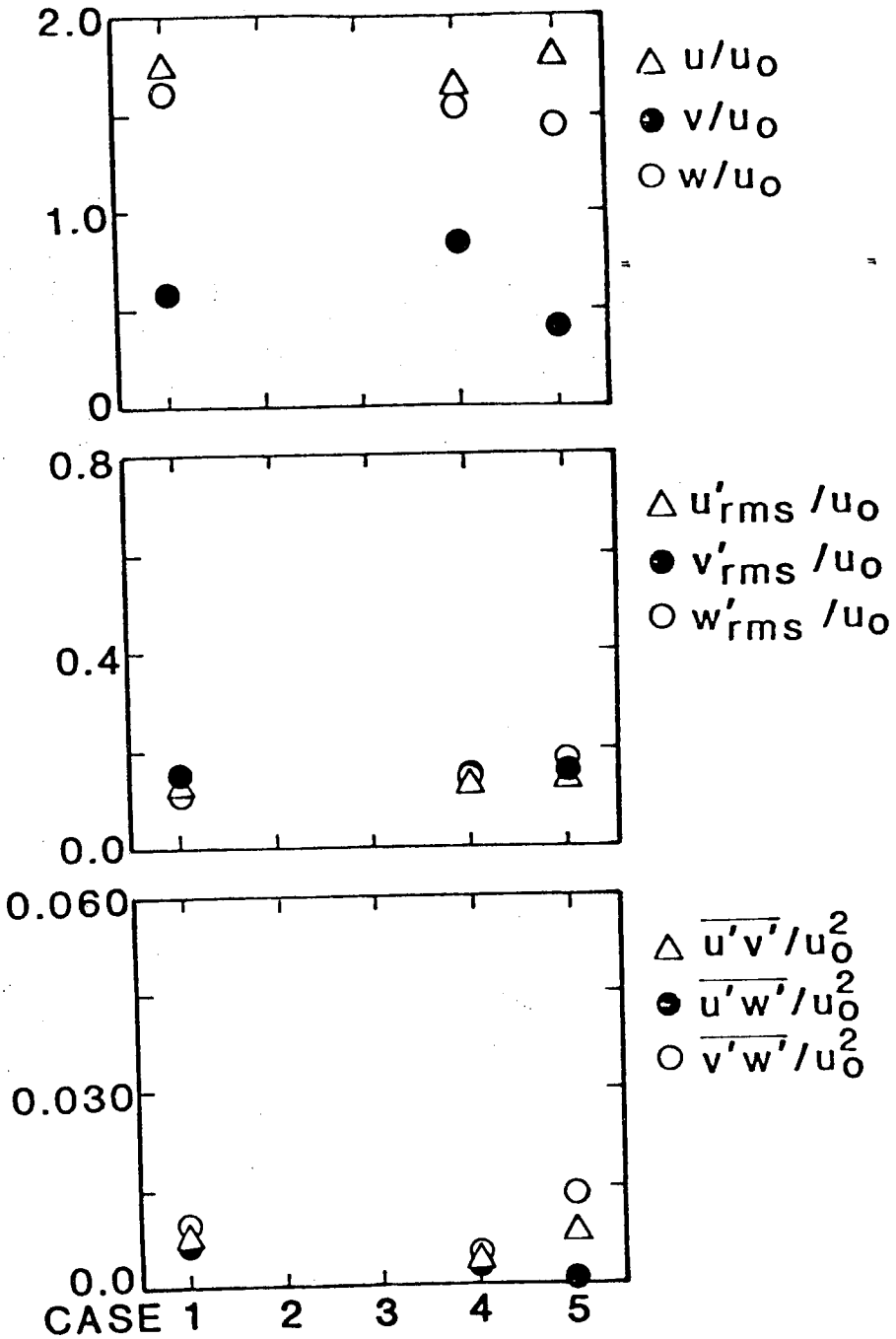

Figure 33. Measurements for Situation D With Different Probe Configuration Cases

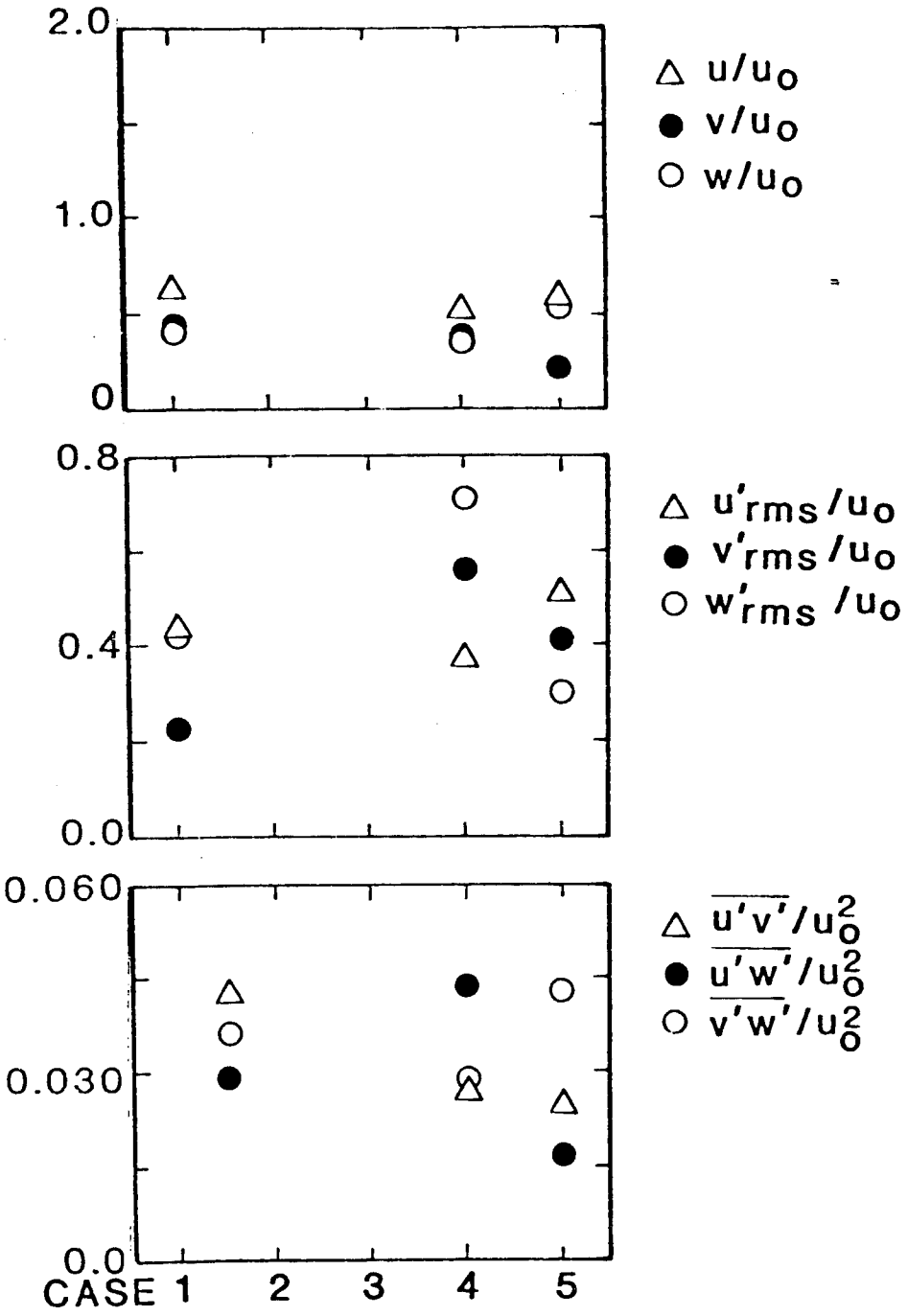

Figure 34. Measurements for Situation E With Different Probe Configuration Cases

1. Report No.	2. Government Accession No.	3. Recipient's Catalog No.
NASA CR-174918		

4. Title and Subtitle	5. Report Date
Turbulence Characteristics of Swirling Flowfields	May 1985
	6. Performing Organization Code

7. Author(s)	8. Performing Organization Report No.
T.W. Jackson and D.G. Lilley	None
	10. Work Unit No.

9. Performing Organization Name and Address	11. Contract or Grant No.
Oklahoma State University School of Mechanical and Aerospace Engineering Stillwater, Oklahoma 74074	NAG 3-74
	13. Type of Report and Period Covered
12. Sponsoring Agency Name and Address	Contractor Report
National Aeronautics and Space Administration Washington, D.C. 20546	14. Sponsoring Agency Code 533-04-1A

15. Supplementary Notes

Final report. Project Manager, James D. Holdeman, Internal Fluid Mechanics Division, NASA Lewis Research Center, Cleveland, Ohio 44135. This report was a dissertation submitted by T.W. Jackson to the Faculty of the Graduate School of Oklahoma State University in partial fulfillment of the requirements for the degree Doctor of Philosophy in December 1984.

16. Abstract

The time-mean and turbulence properties of a confined swirling jet using the six-orientation, single hot-wire technique were obtained. The effect of swirl on a confined, expanding jet is to reduce the size of the corner recirculation zone and generate a central recirculation zone followed by a precessing vortex core. The effect of introducing a contraction nozzle of area ratio four, located two test-section diameters downstream of the inlet, is to dramatically reduce the size and shape of the central recirculation zone for the swirling flows considered. The shear stresses are found to increase by an order of magnitude in the region of the contraction nozzle because of large radial gradients of axial velocity. Reduction of the expansion ratio to D/d = 1 causes the time-mean flowfield to be homogeneous throughout the entire test section with the tangential velocity dominating in the swirling cases. No recirculation zones were observed for these particular flows. Turbulence levels and dissipation rates were found to be low except in the entrance regions and in areas of acceleration in the swirling flow cases.

17. Key Words (Suggested by Author(s))	18. Distribution Statement
Combustor; Swirl; Turbulent flow; Turbulence measurements; Hot wire; Confined swirling jet	Unclassified - unlimited STAR Category 07

19. Security Classif. (of this report)	20. Security Classif. (of this page)	21. No. of pages	22. Price*
Unclassified	Unclassified	265	A12

*For sale by the National Technical Information Service, Springfield, Virginia 22161